Morphometric variability in the extant coccolithophores: implications for the fossil record

by

Alicia Catherine Muzika Kahn

A dissertation submitted to the

Graduate School - New Brunswick

Rutgers, The State University of New Jersey

in partial fulfillment of the requirements

for the degree of

Doctor of Philosophy

Graduate Program in Geological Sciences

written under the direction of

Dr. Marie-Pierre Aubry

and approved by

_____

_____

_____

_____

New Brunswick, New Jersey

October, 2007

ABSTRACT OF THE DISSERTATION

Morphometric variability in the extant coccolithophores: implications for the fossil record

by ALICIA CATHERINE MUZIKA KAHN

Dissertation Director:

Dr. Marie-Pierre Aubry

This detailed quantitative study shows significant intraspecific morphologic variability in species within modern calcareous nannoplankton communities. The link between depth of habitat and particular morphological components may indicate morphological adaptation and functionality. I use fine scale morphological characteristics to differentiate species variants or conversely, to identify polymorphism within species. Rhabdospheres and rhabdoliths of species within the family Rhabdosphaeraceae are analyzed as shallow photic zone proxies and reveal significant intra- and interspecific variability, whereas coccospheres and coccoliths of species in the deep photic zone show notably less variability in size and structure. The intra- and interspecific morphological variability that is noted with depth stratification is applicable to the fossil record in paleoceanographic reconstruction. I compare the extant species of the deep photic zone to the Miocene *Minylitha convallis* and find parallels that imply similar habitats (depth and stratification).

Acknowledgements

First and foremost I must thank my husband, Alessandro, for his unconditional support through the hardest times of this Ph.D. In the final months, when I could not even determine what I wanted to eat, you gave me the perspective to struggle onwards. You are my rock –and that's something, coming from a geologist! I could not have done this without you.

My advisor, Dr. Marie-Pierre Aubry: thank you for all you have taught me in the realm of taxonomy, morphology, microscopy, scientific writing, and scientific observation.

I have consistently enjoyed the sharing of ideas with my external committee member, Dr. Maria Triantaphyllou. Your hospitality during my stay at the University of Athens for collaborative research made an already intellectually stimulating trip invaluable and unforgettable. I thank you for discussing with me your perspective and extraordinary breadth of knowledge.

Thank you to my committee member, Dr. Jim Wright, for encouraging the expansion of the dissertation and for emotional and intellectual support through my M.Sc. and Ph.D. work.

Thank you to my committee member and department chair, Dr. Ken Miller, for also widening the scope of the dissertation in vital ways.

Many thanks to Valentin Starovoytov (Rutgers University) and Dr. Christopher Daniel (Bucknell University) for technical assistance on their S.E.M.s. I especially appreciate the enthusiasm of Chris, Cindy Liutkus, and the Bucknell Geology Department in welcoming me to their department. It was a unique and special opportunity to work on such an exceptional S.E.M. with such good company.

My apologies to my family for my stress level, thank you for still loving me through the process. I am so proud that both Mummy and I will become doctors at the same time. Good luck Samuel in the years to come, Rachel in the last year, and Daddy in weathering all of us!!

Amira, Shai, and Sapo have been mainstays of my writing process, keeping my life in perspective by sleeping all day and occasionally honing my skills as a mouser in the late hours of the day.

Finally I thank the staff, faculty, graduate students, and post-docs of the Department of Geological Sciences and the Institute of Marine and Coastal Sciences at Rutgers University, who have stimulated me, interested me, decompressed me, and provided mutual accompaniment throughout my and their time at Rutgers.

A toast to Dr. Jane, Vanessa, Esquire, and the upcoming Dr. Jess. We did it.

This dissertation work was funded by the Department of Geological Sciences at Rutgers University, NJ, and additionally funded by NSF Grant 0415351 (Dr. Colomban de Vargas), the John Mason Clark 1877 Fellowship in Paleontology and Geology from Amherst College (AK), the Chevron Academic Scholarship (AK), and the Rutgers University Graduate School Special Study Pre-Dissertation Award (AK).

…and now, I live in appreciation of micro/nannoplankton in general, and coccolithophores in particular, that is enriching both scientifically and artistically.

Table of Contents

Chapter 3: Intraspecific variability in the deep photic zone coccolithophorids of the Indian Ocean

List of Tables

List of Figures

Chapter 3

List of Plates

Introduction

m. Sample VANC10MV18A. *Coronosphaera binodata.* (Kamptner 1927) Gaarder in Gaarder and Heimdal 1977

n. Sample VANC10MV03B. *Discophaera tubifera* (Murray and Blackman 1898) Ostenfeld 1900).

o. Sample VANC10MV03B. *Emiliania huxleyi* (Lohmann 1902) Hay and Mohler in Hay et al. 1967.

p. Sample VANC10MV07D. *Florisphaera profunda* Okada and Honjo 1973.

q. Sample VANC10MV07D. *Gephyrocapsa muellerae* Bréhéret 1978.

r. Sample VANC10MV07D. *Gladiolithus flabellatus* (Halldall and Markali 1955) Jordan and Chamberlain 1993.

Plate 2: 30

a. Sample VANC10MV07D. *Gladiolithus striatus* Hagino and Okada 1998.

b. Sample VANC10MV05B. *Helicosphaera pavimentum* Okada and McIntyre 1977.

c. Sample VANC10MV24D. *Helicosphaera wallichii* (Lohmann 1902) Okada and McIntyre 1977.

d. Sample VANC10MV14A. *Homozygosphaera triarcha* Halldal and Markali 1955.

e. Sample VANC10MV26A. *Michaelsaria adriaticus* (Schiller 1914) Manton et al. 1984.

f. Sample VANC10MV03B. *Michaelsaria elegans* Gran 1912 emend. Manton et al. 1984.

g. Sample VANC10MV03B. *Michaelsaria elegans* Gran 1912 emend. Manton et al. 1984.

h. Sample VANC10MV07D. *Oolithotus fragilis* (Lohmann 1912) Martini and Müller 1972.

i. Sample VANC10MV07D. *Oolithotus antillarum* (Cohen 1964) Reinhardt in Cohen and Reinhardt 1968.

j. Sample VANC10MV07D. *Ophiaster formosus* Gran 1912 emend. Manton and Oates 1983.

k. Sample VANC10MV26A. *Palusphaera vandelii* Lecal 1965 emend. Norris 1984.

l. Sample VANC10MV07D. *Papposphaera* sp. type 4 Cros and Fortuño 2002.

m. Sample VANC10MV05B. *Pontosphaera* sp. Lohmann 1902.

n. Sample VANC10MV05B. *Rhabdosphaera clavigera* Murray and Blackman 1898.

o. Sample VANC10MV05B. *Rhabdosphaera stylifera* Lohmann 1902.

p. Sample VANC10MV26A. *Syracosphaera delicata* Cros et al. 2000.

q. Sample VANC10MV03B. *Syracosphaera ossa* (Lecal 1966) Loeblich and Tappan 1968

r. Sample VANC10MV05B. *Syracosphaera pulchra* Lohmann 1902.

Plate 3: 31

a. Sample VANC10MV03B. *Syracosphaera pulchra* HOL *oblonga* type = (*Calyptrosphaera oblonga* Lohmann 1902).

b. Sample VANC10MV07D. *Turrilithus latericidoides* Jordan et al. 1991.

c. Sample VANC10MV24B. *Umbellosphaera irregularis* Paasche in Markali and Paasche 1955.

d. Sample VANC10MV07D. *Umbellosphaera tenuis* (Kamptner 1937) Paasche in Markali and Paasche 1955.

Introduction to the dissertation

1- Background

Coccolithophorids are marine protists, living in the photic zone across the world's oceans. Along with diatoms and dinoflagellates, they comprise the primary eukaryotic phytoplankton in modern oceans. They are used as biostratigraphic markers, as well as indicators of paleoclimate, water column dynamics, and oceanic nutrient concentrations. Their preservable calcite coccoliths (Fig. 1) are found in sediments from the Upper Triassic to the Holocene (Bown 2004). Because few intact coccospheres (Fig. 1) are found in the fossil record, morphologic analysis is mostly restricted to individual coccoliths; however, analysis of extant coccospheres permits co-examination of coccospheres and their constituent coccoliths. Measurements of coccoliths in place on the coccosphere are effective indicators of intraspecific variability, as the relation between the size of the coccosphere and the relative number and size of its coccoliths is comparable. Additionally, such comparative work may help to elucidate the function of both coccospheres and coccoliths, which is as yet unconfirmed (Young 2004).
Extant coccolithophore communities with dominant species allow for quantification of species size from large numbers of coccospheres, thus expanding the database for modern intraspecific variability. The number of measurements in Chapters 1 and 3 of this dissertation is significantly higher than those published and increases the known size variability of coccoliths and coccospheres in the extant (Chapter 1: Tables 4-7, 9; Chapter 3: Tables 2-5). Recent morphological studies in the extant coccolithophores have investigated size range as an indicator of speciation or seasonal change (e.g., Renaud and Klaas 2001; Renaud et al. 2002), and also show the distribution and known size range of

observed species (e.g., Reid 1980; Cros and Fortuño 2002; Young et al. 2003). All new species are defined by the size as well as structure of their coccospheres and coccoliths (e.g., Quinn et al. 2005; Bollmann et al. 2006).

Norris (1984) reviewed extant species within the family Rhabdosphaeraceae in the Indian Ocean. He discussed the particular morphological features of the coccoliths that designate genera within that family, and clarifies the nomenclature. In particular, Norris (1984) provided a key for the monomorphic and dimorphic coccospheres within the family Rhabdosphaeraceae, tying genera to their distinct coccolith structures (for example: monomorphic coccospheres with styliform coccoliths are designated within the genus *Palusphaera*). He discussed those genera with monomorphic coccospheres: *Discosphaera, Palusphaera, Anacanthoica*; and those with dimorphic coccospheres: *Acanthoica, Rhabdosphaera, Algirosphaera*.

Hagino and Okada (2006), Hagino et al. (2005), and Parente et al. (2004) discussed geographical constraint on coccolithophore communities and coccosphere morphology. Hagino and Okada (2006) noted that environmental parameters (nutrient concentrations and temperature) as well as morphological differences in the equatorial and subequatorial Pacific Ocean contrast the morphotypes within *Emiliania huxleyi, Calcidiscus leptoporus, Umbilicosphaera foliosa, U. sibogae,* and *Umbellosphaera tenuis*. Hagino et al. (2005) showed that morphotypes of *E. huxleyi* can be used to recognize particular water masses off the coast of Japan, and that larger specimens are useful in paleoenvironmental reconstruction. In addition, they split *Braarudosphaera bigelowii* into 2 size groupings (<2.5 µm and >4.0 µm) (Hagino et al. 2005). Parente et al. (2004) showed that size differences in the modern *Coccolithus pelagicus* offshore Portugal is

related to latitude, and as such can be used in paleoceanographic interpretation (i.e., *C. pelagicus pelagicus* (smallest) indicates subpolar North Atlantic watermass, *C. pelagicus azorinus* (largest) indicates watermasses from the Azores front).

Numerous publications have documented the splitting of species into distinct size groupings, sometimes corroborated by molecular genetics. Distinction between morphotypes of *Calcidiscus* was determined initially by morphology (Knappertsbusch et al. 1997; Geisen et al. 2002; Renaud et al. 2002; Ziveri et al. 2004), and secondarily confirmed by molecular genetics (Saéz et al. 2003). Renaud et al. (2002), in particular, analyzed modern communities in the northeast/west Atlantic and the Arabian Sea, finding that *C. leptoporus* morphotypes vary seasonally; relative abundances changing with differing nutrient concentrations and/or temperature, both seasonally and latitudinally.

Two communities are observed in the extant coccolithophores, defined by their shallow or deep position within the photic zone (Okada and Honjo 1973). The shallow photic zone species number ~250 (Young et al. 2003) with community composition varying geographically and seasonally (McIntyre and Bé 1967; Okada and McIntyre 1979; Winter et al. 1994). By contrast, the deep photic zone coccolithophore community is of extremely low diversity, comprising <12 species ranging from temperate to tropical latitudes (Okada and Honjo 1973; Baumann et al. 2005). Thus, analysis of morphologic variability in the shallow photic zone coccolithophores must necessarily include a representative number of species within multiple geographically-constrained communities. Due to the small number of species within the deep photic zone

community and their cosmopolitanism, such a broad geographic study may not be necessary.

Several studies have been done in the northern Indian Ocean. Kleijne (1993; 1992) has comprehensively described the distribution of northern Indian Ocean extant coccolithophore genera within the families Coccolithaceae, Umbellosphaeraceae, and Rhabdosphaeraceae. She discusses size variability in the genus *Umbellosphaera*, morphological variation in *Calcidiscus leptoporus* f. *leptoporus*, *Neosphaera coccolithomorpha* and *Umbellosphaera tenuis*, and introduces several new species and morphotypes (Kleijne 1993). She also describes the oceanographic preferences of abundantly occurring species (*D. tubifera, P. vandelii, R. clavigera, A. robusta*) within the family Rhabdosphaeraceae and describes the structure and morphology of their coccospheres and coccoliths (Kleijne 1992).

Andruleit et al. (2003), Friedinger and Winter (1987), and Kleijne (1992, 1993) document extant calcareous nannoplankton in the Indian Ocean from the northern Arabian Sea to the southwestern Indian Ocean. Andruleit et al. (2003) detail the deep photic zone coccolithophores, *F. profunda* and *A. robusta*, and their preferred depth habitat in the northern Arabian Sea. They show that the above taxa live below the thermocline, whether in the shallow or deep photic zone, though they are most abundant when the thermocline is deeper.

In their southwestern Indian Ocean samples, Friedinger and Winter (1987) generally found high abundance (and low diversity) in the samples proximal to the shoreline. They also noted seasonal differences and instability in surface currents strongly effecting the composition of coccolithophore communities.

Kleijne (1992, 1993) shows the range of extant surface water species in the Indian and Atlantic Oceans, the Red and Mediterranean Seas. She provides detailed description of their morphologies and species designations.

Quaternary coccolithophores in the deep photic zone proximal to the Maldives Ridge in the Indian Ocean indicate that downcore abundance changes of *F. profunda, G. flabellatus,* and *A. robusta* assemblages can be used as a proxy for glacial/interglacial cycles (Okada and Matsuoka 1996). Andruleit et al. (2000) analyzed sediment traps in the northeastern Arabian Sea and demonstrate temperature preferences and seasonal fluxes in the extant coccolithophores. Andruleit and Rogalla (2002) identified 3 coccolithophore assemblages in surface sediments of the Arabian Sea. By comparing mean annual nutrient, salinity, temperature, and chlorophyll gradients, they established the significance of certain fossil assemblages in establishing ocean nutrient conditions and proximity to coast or open ocean.

Most coccolithophore genera are depth-stratified and exclusively inhabit their preferred depth (Okada and Honjo 1973). The testable hypothesis providing the basis for this dissertation is that depth-specific coccolithophores (coccospheres and coccoliths) have distinct morphologies that differentiate those in the shallow from those in the deep photic zone. If valid, depth habitat and therefore paleo-ocean conditions can be reconstructed in the fossil record based on coccolith morphology. The deep photic zone is a more stable environment than the shallow photic zone, which interacts with the atmosphere; therefore, I expect to see less intraspecific variability in the coccospheres and coccoliths of the deep photic zone, where low species variability is observed relative to the more

diverse shallow photic zone. The instability of the shallow photic zone forces diversification to a dynamic habitat, whereas the stability of the deep photic zone forces specialization to static conditions.

I present within this dissertation 4 chapters with detailed quantitative and qualitative analyses of morphologic characteristics of species within modern calcareous nannoplankton communities in the shallow and deep photic zones. The overall purpose of these integrated studies was to determine depth habits of coccolithophores species based on morphological differences. I quantify both the variability of coccoliths on their coccospheres and all measured coccoliths in a given species. By analyzing large numbers of coccospheres and coccoliths in these studies, I illustrate the large range of intra- and interspecific variability among modern coccolithophores. Measurements of the shallow photic zone species encompass 4 species within the family Rhabdosphaeraceae and therefore conclusions have limited applicability; whereas, those of the deep photic zone species include 10 of the 12 species within that community and thus I apply the analyses globally. Despite the somewhat narrow dataset, collected from several samples along a southern Indian Ocean transect, I have made comparisons to published morphologic data from more distally located ocean transects in order to increase the global range of the collective dataset.

Several authors (Parente et al. 2004; Hagino et al. 2005; Hagino and Okada 2006) have used coccosphere and coccolith intraspecific size variability to differentiate morphotypes and thus correlate water masses, temperature, and nutrient conditions. The data in this dissertation is unique due to its application to depth habitat reconstruction in the coccolithophores. By analyzing large numbers of coccospheres and coccoliths in the

shallow and deep photic zone I take the first step in creating a global dataset of intraspecific variability as related to depth. Upon further collection of this data, application to the fossil record will indicate paleoceanographic conditions (i.e., upwelling, nutrient concentrations, stratification of the photic zone).

The model of intraspecific size variability among species in the modern deep photic zone community was therefore applied to the Miocene species, *Minylitha convallis*, isolated from nannofossil assemblages. Such comparisons extrapolating paleo-habitats of coccolithophores are highly applicable to paleoceanographic reconstruction, as mentioned above. As shown with Neogene planktonic foraminifera in the Indian Ocean (Wright and Thunell 1988), coccolithophore assemblage composition ultimately may be useful in reconstruction of paleo-circulation in the surface ocean.

Below I present an overview to the coccolithophore communities and assemblages in the analyzed samples and their oceanographic setting. I will also briefly summarize the chapters of the dissertation contained herein.

2- Modern calibration

2.1 Oceanographic and sedimentary setting of the HV Melville Biological and Hydroacoustic Cruise

Filter samples analyzed in this dissertation were taken on an east to west transect across the southern Indian Ocean. The southern Indian Ocean is dominated by a strong subtropical gyre caused by the intersection of the Trade winds and the Westerlies, and is unaffected by seasonal monsoon cycles (Wyrtki 1973).

The western boundary is an anticyclonic subtropical gyre including the Agulhas, as well as the South Equatorial Current, and portions of the west wind drift north of the subtropical convergence. The Agulhas Current is sourced from the South Equatorial Current via south-flowing currents bifurcating to the east and west of Madagascar (Wyrtki 1973). Coccolithophore communities dominating the southwest Indian Ocean within the Agulhas Current and the Agulhas Return Current (Friedinger and Winter 1987) are very similar to those in the northern Indian Ocean (Kleijne et al. 1989).

The easternmost boundary is located proximal to the seasonally variable, shallow Leeuwin Current. Water movement along the western coast of Australia is weak, and no eastern boundary current exists. Seasonal nearshore shallow southern water movement occurs when the southerly wind is weaker from January to July (Wyrtki 1973), during which period the samples were taken (May through June) (Table 1). Along the western Australian coast, warm, low salinity waters are correlated with the Indonesian Throughflow, the South Java Current, and the Leeuwin Current, and have associated low calcareous nannoplankton cell density (Takahashi & Okada 2000).

Neogene surface sediments underlying the Indian Ocean have been examined from Ninety East and Broken Ridges (ODP Leg 121) located in the central part of the Indian Ocean (at the middle of the HV Melville transect), and the Wombat and Exmouth Plateaus off the coast of northwest Australia (ODP Legs 122 and 123) (Peterson et al. 1992). Carbonate accumulation across the Indian Ocean is generally high in the Neogene, with primarily nannofossil ooze dominating on the Broken Ridge (Peterson et al. 1992). The Ninety East Ridge also consists of almost pure carbonate oozes, with some terrigenous input after approximately 8 Ma (Peterson et al. 1992). Cenozoic

sections of ODP Legs 122 and 123 are relatively thin but are comprised of well-preserved foraminiferal- and nannofossil-rich oozes and chalks, with overall carbonate accumulation increasing at ~7-8 Ma (Peterson et al. 1992).

2.2- Coccolithophore communities along the HV Melville transect

The purpose of this study was to identify relatively monospecific calcareous nannoplankton communities from filtered seawater samples for morphologic analysis and collaborative molecular genetic research. During the course of morphologic analysis it became clear that the samples yielded information relevant to a broad scope of subjects (biological, micropaleontological, oceanographic). Diverse coccolithophore communities with generally narrow depth distributions were observed; here I show species photographed across the transect (Pls. 1, 2, 3; see Table 1 for species distribution).

The samples from the HV Melville Biological and Hydroacoustic Cruise transect through the southern Indian Ocean (Fig. 2a) were taken at varying times during the day and night (Table 1) from 0 to ~200m depth. No data were collected for water column nutrient concentrations. Six samples along the transect consisted of frequent to abundant coccospheres and coccoliths (Fig. 3, Table 1). Thirty-five of the 52 samples contained sparse coccospheres and/or coccoliths. Notable among the 52 samples were 11 samples barren of coccolithospheres and coccoliths, and 2 more that were so sparse as to be virtually barren. Many samples, including those that were barren of coccospheres/coccoliths, contained small centric and pennate diatoms, dinoflagellates, silicoflagellates, and chrysophyte cysts. Of particular note along the transect were 2 samples with exceptionally high percentages of species of the family Rhabdosphaeraceae

and another sample with a particularly rich typical deep photic zone community, including 10 morphotypes of *Florisphaera profunda* Okada and Honjo 1973 and 2 unusual new species of the genus *Solisphaera* Bollmann et al. 2006 emend Kahn and Aubry Chapter 2 of this dissertation.

Triantaphyllou et al. (2004) noted a change in community composition dependent on time of day of sampling. That the sampling for this study was done at an inopportune time could explain the high number of barren and sparse samples; however, we see little correlation between time of day and abundance in a sample, although we do see some higher coccolithosphere abundances in the samples in the lower photic zone in the samples taken in the morning (Table 1). We also observe no apparent connection between salinity, temperature, time of day, depth, and coccosphere abundance (Fig. 3). The samples with the most consistently abundant coccospheres and coccoliths were on the eastern side of the transect (especially those samples below 35 m depth). The deep photic zone on the western side was also abundant in coccospheres and coccoliths, though not as consistently as the eastern side. Instead of inhabiting the more oligotrophic open ocean in the middle of the southern Indian gyre, the coccolithophores appear to have preferred the coastal areas along this particular transect (Fig. 2a).

Most species fit into the depth-stratified habitats as described by Reid (1980) and by Okada and Honjo (1973), though *Emiliania huxleyi* ranged from shallow to deep across the transect with little apparent environmental constraint. Several other species ranged in depth, found both in the surface waters and the deeper photic zone, although they were generally less abundant at those depths where they are not characteristic. Those species with a wide depth range are listed here: *Calcidiscus leptoporus, Calciosolenia*

brasilensis, Discosphaera tubifera, Emiliania huxleyi, F. profunda, Gephyrocapsa spp., *Oolithotus antillarum, O. fragilis, Palusphaera vandelii, Rhabdosphaera clavigera, R. stylifera, Syracosphaera* spp., *Umbellosphaera tenuis, U. tenuis, Umbilicosphaera anulus, U. sibogae.*

3- Miocene calibration: ODP Leg 138, Site 846

3.1- Miocene paleoceanography

Calcareous nannoplankton assemblages diversified and expanded globally in the middle Miocene to the late Miocene diversity maximum. This increase in diversity following a period of decline during the late Eocene and Oligocene implies an expansion of warm oligotrophic marine surface waters (Bown et al. 2004). Oxygen isotope data from planktonic foraminifera indicates a stabilization of surface waters (or possible warming) in the low latitudes and rapid cooling in the high latitudes (Savin et al. 1985).

3.2- Miocene phytoplankton assemblages

The samples taken from Leg 138, Site 846 (Fig. 2b) contained coccoliths of *Minylitha convallis* in highly variable concentrations, from barren to dominant (Table 2). Nannoliths of the species *Discoaster*, such as *D. mirabilis*, were abundant in most samples, as were species of the genus *Sphenolithus*. Helicoliths and placoliths of the genera *Helicosphaera* and *Coccolithus*, respectively, were often frequent. Silicoflagellates and diatoms (dominantly pennate, but also round) were abundant in all samples, and occasionally dominated the assemblages. The lack of diversity among the coccolithophore species, as well as the particular genera that were evident in the samples,

points to a high degree of coccolith dissolution. The genera *Minylitha*, *Discoaster*, and *Spenolithus* are all very dissolution resistant, so that their dominance in these samples may not be due to particular paleo-abundance, but merely dissolution of all other constituent species.

4- Summary of the dissertation chapters

4.1- Intraspecific morphotypic variability in the family Rhabdosphaeraceae

Coccospheres of species within the family Rhabdosphaeraceae rarely dominate modern coccolithophore communities. Therefore, the finding of 2 upper photic zone coccolithophore communities along the HV Melville southern Indian Ocean transect dominated by species of the family Rhabdosphaeraceae represents a unique opportunity to analyze large numbers of these coccospheres in addition to begin to characterize the global shallow photic zone coccolithophore community.

4.2- An unusual community of coccolithophores in the deep photic zone

Detailed taxonomic and morphologic description of 2 highly unusual deep photic zone coccolithophores with discussion of their generic and family placement.

4.3- Intraspecific variability in the deep photic zone coccolithophorids of the Indian Ocean

Quantitative and qualitative discussion of an unusually rich deep photic zone community found in the southern Indian Ocean. This community, recognized as specific to the deep photic zone throughout the global oceans (Okada and Honjo 1973), is shown to be

characterized by low inter- and intraspecific morphologic variability both in coccolith and coccosphere morphology.

4.4- Size variability in *Minylitha convallis* (Bukry 1973) emend. Theodoris 1984: implications for paleodepth reconstruction

Analysis of the size of the coccoliths of *M. convallis* and comparison of the variability to that of the coccoliths of species in the deep photic zone. The lack of relative size variability within *M. convallis* assemblages is consistent with the homogeneity we see both in the size of the coccoliths of *F. profunda sensu lato* and other deep photic zone coccolithophores analyzed in chapters 2 and 3. This may suggest that it may have lived in the deep photic zone, implying that high relative abundance of *M. convallis* indicates a deepened nutricline in a well-stratified paleo-water column, as has been shown for high relative abundance of *F. profunda* (Molfino and McIntyre 1990).

References

ANDRULEIT, H., Rogalla, U., 2002. Coccolithophores in surface sediments of the Arabian Sea in relation to environmental gradients in surface waters. Marine Geology, 186: 505-526.

ANDRULEIT, H., Stäger, S., Rogalla, U., Cepek, P., 2003. Living coccolithophores in the northern Arabian Sea: ecological tolerances and environmental control. Marine Micropaleontology, 49:157-181.

ANDRULEIT, H.A., von Rad, U., Bruns, A., Ittekkot, V., 2000. Coccolithophore fluxes from sediment traps in the northeastern Arabian Sea off Pakistan. Marine Micropaleontology, 38: 285-308.

BAUMANN, K.-H., Andruleit, H., Böckel, B., Geisen, M., Kinkel, H., 2005. The significance of extant coccolithophores as indicators of ocean water masses, surface water temperature, and paleoproductivity. Paläontologische Zeitschrift, 79(1): 93-112.

BOLLMANN, J., Cortés, M.Y., Kleijne, A., Østergaard, J., Young, J., 2006. Solisphaera gen. nov. (Prymnesiophyceae), a new coccolithophore genus from the lower photic zone. Phycologia, 45(4): 465-477.

BOWN, P.R., Lees, J.A., Young, J.R., 2004. Calcareous nannoplankton evolution and diversity through time. In: Thierstein, H.R., Young, J.R., Eds., *Coccolithophores: from molecular processes to global impact*. Berlin, Springer-Verlag: 481-508.

CROS, L., Fortuño, J., 2002. Atlas of northwestern Mediterranean coccolithophores. Scientia Marina, 66(1): 7-182.
CROS, L., Kleijne, A., Zeltner, A., Billar, C., Young, J.R., 2000. New examples of holococcolith-heterococcolith combination coccospheres and their implications for coccolithophorid biology. Marine Micropaleontology, 39: 1-34.
FRIEDINGER, P.J., Winter, A., 1987. Distribution of modern coccolithophore assemblages in the southwest Indian Ocean off southern Africa. Journal of Micropaleontology, 6(1): 49-56.
GEISEN, M., Billard, C., Broerse, A., Cros, L., Probert, I., Young, J.R., 2002. Life-cycle associations involving pairs of holococcolithophorid species: intraspecific variation or cryptic speciation? European Journal of Phycology, 37: 531-550.
HAGINO, K., Okada, H., 2006. Intra- and infra-specific morphological variation in selected coccolithophore species in the equatorial and subequatorial Pacific Ocean. Marine Micropaleontology, 58: 184-206.
HAGINO, K., Okada, H., Matsuoka, H., 2005. Coccolithophore assemblages and morphotypes of Emiliania huxleyi in the boundary zone between the cold Oyashio and warm Kuroshio currents off the coast of Japan. Marine Micropaleontology, 55: 19-47.
IGLESIAS-RODRÍGUEZ, M.D., Brown, C., Doney, S.C., Kleypas, J., Kolber, D., Kolber, Z., Hayes, P.K., Falkowski, P.G., 2002. Representing key phytoplankton functional groups in ocean carbon cycle models: coccolithophorids. Global Biogeochemical Cycles, 16(4): 1-19.
KLEIJNE, A., 1993. Morphology, taxonomy and distribution of extant coccolithophorids (calcareous nannoplankton). Drukkerij FEBO B.V., Katwijk.
KLEIJNE, A., 1992. Extant Rhabdosphaeraceae (coccolithophorids, class Prymnesiophyceae) from the Indian Ocean, Red Sea, Mediterranean Sea and North Atlantic Ocean. *Scripta Geologia*, 100:105-167.
KLEIJNE, A., Kroon, D., Zevenboom, W., 1989. Phytoplankton and foraminiferal frequencies in northern Indian Ocean and Red Sea surface waters. Netherland Journal of Sea Research, 24(4): 531-539.
KNAPPERTSBUSCH, M., 1993. Geographic distribution of living and Holocene coccolithophorids in the Mediterranean Sea. Marine Micropaleontology, 21: 219-247.
KNAPPERTSBUSCH, M., Cortés, M.Y., Thierstein, H.R., 1997. Morphologic variability of the coccolithophorid *Calcidiscus leptoporus* in the plankton, surface sediments and from the Early Pleistocene. Marine Micropaleontology, 30: 293-317.
MCINTYRE, A., Bé, A.W.H., 1967. Modern coccolithophores of the Atlantic Ocean – I. Placoliths and cyrtoliths. Deep-Sea Research, 14: 561-597.
MOLFINO, B., McIntyre, A., 1990. Precessional forcing of nutricline dynamics in the equatorial Atlantic. Science, 249: 766-769.
OKADA, H., Honjo, S., 1973. The distribution of oceanic coccolithophorids in the Pacific. Deep Sea Research, 20: 355-374.
OKADA, H., McIntyre, A., 1979. Seasonal distribution of modern coccolithophores in the western North Atlantic Ocean. Marine Biology, 54: 319-328.
OKADA, H., Matsuoka, M., 1996. Lower-photic nannoflora as an indicator of the late Quaternary monsoonal palaeo-record in the tropical Indian Ocean. In: Moguilevsky, A., Whatley, R., Eds., *Proceedings of the ODP and the Marine Biosphere International Conference*. Aberystwyth, ODP: 231-245.

PARENTE, A., Cachão, M., Baumann, K.-H., de Abreu, L., Ferreira, J., 2004. Morphometry of *Coccolithus pelagicus s.l.* (Coccolithophore, Haptophyta) from offshore Portugal, during the last 200 kyr. Marine Micropaleontology, 50(1):107-120.
PETERSON, L.C., Murray, D.W., Ehrmann, W.U., Hempel, P., 1992. Cenozoic carbonate accumulation and compensation depth changes in the Indian Ocean. In: Duncan, R.A., Rea, D.K., Kidd, R.B., von Rad, U., Weissel, J.K., Eds., *Synthesis of results from scientific drilling in the Indian Ocean*. Washington, D.C., American Geophysical Union: 311-333.
QUINN, P.S., Cortés, M.Y., Bollmann, J., 2005. Morphological variation in the deep dwelling coccolithophore *Florisphaera profunda* (Haptophyta). European Journal of Phycology, 40(1): 123-133.
REID, F., 1980. Coccolithophorids of the North Pacific Central Gyre with notes on their vertical and seasonal distribution. Micropaleontology, 26: 151-176.
RENAUD, S., Klaas, C., 2001. Seasonal variations in the morphology of the coccolithophore *Calcidiscus leptoporus* off Bermuda (N. Atlantic). Journal of Plankton Research, 23(8): 779-795.
RENAUD, S., Ziveri, P., Broerse, A.T.C., 2002. Seasonal differences in morphology and dynamics of the coccolithophore *Calcidiscus leptoporus*. Marine Micropaleontology, 46: 363-385.
SAÉZ, A.G., Probert, I., Geisen, M., Quinn, P., Young, J.R., Medlin, L.K., 2003. Pseudo-cryptic speciation in coccolithophores. Proceedings of the National Academy of Sciences, U.S.A., 100(12): 7163-7168.
SAVIN, S.M., Abel, L., Barrera, E., Hodell, D., Keller, G., Kennett, J.P., Killingley, J., Murphy, M., Vincent, E., 1985. The evolution of Miocene surface and near-surface marine temperatures: ocean isotopic evidence. In: Kennett, J.P., Ed., *The Miocene Ocean: paleoceanography and biogeography*. Geological Society of America Memoir 163: 49-82.
TAKAHASHI, K., Okada, H., 2000. Environmental control on the biogeography of modern coccolithophores in the southeastern Indian Ocean offshore of Western Australia. Marine Micropaleontology, 39(1): 73-86.
TRIANTAPHYLLOU, M., Aubry, M.-P., Dimiza, M., Gialouri, D., Dermitzakis, M.D., 2004. Implications of coccolithophore vertical movement during a day-round sampling (Poster Abstract). Journal of Nannoplankton Research, 26(2): 105.
WINTER, A., Jordan, R.W., Roth, P.H., 1994. Biogeography of living coccolithophores in oceanic waters. In: Winter, A., Seisser, W.G., Eds., *Coccolithophores*. Cambridge, Cambridge University Press: 161-177.
WRIGHT, J.D., Thunell, R.C., 1988. Neogene planktonic foraminiferal biogeography and paleoceanography of the Indian Ocean. Micropaleontology, 34(3): 1988.
WYRTKI, K., 1973. Physical oceanography of the Indian Ocean. In: Zeitzschel, B., Ed., *The Biology of the Indian Ocean*. Berlin, Springer-Verlag: 18-36.
YOUNG, J.R., Henriksen, K., Probert, I., 2004. Structure and morphogenesis of the coccoliths of the CODENET species. In: Thierstein, H.R., Young, J.R., Eds., *Coccolithophores: from molecular processes to global impact*. Berlin, Springer-Verlag: 191-216.
YOUNG, J.R., Geisen, M., Cros, L., Kleijne, A., Sprengel, C., Probert, I., Østergaard, J., 2003. A guide to extant coccolithophore taxonomy. *Journal of Nannoplankton Research Special Issue* 1: 1-125.

ZIVERI, P., Baumann, K.-H., Böckel, B., Bollmann, J., Young, J.R., 2004. Biogeography of selected Holocene coccoliths in the Atlantic Ocean. In: Thierstein, H.R., Young, J.R., Eds., *Coccolithophores: from molecular processes to global impact*. Berlin, Springer-Verlag: 327-366.

Introduction

Table captions

Table 1: All samples observed at all sites along HV Melville Hydroacoustic and Biological Sampling Cruise transect in the southern Indian Ocean; data shown for salinity and temperature measurements per sample, time and date of sampling, and species of all coccolithophore per sample.

Table 2: Coccolith abundance (abundant, sparse, barren) of *Minylitha convallis* in all samples taken from ODP Site 846.

Introduction
Tables

Latitude	Longitude	Temperature at surface	Depth	Temperature (oC)	Salinity (‰)	Date	Time of sample start	VANC10MV	*quattrospina*	*robusta*	*gaudii*	*bimurata*	*leptoporus*	*brasiliensis*	sp.	*murrayi*	*divergens*	*cristatus*	*pelagicus*	*gracilis*	*binodata*	*tubifera*	*huxleyi*	*profunda*	spp.	*flabellatus*	*striatus*	*pavimentum*	*wallichii*	spp.	*triarcha*	*adriaticus*	*elegans*	spp.
								Sample name	*Acanthoica*	*Algirosphaera*	*Alisphaera*	*Alveosphaera*	*Calcidiscus*	*Calciosolenia*	*Calciosolenia*	*Calciosolenia*	*Calyptrolithina*	*Ceratolithus*	*Coccolithus*	*Corisphaera*	*Coronosphaera*	*Discosphaera*	*Emiliania*	*Florisphaera*	*Gephyrocapsa*	*Gladiolithus*	*Gladiolithus*	*Helicosphaera*	*Helicosphaera*	*Helicosphaera*	*Homozygosphaera*	*Michaelsaria*	*Michaelsaria*	*Michaelsaria*
-34.827	**32.037**	21.3	35	21.0	35.68	3-May-18	13:35	03B								A						A	A		A			P			P		
			76	21.0	35.68			03C						P								P	A		A						P		
			100	19.0	35.68			03D		P			P	P									A	A	A	P								
-34.361	**37.729**	20.9	7	21.0	35.75	3-May-19	0:12	05A														P	P		P								
			49	21.0	35.74			05B	P				P	P		A		P					A	P	R									R
			85	20.0	35.72			05C																										
			199	17.0	35.67			05E																										
-33.297	**45.365**	21.1	6	21.0	35.73	3-May-21	16:49	07A																										
			52	21.0	35.74			07B																										
			86	20.0	35.76			07C															A		P									
			120	18.0	35.67			07D		P		P	R		R			R				R	P	A	P	P	P					R	
			202	17.0	34.64			07E																										
-31.827	**52.611**	21.7	5	22.0	35.62	3-May-23	17:15	09A															P										
			46	22.0	35.62			09B																										
			74	20.0	35.69			09C															P	P										
			199	15.0	35.52			09E																										
-29.85	**59.844**	22	5	22.0	35.66	3-May-25	12:41	11A										P					P										
			49	22.0	35.70			11B															P											
			102	19.0	35.79			11C															P		P									
			201	15.0	35.60			11E														R												
-23.59	**69.015**	23.1	0			3-May-28	9:30	13A			P							P				P	P											
-22.086	**72.744**	24.1	0			3-May-29	6:05	14surf																										
			45	24.0	35.29			14A														P	P							P			P
			89	24.0	35.42			14B																										
			120	21.0	35.50			14C																										
			150	20.0	35.68			14D																										
			200	19.0	35.83			14E															P	P										
-19.747	**78.01**	25.8	0			3-May-30	18:56	16surf														P	P										
			40					16A										P				P												
			199	20.0	35.69			16E																										
-17.176	**83.676**	25	6	25.0	34.94	3-Jun-01	13:08	18A													P	P	R								P		
			50	25.0	35.04			18B	P	R					R							R	R											
			86	23.0	35.07			18C														P	P											
			200	17.0	35.35			18E																										
-13.963	**89.936**	27.5	5	27.0	34.24	3-Jun-05	1:59	20A														P											
			50	27.0	34.25			20B										R				R											
			100	23.0	34.76			20C								P							P											
			120	21.0	34.87			20D																P										
			201	15.5	34.62			20E		P				R								R	R	P	P	P								
-12.219	**96.787**	28.5	6	28.5	34.02	3-Jun-07	6:06	23A																										
			51	28.2	34.13			23B																										
			76	22.9	34.68			23C																										
-13.212	**104.66**	28	5	28.0	33.88	3-Jun-09	8:41	24A																										
			49	28.3	34.38			24B										P				P		P										
			84	23.8	34.64			24C																										
			121	20.9	34.74			24D		P					R							R	R	P	P	R			R					
			199	14.5	34.63			24E		R					R								R	R	R								R	
						3-Jun-11		26A	P					P			P		P			P	P		R						P	P		
								26B																										
								26C						P		P				P			P		P									
								26D						P									P	P	P									
								26E		P				P								P	P	P	P									

Table 1a.

Latitude	Longitude	Temperature at surface	Depth	Temperature (oC)	Salinity (%0)	Date	Time of sample start	VANC10MV	*fragilis*	*Oolithotus*	*antillarum*	*formosus*	*vandelii*	sp. Type 4	spp.	*Pleurocrysis* cf.	sp.	spp.	*clavigera*	*stylifera*	sp.	spp.	*delicata* cf.	*molischii*	*ossa*	*pulchra*	*pulchra* HOL.	*pulchra* type	*latericoides*	*irregularis*	*tenuis*	*anulus*	*hulburtiana*	*sibogae*	spp.	*sedis*
								Sample name	*Oolithotus*				*Palusphaera*	*Papposphaera*	*Pappomonas*		*Pontosphaera*	*Reticulofenestra*	*Rhabdosphaera*	*Rhabdosphaera*	*Rhabdosphaera*	*Solisphaera*	*Syracosphaera*	*Syracosphaera*	*Syracosphaera*	*Syracosphaera*	*Syracosphaera*	*Syracosphaera*	*Syracosphaera*	*Turrilithus*	*Umbellosphaera*	*Umbellosphaera*	*Umbilicosphaera*	*Umbilicosphaera*	*Umbilicosphaera*	*Umbilicosphaera*	*Incertae*
-34.827	**32.037**	21.3	35	21.0	35.68	3-May-18	13:35	03B		A		A								A	A				P	P			P	A	A	A		P	P
			76	21.0	35.68			03C											P										P	P	P			P		
			100	19.0	35.68			03D		P		P																	P	P	P			P		
-34.361	**37.729**	20.9	7	21.0	35.75	3-May-19	0:12	05A																						P	P					P
			49	21.0	35.74			05B	R										A							A		A			P	P			P		P
			85	20.0	35.72			05C																													
			199	17.0	35.67			05E																													
-33.297	**45.365**	21.1	6	21.0	35.73	3-May-21	16:49	07A																												
			52	21.0	35.74			07B																												
			86	20.0	35.76			07C					P																	A						
			120	18.0	35.67			07D		P	P	R		R		R		R			A		R				P	P	R	R	P		R		
			202	17.0	34.64			07E																												
-31.827	**52.611**	21.7	5	22.0	35.62	3-May-23	17:15	09A																						P						
			46	22.0	35.62			09B																												
			74	20.0	35.69			09C																						P						
			199	15.0	35.52			09E																												
-29.85	**59.844**	22	5	22.0	35.66	3-May-25	12:41	11A																						P						
			49	22.0	35.70			11B																												
			102	19.0	35.79			11C													P				P					P						
			201	15.0	35.60			11E																												
-23.59	**69.015**	23.1	0			3-May-28	9:30	13A					P						P										P		P	P				P
-22.086	**72.744**	24.1	0			3-May-29	6:05	14surf																												
			45	24.0	35.29			14A		P									P									P		P	P		P			
			89	24.0	35.42			14B																												
			120	21.0	35.50			14C																												
			150	20.0	35.68			14D																												
			200	19.0	35.83			14E		P																								P		
-19.747	**78.01**	25.8	0			3-May-30	18:56	16surf											P		P								P	P		P			
			40					16A					P						P									P		P	P		P			P
			199	20.0	35.69			16E																												
-17.176	**83.676**	25	6	25.0	34.94	3-Jun-01	13:08	18A											R									P		P			R		
			50	25.0	35.04			18B					P						P									P		P	R					
			86	23.0	35.07			18C					P			P									P					P	P				P	
			200	17.0	35.35			18E																												
-13.963	**89.936**	27.5	5	27.0	34.24	3-Jun-05	1:59	20A																						P	R					
			50	27.0	34.25			20B											R									R		R			R			
			100	23.0	34.76			20C	P									P						P		P			P						
			120	21.0	34.87			20D		P																										
			201	15.5	34.62			20E		P								P	P						R		R		R	R			R		
-12.219	**96.787**	28.5	6	28.5	34.02	3-Jun-07	6:06	23A																												
			51	28.2	34.13			23B																												
			76	22.9	34.68			23C																												
-13.212	**104.66**	28	5	28.0	33.88	3-Jun-09	8:41	24A																												
			49	28.3	34.38			24B										P			P							P		P						
			84	23.8	34.64			24C																												
			121	20.9	34.74			24D																				R								
			199	14.5	34.63			24E	R										R										R			R			
						3-Jun-11		26A					R								P	P		P			P		R	R						
								26B																												
								26C		P				P													P									P
								26D																												
								26E		P									P								P	P					P		

Table 1b.

Abundant	Sparse	Barren
846_29_2_0	846_29_1_0	846_29_1_40
846_29_2_40	846_29_3_0	846_29_1_80
846_29_3_100	846_29_3_60	846_29_2_100
846_29_3_140	846_29_4_40	846_29_4_80
846_29_4_0	846_29_4_120	
846_29_5_0	846_29_5_40	
846_29_5_60	846_30_1_140	
846_29_5_140		
846_29_6_40		
846_29_6_80		
846_29_6_120		
846_29_7_0		
846_29_7_40		
846_30_1_40		
846_30_1_100		
846_30_2_40		
846_30_2_80		
846_30_2_120		
846_30_3_40		
846_30_3_80		
846_30_3_100		
846_30_4_10		
846_30_4_90		
846_30_4_130		

Table 2.

Introduction

Figure captions

Figure 1: *Emiliania huxleyi* coccosphere to illustrate general coccolithophorid structure. Coccoliths (calcareous or aragonitic shields) surround a single cell to form a coccosphere. S.E.M. photomicrograph taken from polycarbonate filter sampled on the HV Melville Hydroacoustic & Biological Sampling Cruise May/June 2003 along a transect in the Indian Ocean at 115 meters depth.

Figure 2: Location maps

a. Map of transect and sample site locations of the HV Melville Hydroacoustic and Biological Sampling Cruise taken from May to June 2003 in the southern Indian Ocean.

b. Location map of ODP Leg 138, Site 846 in the equatorial Pacific Ocean.

Figure 3: Compilation of values for coccolithophore abundance, salinity, and temperature at all sites and sample depths along the HV Melville transect.

Infilled circle= coccolithophore abundance. Each sample is also labeled here according to depth (A, B, C, D, E).

Infilled triangle= salinity.

Infilled square= water temperature.

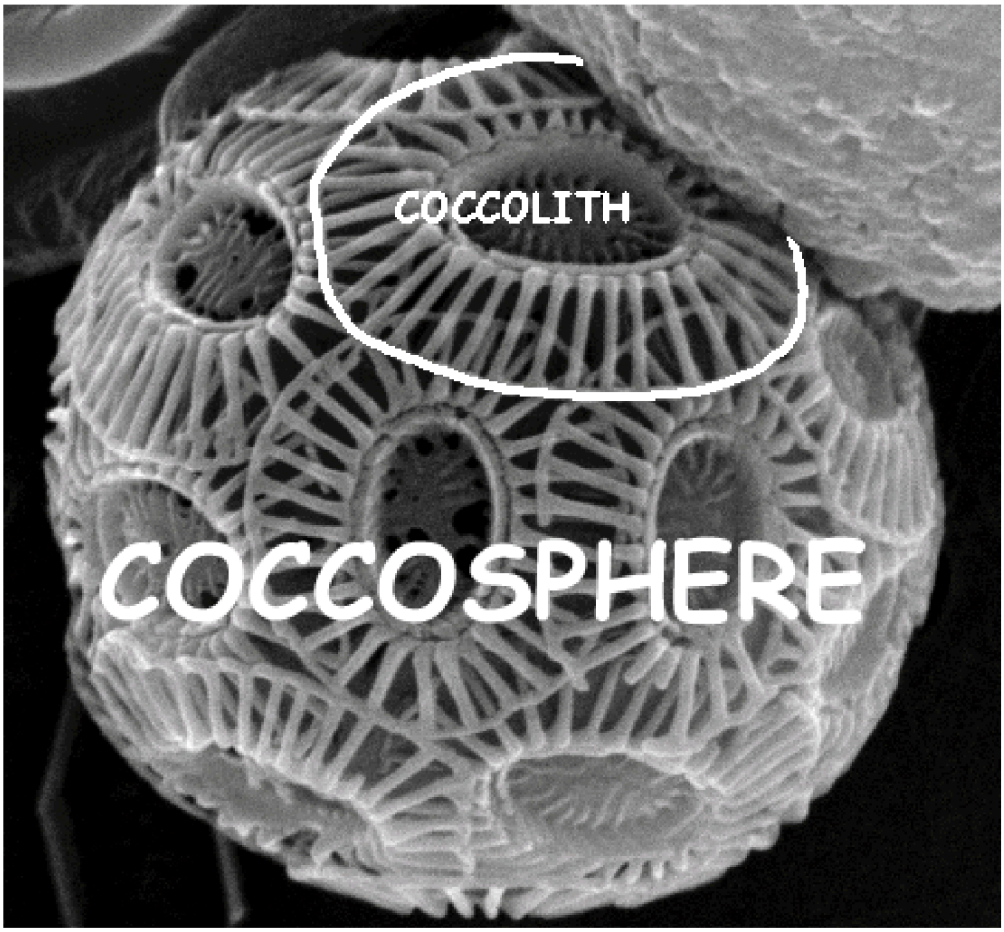

Figure 1

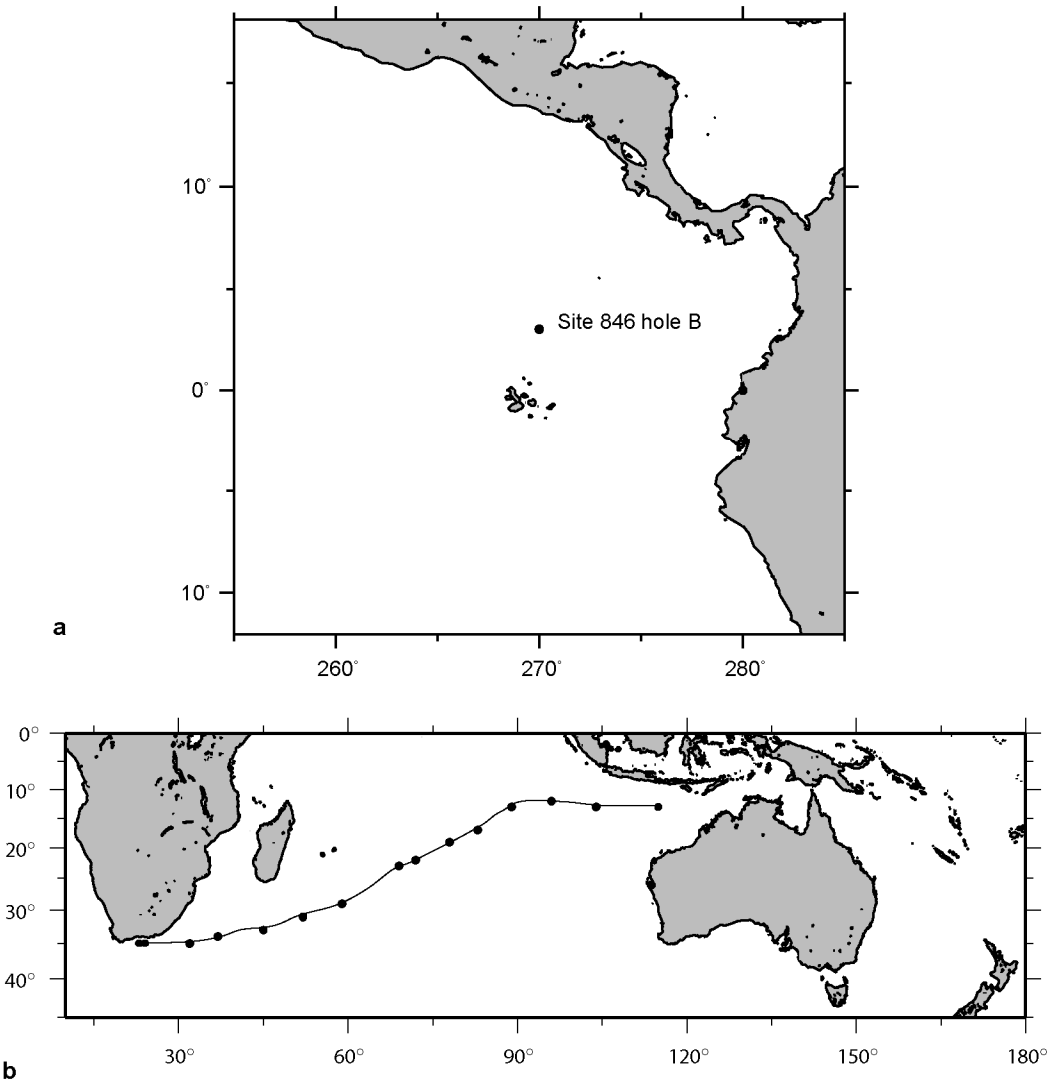

GMT 2006 Apr 27 16:59:44 R.Earley 2006

Figure 2

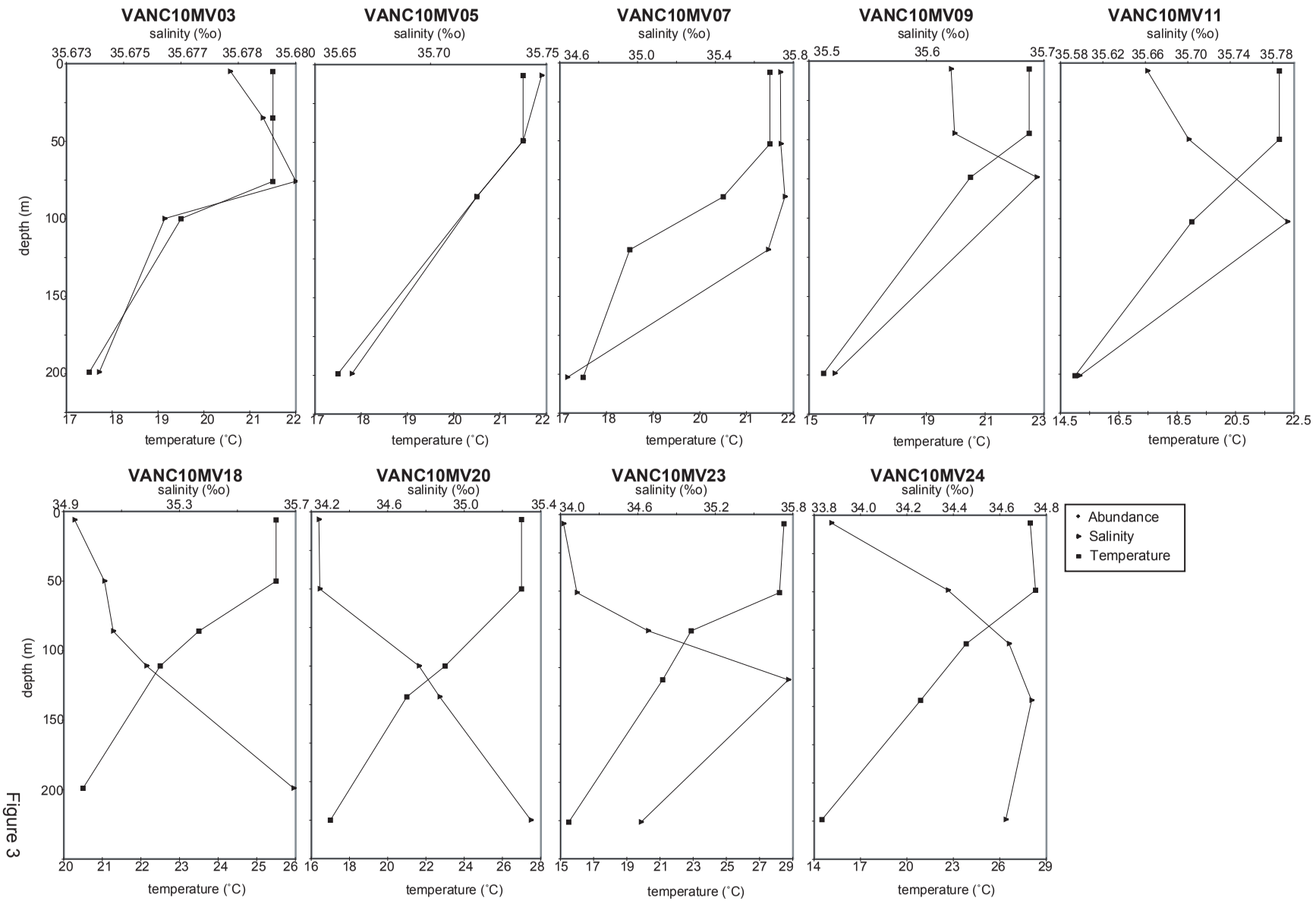
VANC10MV03
VANC10MV05
VANC10MV07
VANC10MV09
VANC10MV11
VANC10MV18
VANC10MV20
VANC10MV23
VANC10MV24
salinity (‰)
temperature (˚C)
depth (m)
Abundance
Salinity
Temperature

Figure 3

Introduction

Plate captions

Plate 1:

a. Sample VANC10MV05B. *Acanthoica quattrospina* Lohmann 1903.

b. Sample VANC10MV07D. *Algirosphaera robusta* (Lohmann 1902) Norris 1984.

c. Sample VANC10MV26A. *Alisphaera gaudii* Kleijne et al. 2002.

d. Sample VANC10MV07D. *Alveosphaera bimurata* (Okada and McIntyre 1977) Jordan and Young 1990.

e. Sample VANC10MV05B. *Calcidiscus leptoporus* (Murray and Blackman 1898) Loeblich and Tappan 1978.

f. Sample VANC10MV05B. *Calciosolenia brasiliensis* (Lohmann 1919) (Deflandre 1945) Young et al. 2003.

g. Sample VANC10MV05B. *Calciosolenia murrayi* Gran 1912.

h. Sample VANC10MV26A. *Calyptrolithina divergens* (Halldal and Markali 1955) Heimdal 1982.

i. Sample VANC10MV05B. *Ceratolithus cristatus* CER *cristatus* type. Kamptner 1950, see also Young et al. 1998 for description of type designations).

j. Sample VANC10MV07D. *Ceratolithus cristatus* CER *rostratus* type. Kamptner 1950, see also Young et al. 1998 for description of type designations).

k. Sample VANC10MV05B. *Ceratolithus* cristatus HET *nishidae* and hoops. Kamptner 1950, see also Young et al. 1998 for description of type designations).

l. Sample VANC10MV26E. *Corisphaera gracilis.* Kamptner 1937.

m. Sample VANC10MV18A. *Coronosphaera binodata.* (Kamptner 1927) Gaarder in Gaarder and Heimdal 1977

n. Sample VANC10MV03B. *Discophaera tubifera* (Murray and Blackman 1898) Ostenfeld 1900).

o. Sample VANC10MV03B. *Emiliania huxleyi* (Lohmann 1902) Hay and Mohler in Hay et al. 1967.

p. Sample VANC10MV07D. *Florisphaera profunda* Okada and Honjo 1973.

q. Sample VANC10MV07D. *Gephyrocapsa muellerae* Bréhéret 1978.

r. Sample VANC10MV07D. *Gladiolithus flabellatus* (Halldall and Markali 1955) Jordan and Chamberlain 1993.

Plate 2:

a. Sample VANC10MV07D. *Gladiolithus striatus* Hagino and Okada 1998.

b. Sample VANC10MV05B. *Helicosphaera pavimentum* Okada and McIntyre 1977.

c. Sample VANC10MV24D. *Helicosphaera wallichii* (Lohmann 1902) Okada and McIntyre 1977.

d. Sample VANC10MV14A. *Homozygosphaera triarcha* Halldal and Markali 1955.

e. Sample VANC10MV26A. *Michaelsaria adriaticus* (Schiller 1914) Manton et al. 1984.

f. Sample VANC10MV03B. *Michaelsaria elegans* Gran 1912 emend. Manton et al. 1984.

g. Sample VANC10MV03B. *Michaelsaria elegans* Gran 1912 emend. Manton et al. 1984.

h. Sample VANC10MV07D. *Oolithotus fragilis* (Lohmann 1912) Martini and Müller 1972.

i. Sample VANC10MV07D. *Oolithotus antillarum* (Cohen 1964) Reinhardt in Cohen and Reinhardt 1968.

j. Sample VANC10MV07D. *Ophiaster formosus* Gran 1912 emend. Manton and Oates 1983.

k. Sample VANC10MV26A. *Palusphaera vandelii* Lecal 1965 emend. Norris 1984.

l. Sample VANC10MV07D. *Papposphaera* sp. type 4 Cros and Fortuño 2002.

m. Sample VANC10MV05B. *Pontosphaera* sp. Lohmann 1902.

n. Sample VANC10MV05B. *Rhabdosphaera clavigera* Murray and Blackman 1898.

o. Sample VANC10MV05B. *Rhabdosphaera stylifera* Lohmann 1902.

p. Sample VANC10MV26A. *Syracosphaera delicata* Cros et al. 2000.

q. Sample VANC10MV03B. *Syracosphaera ossa* (Lecal 1966) Loeblich and Tappan 1968

r. Sample VANC10MV05B. *Syracosphaera pulchra* Lohmann 1902.

Plate 3:

a. Sample VANC10MV03B. *Syracosphaera pulchra* HOL *oblonga* type = (*Calyptrosphaera oblonga* Lohmann 1902).

b. Sample VANC10MV07D. *Turrilithus latericidoides* Jordan et al. 1991.

c. Sample VANC10MV24B. *Umbellosphaera irregularis* Paasche in Markali and Paasche 1955.

d. Sample VANC10MV07D. *Umbellosphaera tenuis* (Kamptner 1937) Paasche in Markali and Paasche 1955.

e. Sample VANC10MV07D. *Umbilicosphaera anulus* (Lecal 1967) Young and Geisen in Young et al. 2003.

f. Sample VANC10MV14A. *Umbilicosphaera hulburtiana* Gaarder 1970.

g. Sample VANC10MV05B. *Umbilicosphaera sibogae* (Weber-van Bosse 1901) Gaarder 1970.

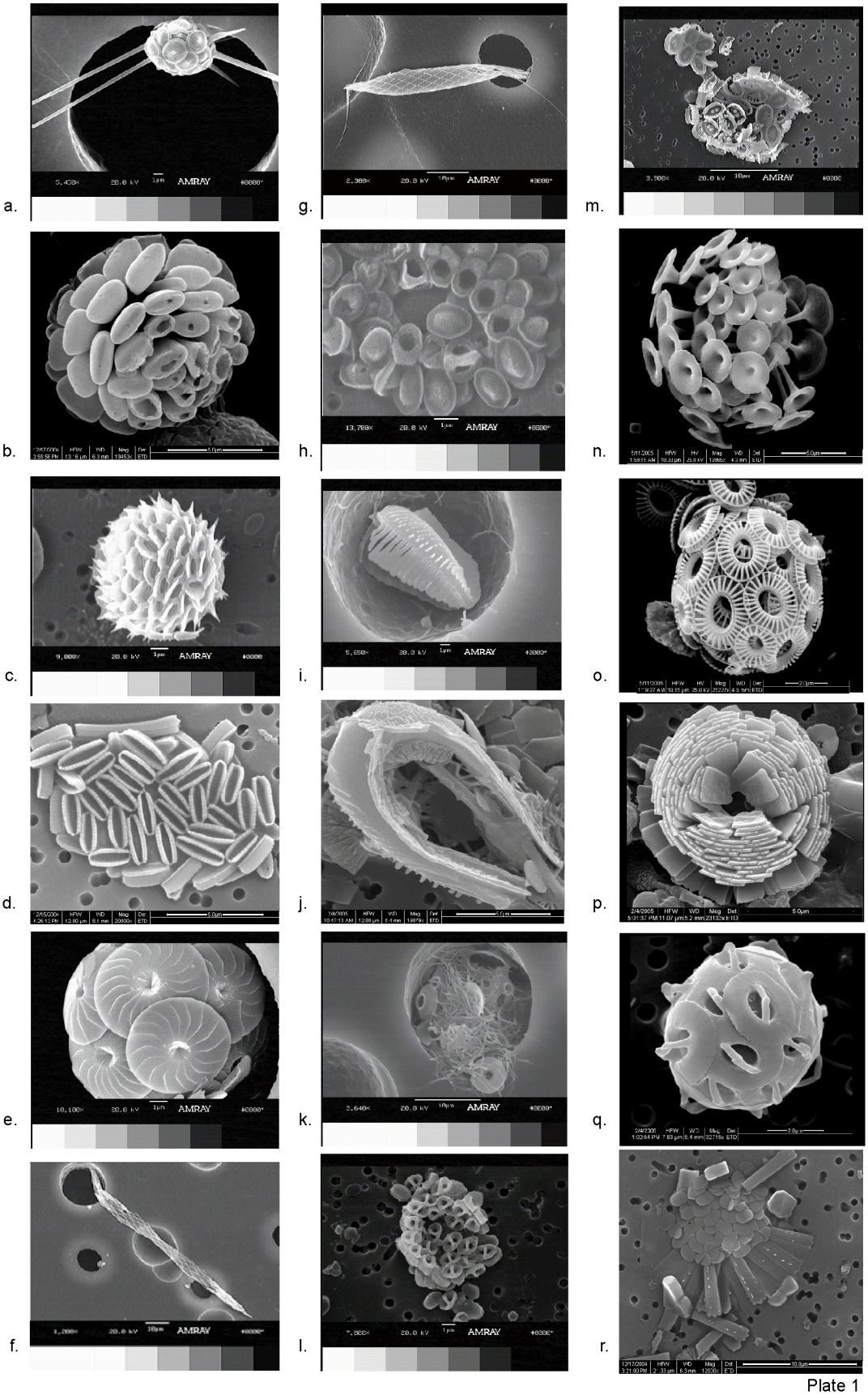

Plate 1

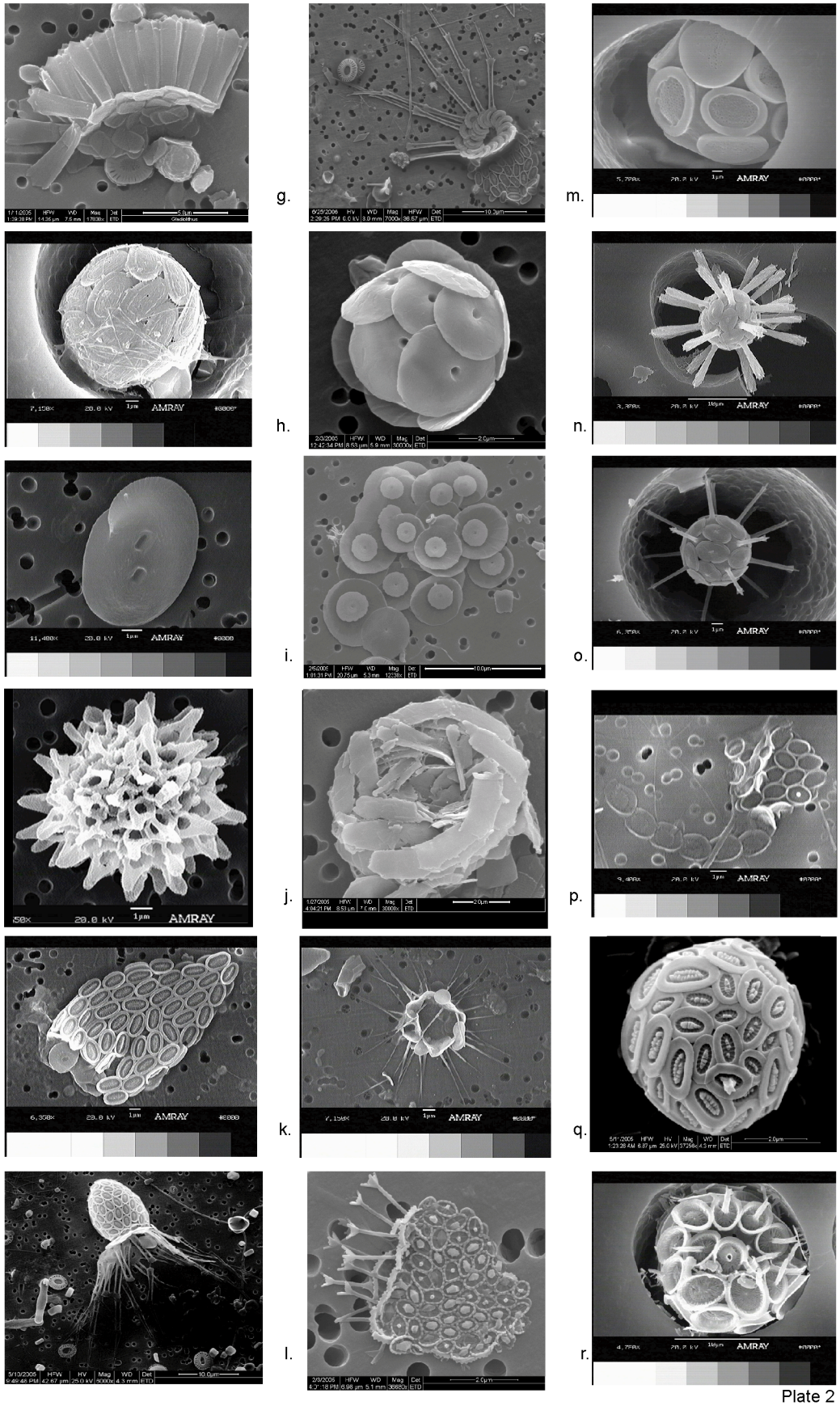

Plate 2

a. 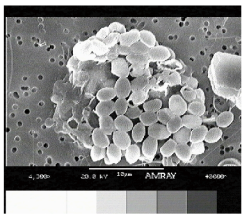

d. 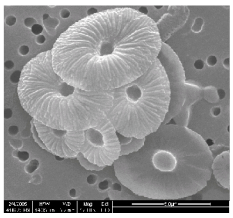

g. 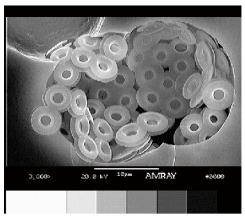

b. 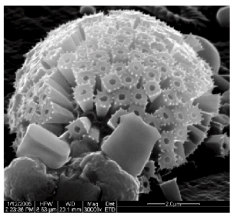

e. 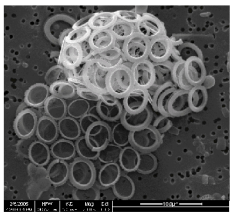

c. 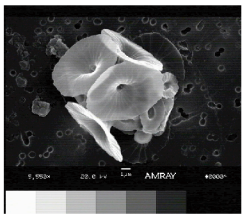

f. 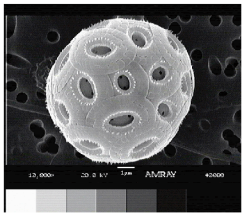

Plate 3

Chapter 1

Intraspecific morphotypic variability in the Family Rhabdosphaeraceae*

*****this chapter published as Kahn, A., Aubry, M.-P., 2006. Intraspecific morphotypic variability in the Family Rhabdosphaeraceae. Micropaleontology, 52(4): 317-342.

Abstract

Detailed inventory of filtered samples taken across the southern Indian Ocean in May-June 2003 yields quantifiable morphological groundwork for species analysis. Two samples were remarkable by their high content in *Discosphaera tubifera*, *Rhabdosphaera clavigera*, *R. stylifera* and *Palusphaera vandelii*, providing us with the opportunity to quantify intraspecific variability in these taxa. Despite its extreme geographic and ecologic restiction, this study is the first to provide an integrated description of rhabdoliths and rhabdospheres based on a large number of specimens. We show that the amplitude of variations varies broadly among Rhabdosphaeraceae species and show that *R. clavigera* and *R. stylifera* are separate taxa. We discuss the implications of our results with regard to species definition, characterisation of dimorphism, and inferences of living communities from fossil assemblages. We also report for the first time on malformations in these taxa.

1. Introduction

The coccolithophores are the object of intensive current research because of their impact in domains as diverse as the food web (Brand 1994), the carbon budget (Westbroek et al. 1993; Ziveri et al. 1999; Baumann et al. 2004; Rost and Riebesell 2004), and the propensity of some species to cause massive blooms that release DiMethyl Sulfide responsible for cloud nucleation (Charlson et al. 1987; Bates et al. 1987; Westbroek et al.

1993; Milliman 1993; Malin and Steinke 2004). In addition, once fossilized, coccoliths constitute excellent time markers and serve increasingly as proxy-indicators of past environmental changes (e.g., Hay 2004; Thierstein et al. 2004; Eleson and Bralower 2005).

In the course of an inventory of coccolithophores collected on filters from water samples taken in the southern Indian Ocean, we encountered two samples exceptionally rich in rhadospheres (i.e., coccospheres consisting of rhabdoliths; Murray and Blackman 1898). This provided us with the opportunity to analyze the intraspecific morphologic variability among four taxa [*Rhabdosphaera clavigera* (Murray and Blackman 1898), *R. stylifera* (Lohmann 1902), *Discosphaera tubifera* (Murray and Blackman 1898) Ostenfeld 1900, and *Palusphaera vandelii* (Lecal 1965)] based on the measurements of a total of 180 rhabdospheres. We describe this variability here, and compare our results with earlier studies.

Although considerable interest on the biology, biogeography and sedimentation of the extant coccolithophores has developed in recent years (see Thierstein et al. 2004) little information is as yet available on the morphologic variations exhibited by the coccoliths that form individual coccospheres. In this study, we integrate measurements on *discrete* rhabdospheres with measurements on their *respective* rhabdoliths. Our objective is to determine whether there is a relationship between the diameter of rhabdospheres and the size and number of their constituent rhabdoliths, with the expectation that this may yield indication as to the role of coccoliths, a role that has remained elusive until now (Young 1994). Additionally, the marked morphological contrasts between the rhabdoliths

secreted by the four species studied here provide us with the opportunity of an interspecific comparison of rhabdospheres.

Site VANC10MV05 is influenced by the Agulhas Current, part of a strong anticyclonic subtropical gyre consisting of the Agulhas, the South Equatorial Current, and portions of the west wind drift north of the subtropical convergence. The Agulhas Current is very strong, pulling its water from the South Equatorial Current via south-flowing currents to the east and west of Madagascar (Wyrtkie 1973). Site VANC10MV26, by contrast, is located along the seasonally variable shallow Leeuwin Current. Water movement along the western coast of Australia is weak, and no eastern boundary current exists. Seasonal nearshore shallow southern water movement occurs when the southerly wind is weaker from January to July (Wyrtkie 1973). Although in very different hydrological settings, these locations are characterized by high salinities both at surface and depth, due to higher evaporation over precipitation, and by rather low nutrient concentrations (Wyrtkie 1973).

2. Methods

2.1. Sample Location and Preparation

The samples analyzed here were taken during the HV Melville VANC10MV Hydroacoustic and Biological Sampling Cruise (May/June 2003). During this cruise 55 water samples, most consisting of 5 liters of sea water, were taken at depths ranging from 0 to 201 m from 13 sites located along a SW-NE transect from Cape Town, South Africa (35^{o}S 20^{o}E) to Port Hedland, Australia (17^{o}S 117^{o}E). All water samples were filtered

through Osmonics polycarbonate filters 47 mm in diameter, with, in most cases, a 0.8 µm pore size. We have examined 55 filters for coccolithophore content. Rhabdospheres were present in low numbers on most filters, but proved to be exceptionally abundant on filters from samples VANC10MV26A and VANC10MV05B.

Sample VANC10MV26A was taken on June 11, 2003 at the western end of the transect (Text-fig. 1). Although its geographic location and water depth are not precisely known, we have studied it for its exceptionally high abundance in *Palusphaera vandelii*. The water depth of the sample is likely in the interval between 0 and 45 m, both because of its "A" label, and its species community. It was filtered with a 0.8 µm pore size.

Sample VANC10MV05B was taken on May 19, 2003 between 00:12 and 01:14 from a depth of 49 m at the eastern end of the Indian Ocean transect (34^{o}S 37 ^{o}E) (Text-fig. 1). Seawater temperature at the time of sampling was 21^{o}C, and salinity was 35.748‰ (Table 1). The 10 to 15 µm pore size of the filters used to capture the coccolithophores was too large to retain some taxa, but this resulted in a remarkable concentration in rhabdospheres of *Discosphaera tubifera*. Rhabdospheres of *R. clavigera* and *R. stylifera* were also common in Sample VANC10MV05B and are analyzed here.

2.2. Scanning Electron Microscope Study

2.2.1. Sample preparation

Halves of each of the 55 filters were made available to us by Colomban de Vargas (Institute of Marine and Coastal Sciences, Rutgers University). The other halves are kept frozen for genetic analysis in view of combining morphologic and molecular taxonomy. A triangular piece (referred to as filter-sample below) was cut out of each filter, running

from its center towards the periphery. Each area thus scanned for rhabdospheres was approximately 8 mm^2. Once mounted onto stubs, sputter coated with gold and palladium, the filter-samples were examined with an Amray S.E.M. in the Electron Imaging Facility, Division of Life Sciences at Rutgers, the State University of NJ.

2.2.2. Inventory

Samples were scanned at 2000x magnification for preliminary inventory. Subsequent detailed morphologic analyses of discrete rhabdoliths and rhabdospheres were performed at magnifications varying between 6000x and 40,000x. Examination of the entire triangular filter-samples resulted in the recovery of a total of 91 and 99 rhabdospheres on filters VANC10MV05B (Table 2) and VANC10MV26A, respectively (Table 2).

2.3. Quantitative analysis

We describe intraspecific variability through the analysis of 5 characters: the size and eccentricity of rhabdospheres and rhabdoliths, and the number of rhabdoliths per rhabdosphere. Thus we have measured 1) all rhabdospheres along two perpendicular axes, a) between the base of the rhabdoliths (inner rhabdosphere) and b) between their distal ends (outer rhabdosphere), and 2) all rhabdoliths along different axes, including a) length of stem, b) longer and shorter diameters of the elliptical base of the stemmed rhabdoliths, c) longer and shorter diameters of discoidal rhabdoliths, and d) shorter and longer diameters of the distal end of the stem of the salpingiform rhabdolith of *D. tubifera* (Text-fig. 2, Table 3). Additionally we have counted the rhabdoliths on all complete rhabdospheres.

3. Taxonomy

The four species analysed here belong to the Family Rhabdosphaeraceae of the Order Syracosphaerales Hay 1977 emend Young et al. (2003), a family that includes at least 20 extant species distributed among 7 genera.

Family Rhabdosphaeraceae Haeckel 1894

The Family Rhabdosphaeraceae is characterized by the secretion of a specific type of coccolith, termed rhabdolith in the morphostructural sense of Kleijne (1992) and Aubry (1999). Rhabdoliths consist of a typical number of concentrically arranged cycles of elements. Rhabdoliths in the genera *Rhabdosphaera*, *Discosphaera* and *Palusphaera* comprise three cycles (Text-fig. 3). The innermost cycle consists of lamellar elements in *Discosphaera*, and of rod-shaped elements in *Rhabdosphaera* and *Palusphaera*. It fills the central area forming a slightly concavo-convex cover in discoidal rhabdoliths. More commonly, it develops into a spirally structured distal stem. Stemmed rhabdoliths may be styliform, sacculiform, helatoform, claviform, or salpingiform, depending on shape. Rhabdospheres consist of salpingiform rhabdoliths in *D. tubifera* (Text-fig. 3, Plate 1), and styliform rhabdoliths in *P. vandelii* (Text-fig. 3, Plate 2). In both species, the rhabdosphere has been described as monothecate, and the base of the rhabdolith is mostly circular. Rhabdospheres of *R. clavigera* and *R. stylifera* are dithecate. They consist, respectively, of claviform and helatoform rhabdoliths with an elliptical base, and include an outer theca of discoidal rhabdoliths (Text-fig. 3, Plate 3).

3.1. *Discosphaera tubifera* (Murray and Blackman 1898) Ostenfeld 1900

Discosphaera tubifera, the only extant species of the genus, is a distinctive taxon and the type species of *Discosphaera* Haeckel 1894. The basic morphology of the rhabdosphere and rhabdoliths have been comprehensively described by Kleijne (1992). The rhabdosphere is described as spherical, 15-20 µm in diameter, consisting of about 50 salpingiform rhabdoliths with a stem 4.5 to 7 µm in length.

Norris (1984) reported *D. tubifera* as common from May through mid-July 1963 in surface waters (0-48m) of the Indian Ocean, but Kleijne (1992) found it to be only occasional during the same months of 1985 in surface waters of the northeastern Indian Ocean.

3.2. *Palusphaera vandelii* Lecal 1965 emended Norris 1984

The genus *Palusphaera* Lecal 1965 emended Norris 1984 is known only from extant communities. *Palusphaera vandelii* is the only formally described species. The morphology of its styliform rhabdoliths with their characteristic long stem was described by Norris (1984; as cyrtoliths: see discussion in Aubry 1999), but the rhabdosphere is poorly known because it is generally collapsed on filter-samples.

Norris (1984) found *P. vandelii* to be common in surface waters of the western Indian Ocean during July of Year 1963. In contrast, Kleijne found it to be occasional in surface waters (0-5 m) of the northeastern Indian Ocean during June and July of Year 1985.

3.3. *Rhabdosphaera clavigera* Murray and Blackman 1898 and *Rhabdosphaera stylifera* Lohmann 1902.

The genus *Rhabdosphaera* was introduced by Haeckel 1894. *Rhabdosphaera clavigera* is its type species. The name *R. clavigera* was introduced to describe spherical rhabdospheres consisting of numerous rhabdoliths with club-shaped projections. Lohmann (1902) described *R. stylifera* for rhabdospheres formed of rhabdoliths with thin, parallel-sided stems and broad proximal bases. According to Lohmann (1902), the rhabdosphere of *R. stylifera* consists of fewer, less closely spaced rhabdoliths than that of *R. clavigera*.

Several authors have proposed that *R. stylifera* is a junior synonym of *R. clavigera*, based on the fact that rhabdospheres with rhabdoliths typical of each species are common (see discussion in Aubry 1999). In our material the distinction between the two species is unambiguous and they are treated separately.

Norris (1984) noted that *R. clavigera* (inclusive of *R. stylifera*) was common in surface waters of the Indian Ocean during May to mid-July of Year 1963, in contrast to Kleijne (1992) who remarked on its rarity in the northeastern Indian Ocean in June-July of 1985.

4. Intraspecific variability in plankton samples VANC10MV26A and VANC10MV05B

4.1. *Discosphaera tubifera* (Plate 1)

Filter sample VANC10MV05B yielded 67 rhabdospheres of *D. tubifera*, representing approximately 45% of the total number (150) of coccospheres recorded in the filter-sample (Table 2). Because the large pore size of the filter must have resulted in the loss of small coccospheres, this percentage is certainly an overestimate of the original richness of the coccolithophore community in *D. tubifera*. It remains however that since

all filters represent the same amount of seawater (5 liters), *D. tubifera* must have been abundant in the community that filter VANC10MV05B represents.

The filter-sample from VANC10MV26A yielded only isolated rhabdoliths of *D. tubifera*; it is not taken into account in this study.

4.1.1. The rhabdosphere

The rhabdospheres of *D. tubifera* are spherical to subspherical. The eccentricity of their inner rhabdosphere varies between 1 and 0.8, with a mean of 0.9 (Table 4). The diameter of the inner rhabdosphere varies between 4.1 and 6.5 µm; that of the outer rhabdosphere between 9.7 to 17.4 µm (Text-fig. 4a, Table 4). The largest inner rhabdosphere was almost twice as large as the smallest inner rhabdosphere. The largest outer rhadosphere was 1.6 times larger than the largest outer rhabdosphere. However, there is little correlation between the diameter of the inner and outer rhabdospheres, except at the extremes of the size range (Text-fig. 4a). The smallest and largest inner rhabdospheres were also, respectively, the smallest and largest outer rhabdospheres; however, a 5 µm inner rhabdosphere may correspond as well to a 13 µm or a 15.5 µm outer rhabdosphere. The average number of rhabdoliths on a single rhabdosphere is 48.5 (Table 4). However, the number of rhabdoliths per rhabdosphere varies considerably, from 29 to 66. Further, this number does not correlate with the diameter of the inner rhabdosphere, itself a proxy of the cell size. A ~4.5 µm-cell may bear as many as 55 rhabdoliths whereas a ~6.5 µm-cell may be enveloped by as few as 52 or as many as 63 rhabdoliths (Text-fig. 4b).

4.1.2. The salpingiform rhabdoliths

The length of the rhabdoliths varies greatly both on individual rhabdospheres and between rhabdospheres (Text-fig. 4c). The smallest rhabdolith recorded measured 2.2 µm; the largest measured 6.4 µm, which is almost three times larger (Table 4). The bases of the rhabdoliths are sub-circular, with a mean eccentricity of 0.8 (Text-fig. 4d). There is little variability in the diameter of the base of the rhabdoliths either on a single rhabdosphere (Text-fig. 4e) or among rhabdospheres (Text-fig. 4f), the maximum difference being only 1.6 µm. The distal ends of the rhabdoliths are more circular than their bases, their eccentricity averaging 0.9. However their diameters are highly variable both on single rhabdospheres and between rhabdospheres. The shortest diameter was 0.9 µm, the longest 5.1 µm (Table 4). The largest range on a single rhabdosphere was from 1.2 to 4.2 µm. Thus, on a single rhabdosphere, some rhabdoliths may be as much as 3 times longer than others, the proximal diameter may be 1.3 to1.4 times that of others, and the distal diameter (distal part of the stem) may be 5 times larger than that of others.

4.2. *Palusphaera vandelii* (Plate 2)

Ninety-seven rhabdospheres of *P. vandelii* were observed on filter-sample VANC10MV26A. These represent 51% of a total of 190 coccospheres (comprising 18 different species) recorded on the filter (Table 2). In contrast 2 rhadospheres of this species were found among 150 coccospheres of various species on the filter-sample VANC10MV05B (Table 2).

All rhabdospheres were collapsed. This is easily explained by the lack of rigidity of the rhabdoliths themselves. Their base is very thin and the long and delicate stems easily curve under pressure (Plate 2, figs. 1-5). This restricts considerably the amount of

data collectable to describe intraspecific variability in the species. Of the 97 collapsed rhabdospheres, only 23 were suitable for counts of rhabdoliths because these had fallen in radiating patterns such that the original rhabdospheres were easily reconstructed (e.g., Plate 2, figs. 1-2). Only 80 rhabdospheres were suitable for measurement of diameter, because although assumed complete, the rhabdoliths on 17 of the rhabdospheres had fallen in a disorganized fashion (e.g., Plate 2, figs. 3-4).

4.2.1. The rhabdosphere

The inner rhabdosphere of *P. vandelii* is small, varying in diameter between 2.7 and 5.8 µm with a mean of 3.9 µm (Text-fig. 5a, Table 5). The eccentricity could not be measured from collapsed rhabdospheres. The number of rhabdoliths varies between 20 and 75, with a mean of 42 (Table 5). There would appear to be no correlation between the diameter of the inner rhabdosphere and the number of constituent rhabdoliths (Text-fig. 5b). However, 57% of the rhabdospheres comprised between 40 and 50 rhabdoliths.

4.2. The styliform rhabdoliths

The variation in size of the diameter of the base of the rhabdoliths is considerable, ranging between 0.7 µm and 2.2 µm (Text-fig. 5c, Table 5). Similarly, the length of individual rhabdoliths on single rhabdospheres or between rhabdospheres varies greatly (Text-fig. 5d). The maximum difference in length among rhabdoliths on a single rhabdosphere is 6.1 µm, the shortest rhabdolith measuring 1.6 µm, the largest 7.7 µm. The maximum difference in length of rhabdoliths between rhabdospheres is 8.2 µm, the shortest rhabdolith being 1.6 µm and the longest 9.8 µm (Table 5).

4.3. *Rhabdosphaera clavigera* (Plate 3, figs. 2, 4, 6)

Ten complete rhabdospheres of *R. clavigera* were found among a total of 150 complete coccospheres of various species on filter-sample VANC10MV05B. No rhabdospheres of *R. clavigera* were found on filter-sample VAN10MV26A.

4.3.1. The rhabdosphere

The rhabdosphere of *R. clavigera* is sub-spherical. The eccentricities (as measured from two rhabdospheres) are 0.88 and 0.95. The diameter of the inner rhabdosphere varies between 8.7 and 10.5 µm (with a mean of 9.8 µm) (Text-fig. 6a, Table 6). The diameter of the outer rhabdosphere varies between 19.3 and 26.9 µm (with a mean of 23.5 µm) (Text-fig. 7a, Table 6).

The number of discoidal rhabdoliths varies between 8 and 26 per rhabdosphere (with a mean of 19) (Text-fig. 7b, Table 6). The number of claviform rhabdoliths per rhabdosphere varies between 14 and 26 (with a mean of 21.8) (Text-fig. 7b, Table 6). Thus, on average, the exotheca comprises slightly fewer (discoidal) rhabdoliths than the endotheca (of claviform rhabdoliths). The ratio of discoidal to claviform rhabdoliths on a single rhabdosphere varies between 0.6 and 1.1.

4.3.2. The rhabdoliths

Claviform rhabdoliths vary substantially in length among rhabdospheres (Text-fig. 6b). The shortest measured 6.1 µm, the largest 10.9 µm (Table 6). The mean length among the 10 rhabdospheres was 8.4 µm, with variation on individual rhabdospheres as well (Text-fig. 6b). The size difference is 0.7 µm on average, and the maximum difference

was 2.3 µm (from 8 to 10.3 µm; rhabdosphere 1 in Text-fig. 6b). The amplitude of variation in the diameter of the base of the claviform rhabdoliths cannot be established because these are covered by the exotheca. The discoidal rhabdoliths (exotheca) are elliptical, with an average eccentricity of 0.7 (Table 6). The average diameter of the long and short axes of the discoidal rhabdoliths are 4.2 and 2.9 µm, respectively (Text-fig. 6c, Table 6).

4.4. *Rhabdosphaera stylifera* (Plate 3, figs. 1, 3, 5)

Twelve rhabdospheres of *R. stylifera* were found on the same filter-sample (VANC10MV05B) on which the 10 rhabdospheres of *R. clavigera* were found. The 2 species represent, respectively, 6.6 and 8% of the total community of species collected as rhabdospheres on the filter sample (Table 2). Filter sample VANC10MV26A contained 2 rhabdospheres of *R. stylifera* in a total of 190 coccospheres recorded (Table 2).

4.4.1. The rhabdosphere

The diameter of the inner rhabdosphere of *R. stylifera* varies between 4.4 and 7.6 µm (with a mean of 6.2 µm) (Text-fig. 6a, Table 6). Its outer rhabdosphere varies between 7.8 and 16.1 µm (with a mean of 12.9 µm) (Text-fig. 8a, Table 6). The rhabdospheres comprise a total number of 15-43 rhabdoliths (Table 6), the discoidal rhabdoliths being generally more numerous than the helatoform rhabdoliths (Text-fig. 8b). The difference in number between the two, however, is slight: the discoidal:helatoform rhabdolith ratio varies between 0.7 and 1.8. The number of discoidal rhabdoliths varies between 7 and 24

per rhabdosphere (mean=14); that of helatoform rhabdoliths varies between 8 and 21 (mean= 13.5) (Table 6).

4.4.2. The rhabdoliths

The length of helatoform rhabdoliths varies among rhabdospheres by 2.3 µm. The shortest measures 2.9 µm, and the longest 5.2 µm (mean= 4.3 µm) (Text-fig. 6b, Table 6). On a single rhabdosphere, the mean difference in length between helatoform rhabdoliths is 0.4 µm. The greatest range in length between rhabdoliths on a single rhabdosphere was 0.7 µm (4.5-5.2 µm) (Text-fig. 6b). As in *R. clavigera*, the bases of the helatoform rhabdoliths are covered by the discoidal rhabdoliths. The latter are elliptical (Text-fig. 6c), with a mean eccentricity of 0.6 (Table 6). Their diameters along their long and short axes average 3.1 and 1.8 µm, respectively (Table 6).

5. Discussion

Species of the Family Rhabdosphaeraceae, though common, rarely dominate living communities (Kleijne 1992; Honjo and Okada 1974; Nishida 1979; Okada and McIntyre 1979; McIntyre et al. 1970). At 49 m water depth (VANC10MV05B), they constituted 61% of the total community and at a higher depth (0-45m) (VANC10MV26A), they constituted 52% of the total community, with *D. tubifera* and *P. vandelii* each occurring in significantly larger numbers than any other individual species. (Interestingly, at the opposite sides of the Indian Ocean the 2 species traded dominance, at least momentarily, from unequivocal dominance of 45-51% to approximately 0-1% of the assemblage). This study is therefore the first to address intraspecific variability in the

family based on a large collection of specimens. Yet, because our sampling is punctual, both geographically and temporally, we may not describe the variability extremes in either species. Similar analyses from locations in different hydrological regimes, and time series analyses at selected sites will be necessary to comprehend the patterns of morphologic variability for any given species. As restricted as they are, our data have nevertheless important implications with regard to species definition, characterisation of dimorphism, and inferences of living communities from fossil assemblages. They are discussed in turn.

5.1. Species definition

The morphologic variations that we describe here generally agree with variations reported in the literature (Tables 4-7). Whereas this is true for mean values, the amplitude of variations is greater in our samples than described elsewhere, which we attribute to the larger number of specimens measured for each species in this study. Interestingly, despite an apparent homogeneity in shape, the size variation is surprisingly high in the four taxa studied here.

5.1.1. *Discosphaera tubifera*

Discosphaera tubifera occurs frequently in the Indian Ocean (Text-fig. 9), (although generally more dominant on the western part of the transect than on the eastern part). This is an easily identifiable species, with apparently (but superficially) little variation in size or shape between rhabdospheres (Plate 1, Text-fig. 10).). Although the average length (4.3 µm) of the rhabdoliths is usually less than the diameter of the rhabdosphere

(3.9-6.5 µm; average=5.0 µm), their maximum length (3.2-6.4 µm; average=5.0 µm) is often greater than the diameter of the rhabdosphere (Text-fig. 4g).

Comparison of the amplitude of the variations described here among rhabdospheres of *D. tubifera* with published data (Clochiatti 1971a; Norris 1984; Kleijne 1992; Cros and Fortuño 2002) indicates that an accurate description of morphological variations is attainable only by measuring a large collection of individuals (Table 4). In any case, this comparison supports our demonstration that morphologic variations in our collection of specimens of *D. tubifera* follow a unimodal distribution, implying that this is a discrete, well-differentiated taxon for which we do not expect to find cryptic species (Text-Fig. 10).

5.1.2. *Palusphaera vandelii*

Palusphaera vandelii occurs in small numbers in the Indian Ocean (Text-fig. 9), its abundance increasing in shallow coastal communities (e.g., Sample VANC10MV26A; Text-fig. 1). As in *D. tubifera*, the overall similarity in shape among the rhabdospheres of *P. vandelii* conceals marked variations in the number and size of component rhabdoliths. These variations follow a unimodal distribution (Text-fig. 10), implying that this taxon is well defined. The diameter and eccentricity of the proximal side of the rhabdoliths are relatively constant, but the length of the styliform stem varies significantly, by an average of 6.5 µm among different rhabdospheres, 4.6 µm on a single rhabdosphere (Text-fig. 5e). No pattern emerges concerning the relation between the diameter of the basal side of the styliform rhabdoliths and their length. The size range is

larger in this study than in previous studies in which fewer rhabdospheres were measured (Table 5).

Estimates from collapsed rhabdospheres show strong variations in the number of styliform rhabdoliths per rhabdosphere, but, as in *D. tubifera*, no correlation occurs between rhabdolith number and rhabdosphere diameter (Text-fig. 5b). The differences between rhabdospheres are well marked, although with only collapsed rhabdospheres it is difficult to unequivocally determine that rhadoliths were not shed from the rhabdospheres with fewer rhabdoliths. Rhabdoliths are extremely closely spaced on some rhabdospheres (Plate 2, fig. 5), with up to 75 rhabdoliths surrounding a 4.4 µm diameter cell. Other rhabdospheres are not as closely packed (e.g., Plate 2, fig. 2); a 5.8 µm cell is surrounded by 49 styliform rhabdoliths.

5.1.3. *Rhabdosphaera clavigera*

The number of whole rhabdospheres of *R. clavigera* is low, but we measured all whole rhabdospheres as well as rhabdoliths on whole and collapsed rhabdospheres. The total number of rhabdoliths per rhabdosphere varies from 22-52 (Table 6). The number of rhabdoliths on each discrete sphere also varies; 50% of rhabdospheres consist of an equal number of (0-2 variation) of claviform and discoidal rhabdoliths. In the other 50%, the claviform rhabdoliths outnumber the discoidal rhabdoliths.

As for previous species, no apparent correlation exists between the length of the claviform rhabdoliths and the diameter of the rhabdosphere (Text-fig. 6d). The diameter of the outer rhabdosphere is 2.5-3 times that of the inner rhabdopshere; however, the mean length of the claviform rhabdoliths is slightly less than the diameter of the

rhabdosphere, indicating that the longer than average rhabdoliths account for the greater size difference between the inner and outer rhabdosphere. Large variations in the length of the claviform rhabdoliths and in the diameter of the base of the discoidal rhabdoliths are notable.

5.1.4. *Rhabdosphaera stylifera*

The total number of rhabdoliths on a single rhabdosphere varies from 15 to 41 (Table 6). The difference in the number of helatoform vs. discoidal rhabdoliths is small (Text-fig. 8b). On 73% of the rhabdospheres it varies between 0 and 3. In the remaining 27% rhabdospheres it varies between 5 and 7. In addition, no apparent pattern emerges as to which rhabdolith-type dominates the rhabdosphere. As in *R. clavigera*, the number of rhabdoliths per rhabdosphere varies, although the amplitude of variation is generally less than in *R. clavigera*.

The outer rhabdosphere is slightly greater than twice the diameter of the inner rhabdosphere (with 1 exception: inner is 1.8 times smaller than outer); however, the mean length of the helatoform rhabdoliths is slightly less than the diameter of the rhabdosphere, indicating, as with *R. clavigera*, that the longer rhabdoliths account for the greater than 200% size increase from inner to outer rhabdosphere. As in other species there is no correlation between the length of the rhabdoliths and the diameter of the rhabdosphere (Text-fig. 6d). Also, variations in the diameter of the rhabdospheres and discoidal rhabdoliths, and in the length of the helatoform rhabdoliths are easily observable through our measurements.

5.1.5. *Rhabdosphaera. clavigera* and *R. stylifera*

Rhabdosphaera clavigera and *R. stylifera* have been distinguished as separate species (Clochiatti 1971; Kleijne and Jordan 1990; Steinmetz 1991) or they have been regarded as distinct morphotypes of a single species (the name *clavigera* having historical priority) (Norris 1984; Kleijne 1992; Young et al. 2003). We show here that there is little morphological overlap between the *R. clavigera*- and *R. stylifer*a-morphotypes (Plate 3). When plotted together for the two species in our material, size variations and other parameters show bimodal distribution (Text-fig. 11). The most obvious morphologic difference is the shape of the rhabdolith, claviform vs. helatoform. *Rhabdosphaera clavigera* has rhabdoliths with club-shaped stems formed by the lamellar/cuneate cycle that thickens as it spirals outwards towards the distal end, and terminating in a single papilla rising above symmetric pentameral spiraling elements (Text-fig. 3c; Plate 3, figs. 2, 4, 6). *Rhabdosphaera stylifera* has helatoform rhabdoliths similarly formed by a lamellar/cuneate cycle, terminating in a single papilla rising above symmetric pentameral spiraling elements, but the helatoform rhabdolith is of constant thickness (Text-fig. 3c; Plate 3, figs.1, 3, 5).

Differences in rhabdolith shape aside, *R. clavigera* is considerably larger than *R. stylifera* in all morphological aspects in our material. The diameter of the rhabdosphere of *R. stylifera* averages 63% that of *R. clavigera*, with no overlap between the two (Text-fig. 6a). Similarly, the mean length of the helatoform rhabdoliths of *R. stylifera* is 50% that of the claviform rhabdoliths of *R. clavigera* (Text-fig. 6b). The distribution of the mean diameters of the rhabdospheres of *R. clavigera* and *R. stylifera* plotted against the mean

lengths of their respective rhabdoliths also illustrates a significant size contrast (Text-fig. 6e).

Although smaller, the difference in diameter among the discoidal rhabdoliths is also notable; the discoidal rhabdoliths are approximately 20% larger in *R. clavigera* than in *R. stylifera* (Text-fig. 6c). The discoidal rhabdoliths of *R. clavigera* are generally rounder (mean=0.7), those of *R. stylifera* generally more elliptical (mean=0.6) (Table 6). In addition, the ratio between the minimum and maximum diameter of the rhabdospheres of *R. stylifera* differ from that of *R. clavigera* (0.6 versus 0.8). The ratio between the minimum and maximum diameter of the discoidal rhabdoliths (0.8) and between the minimum and maximum length of the helatoform rhabdoliths (0.6) are the same as for the claviform rhabdoliths of *R. clavigera*.

The ranges of published measurements on *R. clavigera* and *R. stylifera* are within the amplitude of variability that we describe here (Tables 6-7). We have also measured rhabdospheres of the two species using published photographs (Table 8). Some of these measurements agree well with our data, but several rhabdospheres of *R. stylifera* are considerably larger than those in our samples. In particular, an isolated rhabdosphere of *R. stylifera* (Young et al. 2005) is not only almost 50% larger than our largest rhabdosphere of *R. stylifera* but also 1% larger than our largest rhabdosphere of *R. clavigera.* Clearly, and as acknowledged above, our sample is too local to represent the full scope of intra- and interspecific variability; however, no rhabdosphere of *R. clavigera* was documented from the same community in which this remarkably large rhabdosphere of *R. stylifera* (of unknown location) occurred, and it may be that the former species would have been proportionally larger than the latter. We did not find published

photographs of both *R. stylifera* and *R. clavigera* sampled from the same location. We propose that it is not the absolute size that characterizes either species, but the relative difference in their size in a given community of coccolithophore. This must be further analyzed.

Hybridization has been offered to explain mixed rhabdospheres that simultaneously bear claviform (*R. clavigera*) and helatoform (*R. stylifera*) rhabdoliths (Gaarder and Hasle 1971; Borsetti and Cati 1972; Nishida 1979, 1985; Hallegraeff 1984; Kleijne 1992). Because of the shared global distribution of the 2 species (Pacific, Indian, Atlantic Oceans, Mediterranean and Red Seas (Text-fig. 9; Norris 1984; Kleijne 1992) hybridization is conceivable, but still remains to be proven.

5.2. Characterization of and comparison between rhabdospheres of different species

5.2.1. Dithecatism and polymorphy

A survey of the literature reveals major differences between coccospheres, not only with regard to the well-documented dithecatism and polymorphism in some species (see Young et al., 2005), but also to the manner in which coccoliths relate to one another on coccospheres. The rhabdospheres of *R. stylifera* and *R. clavigera* comprise two concentric layers of coccoliths, each with coccoliths of similar structure but different morphologies. They are regarded as dithecate (Kleijne 1992) or polymorphic (Young et al. 2003). We follow Kleijne in interpreting them as dithecate because the two layers (exo- and endotheca) are clearly distinct. Dithecatism in these two species may contribute to strengthening the rhabdosphere, the exotheca of discoidal rhabdoliths securing the endotheca formed by large rhabdoliths with heavy stems.

The rhabdosphere of *D. tubifera* is regarded as monomorphic (Kleijne, 1993). Yet, regardless of the number of constituent rhabdoliths, it comprises rhabdoliths of substantially different length (differing by a factor of 3) and distal diameter (differing by a factor of 5). In our view the rhabdosphere of *D. tubifera* is polymorphic. Although of apparent uniformity, it may be likened to coccospheres with more obvious morphological contrasts, as in *Umbellosphaera* species. The same is true for *P. vandelii* in which the size of the rhabdoliths on a single rhabdosphere varies greatly.

5.2.2. Relation between growth and size

In *D. tubifera* the number of rhabdoliths per rhabdosphere varies considerably, as does their length. This could be related to the growth of the rhabdosphere and cellular division, in a manner similar to that noted in cultures of *Emiliania huxleyi* (Linschooten et al. 1991). However, there is virtually no correlation between the diameter of the rhabdosphere and the number of component rhabdoliths. Although the largest and smallest rhabdospheres have the largest and lowest numbers of rhabdoliths, respectively, rhabdospheres of intermediate size have variable numbers of rhabdoliths of variable size (Text-fig. 4h). The cause(s) for wide variations in the number of rhabdoliths constituting the rhabdosphere of *D. tubifera* thus requires investigation. This is true also for *P. vandelii*.

The mode of formation of the stem of rhabdoliths is a puzzle. Like other heterococcoliths, rhabdoliths are likely to form intracellularly. Yet, the length of the stemmed rhabdoliths often exceeds the cell diameter in all 4 species. Lecal (1965)

reported that the stem forms after the extrusion of the rhabdoliths from the cell, which requires confirmation.

5.2.3. Outer versus inner rhabdosphere

The overlapping bases of the rhabdoliths form a solid, albeit articulate, sphere that we call here "inner rhabdosphere". The distal ends of rhabdoliths delineate concretely (as in *D. tubifera*) or virtually (as in *Rhabdosphaera* spp.) a second sphere that we call the "outer rhabdosphere." In *D. tubifera* the distal end of the rhabdoliths imbricate, forming a continuous but irregular envelope with alternating depressed and protruding areas depending on the length of adjacent rhabdoliths (Plate 1, fig. 3, Text-figs. 2a, 12a). The shape and arrangement of the rhabdoliths produce a pseudo-dithecatism, the inner and outer rhabdospheres being, respectively, endotheca and exotheca. In truly dithecate species, the endotheca and exotheca are separate. Dithecatism is a characteristic of the Family Syracosphaeraceae, the most diversified (successful) family of extant coccolithophores. In addition to the flotation devices that the salpingiform rhabdoliths may represent, the pseudo-dithecatism in *D. tubifera* may be a morphologic convergence, dithecatism possibly providing a definitive, albeit undiscovered, advantage to the living cell in the modern ocean (see further discussion in Aubry 2006).

In *Rhabdosphaera* spp. the virtual outer rhabdosphere is highly discontinuous, but because of the variable size of rhabdoliths the outer coccosphere is also irregular (Text-fig. 12b).

5.2.4. Paleobiological reconstructions

Most coccospheres disintegrate during sedimentation, so that calcareous nannofossil oozes are essentially comprised of a multitude of separate coccoliths. Given the number of coccoliths per coccosphere of any discrete taxon it is possible to estimate the number of cells that contributed to a measured number of sedimented coccoliths of this taxon. In turn this permits determination of past sedimentary fluxes and oceanic production by the coccolithophores (Kleijne 1991; Knapperbusch 1993; Boerse et al. 2000a-c; Ziveri and Thunell 2000). In order to assist the conversion of coccolith number into cell number, Yang and Wei (2003) have provided an estimate of the number of coccoliths per coccospheres in 141 extant species based on a literature search. Their report underestimates strongly the variability of the number of coccoliths per coccosphere in the species studied here (Table 9). Our study shows that, at least for these species, the conversion of a number of coccoliths into a number of cells is not straightforward. At the same time, it provides the limits within which the conversion is valid for each species, and upon which minimal and maximal production can be restituted from fossil evidence. It also provides two useful values, mean and mode (for *D. tubifera* and *P. vandelii*) upon which to establish the conversion for a reliable approximation of cell numbers and production.

6. Malformation

Malformed rhabdopheres and rhabdoliths occur in our samples. In Sample VANC10MV05B malformation affected 6% of the rhabdospheres of *D. tubifera*, 10% of those of *R. clavigera*, and 50% of those of *R. stylifera* (Table 1). In Sample VANC10MV26A 10% of the rhabdospheres of *P. vandelii* and 50% of those of *R.*

stylifera were malformed (Table 2). Coarsely calcified rhabdoliths and increased ellipticity of rhabdospheres and of the base of rhabdoliths are diagnostic of malformation (Plate 2, fig. 6; Plate 4; Plate 5). The distal end of the rhabdoliths of *D. tubifera*, *R. clavigera*, and *R. stylifera*, and the proximal end of those of *P.vandelii* appear shriveled (Plate 2, fig. 6; Plate 4; Plate 5, figs. 1, 4, 5, 7).

Malformation is rampant among the coccolithophores recovered along the Melville transect. It is unevenly distributed and affects almost all taxa indiscriminately. What might be identified as small variations in species morphology may in fact reflect minimal malformation (?undercalcification) (Plate 5, figs. 1-3, 5-6). In *D. tubifera*, some rhabdospheres bear incomplete salpingiform rhabdoliths whose distal end is barely or irregularly formed (Plate 4, fig. 2). Other rhabdospheres are irregularly elliptical; the proximal ends of the rhabdoliths have irregular shapes, the distal ends are incompletely or irregularly formed (Plate 4, figs. 1, 3-4).

Rhabdospheres of *P. vandelii* are less severely malformed than those of *D. tubifera* and *R. stylifera*. The proximal end of the styliform rhabdoliths is commonly malformed, usually rippled (instead of relatively flat) giving the rhabdoliths an irregular appearance (Plate 2, fig. 6). The extended papilla is occasionally poorly crystallized (Plate 2, fig. 6)

Malformation of *R. stylifera* may be occasionally severe, implying that this species is more sensitive to environmental problems. No data are available on the water chemistry, atmospheric conditions, or viral/bacterial concentrations that would help determine a possible cause for malformation. However, it is clear that *R. stylifera* is more sensitive to environmental factors than the other three species. Most of its malformed rhabdospheres are coarsely shaped with poorly formed helatoform rhabdoliths. One rhabdosphere was

so malformed that it was difficult to determine it to species level. Its discoidal rhabdoliths are strongly curved, relatively small and spherical (vs. normal rhabdospheres which have larger, more elliptical discoidal rhabdoliths) (Plate 5, fig. 4).

Our observation of malformation in *R. clavigera* is limited to several collapsed discoidal and claviform rhabdoliths. In these rhabdoliths the proximal end is truncated and/or the tips of the claviform stem are rounded (Plate 5, fig. 7).

Interestingly, although more rhabdospheres of *R. stylifera* than *R. clavigera* were found malformed (artifact due to sample size?), a higher percentage of rhabdospheres of *R. clavigera* than of *R. stylifera* were collapsed (Table 6). This may indicate that though the rhabdosphere of *R. stylifera* is more prone to malformation, it is structurally stronger than that of *R. clavigera.* The rhabdospheres of *R. stylifera* are smaller than those of *R. clavigera*, and their narrow helatoform rhabdoliths may be lighter, thus causing less pressure on the inner rhabdospheres. The thick club-shaped claviform rhabdoliths that form the large rhabdospheres of *R. clavigera* are "top-heavy" causing great pressure on the inner rhabdospheres, which thus may be prone to collapse.

Malformation has been reported in several coccolithophore taxa (Kleijne 1990; Girardeau et al. 1993; Triantaphyllou et al. 2002; Dimiza et al. 2003; Crudeli et al. 2004; Yang et al. 2004), most commonly in *Emiliania huxleyi*. However, to our knowledge, no malformation has as yet been reported in the family Rhabdosphaeraceae. In our study of samples from the HV Melville transect, malformation is restricted to samples from the upper photic zone (upper 50 m), and from relatively coastal locations (both eastern and western boundaries of the southern Indian Ocean). Deeper samples (60-200 m) were free

from malformation. We note in passing that the two samples described here did not contain the largest percentage of malformed specimens along the transect.

Conclusions

Through the measurement of selected morphological parameters that describe rhabdospheres and rhabdoliths we have documented intraspecific variability among 4 species of the family Rhabdosphaeraceae. We show that detailed studies of large collections of specimens are necessary to thoroughly describe intraspecific variability. To be comprehensive, this study requires additional morphologic description of the same taxa sampled in different hydrological settings, allowing description of the complete spectrum of intraspecific variability in relation to biogeography. This study provides however an initial framework for comparative analysis between morphology and molecular biology, in an attempt to clarify the extent of cryptic speciation in coccolithophores

We show here that *D. tubifera* and *P. vandelii* each exhibit a *continuum* of intraspecific variations, suggesting that these are genetically homogeneous taxa. In contrast to recent work, we show that *R. clavigera* and *R. stylifera* are distinctive taxa, and propose that their intraspecific variability remains essentially unknown.

We have described the rhabdospheres of *D. tubifera* and *P. vandelii* as polymorphic, in contrast to current descriptions; and we have established that the rhabdosphere of *D. tubifera* represent a case of pseudo-dithecatism. We show that detailed quantitative analysis of intraspecific variations allow determination of uncertainties in

paleoproduction as inferred from coccolith frequency. Finally we report for the first time on malformation in the Family Rhabdosphaeraceae.

Acknowledgements

We warmly thank Valentin Starovoytov for his technical assistance on the S.E.M. and Ryan Earley for helping us with the maps. We acknowledge an anonymous reviewer for valuable comments on this manuscript. This study was partially funded by NSF Grant 0415351 (C. de Vargas).

References

ANDRULEIT, H., Geisen, M., Stäger, S., 2006. Stereo-microscopy of coccolithophores – modern applications for imaging and morphological analysis. *Journal of Nannoplankton Research*, 28(1):1-16.

AUBRY, M.-P., 2006. A major Pliocene calcareous nannoplankton turnover: Change in morphological strategy in the photic zone. In: Monechi, S., Rampino, M., and Coccioni, R., Eds., *Mass Extinctions and Other Large Ecosystem Perturbations: Causes and Consequences.* Geological Society of America, Special Paper 424: 25-51.

AUBRY, M.-P., 1999. Handbook of Cenozoic Calcareous Nannoplankton., Book 5: Heliolithae (Zygoliths and Rhabdoliths). New York, Micropaleontology Press: 1-368.

BATES, T.S., Charlson, R.J., and Gammon, R.H., 1987. Evidence for the climatic role of biogenic sulfur. *Nature*, 329:319-321.

BAUMANN, K.-H., Andruleit, H., Böckel, B., Geisen, M., Kinkel, H., 2005. The significance of extant coccolithophores as indicators of ocean water masses, surface water temperature, and paleoproductivity. *Paläontologische Zeitschrift*, 79(1): 93-112.

BAUMANN, K.-H., Böckel, B., and Frenz, M., 2004. Coccolith contribution to South Atlantic carbonate sedimentation. In: Thierstein, H.R., Young, J.R., Eds., *Coccolithophores: from molecular processes to global impact*. Berlin, Springer-Verlag: 367-402.

BORSETTI, A.M., Cati, F., 1972. Il nannoplankton calcaero vivente nel Tirreno centro-meridionale. *Giorn. Geol*., Ser. 2a, 38:395-414.

BRAND, L.E., 1994. Physiological ecology of marine coccolithophores. In: Winter, A., Siesser, W., Eds., *Coccolithophores*. Cambridge University Press, Cambridge: 39-49.

BROERSE, A.T.C., Brummer, G.-J.A., van Hinte, J.E., 2000a. Coccolithophore export production in response to monsoonal upwelling off Somalia (northwestern Indian Ocean). *Deep-Sea Reseach II*, 47: 2179-2206.

BROERSE, A.T.C., Ziveri, P., van Hinte, J.E., Honjo, S., 2000b. Coccolithophore (-$CaCo_3$) flux in the Sea of Okhotsk: seasonality, settling and alteration processes. *Marine Micropaleontology*, 39: 179-200.
BROERSE, A.T.C., Ziveri, P., van Hinte, J.E., Honjo, S., 2000c. Coccolithophore export production, species composition, and cocolith-$CaCo_3$ fluxes in the NE Atlantic (34^oN 21^oW and 48^oN 21^oW). *Deep Sea Research II*, 47: 1877-1906.
CHARLSON, R.J., Lovelock, J.E., Andreae, M.O., and Warren, S.G., 1987. Oceanic phytoplankton, atmospheric sulfur, cloud albedo, and climate. *Nature*, 326:665-661.
CLOCHIATTI, M., 1971a. Remarques sur quelques rhabdolithes de Méditerranée. *Cahiers Micropal.* Ser. 2(9):1-8.
CLOCHIATTI, M., 1971. Contribution à l'étude du nannoplancton calcaire du Néogène d'Afrique du Nord. *Mém. Nat. Hist. Nat*., série C, XXIII, 1-135pp.
CROS, L., Fortuño, J.-M., 2002. Atlas of Northwestern Mediterranean Coccolithophores. *Scientia Marina*, 66(1):1-186.
CRUDELI, D., Young, J.R., Erba, E., de Lange, G.J., Henriksen, K., Kinkel, H., Slomp, C.P., Ziveri, P., 2004. Abnormal carbonate diagenesis in Holocene-late Paleocene sapropel-associated sediments from the Eastern Mediterranean; evidence from *Emiliania huxleyi* coccolith morphology. *Marine Micropaleontology*, 52:217-240.
DIMIZA, M., Triantaphyllou, M., Dermitzakis, M.D., 2003. *Emiliania huxleyi* dynamics in the summer coccolithophore assemblages of Andros Island (middle Aegean Sea) coastal environments: first results. *Coccolithophores 2003: INA Workshop on extant coccolithophorid research, Abstracts Volume*. Gaia No. 11, Athens, Greece, 47-50.
ELESON, J.W., Bralower, T.J., 2005. Evidence of surface water temperature and productivity at the Cenomanian/Turonian boundary. *Micropaleontology*, 51(4): 319-332.
GAARDER, K.R. and Hasle, G.R., 1971. Coccolithophorids of the Gulf of Mexico. *Marine Science Bulletin*, 21(2):519-544.
GIRARDEAU, J., Monteiro, P.M.S., Nikodemus, K., 1993. Distribution and malformation of living coccolithophores in the northern Benguela upwelling system off Namibia. *Marine Micropaleontology*, 22:93-110.
HAECKEL, E., 1894. Systematische phylogenie der prosisten und pflanzen. Berlin, G. Reimer: i-xv, 1-400.
HALLEGRAFF, G.M., 1984. Coccolithophorides (calcareous nannoplankton) from Australian waters. *Botanica Marina*, 27:229-247.
HAY, W.W., 2004. Carbonate fluxes and calcareous nannoplankton. In: Thierstein, H.R., Young, J.R., Eds., *Coccolithophores: From Molecular Processes to Global Impact*. Berlin, Springer-Verlag: 509-528.
HONJO, S. and Okada, H., 1974. Community structure of coccolithophores in the photic layer of the mid-Pacific. *Micropaleontology*, 20:209-230.
KLEIJNE, A., 1992. Extant Rhabdosphaeraceae (coccolithophorids, class Prymnesiophyceae) from the Indian Ocean, Red Sea, Mediterranean Sea and North Atlantic Ocean. *Scripta Geologia*, 100:105-167.
KLEIJNE, A., 1991. Holococcolithophorids from the Indian Ocean, Red Sea, Mediterranean Sea and North Atlantic Ocean. *Marine Micropaleontology*, 17: 1-76.
KLEIJNE, A., 1990. Distribution and malformation of extant calcareous nannoplankton in the Indonesian Seas. *Marine Micropaleontology*, 16:293-316.

KLEIJNE, A. and Jordan, R.W., 1990. Proposed changes to the classification system of living coccolithophorids, II., INA Newsletter, 12:13.
KNAPPERTSBUSCH, M., 1993. Geographic distribution of living and Holocene coccolithophorids in the Mediterranean Sea. *Marine Micropaleontoloy*, 21: 219-247.
LECAL, J., 1965. A propos des modalités d'élaboration des formations épineuses des Coccolithophoridés. *Protistologica*, 1(2):63-70.
LINSCHOOTEN, C., van Bleijswijk, J.D.L., van Emburn, P.R., de Vrind, J.P.M., Kempers, E.S., Westbroek, P., de Vrind-de Jong, E.W., 1991. Role of the light-dark cycle and medium composition on the production of coccoliths by *Emiliania huxleyi* (Haptophyceae). *Journal of Phycology*, 27: 82-86.
LOHMANN, H., 1902. Die Coccolithophoridae, eine Monographie der Coccolithen bildenden Flagellaten, zugleich ein Beitrag zur Kenntnis des Mittelmeerauftriebs. *Arch. Protistenk*., 1(1):89-165.
MALIN, G., and Steinke, M., 2004. Dimethyl sulfide production: what is the contribution of the coccolithophores. In: Thierstein, H.R., Young, J.R., Eds., *Coccolithophores: from molecular processes to global impact*. Berlin, Springer-Verlag: 127-164.
McINTYRE, A., Bé, A.W.H., and Roche, M.B., 1970. Modern Pacific Coccolithophorida: a paleontological thermometer. *Transactions of the New York Academy of Science*, Series II, 32: 720-731.
MILLIMAN, J.D., 1993. Production and accumulation of calcium carbonate in the ocean: budget of a non-steady state. *Global Biogeochemical Cycles*, 7:927-957.
MURRAY, G., and Blackman, V.H., 1898. On the nature of the coccospheres and rhabdospheres. Philos. Trans. Royal Society of London, 190B: 427-441.
NISHIDA, S., 1979. Atlas of Pacific nannoplanktons. *News Osaka micropaleontol. Special Paper*, 3:1- 31.
NORRIS, R.E., 1984. Indian Ocean nannoplankton. I, Rhabdosphaeraceae (Prymnesiophyceae) with a review of extant taxa. *Journal of Phycology*, 20:27-41.
OKADA, H., and McIntyre, A., 1979. Seasonal distribution of modern coccolithophores in the western North Atlantic Ocean. *Marine Biology*, 54:319-328.
OSTENFELD, C., 1900. Über Coccosphaera. Zool. Anz., 23, 612:198-200.
ROST, B. and Riebesell, R., 2004. Coccolithophore calcification and the biological pump: response to environmental changes. In: Thierstein, H.R., Young, J.R., Eds., *Coccolithophores: from molecular processes to global impact*. Berlin, Springer-Verlag: 99-126.
STEINMETZ, J.C., 1991. Calcareous nannoplankton biocoenosis: sediment trap studies in the Equatorial Atlantic, Central Pacific, and Panama Basin. In: Honjo, S., Ed., *Ocean biocoenosis series no. 1*. Woods Hole, Woods Hole Oceanographic Institution: 1-85.
TRIANTAPHYLLOU, M.V., Dermitzakis, M.D., Dimiza, M.D., 2002. Holo- and Heterococcolithophores (calcareous nannoplankton) in the gulf of Korthi (Andros island, Aegean Sea, Greece) during late summer 2001. *Revue Paléobiol*., Genève, 21(1):353-369.
THIERSTEIN, H.R., Córtes, M.Y., and Haidar, A.T., 2004. Plankton community behavior on ecological and evolutionary timescales: when models confront evidence. In: Thierstein, H.R., Young, J.R., Eds., *Coccolithophores: from molecular processes to global impact*. Berlin, Springer-Verlag: 455-480.

WESTBROEK, P., Brown, C.W., Van Bleijswijk, J., Brownlee, C., Brummer, G.J., Conte, M., Egge, J., Farnandez, E., Jordan, R., Knappertsbusch, M., Stefels, J., Veldhuis, M., Wal, P., Van Der Waal, P., and Young, J.R., 1993. A model system approach to biological climate forcing: the example of *Emiliania huxleyi*. *Global and Planetary Change*, 8:27-46.

WINTER, A., Seisser, 1994. Atlas of Living Coccolithophores. In: Winter, A., Seisser, W.G., Eds., *Coccolithophores*. Cambridge, Cambridge University Press: 107-159.

WYRTKIE, K., 1973. Physical oceanography of the Indian Ocean. In: Zeitzschel, B., Ed., *The Biology of the Indian Ocean*. Berlin, Springer-Verlag: 18-36.

YANG, T., Wei, K., Chen, M., Ji, S., Gong, G., Lin, F., Lee, T., 2004. Summer and winter distribution and malformation of coccolithophores in East China Sea. *Micropaleontology*, 50:1, 157-170.

YANG, T.-N., and Wei, K.-Y., 2003, How many coccoliths are there in a coccosphere of the extant coccolithophorids? A compilation, Journal of Nannoplankton Research, v. 25, p. 7-15.

YOUNG, J.R., Geisen, M., Probert, I., 2005. A review of selected aspects of coccolithophore biology with implications for paleodiversity estimation. *Micropaleontology*, 51(4):267-288.

YOUNG, J.R., Henriksen, K., Probert, I., 2004. Structure and morphogenesis of the coccoliths of the CODENET species. In: Thierstein, H.R., Young, J.R., Eds., *Coccolithophores: from molecular processes to global impact*. Berlin, Springer-Verlag: 191-216.

YOUNG, J.R., Geisen, M., Cros, L., Kleijne, A., Sprengel, C., Probert, I., Østergaard, J., 2003. A guide to extant coccolithophore taxonomy. *Journal of Nannoplankton Research Special Issue* 1: 1-125.

ZIVERI, P., Thunell, R.C., 2000. Coccolithophore export production in Guaymas Basin, Gulf of California: response to climate forcing. *Deep Sea Research II*, 47: 2073-2100.

ZIVERI, P., Young, J.R., Van Hinte, J.E., 1999. Coccolithophore export production and accumulation rates. *Georesearch Forum*, 5:41-56.

Chapter 1

Table captions

Table 1: Stations VANC10MV05 and VANC10MV26: Conditions at time of sampling.

Table 2: Rhabdosphere occurrences on Filter-samples VANC10MV05B and VANC10MV26A.

Table 3: Characters measured in this study (See Fig. 2)

Table 4: Measurements of rhabdosphere and salpingiform rhabdoliths of *D. tubifera* from filter-sample VANC10MV05B, and comparison with published data. Malformed rhabdospheres were exluded from measurements. Bold values are those cited in text.

Table 5: Measurements of rhabdosphere and styliform rhabdoliths of *P. vandelii* from filter-sample VANC10MV26A, and comparison with published data. Malformed rhabdospheres were exluded from measurements. Bold values are those cited in text.

Table 6: Measurements of rhabdosphere and clavi/helatoform rhabdoliths of *R. clavigera* and *R.stylifera* from filter-sample VANC10MV05B, and comparison with published data. Malformed rhabdospheres were exluded from measurements. Bold values are those cited in text.

Table 7: Comparison between published measurements on rhabdoliths of *R. clavigera* and *R.stylifera* with our data.

Table 8: Measurements of *R. clavigera* and *R.stylifera* based on published photographs.

Table 9: Comparison between published measurements of numbers of rhabdoliths per rhabdosphere in *D. tubifera*, *P. vandelii*, *R. clavigera*, and *R.stylifera* and our data; a) and b) are values from 2 different sources (respectively, Kleijne 1992 and Knappertsbusch 1993).

Chapter 1
Tables

CTD Station	Sample	Date	Time started	Time finished	Ambient temperature °C	Depth m	Salinity ‰	Water filtered L
VANC10MV05	B	03-May-19	0:12	1:14	21.00	49	35.74	5
VANC10MV26	A	03-June-11	Un-known	Un-known	Unknown	Unknown	Un-known	5

Table 1.

Species	Sample Number	Total coccospheres	Complete coccospheres	Percent of total species	Collapsed coccospheres
Discosphaera tubifera	05B 26A	67	64	45	3
Palusphaera vandelii	05B 26A	2 97		1 51	2 97
Rhabdosphaera clavigera	05B 26A	10	3	7	7
Rhabdosphaera stylifera	05B 26A	12 2	9 2	8 1	3
Other species	05B 26A	59 91		39 48	

Table 2.

Species	Rhabdosphere/ Rhabdolith	Measurement	**Feature**
Discosphaera tubifera	Rhabdosphere	Diameter	Outer rhabdosphere
			Inner rhabdosphere
		Eccentricity	
	Salpingform process	Length	Process
		Diameter	Distal part
			Proximal part
		Eccentricity	Distal part
			Proximal part
Rhabdosphaera clavigera	Rhabdosphere	Diameter	Outer rhabdosphere
			Inner rhabdosphere
		Eccentricity	
	Claviform process	Length	Process
		Diameter	Proximal part
			Discoidal rhabdolith
		Eccentricity	Proximal part
		Eccentricity	Discoidal rhabdolith
Rhabdosphaera stylifera	Rhabdosphere	Diameter	Outer rhabdosphere
			Inner rhabdosphere
		Eccentricity	
	Helatoform process	Length	Process
		Diameter	Proximal part
			Discoidal rhabdolith
		Eccentricity	Proximal part
			Discoidal rhabdolith
Palusphaera vandelii	Rhabdosphere	Diameter	Inner rhabdosphere
			Outer rhabdosphere
	Styliform rhabdolith		Proximal part
		Eccentricity	Proximal part
		Length	Process

Table 3.

Discosphaera tubifera					
		(Ostenfeld, 1900)	**(Kleijne, 1992)**	**(Cros & Fortuño, 2002)**	**Sample 05B this paper**
# of rhabdospheres	total			6	67 (-70)
	complete			6	36
	collapsed				18
	broken rhabdoliths				5
	partially hidden				4
	malformed/dissolved/overgrown				4
Diameter of inner rhabdosphere	min			4.5	4.1
	max			6.5	6.5
	mean	6.0	6.0		5.3
	std dev				1.8
Eccentricity of inner rhabdosphere	min				**0.8**
	max				**1.0**
	mean				**0.9**
Diameter of outer rhabdosphere	min	15.0	15.0	12.5	9.7
	max	20.0	20.0	16	17.4
	mean				13.9
	std dev				1.9
Eccentricity of outer rhabdosphere	min				0.7
	max				1.0
	mean				0.9
# of rhabdoliths	min				**29**
	max				**66**
	2nd less min				35
	2nd less max				60
	mean	50	50		**48.5**
Length of rhabdolith	min			3.3	**2.2**
	max			5.7	**6.4**
	mean			4.0-5.0	4.3
	std dev				0.95
Eccentricity of base of rhabdolith	min	0.7			0.4
	max	0.8			1.0
	mean				**0.8**
Long axis of base of rhabdolith	min		1.7		0.9
	max	2.4	2.4		2.3
	mean				1.7

Table 4.

Short axis of base of rhabdolith	min	1.4	1.4		0.7
	max		1.6		2.1
	mean				1.6
Eccentricity of distal part of rhabdolith	min				0.4
	max				1.0
	mean				**0.9**
Short axis of distal part of rhabdolith	min	2.0	2.00		1.0
	max				**5.1**
	mean				3.1
	std dev				0.6
Long axis of distal part of rhabdolith	min				**0.9**
	max	4.2	4.20		4.3
	mean				2.8
	std dev				0.7

Table 4.

Palusphaera vandelii				
		(Kleijne, 1992)	**(Cros & Fortuño, 2002)**	**Sample 26A this paper**
# of rhabdospheres	total		10	97
	complete		2	23
	collapsed		8	97
	malformed			10(12)
Diameter of inner rhabdosphere	min		4	**2.7**
	max		5	**5.8**
	mean			**3.9**
Diameter of outer rhabdosphere	min		10	
	max		14	
	mean			
# of rhabdoliths	min			**20**
	max			**75**
	mean	40		**42.2**
Diameter of proximal side of rhabdolith	min	2	1.2	**0.7**
	max	2.3	2.1	**2.2**
	mean		1.5-1.9	1.4
	std dev			0.2
Length of rhabdolith	min		3.5	**1.6**
	max	>10	9	**9.8**
	mean			5.1
	std dev			1.2

Table 5.

***Rhabdosphaera* spp.**		***R. stylifera*** **(Murray & Blackman, 1898)**	***R. clavigera*** **(Lohmann, 1902)**	***R. "clavigera"*** **(Kleijne, 1992)**	***R. "clavigera"*** **(Cros & Fortuño, 2002)**	***R. clavigera*** **Sample 05B this paper**	***R. stylifera*** **Sample 05B this paper**
# of rhabdospheres	total				15	**10**	**12**
	complete				15	3	9
	collapsed					7	3
	malformed						5
Diameter of inner rhabdosphere	min	5	7.9	7.9	6	**8.7**	**4.4**
	max	10	8.6	8.6	10.5	**10.5**	**7.6**
	mean				8-9.2	**9.8**	**6.2**
Diameter of outer rhabdosphere	min	16	18.7	18.7	14	**19.3**	**7.8**
	max	19	19.7	19.7	21	**26.9**	**16.1**
	mean				17-20	**23.5**	**12.8**
# of discoidal rhabdoliths	min		15	15	12	**8**	**7**
	max		20	20	32	**26**	**24**
	mean					**19**	**14.1**
# of clavi/helatoform rhabdoliths	min				10	**14**	**8**
	max				32	**26**	**21**
	mean		20 +/-	20		**21.8**	**13.5**
Length of clavi/helatoform rhabdolith	min				3.7	**6.1**	**2.9**
	max				5.8	**10.9**	**5.2**
	mean		5 +/-	5	5.0-5.3	**8.4**	**4.3**
	std dev					**1.4**	**0.6**
Eccentricity of rhabdolith	min					0.4	0.5
	max					1.0	0.7
	mean					0.7	**0.6**
Long axis of discoidal rhabdolith	min		1.8	3	3.1	3.0	2.3

Table 6

	max		3.7	3.7	3.9	5.2	4.0
	mean				3.3-3.7	**4.2**	**3.1**
	std dev					**0.4**	**0.5**
Short axis of discoidal rhabdolith	min		0.6	1.8	2.5	1.8	1.3
	max		0.65	2.4	2.8	4.3	2.4
	mean					**2.9**	**1.8**
	std dev					**0.25**	**0.5**
Long axis of clavi/helatoform rhabdolith base	min			3.4			
	max			3.5			
Short axis of clavi/helatoform rhabdolith base	min			2.4			
	max			2.7			

Table 6.

	R. clavigera			*R. stylifera*		
	Max Diameter	Max Diameter	Max Length	Max Diameter	Max Diameter	Max Length
	discoidal rhabdolith	claviform rhabdolith	claviform rhabdolith	discoidal rhabdolith	helatoform rhabdolith	helatoform rhabdolith
Lohmann 1902	3.7					
Deflandre & Fert 1954	4.1	1.9	8	4.3	1.3	6.5
Halldal & Markali 1955				3.5	0.7	7.5
Cohen 1964	5	0.7	11	3.5	0.5	6
Cohen 1965a	3.8	0.9	13	2.7	0.45	4.3
Cohen 1965b	4.1	0.7	6.3			
Hay et al. 1967	5.5	1	9.4			
MacIntyre & Bé 1967				3.4	0.6	5
Boudreaux & Hay 1969	3.3	1.8	8.6	3.1	0.4	4.9
Bartolini 1970	4.6	1.1	8.2			
Clocchiatti 1971	4.2	0.8	7.6			
Clocchiatti 1971a	4.8	2	8	4.3	1.3	7.3
Kleijne 1992		3.5				
Cros and Fortuño 2002	3.9		5.8			
This paper	**5.2**		**10.9**	**4**		**5.2**
Avg	**4.35**	**1.44**	**8.8**	**3.6**	**0.75**	**5.8**
Min	3.3	0.7	5.8	2.7	0.4	4.3
Max	5.5	3.5	13	4.3	1.3	7.5

Table 7. Data from Clochiatti 1971a. Additional data from Kleijne (1992), Cros and Fortuño (2002), and data herein.

Author	Species	**Inner diameter (µm)**	Outer diameter (µm)	Mean length of clavi/helatoform rhabdoliths (µm)
Winter & Seisser 1994	R. clavigera	6.2	14.9	5.3
Winter & Seisser 1994	R. stylifera	6.6	15.2	5.2
Kleijne 1992	R. stylifera	7.0	13.0	3.9
Andruleit et al. 2006	R. stylifera	7.3	14.8	5.2
Cros & Fortuño 2002	R. stylifera	8.4	16.0	4.9
Cros & Fortuño 2002	R. stylifera	8.9	18.0	5.4
Young et al. 2005	R. stylifera	9.6	20.8	5.8
Young et al. 2002	R. stylifera	11.0	19.5	6.4

Table 8.

		(Yang and Wei 2003)		Our data		
		Number of rhabdoliths per rhabdosphere				
Species	Type of rhabdolith	Mean	Range	Range	Mean	Mode
D. tubifera	Salpingiform	a) ~50 b) 64		29-66	48.5	48
P. vandelii	Styliform	40	50 - >100	20-75	42.2	40
R. clavigera	Discoidal Helatoform	38 ~20	15 – 22	8-26 14-26	19 21.8	

Table 9.

Chapter 1

Figure captions

Figure 1: Location of sites.

Figure 2: Parameters measured in this study (see also Table 3) for a. *D. tubifera*, b. *R. stylifera*, c. *P. vandelii*, d. *R. clavigera*. D= diameter. L= length.

Figure 3: Distinctive morphology and structure of the rhabdoliths analyzed in this study (From Aubry 1999).

a. Structure of base on distal side

b. Structure of base on proximal side

c. Cross section of rhabdolith

d. Side view of stem of rhabdolith and proximal view of base

Figure 4: Intraspecific variability in *D. tubifera*.

Black dot= mean. Bar= amplitude.

a. Comparison of mean diameter of inner and outer rhabdospheres.

b. Comparison of the diameter of inner rhabdospheres vs. the number of salpingiform rhabdoliths. Note the lack of correlation between the two characters.

c. Mean length of individual rhabdoliths on successive rhabdospheres. Mean and amplitude of size variation of the length of rhabdoliths on individual rhabdospheres. X-axis= rhabdospheres arranged in order of increasing mean length of rhabdolith. Y-axis= bar shows lengths of all rhabdoliths per discrete rhabdosphere.

d. Comparison of eccentricity of the basal part of the salpingiform rhabdoliths on rhabdospheres.

e. Comparison of mean diameter (long and short axes) of the base of rhabdoliths.

f. Mean diameter of long and short axes of base of rhabdoliths.

g. Comparison of the mean length of rhabdoliths vs. mean diameter of the inner rhabdospheres. Note the lack of correlation between diameter of the rhabdosphere and the length of the rhabdolith and that the diameter of the rhabdospheres is sometimes less than length of salpingiform rhabdoliths.

h. Comparison of the mean diameter of rhabdospheres to the number of rhabdoliths.

Figure 5: Intraspecific variability in *P. vandelii*.

Black dot= mean. Bar= amplitude.

a. Comparison of mean diameter of rhabdospheres.

b. Comparison of mean diameter of rhadospheres and number of component rhabdoliths.

c. Mean diameter of the base of individual styliform rhabdoliths.

d. Mean length of rhabdoliths.

e. Comparison of the mean diameter of the base and the mean length of the rhabdoliths.

Figure 6: Inter- and intraspecific variability in *R. clavigera* and *R. stylifera*.

Outlined dot= mean of *R. clavigera*. Black square= mean of *R. stylifera*. Bar= amplitude.

a. Mean diameter of inner rhabdospheres.

b. Comparison of mean length of clavi/helatoform rhabdoliths. Measurements include rhabdoliths on both intact and partially collapsed rhabdospheres.

c. Comparison of mean diameter of long and short axes of discoidal rhabdoliths.

d. Comparison of number of clavi/helatoform rhabdoliths vs. the number of discoidal rhabdoliths per rhabdosphere.

e. Comparison of mean diameter of rhabdospheres vs. mean length of rhabdoliths.

Figure 7: Intraspecific variability in *R. clavigera*.

a. Mean diameters of inner vs. outer rhabdospheres.

b. Comparison of number of claviform vs. discoidal rhabdoliths.

Figure 8: Intraspecific variability in *R. stylifera*.

a. Mean diameters of the inner and outer rhabdospheres.

b. Comparison of the number of helatoform vs. discoidal rhabdoliths.

Figure 9: Map of the Indian Ocean showing the occurrences of *D. tubifera, P. vandelii, R. clavigera,* and *R. stylifera*. Compiled from Kleijne (1992), and Norris (1984), and data herein.

Figure 10: Unimodal variability of various morphological characters in *D. tubifera* and *P. vandelii*.

Figure 11: Unimodal variability of various morphological characters in *R. clavigera* and *R. stylifera*.

Figure 12: Side view of rhabdospheres with varying numbers of rhabdoliths:

a. *Discosphaera tubifera*. Upper right: rhabdosphere with few rhabdoliths; lower right: rhabdosphere with many imbricating rhabdoliths (representation of imbrication is coarse)

b. *Rhabdosphaera clavigera* (right) and *R. stylifera* (left).

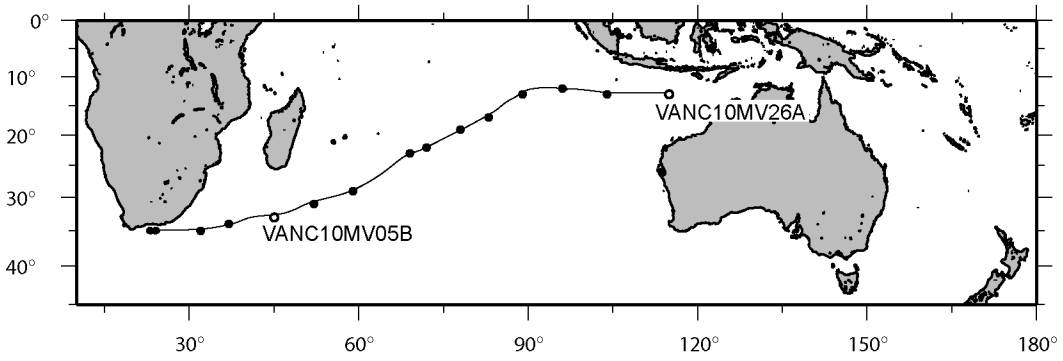

GMT 2006 Apr 27 16:59:44 R.Earley 2006

Figure 1

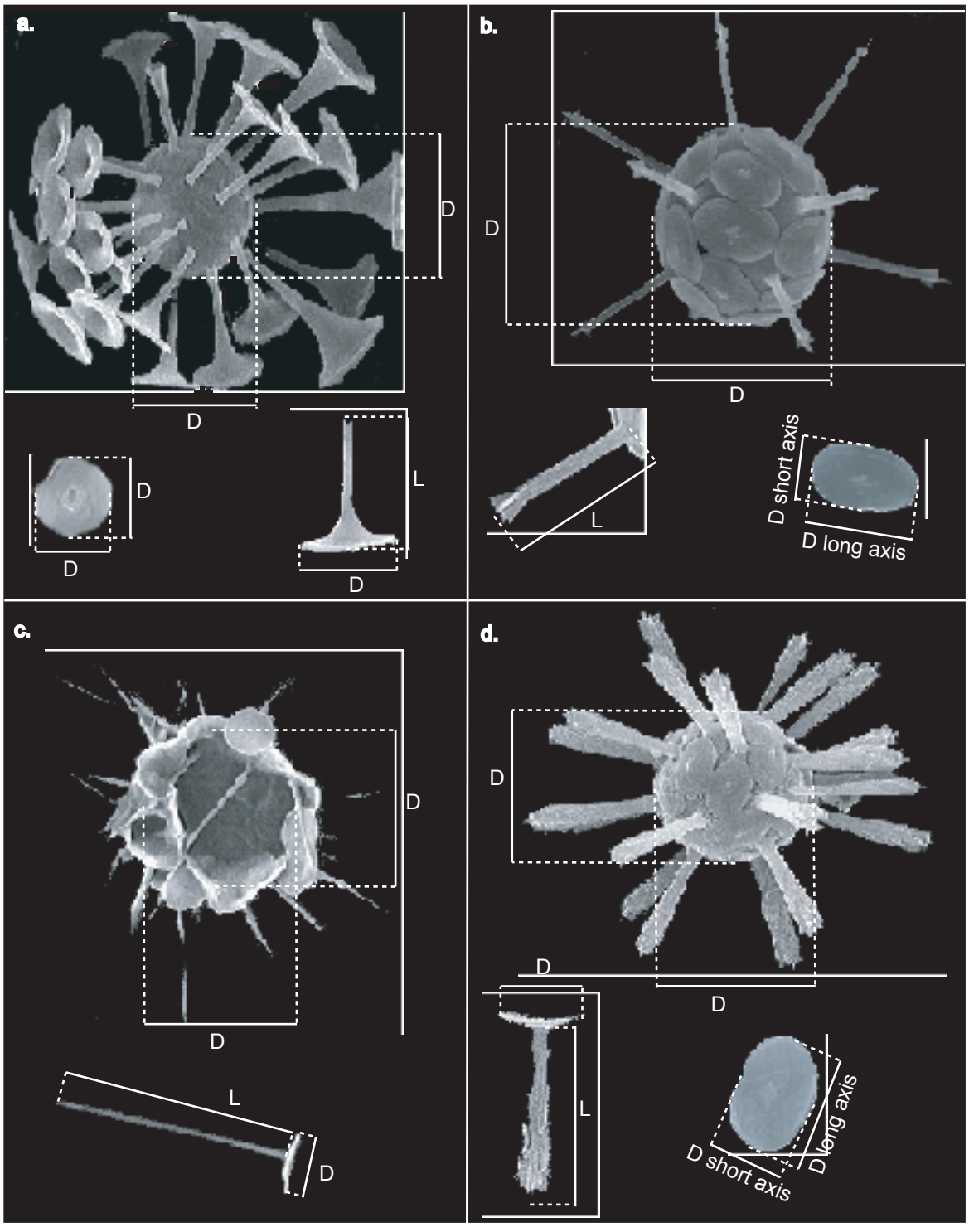
a.
D
D
D
D
L
D
b.
D
D
L
D short axis
D long axis
c.
D
D
L
D
d.
D
D
D
L
D short axis
D long axis

Figure 2

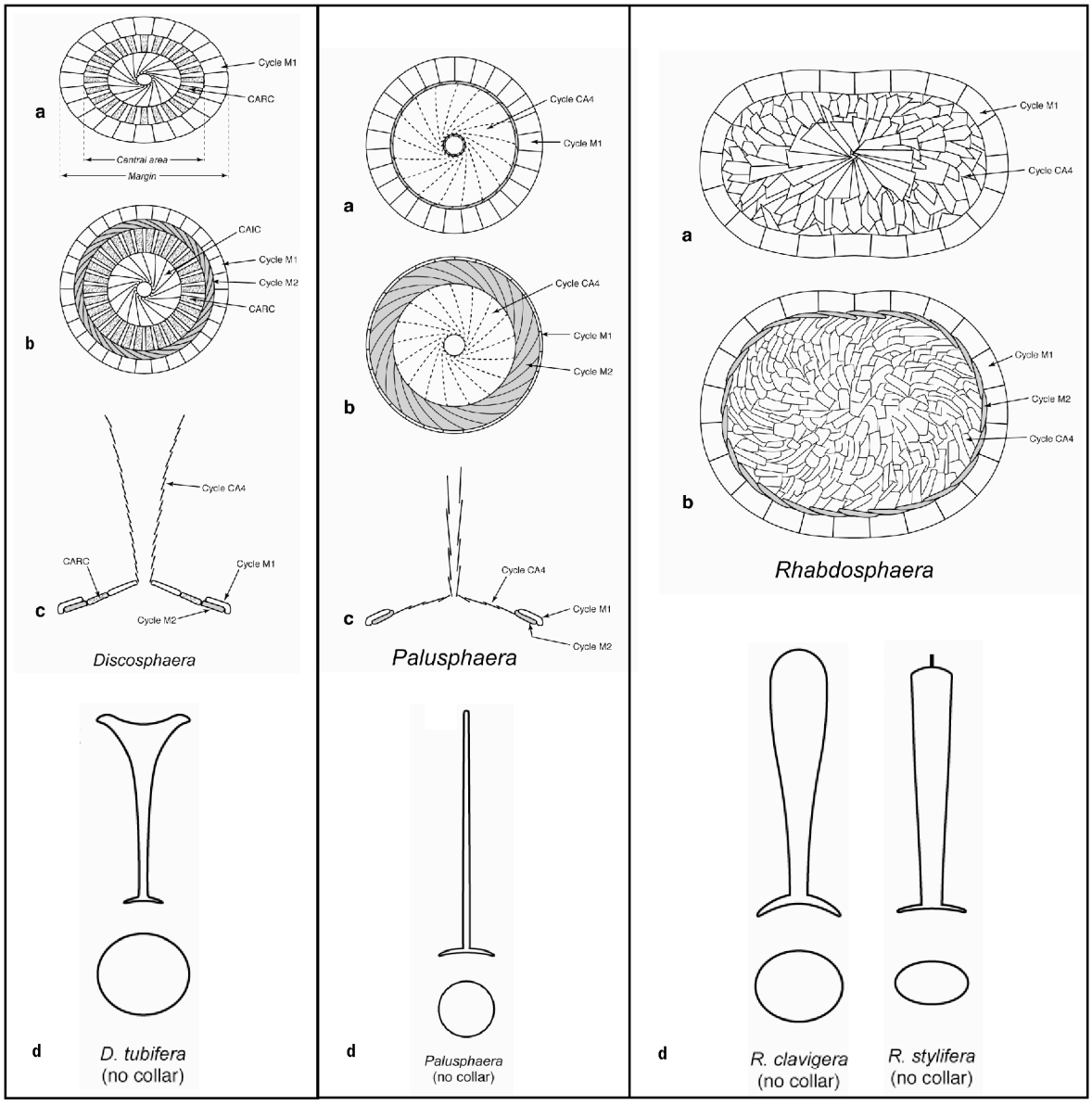

a. *D. tubifera* b. *P. vandelii* c. *R. clavigera, R. stylifera*

Figure 3

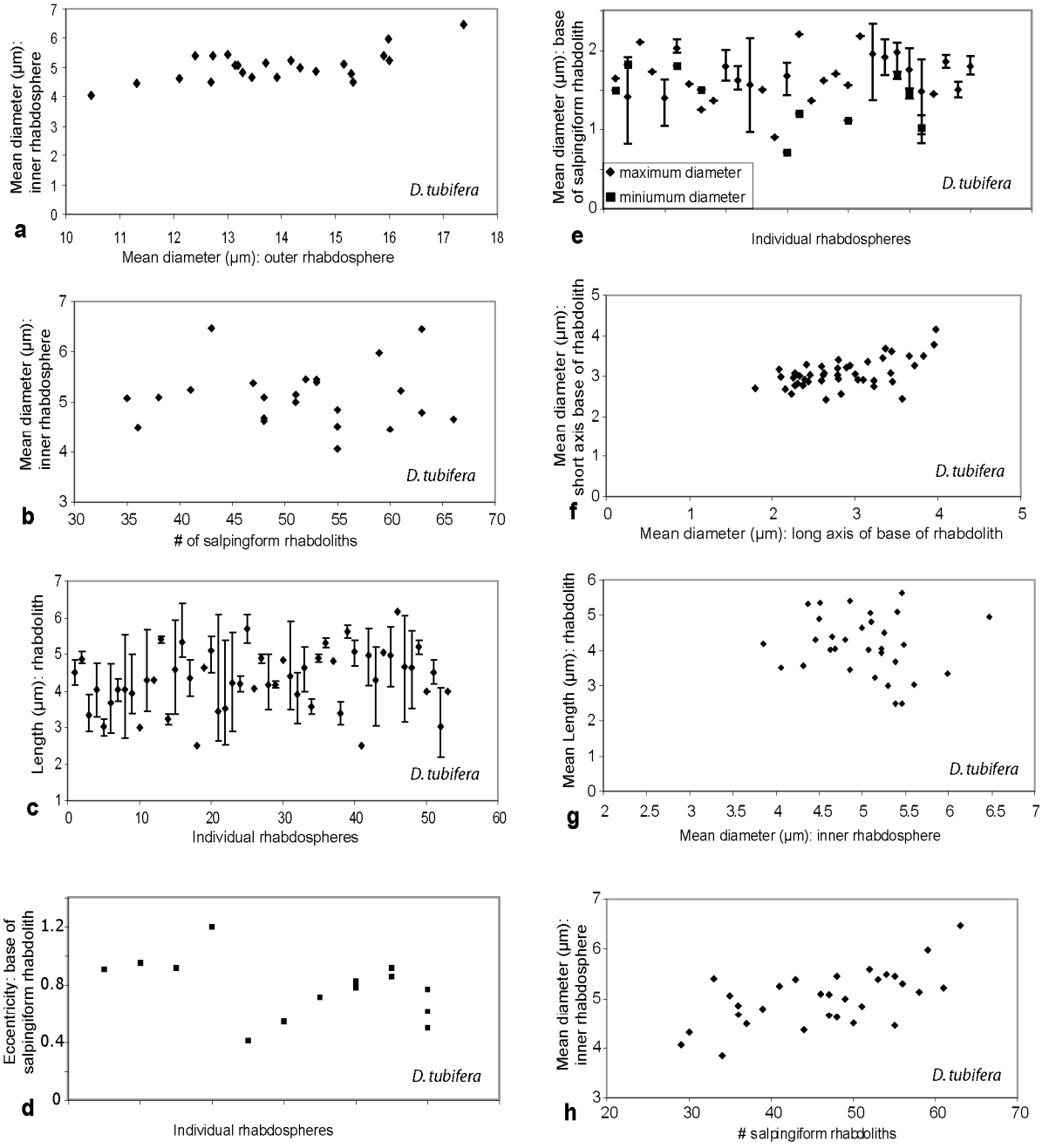
a
Mean diameter (µm): inner rhabdosphere
Mean diameter (µm): outer rhabdosphere
D. tubifera
b
Mean diameter (µm): inner rhabdosphere
# of salpingform rhabdoliths
D. tubifera
c
Length (µm): rhabdolith
Individual rhabdospheres
D. tubifera
d
Eccentricity: base of salpingiform rhabdolith
Individual rhabdospheres
D. tubifera
e
Mean diameter (µm): base of salpingiform rhabdolith
maximum diameter
miniumum diameter
Individual rhabdospheres
D. tubifera
f
Mean diameter (µm): short axis base of rhabdolith
Mean diameter (µm): long axis of base of rhabdolith
D. tubifera
g
Mean Length (µm): rhabdolith
Mean diameter (µm): inner rhabdosphere
D. tubifera
h
Mean diameter (µm): inner rhabdosphere
salpingiform rhabdoliths
D. tubifera

Figure 4

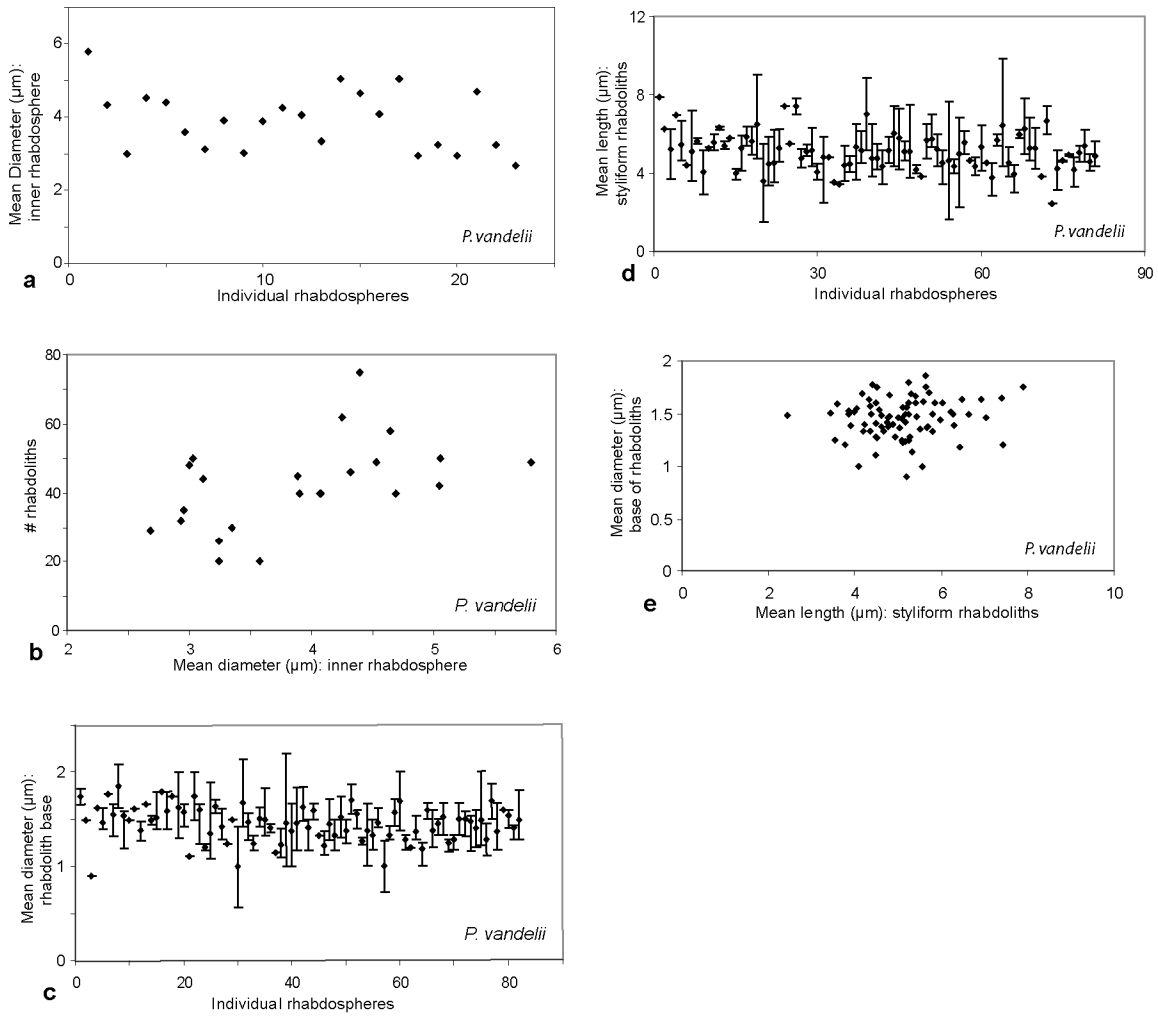
Mean Diameter (µm): inner rhabdosphere
P.vandelii
a
Individual rhabdospheres
Mean length (µm): styliform rhabdoliths
P.vandelii
d
Individual rhabdospheres
rhabdoliths
P. vandelii
b
Mean diameter (µm): inner rhabdosphere
Mean diameter (µm): base of rhabdoliths
P.vandelii
e
Mean length (µm): styliform rhabdoliths
Mean diameter (µm): rhabdolith base
P. vandelii
c
Individual rhabdospheres

Figure 5

Figure 6

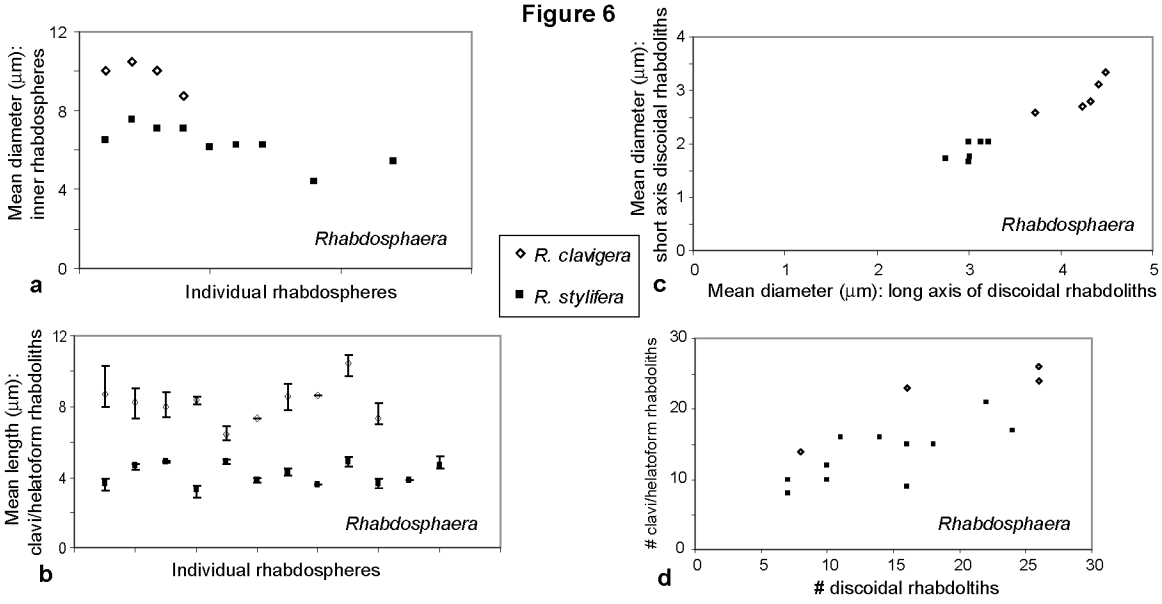

Figure 7

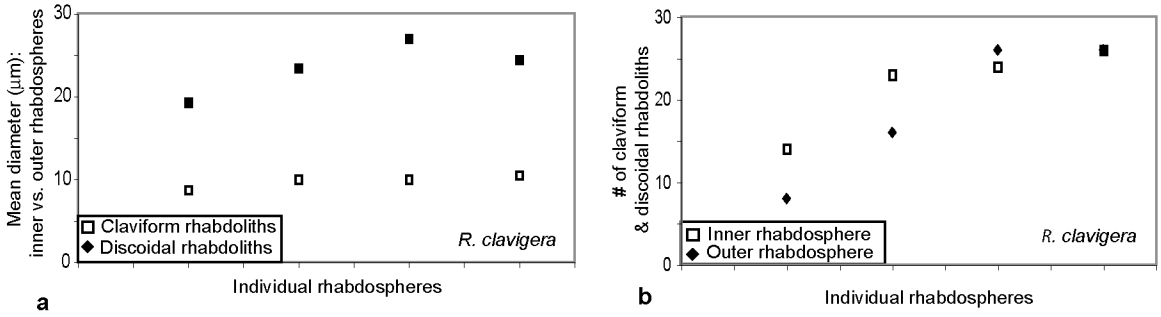

Figure 8

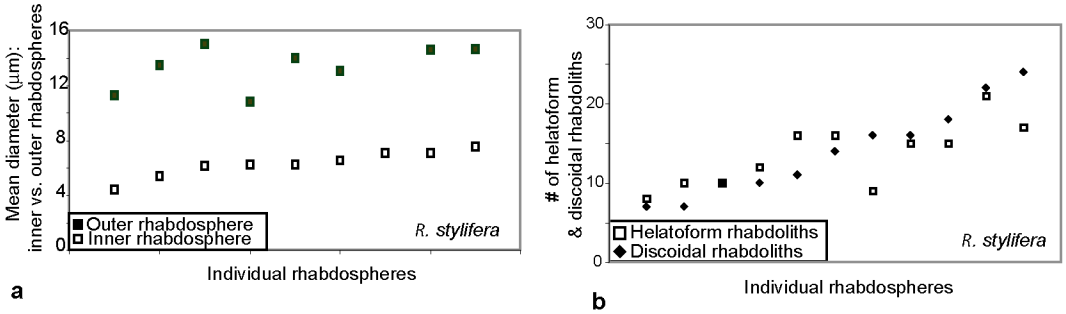

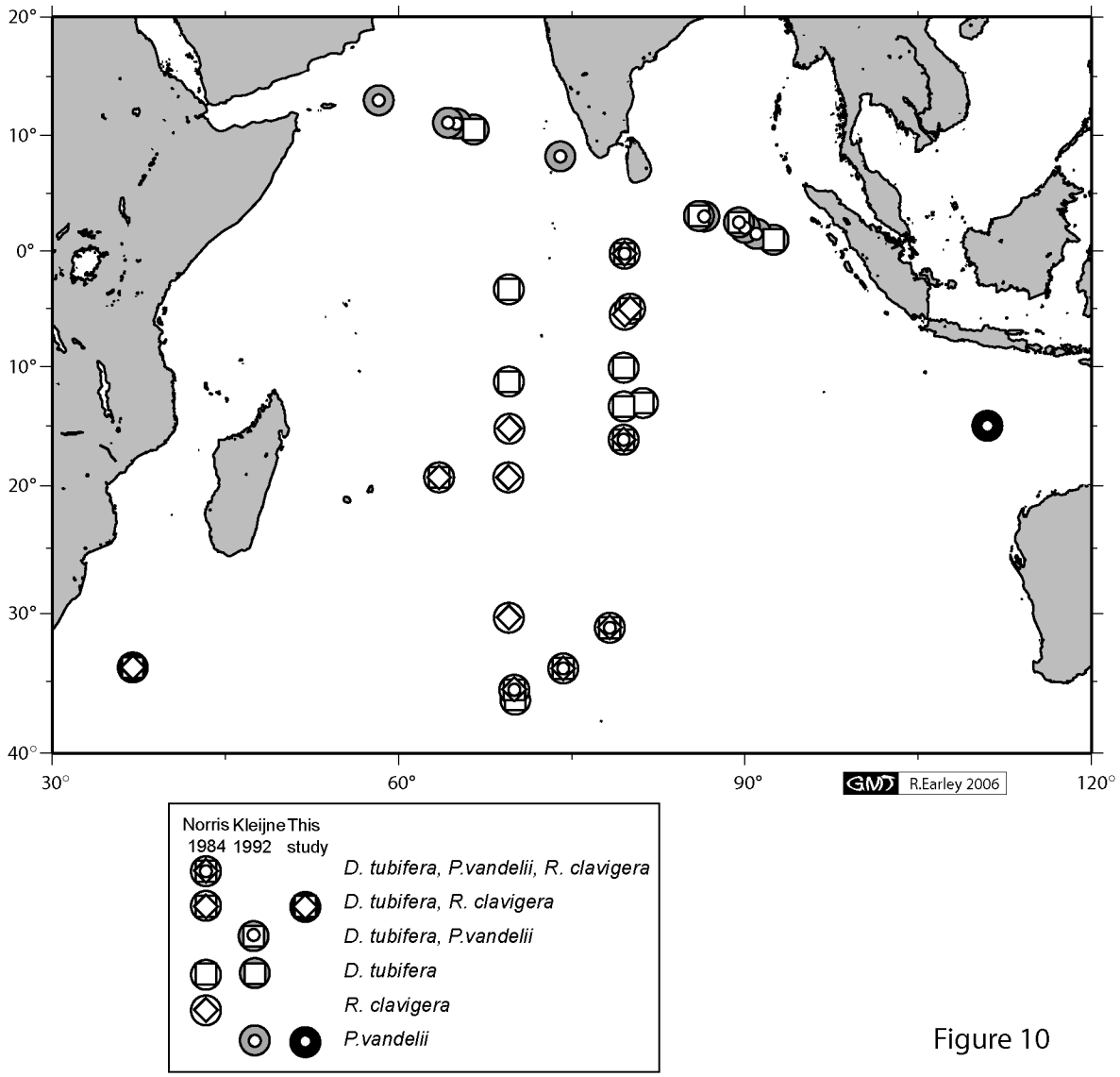
20°
10°
0°
10°
20°
30°
40°
30°
60°
90°
120°
GMT R.Earley 2006
Norris 1984
Kleijne 1992
This study
D. tubifera, P.vandelii, R. clavigera
D. tubifera, R. clavigera
D. tubifera, P.vandelii
D. tubifera
R. clavigera
P.vandelii

Figure 10

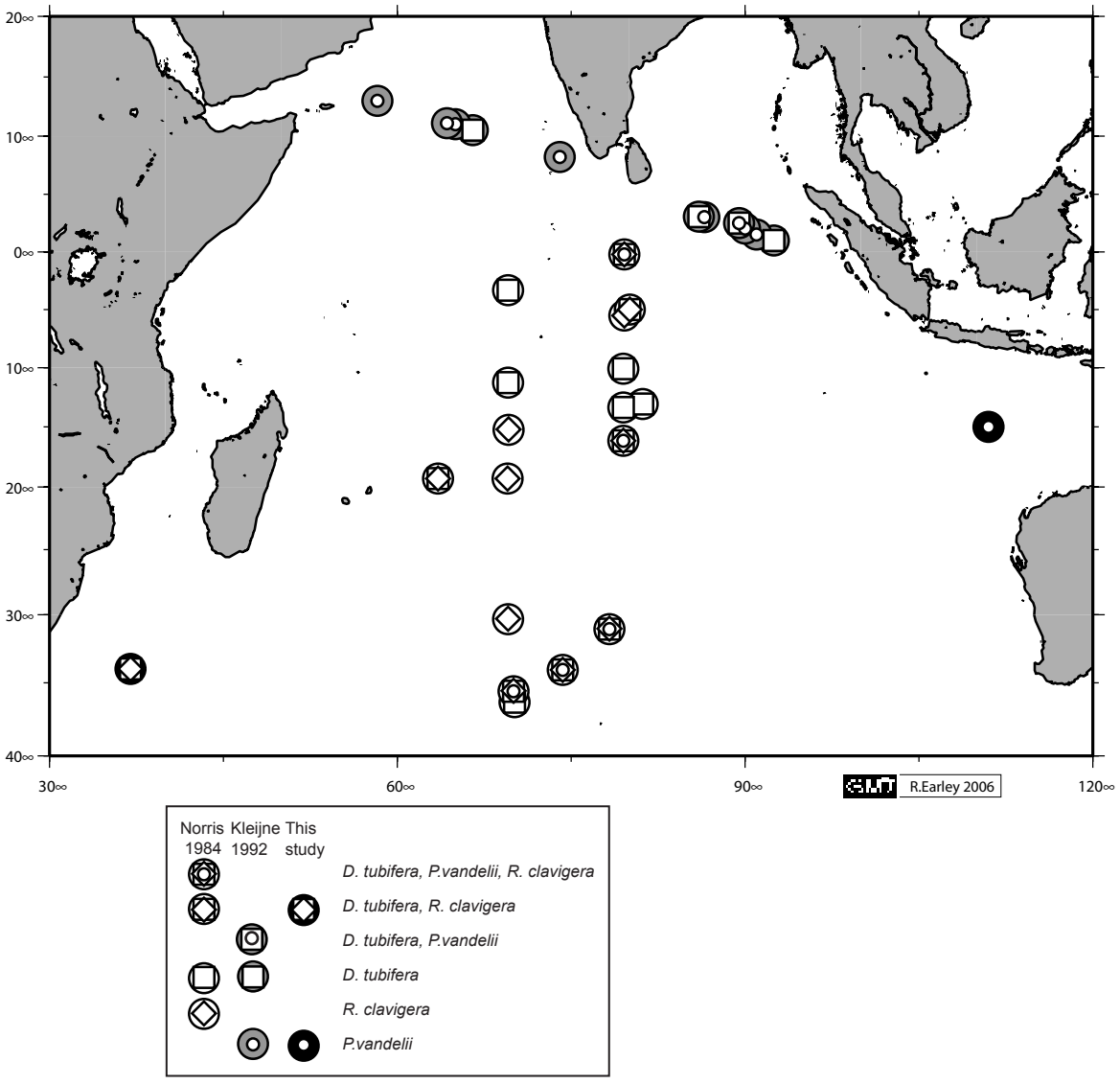
20∞
10∞
0∞
10∞
20∞
30∞
40∞
30∞
60∞
90∞
120∞
R.Earley 2006
Norris 1984
Kleijne 1992
This study
D. tubifera, P.vandelii, R. clavigera
D. tubifera, R. clavigera
D. tubifera, P.vandelii
D. tubifera
R. clavigera
P.vandelii

Figure 9

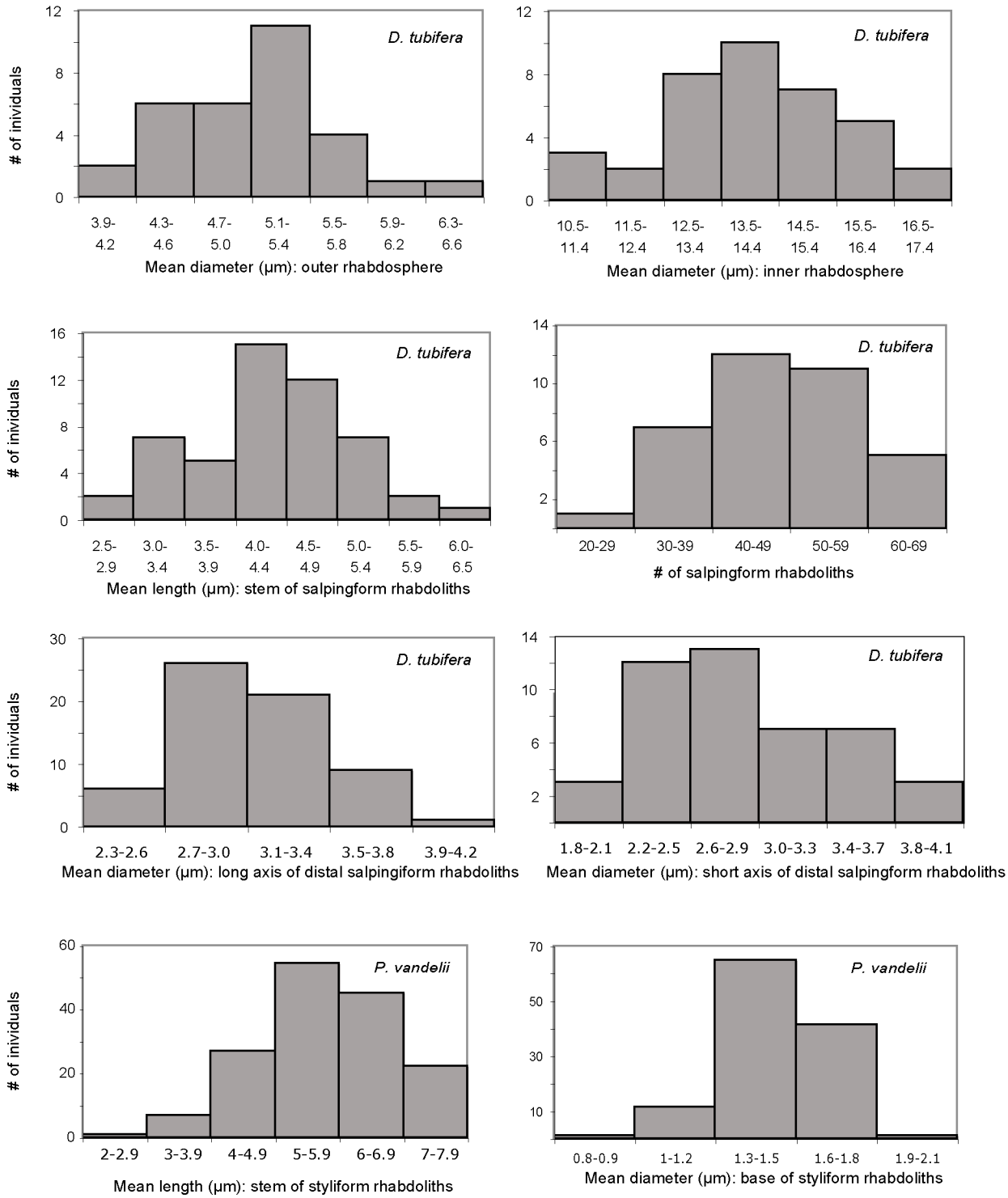
D. tubifera
# of inividuals
Mean diameter (µm): outer rhabdosphere
Mean diameter (µm): inner rhabdosphere
Mean length (µm): stem of salpingform rhabdoliths
# of salpingform rhabdoliths
Mean diameter (µm): long axis of distal salpingiform rhabdoliths
Mean diameter (µm): short axis of distal salpingform rhabdoliths
P. vandelii
Mean length (µm): stem of styliform rhabdoliths
Mean diameter (µm): base of styliform rhabdoliths

Figure 10

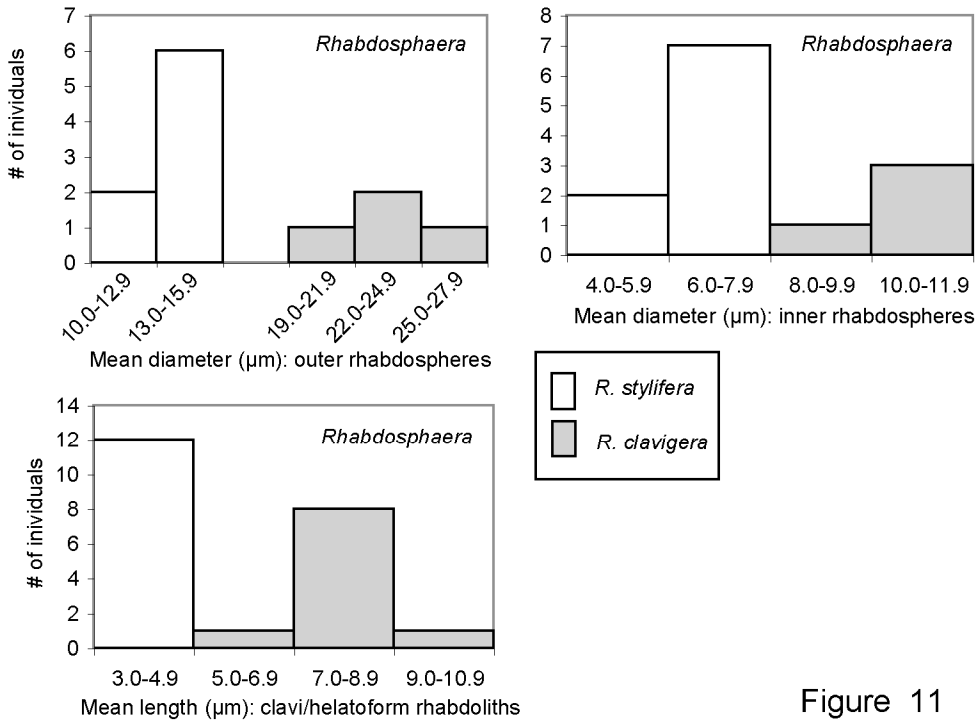
Rhabdosphaera
# of inividuals
0
1
2
3
4
5
6
7
10.0-12.9
13.0-15.9
19.0-21.9
22.0-24.9
25.0-27.9
Mean diameter (µm): outer rhabdospheres
Rhabdosphaera
0
1
2
3
4
5
6
7
8
4.0-5.9
6.0-7.9
8.0-9.9
10.0-11.9
Mean diameter (µm): inner rhabdospheres
R. stylifera
R. clavigera
Rhabdosphaera
# of inividuals
0
2
4
6
8
10
12
14
3.0-4.9
5.0-6.9
7.0-8.9
9.0-10.9
Mean length (µm): clavi/helatoform rhabdoliths

Figure 11

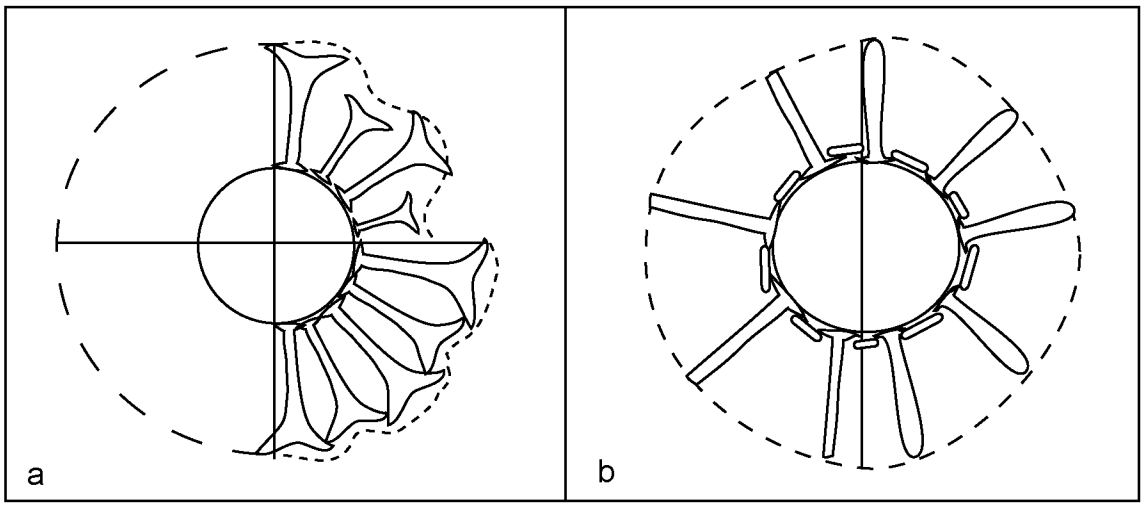

Figure 12

Chapter 1

Plate captions

Plate 1: Figs. 1, 4-6; bar=1 μm. Figs. 2-3; bar=10 μm. 1-6. *Discosphaera tubifera*. Filter-sample VANC10MV05B.

3. *Ceratolithus cristatus* hoops covering lower right salpingiform rhabdoliths.

5: Note detailed view of proximal side of salpingiform rhabdoliths within collapsed rhabdosphere.

Note that the stemmed rhabdoliths cover the inner rhabdosphere very differently in different rhabdospheres, from complete obstruction of the inner rhabdosphere, (fig. 3) to very sparse coverage (fig. 5).

Plate 2: Figs 1-6; bar=1 μm. 1-6. *Palusphaera vandelii*. Filter-sample VANC10MV26A.

1-2, 5: Collapsed rhabdosphere with styliform rhabdoliths in place.

3-4: Collapsed rhabdospheres with out of place styliform rhabdoliths.

6: Collapsed rhabdosphere with poorly formed styliform rhabdoliths.

Plate 3: Figs. 3; bar=1 μm. Fig. 1-2, 4-6; bar=10 μm. 1,3,5. *Rhabdosphaera stylifera*; 2, 4, 6. *Rhabdosphaera clavigera*. Filter-sample VANC10MV05B.

1, 3, 5: Note scale bar relative to that of figs. 2, 4, 6 and the stylus-shaped helatoform rhabdoliths.

2, 4, 6: Note larger size relative to figs. 1, 3, 5, and club-shaped claviform rhabdoliths.

2: Note isolated spine of *Meringosphaera mediterranea* Lohmann above *R. clavigera*.

Plate 4: Figs. 1-4; bar=1 μm. 1-4. *Discosphaera tubifera*. Filter-sample VANC10MV05B.

1: Elliptical rhabdosphere with poorly formed salpingiform rhabdoliths.

2: Spherical to subspherical rhabdospheres with irregularly formed salpingiform rhabdoliths.

3: Extremely irregularly shaped rhabdosphere with very poorly formed and broken salpingiform rhabdoliths.

4: Irregularly shaped rhabdosphere with broken salpingiform rhabdoliths.

Plate 5: Figs. 1-6; bar=1 μm. Fig. 7; bar=10 μm. 1-6. *Rhabdosphaera stylifera*.

1-3, 5-7. Filter-sample VANC10MV05B. 4. Filter-sample VANC10MV26A.

1, 5-7: Elliptical irregularly shaped rhabdosphere with poorly formed discoidal and helatoform rhabdoliths.

2-3. Collapsed, flattened rhabdospheres with poorly formed discoidal and helatoform rhabdoliths.

4. Extremely irregularly shaped rhabdosphere with poorly formed, highly curved discoidal and helatoform rhabdoliths.

7. *Rhabdosphaera clavigera.* Poorly formed, broken discoidal and claviform rhabdoliths.

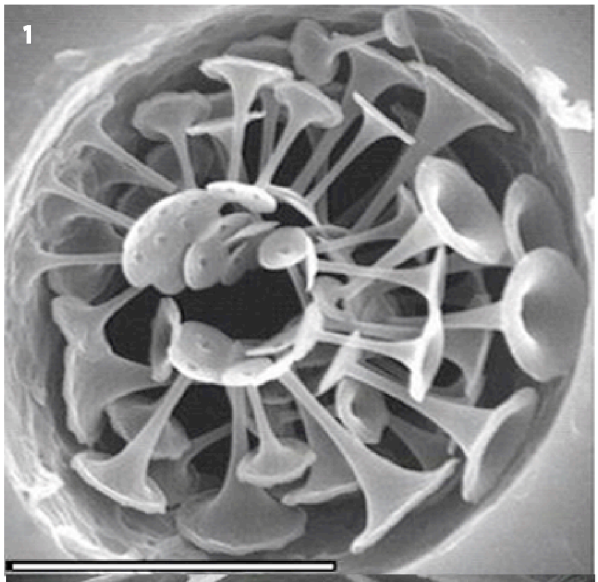

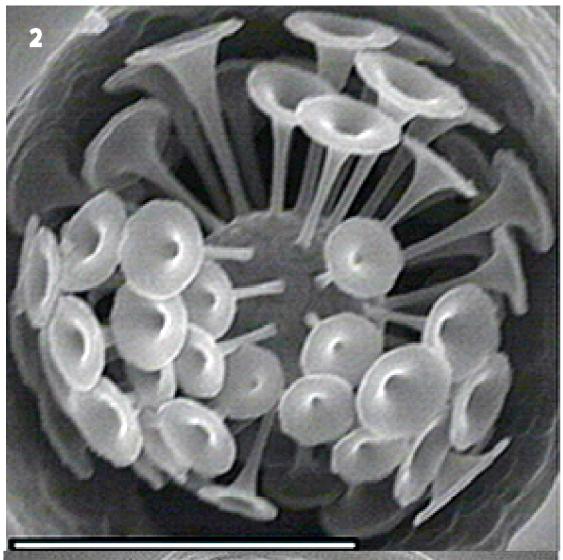

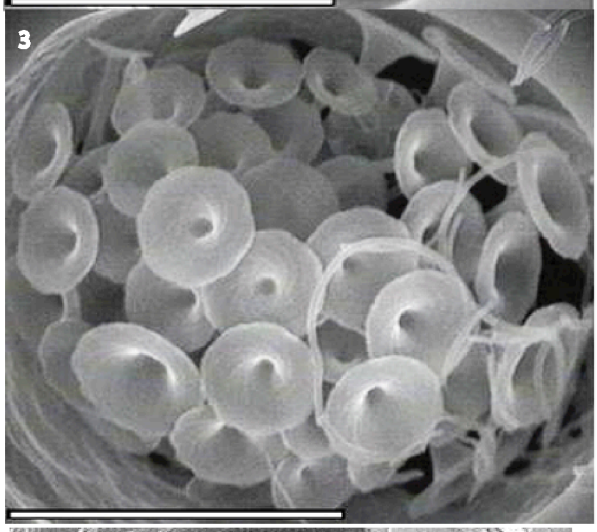

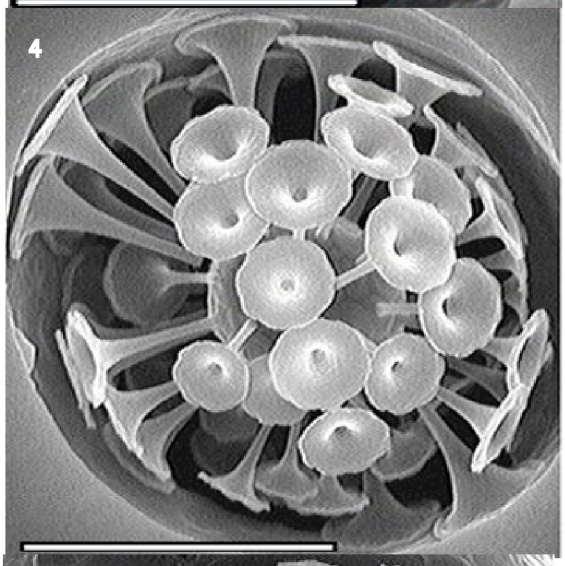

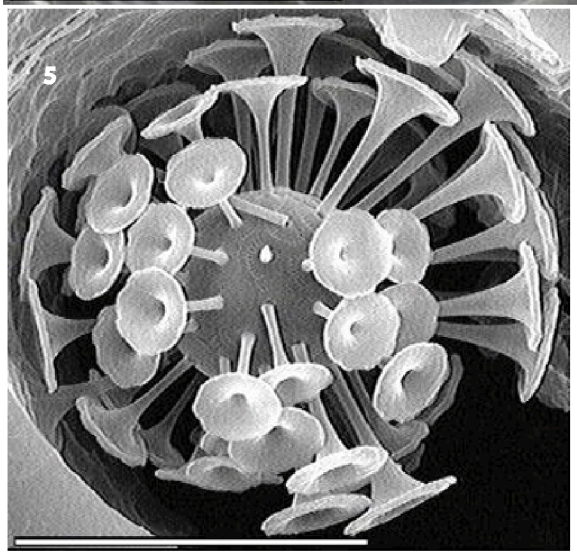

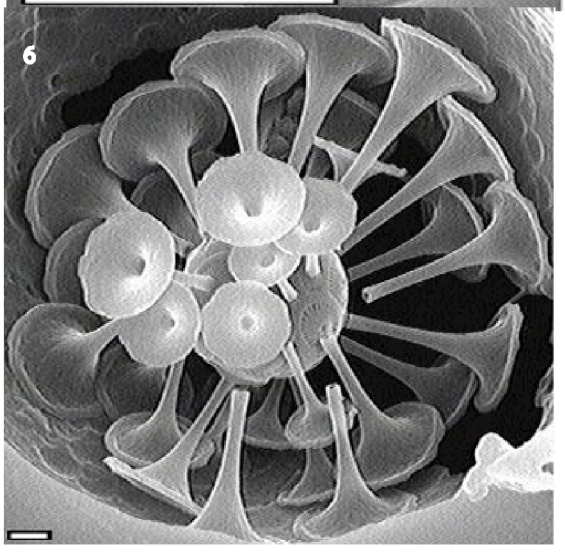

Plate 1

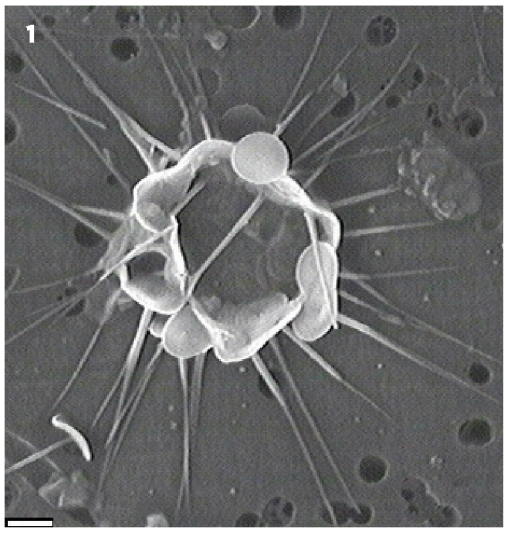

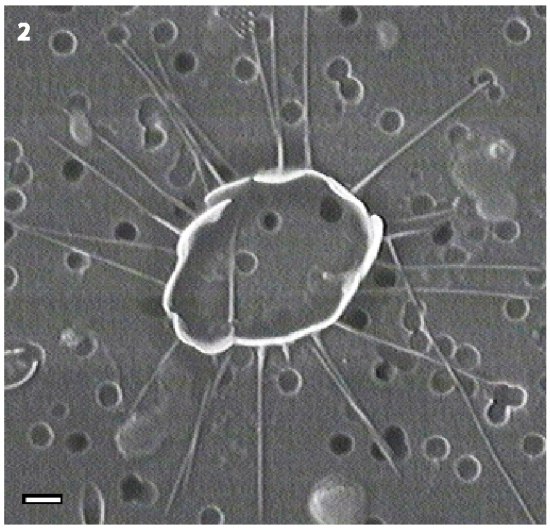

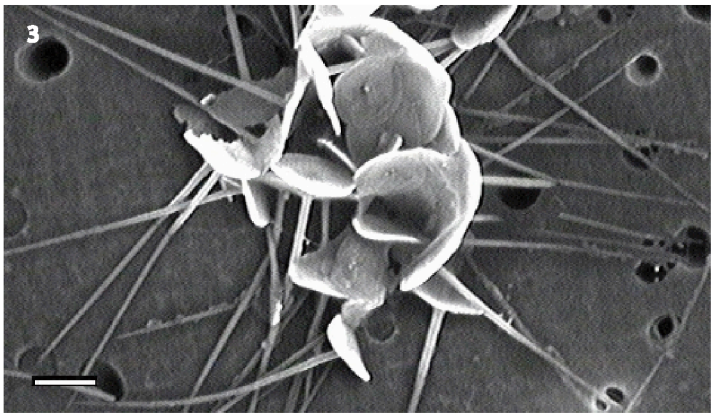

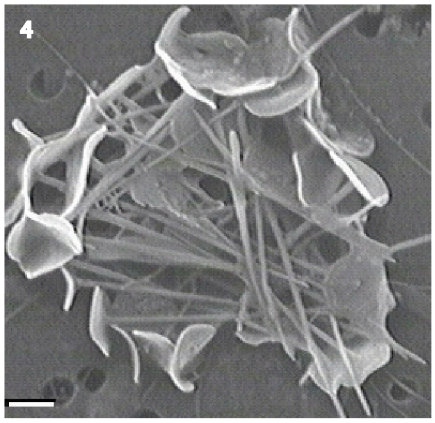

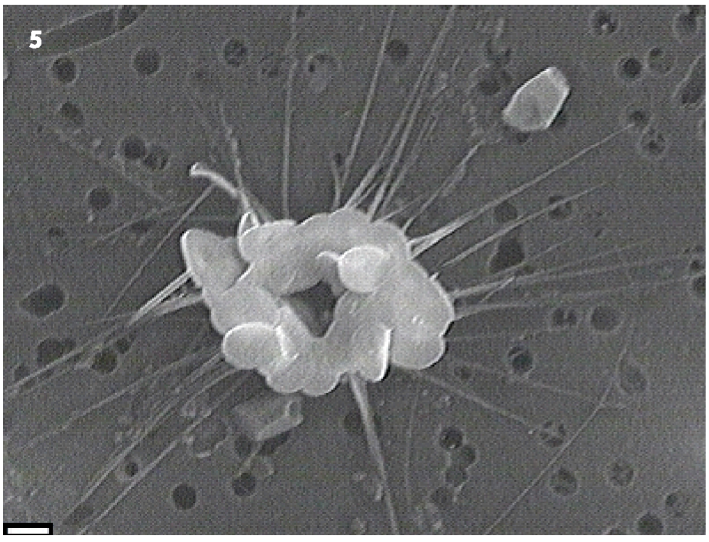

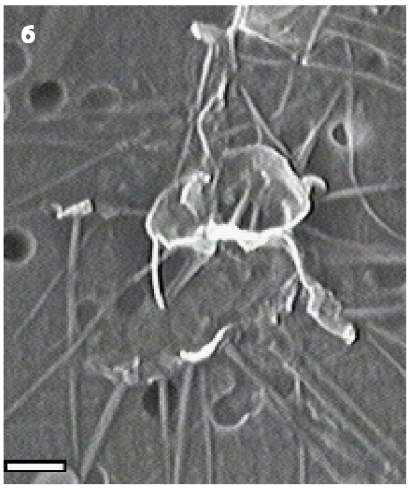

Plate 2

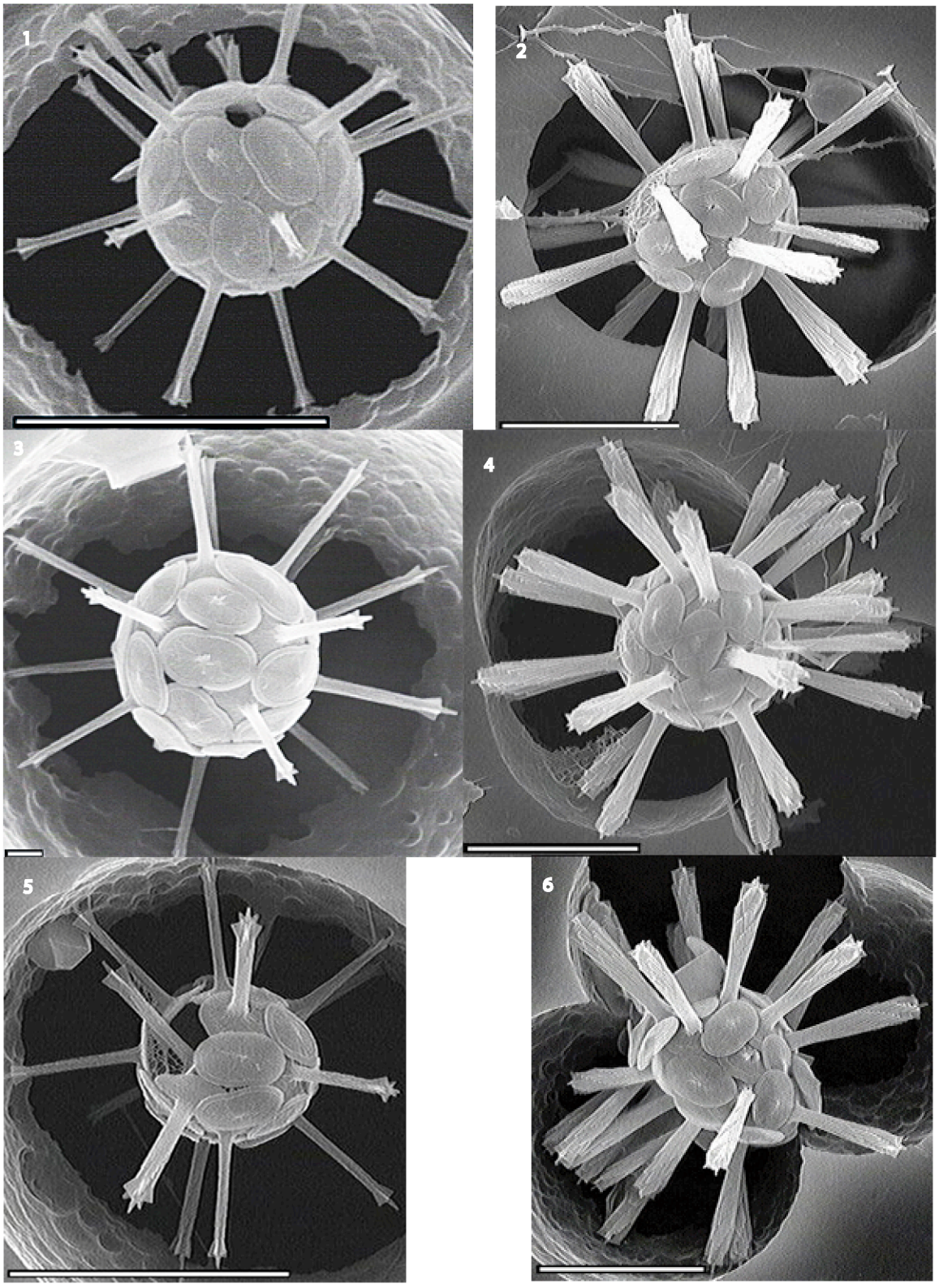

Plate 3

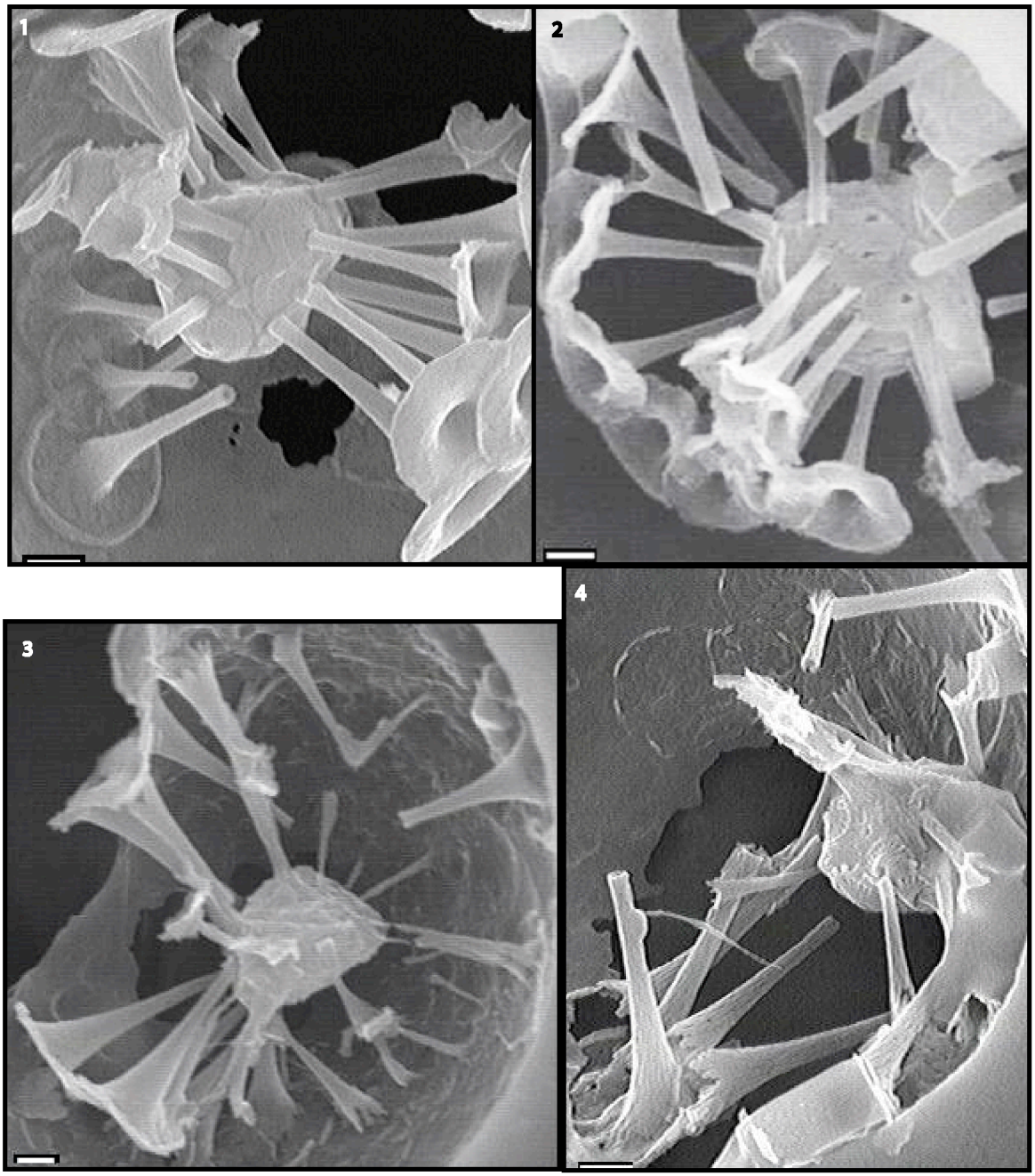

Plate 4

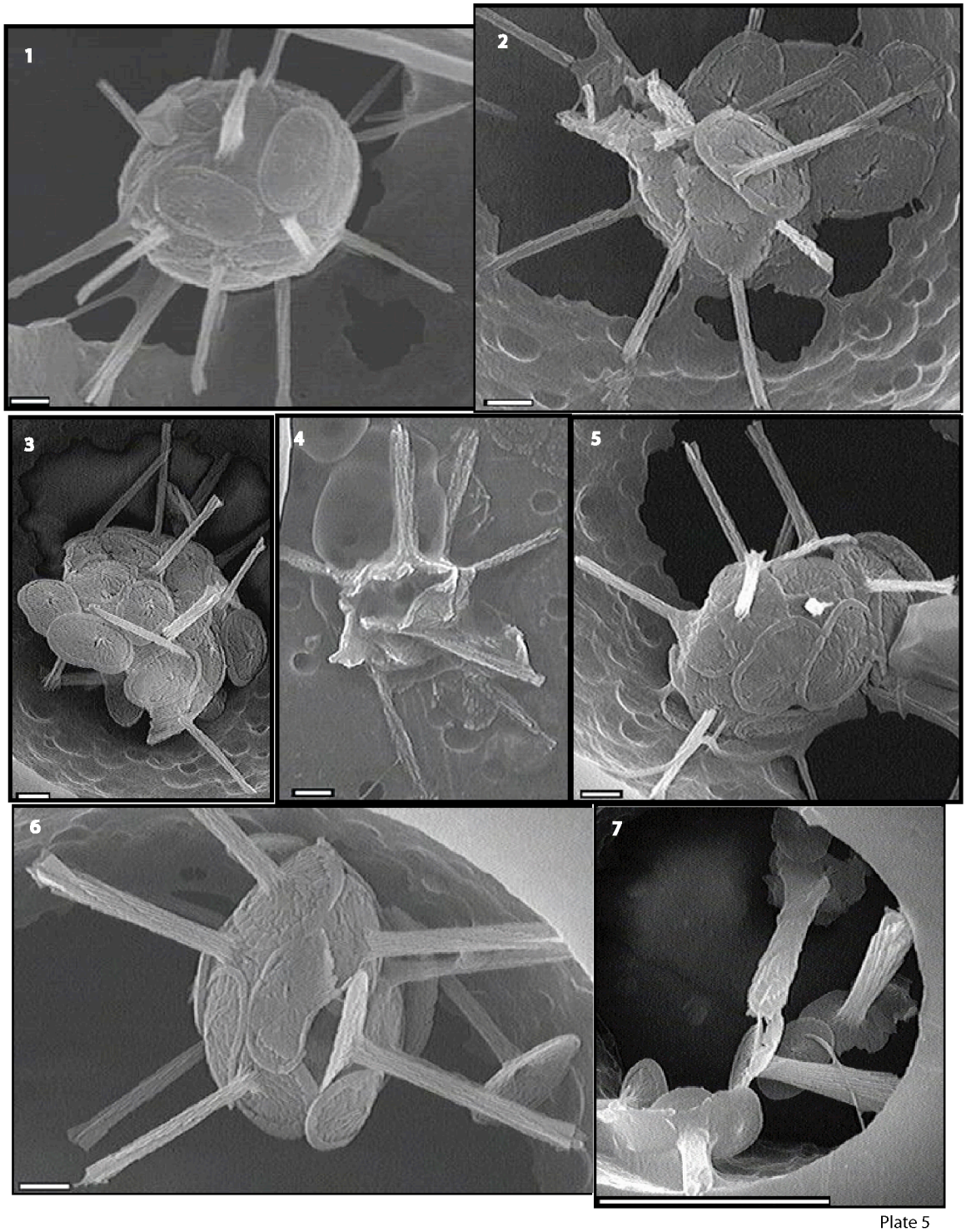

Plate 5

Chapter 2

An unusual coccolithophore community within the deep photic zone in the Indian Ocean*

*this chapter is the basis for Aubry, M.-P. and Kahn, A., 2006. Coccolithophores from the deep photic zone of the Indian Ocean: a case for morphological convergence as a forcing mechanism in the evolution of the calcareous nannoplankton. Micropaleontology, 52(5): 411-431.

Abstract

I describe 2 new forms of coccolithophores from the deep photic zone. These forms are complex and strongly morphologically differentiated from other coccolithophore genera. They are comprised of the smallest yet described coccospheres and constituent coccoliths, which are differentiated by their positions on the coccosphere, and are unusual in shape, structure, and degree of varimorphism. They are found in relatively high concentrations within the deep photic zone in the Indian Ocean along with *Florisphaera profunda*.

1- Introduction

The deep photic zone (DPZ) is inhabited by a specific coccolithophore community (Okada and Honjo 1973). In the course of an investigation of the intraspecific variability within this community in the Indian Ocean, I encountered 4 taxa that are unusual by their minuteness, the hemispheric shape of their coccospheres, and the 3 different morphologies of coccoliths asymmetrically arranged on the coccosphere. The coccoliths are identifiable by both their morphologies and their arrangement on the coccosphere. In this chapter, I describe these 4 taxa.

2- Methods

The coccospheres described here were collected from sample VANC10MV07D (HV Melville Hydroacoustic and Biological Sampling Cruise), taken on May 3, 2003 (between 16:49 and 17:45 h) at a depth of 120 m on the eastern side (33°17.91'S, 45° 21.72'E) of the Indian Ocean (Fig. 1). Seawater temperature and salinity at the sample location (120 m) were 18°C, and 35.67‰, respectively. Five liters of seawater were vacuum filtered onto a polycarbonate (Osmonics) filter 47 mm diameter with a 0.8 µm pore size. I examined approximately 8 mm^2 of the filter at magnifications ranging from 5000x to 120,000x using an S.E.M., and systematically photographed all coccospheres encountered on the filter. Photographs were then used for measurements using Image J graphics measuring program.

The forms described here represent a small percentage (8%) of the 670 coccospheres (representing 23 species) in our sample, which is strongly dominated (42.3%) by *Florisphaera profunda sensu lato*. *Emiliania huxleyi*, *A. robusta*, and *G. flabellatus* and *G. striatus*, were found in lower concentrations (4.7%, 4.0%, 1.9%, and 0.9%, respectively). All coccospheres of interest in this paper were found flattened on the filter, indicating that the cell has collapsed during vacuum filtering.

3- Observations

Among the 4 taxa discussed here, 2 are undescribed. I refer to them as Coccolithophore sp. Z and Coccolithophore sp. 1, after Cros and Fortuño (2002), who named Coccosphere sp. 1 from the northwest Mediterranean Sea. Coccolithophore sp. Z is represented here by 21 coccospheres, Coccolithophore sp. 1 by 14

coccospheres. In both forms the coccospheres and coccoliths are exceptionally tiny (diameters of coccosphere and proximal side of coccoliths range from 3.1 to 5.9 μm and 0.7 to 1.3 μm, respectively) (Table 1). The coccospheres are roughly hemispherical. I refer to the convex side as the domal side and the planar, or slightly concave, side as the antidomal side. They consist of coccoliths that are differentiated according to morphology and by position on either the domal or antidomal side of the coccosphere (Pls. 1, 2).

On the antidomal side in both forms, randomly arranged jointive to slightly overlapping discoidal coccoliths form a single layer in the central area which is overlapped peripherally by a girdle of regularly arranged distally convex discoidal coccoliths (Pls. 1e, 2a-b; Figs. 2a, 3a). In Coccolithophore sp. Z, the centrally located discoidal coccoliths are concave distally whereas in Coccolithophore sp. 1 they have a long narrow protrusion. The girdle coccoliths (of both forms) are elliptical with a narrow rim composed of narrow rectangular elements (Pls. 1e, 2a-b, 3c; Figs. 2c, 3c). The lamellar cycle is composed of polygonal elements that radiate into a slightly raised broad central area.

The centrally located coccoliths on the planar side contrast strongly in morphology between Coccolithophore sp. Z and Coccolithophore sp. 1. Those of Coccolithophore sp. Z are elliptical and slightly concave on the distal side (Pl. 3b; Fig. 2d). The coccolith is comprised of polygonal elements which form a crudely radial pattern, with variable termination at the center of the coccolith, either 1. a concave suture parallel to the long axis of the coccolith (Pl. 3b; Fig. 2d), or 2. several polygonal elements overlapping the suture to form a slightly raised central area (Pl. 1f; Fig. 2d).

Those of Coccolithophore sp. 1 are similarly elliptical but they have a wide asymmetrical rim, so that the rim along the long axis is relatively wider than that along the short axis of the coccolith. The lamellar cycle consists of polygonal elements oriented roughly perpendicular to the base and rising into a narrow protrusion parallel to and spanning the length of the long axis of the coccolith (Pl. 3f; Fig. 3d).

On the domal side, the coccospheres of both forms consist of sacculiform coccoliths with a round base, which overlap slightly (Pls. 1a-b, 2c-f; Figs. 2a, 3a). They are arranged tightly and regularly across the domal side (Pl. 1a-b; Fig. 2a). A narrow rim of radial elements comprises the outer cycle of the round base of the domal coccoliths. The inner cycle is comprised of radial elements that meet to form an irregular suture at the center of the coccolith. The central area overlaps the inner cycle, and is comprised of polygonal elements oriented almost perpendicular to the base. These elements are imbricated and rise radially into an elongate cylinder of constant thickness, to a distal terminus, which terminates smoothly (Pls. 2c-f, 3d-e; Fig. 3b) or in a short papilla (Pls. 1a-d, 3a, j; Fig. 2b). Although the protrusions of Coccolithophore sp. Z are usually cylindrical, they are varimorphic, ranging from a bell-shaped low asymmetrical cylinder to an elongate cylinder of constant thickness. The domal coccoliths of Coccolithophore sp. 1 differ from those in Coccolithophore sp. Z by the absence of a distal papilla, and by their homogeneity.

Due to the presence of 3 different types of coccoliths I describe the coccosphere as trimorphic. The 3 types of coccoliths are comprised of spiraling elements rising to variable heights, highly reminiscent of cedar cones; I therefore refer to the coccoliths

as cedriliths for structural clarity from hereon (Table 2; Pl. 3). Specifically I refer to the antidomal cedriliths as discoidal cedriliths due to their overall elliptical shape outline. I refer to the convex discoidal cedriliths observed on both Coccolithophore sp. Z and 1 as tumular due to the mound-shape into which the polygonal elements rise (Table 2; Pl. 3b-c, e; Figs. 2c, 3c). The concave discoidal cedriliths of Coccolithophore sp. Z are termed cupuliform due to their depressed central area (Table 2; Pl. 3b; Fig. 2d). The discoidal cedriliths observed only on Coccolithophore sp. 1 are termed gibbous due to their long narrow protrusion (Table 2; Pl. 3f; Fig. 3d). The domal cedriliths are termed sacculiform due to their cylindrical protrusion.

4- Generic discussion and placement

4.1- Comparison of forms a and b with species of the genus *Solisphaera* Bollmann, Cortés, Kleijne, Østergaard & Young 2006. emend. Kahn and Aubry

Coccolithophore sp. Z and Coccolithophore sp. 1 are similar to *S. emidasia, S. blagnacensis,* and *S. helianthiformis* in the configuration of their coccospheres and structure of their coccoliths. These 5 taxa have in common highly unusual coccospheres unknown in other forms. Below I compare the shape of the coccospheres as well as the positioning and structure of the three kinds of coccoliths on the coccospheres of Coccolithophore sp. Z and Coccolithophore sp. 1 with those of the species within the genus *Solisphaera*.

The coccospheres of all of the above appears to be hemispheric (Figs. 2a, 3a, 4a). The domal side is comprised of a single type of coccolith with a sacculiform

(Coccolithophore sp. Z and Coccolithophore sp. 1) or peltiform (*S. emidasia, S. blagnacensis, S. helianthiformis*) protrusion. These coccoliths are upright in a convex shape similar to that formed by the tubular coccoliths of *Gladiolithus*. The coccoliths of Coccolithophore sp. Z, Coccolithophore sp. 1, and *S. helianthiformis* are sacculiform (Pl. 3a, d, j, k; Figs. 2b and 3b), in contrast with those of *S. emidasia* and *S. blagnacensis* which are peltiform, rising from their base into a flat central polygonal protrusion akin to the hilt of a sword (Pl. 3g, h, l; Fig. 4b). Yet, despite the contrast in basic shape, the positioning and morphology of the imbricating polygonal elements of all the domal coccoliths is equivalent (Pl. 3a, g, j, k; Figs. 2b, 3b, 4b). The slightly convex antidomal side of the coccospheres is comprised of 2 kinds of flatter elliptical coccoliths. The antidomal coccoliths of *S. emidasia*, *S. blagnacensis*, and *S. helianthiformis* are easily differentiated both by morphology and position on the coccosphere. The overlapping endothecal coccoliths cover the entire antidomal side, and are loosely covered by the exothecal coccoliths (Pl. 4b, d; Figs. 4a, 5a). In contrast, the cupuliform and gibbous cedriliths of Coccolithophore sp. Z and Coccolithophore sp. 1, respectively, cover the center of the antidomal side with the girdle (tumular) cedriliths positioned laterally (Pls. 1e-f, 3a-b). The exothecal coccoliths of *S. emidasia, S. blagnacensis*, *S. helianthiformis,* appear to be significantly thicker than the endothecal coccoliths.

I see very distinctive similarities between certain coccoliths on different coccospheres. The lamellar cycle of the sacculiform cedrilith of Coccolithophore sp. Z is generally cylindrical, but is sometimes shortened and thickened into a bell shape.

This bell shape is similar to the lamellar cycle of the domal coccoliths of *S. helianthiformis*, which form an elongate bell shape with an extended narrow spine. Similarly, the exothecal coccoliths of *S. blagnacensis* and cupuliform cedriliths of Coccolithophore sp. Z are comparable in structure and varimorphism. Both are elliptical with a broad rim formed by the bending of the elements comprising the convex central area. Both terminate at the center in a suture, which is sometimes obscured by elements that extend over the suture (varimorphism) (Fig. 2d and 4c).

I place Coccolithophore sp. Z and Coccolithophore sp. 1 within the genus *Solisphaera* due to the following parallels between them: 1. hemispheric structure of the coccospheres, 2. coccospheres comprised of coccoliths differentiated morphology and by position on the coccosphere 3. three types of varimorphic coccoliths: 1 type of sacculiform coccolith, and 2 types of discoidal coccoliths, 4. structure and positioning of the polygonal elements that compose the coccoliths. With the generic placement of Coccolithophore sp. Z and Coccolithophore sp. 1 into *Solisphaera*, I extend the term cedrilith to the coccoliths of *S. blagnacensis* (Table 2; Pl. 3), *S. emidasia*, and *S. helianthiformis*. The concave discoidal cedriliths of Coccolithophore sp. Z, *S. blagnacensis*, *S. emidasia*, and *S. helianthiformis* are termed cupuliform due to their depressed central area. I refer to the scaley, slightly convex discoidal cedriliths on the antidomal side of the coccospheres of *S. blagnacensis*, *S. emidasia*, and *S. helianthiformis* as scutate. The domal-side cedriliths are referred to as sacculiform (*S. turbinella* and *S. galbula*) or peltiform (*S. blagnacensis*, *S. emidasia*, *S. helianthiformis*) cedriliths due to their cylindrical swollen or flattened protrusion, respectively. Some of the strong similarities among the coccoliths of different

species and forms may indicate morphologic convergence within the genus *Solisphaera*.

4.2- Discussion of the peltiform cedriliths of the *Solisphaera* genus

The genus *Solisphaera* was so named for the distinctive corona Bollmann et al. (2006) describe as surrounding the domal side of the coccospheres of this genus. According to Bollmann et al. (2006), domal "coronal" cedriliths ring the domal-side "body" cedriliths in a position perpendicular to the orientation of those "body" cedriliths, and parallel to the orientation of the antidomal discoidal cedriliths. I propose that the corona is not parallel to the discoidal cedriliths as described, but instead that the distinctive sun-like shape (e.g., Pl. 4e) was created by the "coronal" cedriliths collapsing from an originally upright position parallel to the domal "body" cedriliths. This can be seen from both domal and antidomal sides of the coccospheres (Pl. 4), where all or most of the domal "coronal" and "body" coccoliths remain upright, not having yet collapsed downwards. It can also be seen in coccospheres of other genera, such as *F. profunda*, where a similar collapse of equatorial polygoliths is observed (Pl. 5). The "coronal" cedriliths do not form a corona that sticks out perpendicular from the other "body" cedriliths, instead, these cedriliths merely comprise the intraspecifically size variable "body" cedriliths on the domal of the coccosphere. I therefore refer to the "coronal" and "body" cedriliths from Bollmann et al. (2006) as one in the same peltiform cedriliths and consider the coccosphere trimorphic. I term the domal cedriliths cupuliform and scutate cedriliths (exothecal and endothecal; see Table 2 and Pl. 3 for clarification) instead of heavily and lightly

calcified coccoliths as in Bollmann et al. (2006), respectively, for specificity in coccosphere and cedrilith structure and position. Cupuliform refers to the concave shape of the exothecal cedrilith and scutate refers to the scaley slightly convex shape of the endothecal cedrilith.

Conclusions

I have found in abundance 2 very unique forms that have only been found in the DPZ. These forms are differentiated from other extant taxa by their trimorphic hemispheric coccospheres and highly unusual cedriliths, which can be distinguished both by morphology and by location on the coccosphere. Although I do note varimorphism in many extant forms (see Young et al. 2003 or Cros and Fortuño 2002 for compilations), I do not see trimorphic coccospheres with varimorphism unassociated with any flagellar opening as I note in the forms I describe here. This similarity in form and structure may be indicative of inter- and intraspecific morphological convergence among coccolithophores. Such convergence implies similar functionality of coccospheres and coccoliths across families.

I describe the 2 forms within the *Solisphaera* genus but also emend its generic description to clarify the structure of the coccosphere and polymorphic sacculiform/peltiform cedrilith. Finally, a new family Solisphaeraceae Aubry and Kahn 2006 is introduced to encapsulate the 5 new species within the *Solisphaera* genus.

Acknowledgements

I express my deepest gratitude to Dr. Christopher Daniel, Bucknell University Geology Department, and Valentin Starovoytov, Rutgers University Biological Sciences Department, for their supportive technical assistance during S.E.M. sessions. My sincerest thanks to Connie Sanchetta for her Latin translations. I am thankful to Colomban de Vargas for providing the filters from the 2003 HV Melville cruise, Maria Triantaphyllou for discussions, and Ryan Earley for help with the drafting of maps.

References

AUBRY, M.-P., Kahn, A., 2006. Coccolithophores from the deep photic zone of the Indian Ocean: a case for morphological convergence as a forcing mechanism in the evolution of the calcareous nannoplankton. Micropaleontology, 52(5): 411-431.

BOLLMANN, J., Cortés, M.Y., Kleijne, A., Østergaard, J., Young, J., 2006. *Solisphaera* gen. nov. (Prymnesiophyceae), a new coccolithophore genus from the lower photic zone. *Phycologia*, 45(4): 465-477.

CROS, L., Fortuño, J., 2002. Atlas of northwestern Mediterranean coccolithophores. *Scientia Marina*, 66(1): 7-182.

OKADA, H., Honjo, S., 1973. The distribution of oceanic coccolithophorids in the Pacific. *Deep Sea Research*, 20: 355-374.

YOUNG, J.R., Geisen, M., Cros, L., Kleijne, A., Sprengel, C., Probert, I., Østergaard, J., 2003. A guide to extant coccolithophore taxonomy. *Journal of Nannoplankton Research Special Issue* 1: 1-125.

Taxonomy

We emend the species description of the genus *Solisphaera*. We also designate Coccolithophore sp. Z and Coccolithophore sp. 1 as new species, *S. turbinella* and *S. galbula*, respectively, within the genus *Solisphaera*.

Division Haptophyta Hibberd 1972 ex Edwardsen and Eikrem in Edwardsen et al. 2000
Class Prymnesiophyceae Hibberd 1976; emend Cavalier-Smith in Cavalier-Smith et al. 1996
Order Syracosphaerales Hay 1977; emend. Young et al., 2003

Family Solisphaeraceae (*incertae sedis* aff. Rhabdosphaeraceae Bollmann, Cortés, Kleijne, Østergaard and Young 2006) Aubry and Kahn 2006
Genus *Solisphaera* Bollmann, Cortés, Kleijne, Østergaard & Young 2006. emend. Kahn and Aubry
Solisphaera nov. gen. Bollmann, Cortés, Kleijne, Østergaard & Young 2006.
Trimorphic hemispheric coccosphere comprised of varimorphic cedriliths differentiated by morphology and position on the coccosphere. Domal side comprised of upright varimorphic cedriliths with sacculiform/peltiform protrusion. Dithecate planar side comprised of 2 types of discoidal cedriliths with variably sized protrusions, located centrally, laterally or across the entire base.

Type species: *Solisphaera emidasia* Bollmann, Cortès, Kleijne, Østergaard and Young 2006 emend. Kahn and Aubry
Solisphaera turbinella sp. nov. Kahn and Aubry
(L. *turbinella*= helicoidal)
"Saturnulus" sp. Young et al. 2003, Plate 27, fig. 13, p. 61.

Latin description: Parvissima, monothecata, tres formas dissimiles coccolitharum habens, late hemiglobosa; coccosphaera cedrilithis domalibus et antidomalibus distinctissimis composita, cingulum equatorialis cedrilithis propriis compositum. Cedrilithi domales sacculiformes, cum fundamento lato rotundo et orbe centrale lamellato intorte surgens, eminentia cylindrica terminata in papillam brevem fiens. Cedrilithi antidomales cupuliformes, leviter concavi. Cingulum proprium cedrilithis tumularibus compositum.

English description: Very small, monothecate, trimorphic, broadly hemispherical, coccosphere consisting of markedly distinct domal and antidomal cedriliths and with an equatorial girdle of specialized cedriliths. Domal cedriliths are sacculiform with a wide circular base and the central lamellar cycle rises in spiral fashion into a cylindrical protrusion terminated by a short papilla. Antidomal cedriliths are cupuliform. The specialized girdle consists of tumular cedriliths.

Coccosphere: total number of coccoliths per coccosphere: >100; with 34 to 70 sacculiform, 13 to 21 cupuliform and 20 to 30 tumular cedriliths. Equatorial diameter: 3.1 to 5.3 µm.

Sacculiform cedriliths: long axis of base: 0.1 to 1.0 µm; short axis of base: 0.7 to 0.8 µm; height to papilla: 0.2 to 0.7 µm; height of papilla: 0.1 to 0.2 µm.
Cupuliform cedriliths: long axis: 0.7 to 1.2 µm; short axis: 0.6 to 0.9 µm.
Tumular cedriliths: long axis: 0.9 to 1.2 µm; short axis: 0.7 to 0.9 µm.

Type material: Rutgers University Micropaleontology Laboratory S.E.M. stub from filter-sample VANC10MV07D_b collected at type locality.

Type repository: Rutgers University Department of Geological Sciences.
Type locality: Indian Ocean, Site VANC10MV07D; 33°17.91'S, 45°21.72'E), recovered on 3 May 2003 (between 16:49 and 17:45 h) at a depth of 120 m where seawater temperature was 18°C and salinity 35.67‰.
Holotype: Plate 2, Fig. a
Ethymology: L. *turbinella* = helicoidal
Number of coccospheres analyzed: 21 (all were collapsed).

Distribution: We encountered this species at only one locality in the deep photic zone of the southern Indian Ocean. Also reported and illustrated (as *Algirosphaera* sp.) in the Emidas database (hhtp://www.emidas.ethz.ch) Image 858 from 100 m water depth in the North Pacific Ocean.

Solisphaera galbula sp. nov. Kahn and Aubry
(L. *galbula*= cypress cone)
Coccolithophore sp. 1 Cros and Fortuño 2002, Figs. 110C, D, p. 172.
"Saturnulus" sp. Young et al. 2003, Plate 27, fig. 14, 15, p. 61.
Latin description: Parvissima, monothecata, tres formas dissimiles coccolitharum habens, coccosphaera late hemiglobosa, cedrilithis domalibus et antidomalibus distinctissimis composita; cedrilithi antidomales formas diversas habens, gradatim mutans uno ad altrum; cingulum equatorialis cedrilithis propriis composito. Cedrilithi domales sacculiformes, cum fundamento lato rotundo et orbe centrale lamellato intorte surgens, eminentia cylindrica cum apice rotundo fiens. Cedrilithi antidomales convexissimi, cum eminentia ad cingulum conspicue dilatans. Cingulum proprium cedrilithis tumularibus compositum.

English description: Very small, monothecate, trimorphic, broadly hemispherical coccosphere, strongly varimorphic on the antidomal side, consisting of markedly distinct domal and antidomal cedriliths and with an equatorial girdle of specialized cedriliths. Domal cedriliths are sacculiform with a wide circular base, and the central lamellar cycle rises in spiral fashion into a cylindrical protrusion with rounded top. Antidomal cedriliths are gibbous, with protrusion noticeably broadening towards girdle. Specialized girdle consists of tumular cedrilihs.

Coccosphere: Total number of coccoliths per coccosphere: >100; with 32 to 63 sacculiform, 27 to 41 gibbous and 21 to 36 tumular cedriliths. Equatorial diameter: 4.2 to 5.9 µm.
Sacculiform cedriliths: long axis of base: 0.6 to 0.9 µm; short axis of base: 0.7 to 0.7 µm; long axis of protrusion: 0.6 to 0.9 µm; short axis of protrusion 0.2 to 0.3 µm; height of protrusion: 0.2 to 0.3 µm.
Gibbous cedriliths: long axis: 0.6 to 1.2 µm; short axis: 0.5 to 1.1 µm.
Tumular cedriliths: long axis: 0.8 to 1.3 µm; short axis: 0.5 to 0.7 µm.

Type material: Rutgers University Micropaleontology Laboratory S.E.M. stub of filter-sample VANC10MV07D_b, collected at type locality.
Type repository: Rutgers University Department of Geological Sciences.

Type locality: Indian Ocean Site VANC10MV07D (33°17.91'S, 45°21.72'E); filter sample recovered on 3 May 2003 (between 16:49 and 17:45 h) at a depth of 120 m where seawater temperature was 18°C and salinity 35.67‰.
Holotype: Plate 3, Fig. c
Ethymology: L. *galbula* = cypress cone
Number of coccospheres analyzed: 14 (all were collapsed)

Distribution: We encountered this species at only one locality in the deep photic zone of the southern Indian Ocean. Also illustrated from the Mediterranean Sea where it was recovered (17 September 1996 off southeastern Spain (41°19.3'N, 3°33.5'E) at 57 m water depth (Cros and Fortuño 2002). Illustrated but undifferentiated from *S. turbinella* in Young et al. (2003)

Solisphaera blagnacensis Bollmann, Cortés, Kleijne, Østergaard & Young 2006. emend. Kahn and Aubry
Solisphaera blagnacensis Bollmann, Cortés, Kleijne, Østergaard & Young 2006.
"Saturnulus blagnacensis" Young et al. 2003, Plate 27, figs. 7 and 10, p. 61.

Very small, trimorphic, broadly hemispheric coccosphere, monothecate on the domal side, dithecate on the antidomal side, consisting of markedly distinct domal and antidomal cedriliths and with an equatorial girdle of unspecialized variably-sized cedriliths. Domal cedriliths are peltiform, arranged in a single layer. Antidomal cedriliths are arranged in two layers, an inner layer of scutate cedriliths and an outer layer of cupuliform cedriliths.

Coccosphere: Total number of coccoliths per coccosphere: >100; with 31 to 51 peltiform, 11 to 14 cupuliform and 9 to 13 scutate cedriliths. Equatorial diameter: 4.1 and 6.2 µm, with an average of 4.8 µm.
Peltiform cedrilith: long axis of base: 0.7 to 1.3 µm; short axis of the base: 0.6 to 0.8 µm; height: 0.6 to 1.0 µm.
Cupuliform cedriliths long axis: 0.9 to 1.6 µm; short axis: 0.7 to 1.1 µm;
Scutate cedriliths: Long axis of base: ~1.0 to 1.5 µm; short axis of base: ~0.5 µm; cannot be measured accurately because partly covered by cupuliform cedriliths.

Distribution: The species was described from the deep photic zone (150 m) in the subtropical (near Canary Islands) North Atlantic Ocean and was reported from the central equatorial Pacific Ocean and western Mediterranean (Alboran) Sea (Bollmann et al. 2006). Its geographic distribution is now extended to the southern Indian Ocean. The seawater temperature (18°C) and salinity (35.67‰) at our Indian Ocean site falls within the ranges of temperature (~15.7-21.2°C) and salinity (34.7-37‰) at the other locations.

Chapter 2

Table captions

Table 1: Measurements of sacculiform/peltiform cedriliths and discoidal cedriliths of *S. turbinella*, *S. galbula*, *S. blagnacensis*, and *S. emidasia* from filter-sample VANC10MV07D (in bold print) compared with measurements from published manuscripts: *S. galbula* (Cros and Fortuño 2002) (in italics); *S. blagnacensis* and *S. emidasia* (Bollmann et al. 2006) (in plain text).

Table 2: Different types of sacculiform/peltiform cedriliths and discoidal cedriliths found in 5 species within the *Solisphaera* genus. Coccolithophore sp. 1 comprises sacculiform, tumular and cupuliform cedriliths, Coccolithophore sp. 2 comprises sacculiform, gibbous and tumular cedriliths; *S. blagnacensis* comprises peltiform, scutate and cupuliform cedriliths. If we note that the sacculiform and peltiform types are morphologically very close, *S. blagnacensis* appears very similar to Coccolithophore sp. 1.

		this paper			Cros & Fortuño 2002 and Bollmann et al. 2006		
		average	**min**	**max**	average	min	max
S. turbinella							
total # of individuals		**21**					
# with all cedriliths visible		**7**					
coccosphere	diameter	**4.5**	**3.1**	**5.3**			
# with domal side visible		**9**					
sacculiform cedriliths	#	**50**	**34**	**70**			
sacculiform cedriliths base	long axis	**0.8**	**0.1**	**1.0**			
sacculiform cedriliths base	short axis	**0.8**	**0.7**	**0.8**			
sacculiform cedriliths	height to papilla	**0.5**	**0.2**	**0.7**			
sacculiform cedriliths	height of papilla	**0.1**	**0.1**	**0.2**			
# with antidomal side visible		**5**					
tumular cedriliths	#	**25**	**20**	**30**			
tumular cedriliths	long axis	**1.1**	**0.9**	**1.2**			
tumular cedriliths	short axis	**0.8**	**0.7**	**0.9**			
cupuliform cedriliths	#	**17**	**13**	**21**			
cupuliform cedriliths	long axis	**1.0**	**0.7**	**1.2**			
cupuliform cedriliths	short axis	**0.8**	**0.6**	**0.9**			
S. galbulus							
total # of individuals		**14**			*Not given*		
# with all cedriliths visible		**2**					
coccosphere	diameter	**5.0**	**4.2**	**5.9**		*4.5*	*6.5*
# with domal side visible		**6**					
sacculiform cedriliths	#	**51**	**32**	**63**			
sacculiform cedrilith base	long axis	**0.7**	**0.6**	**0.9**		*0.9*	*1.5*
sacculiform cedrilith base	short axis	**0.7**	**0.7**	**0.7**			
sacculiform cedrilith	height	**0.6**	**0.5**	**0.7**			
sacculiform cedrilith distal end	long axis	**0.8**	**0.6**	**0.9**			
sacculiform cedrilith distal end	short axis	**0.3**	**0.2**	**0.3**			
# with antidomal side visible		**5**					
tumular cedriliths	long axis	**1.1**	**0.8**	**1.3**			
tumular cedriliths	short axis	**0.6**	**0.5**	**0.7**			
gibbous cedriliths	#	**33**	**27**	**41**			
gibbous cedriliths	long axis	**1.0**	**0.6**	**1.2**			
gibbous cedriliths	short axis	**0.6**	**0.5**	**1.1**			
S. blagnacensis							
total # indiv		**14**			Not given		
coccosphere	diameter	**4.8**	**4.1**	**6.2**	7.5		
# with domal side visible		**11**					
peltiform cedriliths	#	**41**	**32**	**51**		51	68
peltiform cedrilith proximal side	long axis	**1.0**	**0.7**	**1.3**		0.9	1.4
peltiform cedrilith proximal side	short axis	**0.7**	**0.6**	**0.8**		0.6	0.9
peltiform cedrilith	height	**0.8**	**0.6**	**1.0**			
peltiform cedrilith distal side	long axis	**1.0**	**0.6**	**1.2**			
peltiform cedrilith distal side	short axis	**0.2**	**0.1**	**0.3**			
# with antidomal side visible		**4**					
cupuliform cedriliths	#	**13**	**11**	**14**		10	14
cupuliform cedrilith	long axis	**1.3**	**0.9**	**1.6**	1.4		

Table 1

cupuliform cedrilith	short axis	**0.9**	**0.7**	**1.1**	1.0		
scutate cedriliths	#	**11**	**9**	**13**			
S. emidasia							
total # indiv		**1**			Not given		
coccosphere	diameter	**6.6**			7.0	5.0	6.0
# with domal side visible		**1**					
peltiform cedriliths	#	**18**				13	24
peltiform cedrilith	base L	**1.1**	**1.0**	**1.1**			
peltiform cedrilith	height	**1.0**	**0.8**	**1.2**	1.5		
peltiform cedrilith	top L	**1.1**	**1.1**	**1.2**	0.9		

Table 1.

	domal side			antidomal side		girdle		
	sacculiform	cupuliform	scutate	gibbous	scutate	cupuliform	peltiform/ petaliform	tumular
S. turbinella (Coccolithophore sp. Z)	SC	CC						TC
S. galbulus (Coccolithophore sp. 1)	SC			GC				TC
S. blagnacensis					ScC	CC	PC	
S. emidasia			ScC		ScC		PC	
S. helianthiformis			ScC		ScC		PaC	

Table 2.

Chapter 2

Figure captions

Figure 1: HV Melville transect and location of Site VANC10MV07.

Figure 2: Distinctive morphology and structure of the cedriliths and coccospheres of *S. turbinella*.

a. Structure of coccosphere. Sacculiform cedriliths are arranged tightly (bases slightly overlap) and regularly across the domal side. On the antidomal side of the coccosphere tumular cedriliths are positioned as a girdle around the centrally located cupuliform cedriliths, which are are randomly arranged jointive to slightly overlapping to form a single layer.

b. Structure of sacculiform cedrilith. Although the protrusions of *S. turbinella* are usually cylindrical they range in shape from a bell-shaped low asymmetrical cylinder to an elongate cylinder of constant thickness. They are distinct from those of *S. galbula* by such varimorphism and also by the presence of a distal papilla.

c. Structure of tumular cedrilith. The base is elliptical with a narrow rim composed of narrow rectangular elements. Note the inner cycle is overlapped by the central area and we suggest it is comprised of radial elements that terminate in a narrow suture. The central area is composed of polygonal elements that radiate into a slightly raised broad central area.

d. Various structures of cupuliform cedrilith. They are elliptical and slightly concave on the distal side and are comprised of polygonal elements, which form a crudely radial pattern, with variable termination at the center of the coccolith, either 1. a concave suture parallel to the long axis of the coccolith, or 2. several polygonal elements overlapping the

suture to form a slightly raised central area. The 2 variations of termination represent the varimorphism of this cedrilith; from the center of the antidomal side of the coccosphere to the girdle tumular cedriliths, the cupuliform discodal cedriliths progress in structure from smoothly concave with a visible suture, to concave with a low mound of polygonal elements obscuring the suture, to an increasingly broad mound at which point their structure is parallel to those of the tumular cedriliths.

Figure 3: Distinctive morphology and structure of the cedriliths and coccospheres of *S. galbula*.

a. Structure of coccosphere. Sacculiform cedriliths are arranged tightly (bases slightly overlap) and regularly across the domal side. Tumular cedriliths are positioned as a girdle around the centrally located gibbous cedriliths on the antidomal side of the coccosphere.

b. Structure of sacculiform cedrilith. The domal coccoliths of *S. galbula* differ from those in *S. turbinella* by the absence of a distal spine and by the homogeneity in shape between the cedriliths.

c. Structure of tumular cedrilith. See description in Fig. 2c.

d. Structure of gibbous cedrilith. Elliptical with a wide asymmetrical rim, so that the rim along the long axis is relatively wider than that along the short axis of the coccolith. The lamellar cycle consists of polygonal elements oriented roughly perpendicular to the base and rising into a narrow protrusion parallel to and spanning the length of the long axis of the cedrilith.

Figure 4: Distinctive morphology and structure of the cedriliths and coccospheres of *S. blagnacensis*.

a. Structure of coccosphere. Peltiform cedriliths are located across the domal side of the coccosphere; the larger peltiform cedriliths are located equatorially, and the smaller ones centrally. Scutate cedriliths are arranged randomly across the antidomal side and are overlapping peripherally and incompletely across the center by cupuliform cedriliths on the antidomal side of the coccosphere.

b. Structure of peltiform cedrilith with 2 sizes of peltiform protrusion. The base has a narrow rim, and an inner cycle comprised of radiating elements. The central area is comprised of a flat central polygonal protrusion comprised of imbricating polygonal elements.

c. Various structures of cupuliform cedrilith. They are elliptical and slightly concave on the distal side and are comprised of polygonal elements, which form a crudely radial pattern, with variable termination at the center of the coccolith, either 1. a concave suture parallel to the long axis of the coccolith, or 2. several polygonal elements overlapping the suture to form a slightly raised central area.

d. Scutate cedrilith. These are comprised of a narrow rim of radial elements and a broad central area comprised of polygonal elements in radial position, terminating at the center by slightly overlapping each other.

Figure 5: Distinctive morphology and structure of the cedriliths and coccospheres of *S. emidasia*.

a. Structure of coccosphere. The domal side of the coccosphere is comprised of scutate discoidal cedriliths. The antidomal side is comprised of scutate cedriliths, overlapped peripherally by cupuliform cedriliths. Peltiform cedriliths are located equatorially, forming a girdle with cupuliform cedriliths.

b. Structure of peltiform cedrilith. See description from Fig. 4b. The central protrusion is thinner than that of S. blagnacensis and the sides are straighter, forming a more geometric shape.

c. Various structures of cupuliform cedrilith. See description from Fig. 4c.

d. Scutate cedrilith. See description from Fig. 4d.

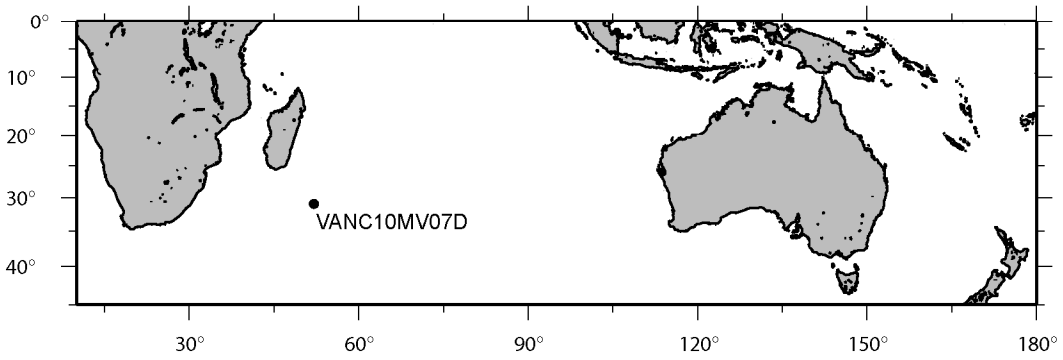

GMT 2006 Apr 27 16:59:44 R.Earley 2006

Figure 1

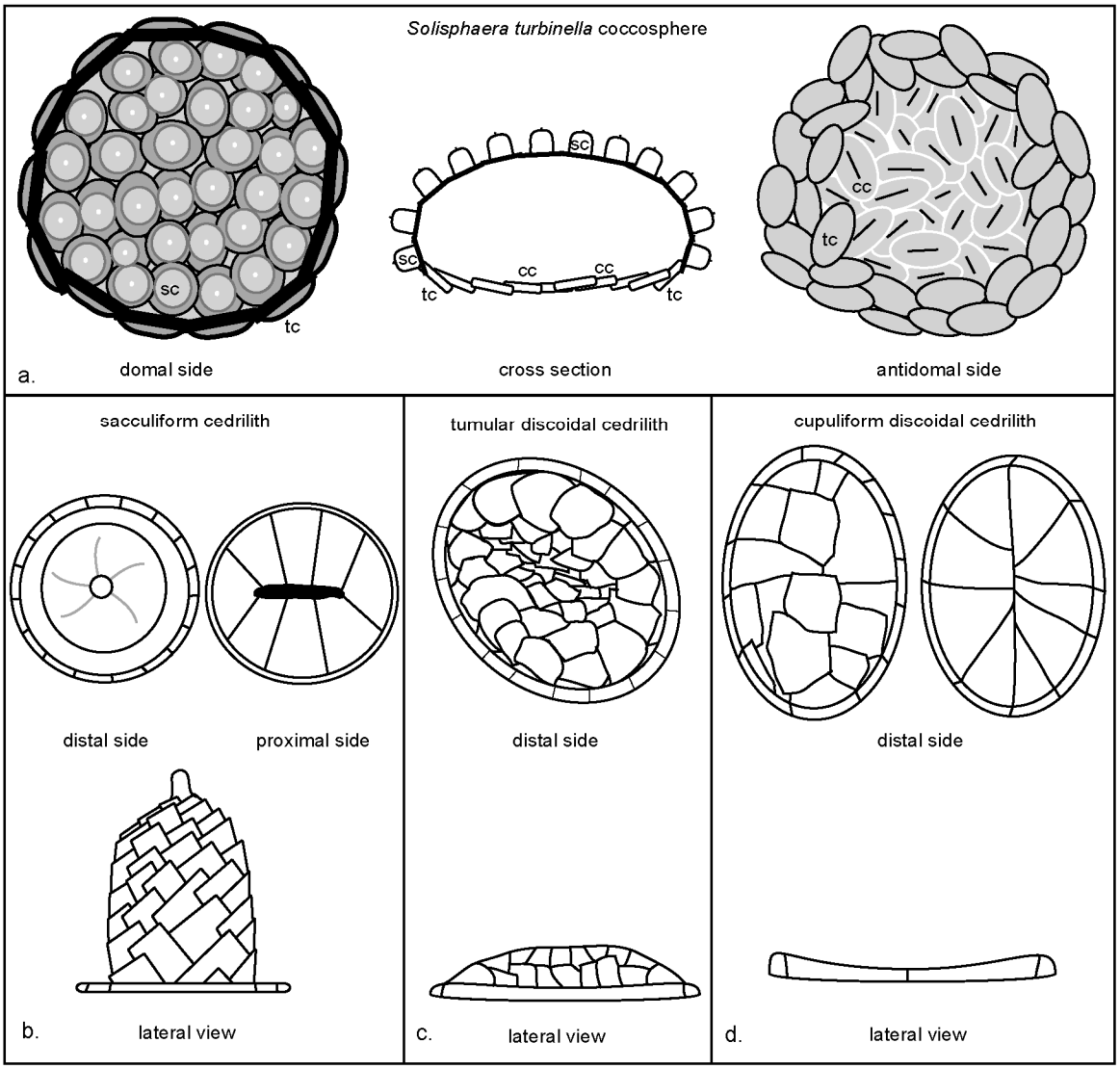
Solisphaera turbinella coccosphere
sc
tc
cc
a.
domal side
cross section
antidomal side
sacculiform cedrilith
distal side
proximal side
b.
lateral view
tumular discoidal cedrilith
distal side
c.
lateral view
cupuliform discoidal cedrilith
distal side
d.
lateral view

Figure 2

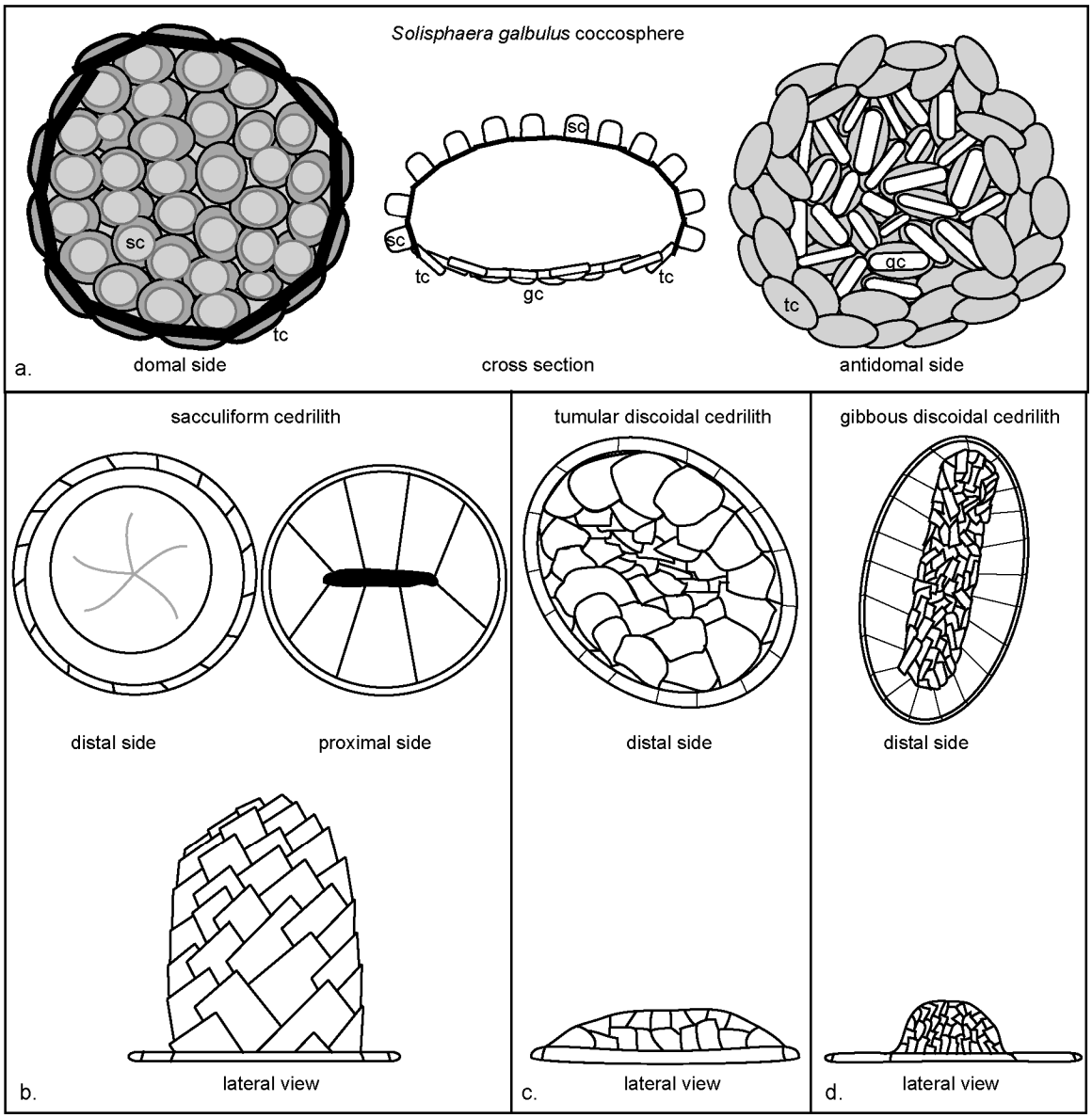
Solisphaera galbulus coccosphere
sc
tc
sc
sc
tc
gc
tc
gc
tc
a.
domal side
cross section
antidomal side
sacculiform cedrilith
distal side
proximal side
b.
lateral view
tumular discoidal cedrilith
distal side
c.
lateral view
gibbous discoidal cedrilith
distal side
d.
lateral view

Figure 3

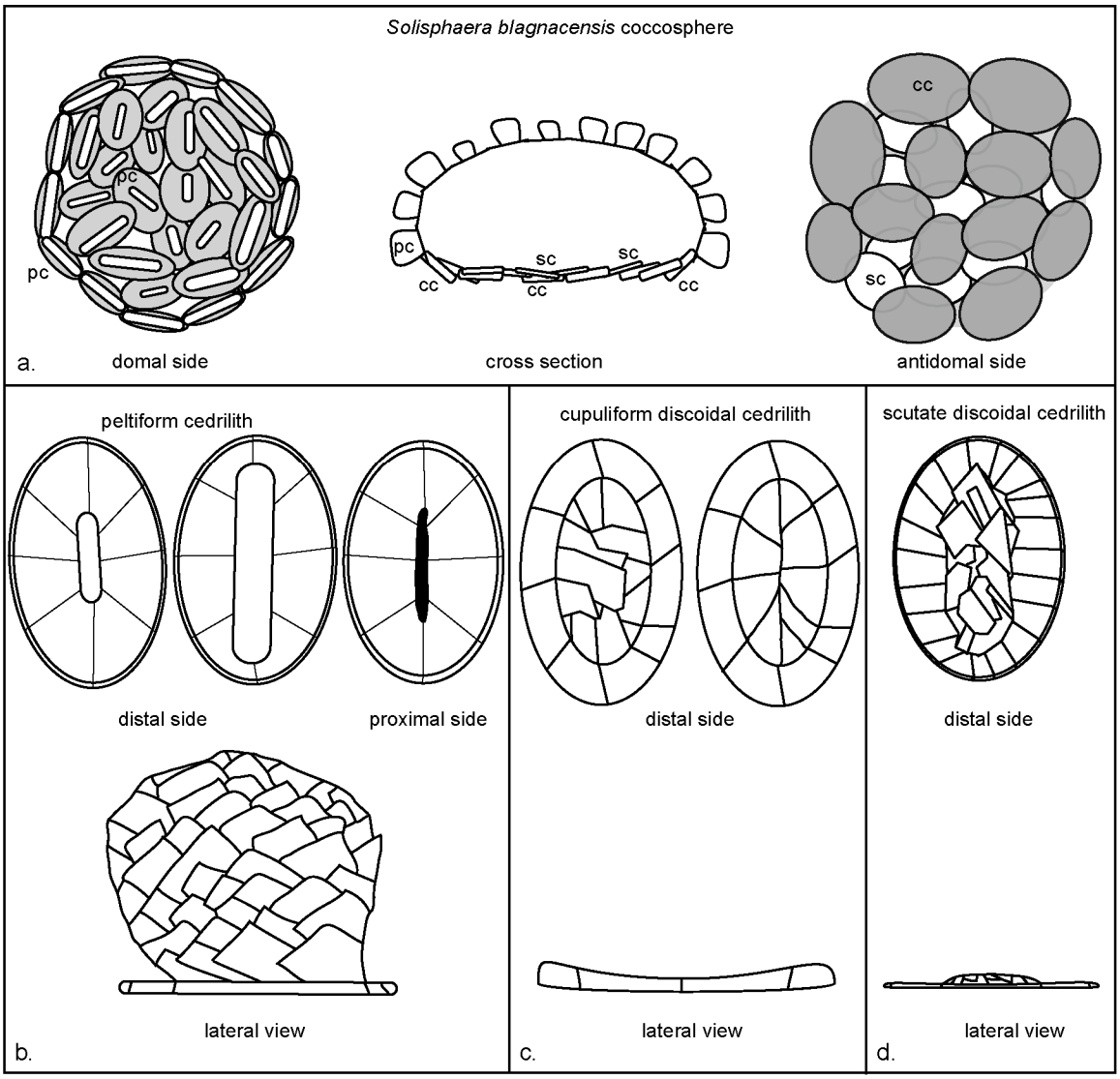
Solisphaera blagnacensis coccosphere
pc
pc
a.
domal side
pc
sc
sc
cc
cc
cc
cross section
cc
sc
antidomal side
peltiform cedrilith
distal side
proximal side
b.
lateral view
cupuliform discoidal cedrilith
distal side
c.
lateral view
scutate discoidal cedrilith
distal side
d.
lateral view

Figure 4

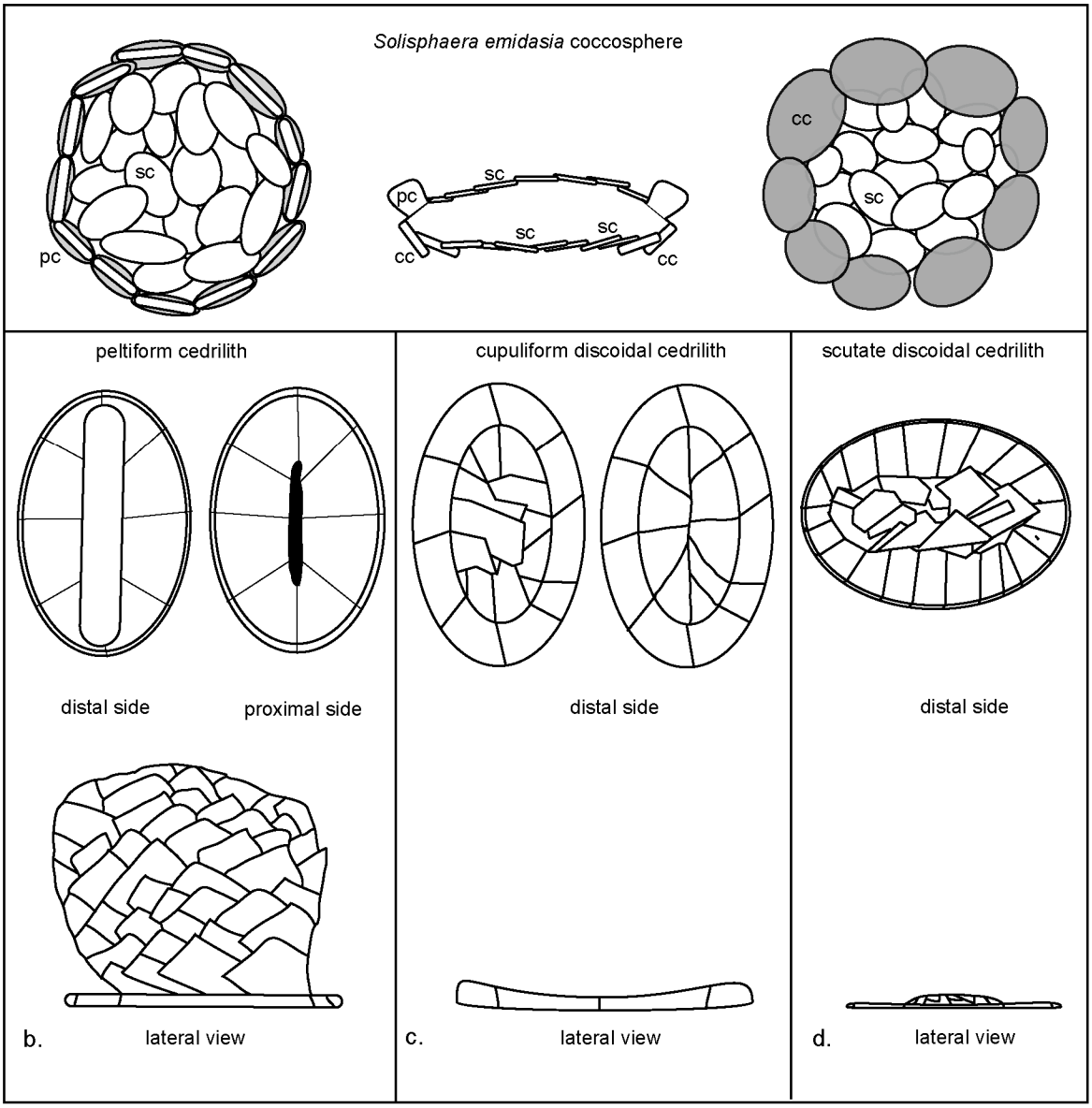
Solisphaera emidasia coccosphere
sc
pc
sc
pc
sc
sc
cc
cc
cc
sc
peltiform cedrilith
distal side
proximal side
b.
lateral view
cupuliform discoidal cedrilith
distal side
c.
lateral view
scutate discoidal cedrilith
distal side
d.
lateral view

Figure 5

Chapter 2

Plate captions

Plate 1: Figs. a-f; bar=2 μm. a-f: *Solisphaera turbinella*.

a-d: Domal side of coccosphere.

c: Note bending of coccosphere partially showing antidomal side of coccosphere.

e-f: Antidomal side of coccosphere.

Plate 2: Figs. a-f; bar=2 μm. a-f: *Solisphaera galbula*.

a-b: Antidomal side of coccosphere.

c-f: Domal side of coccosphere.

Plate 3: Figs. a-f; bar=2 μm. a-c, j: *S. turbinella*; d-f, k: *S. galbula*; g-i, l: *S. blagnacensis*.

a, d: Sacculiform cedriliths.

b: Cupuliform and tumular discoidal cedriliths.

c: Tumular cedriliths.

e: Sacculiform cedrilith and tumular discoidal cedriliths. Note discoidal cedrilith in transitional form between the low mound of the tumular cedrilith and the narrow raised protrusion of the gibbous cedriliths.

f: Gibbous discoidal cedriliths.

g, h: Peltiform cedriliths.

i: Cupuliform and scutate discoidal cedriliths.

j: Proximal view of sacculiform cedrilith.

k: Proximal view of sacculiform cedrilith.

l: Proximal view of peltiform cedrilith.

Plate 4: Figs. a-f; bar=2 μm. a-f: *Solisphaera blagnacensis*.

a, c, e: Domal side of coccosphere.

b, d: Antidomal side of coccosphere

f: Assorted sacculiform cedriliths and cupuliform discoidal cedriliths.

Plate 5: Fig. a-c; bar=2 μm. Figs. d-e; bar=5 μm. a: *Solisphaera blagnacensis*. b: *Solisphaera emidasia*. c-e: *Florisphaera profunda*.

a: Domal side of coccosphere with some peltiform cedriliths collapsed into a corona, and some upright.

b: Domal side of coccosphere illustrating peltiform cedriliths collapsed into a coronal shape.

c-e: Domal side of coccosphere with outer polygoliths collapsed. Note coronal shape of fallen polygoliths.

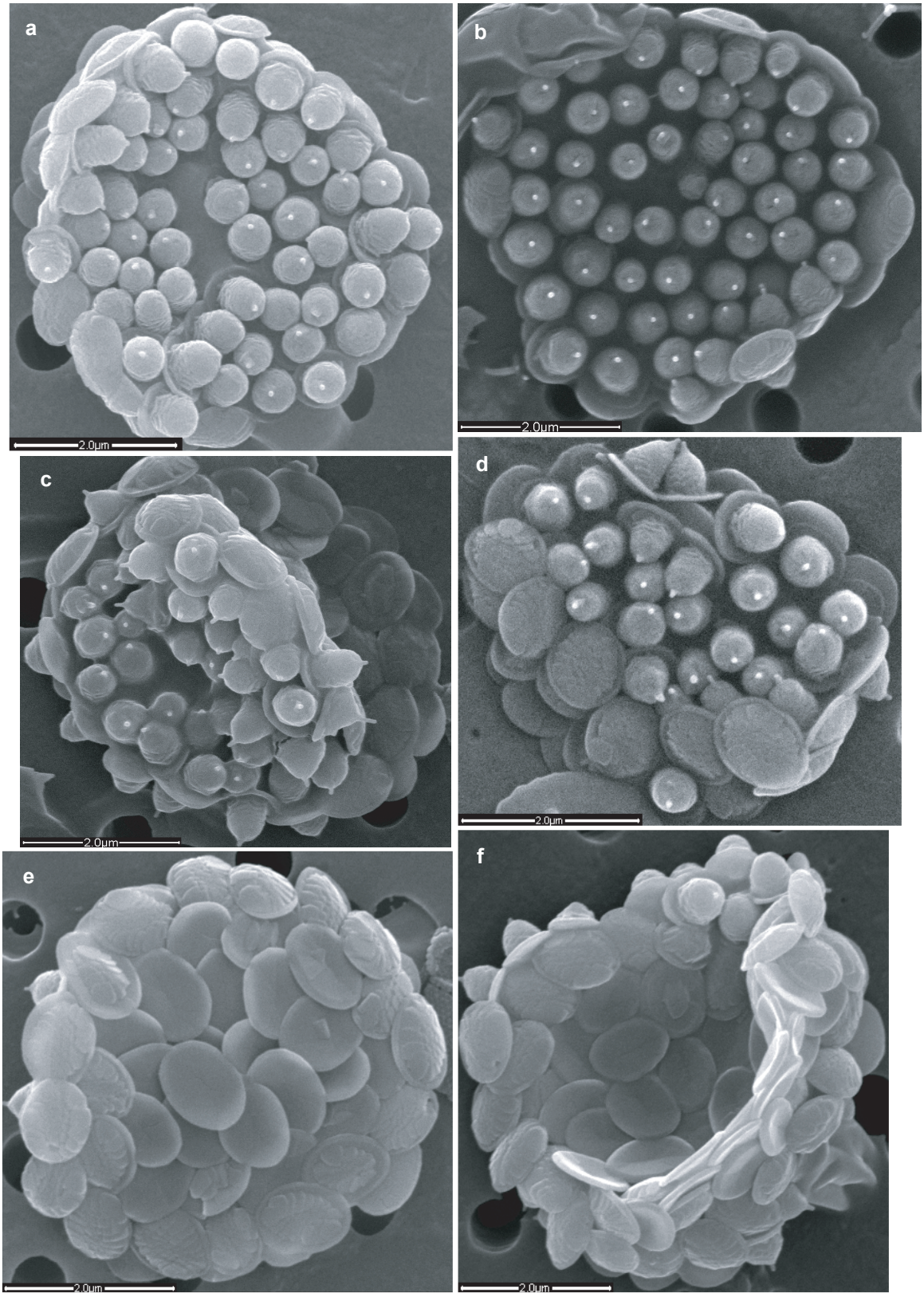

Plate 1

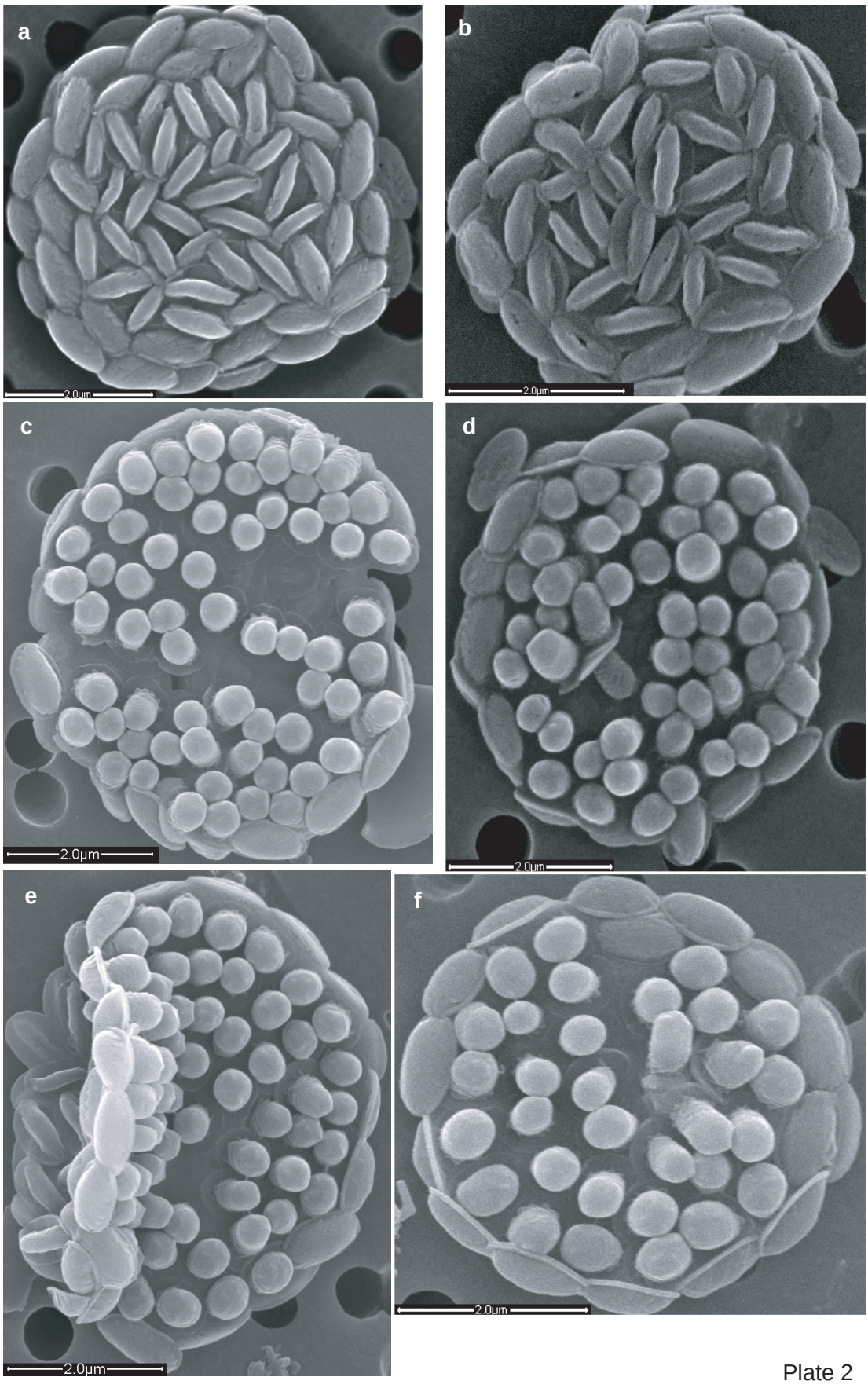

Plate 2

Solisphaera turbinella

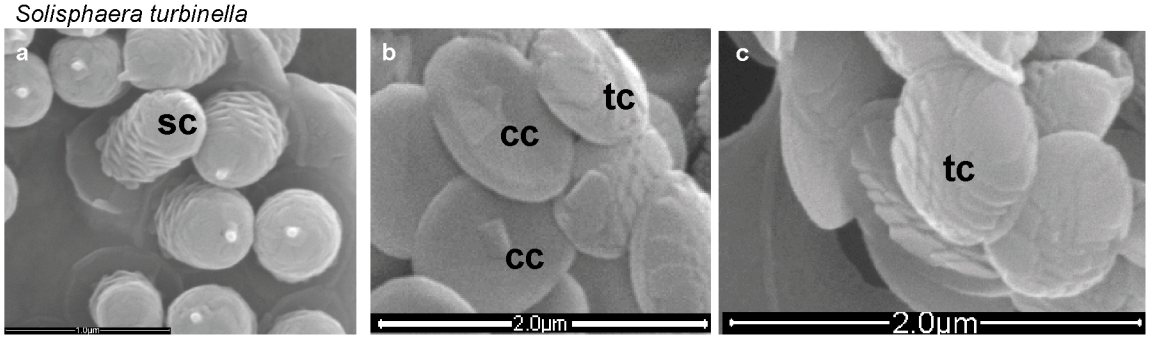

Solisphaera galbulus

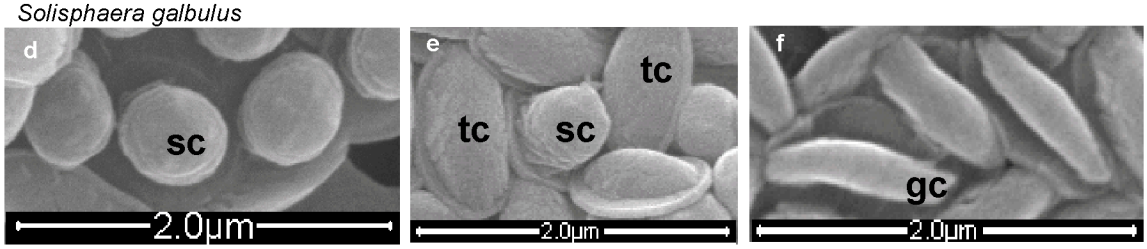

Solisphaera blagnacensis

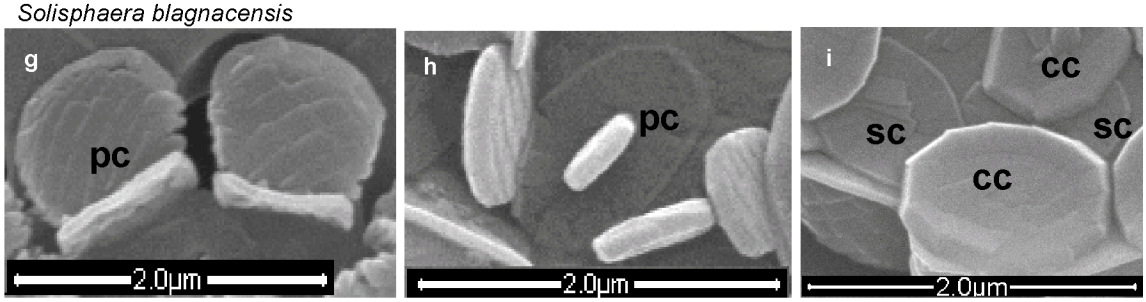

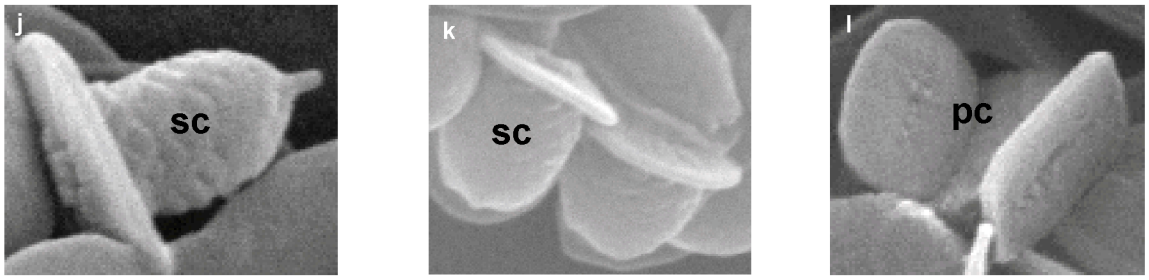

Plate 3

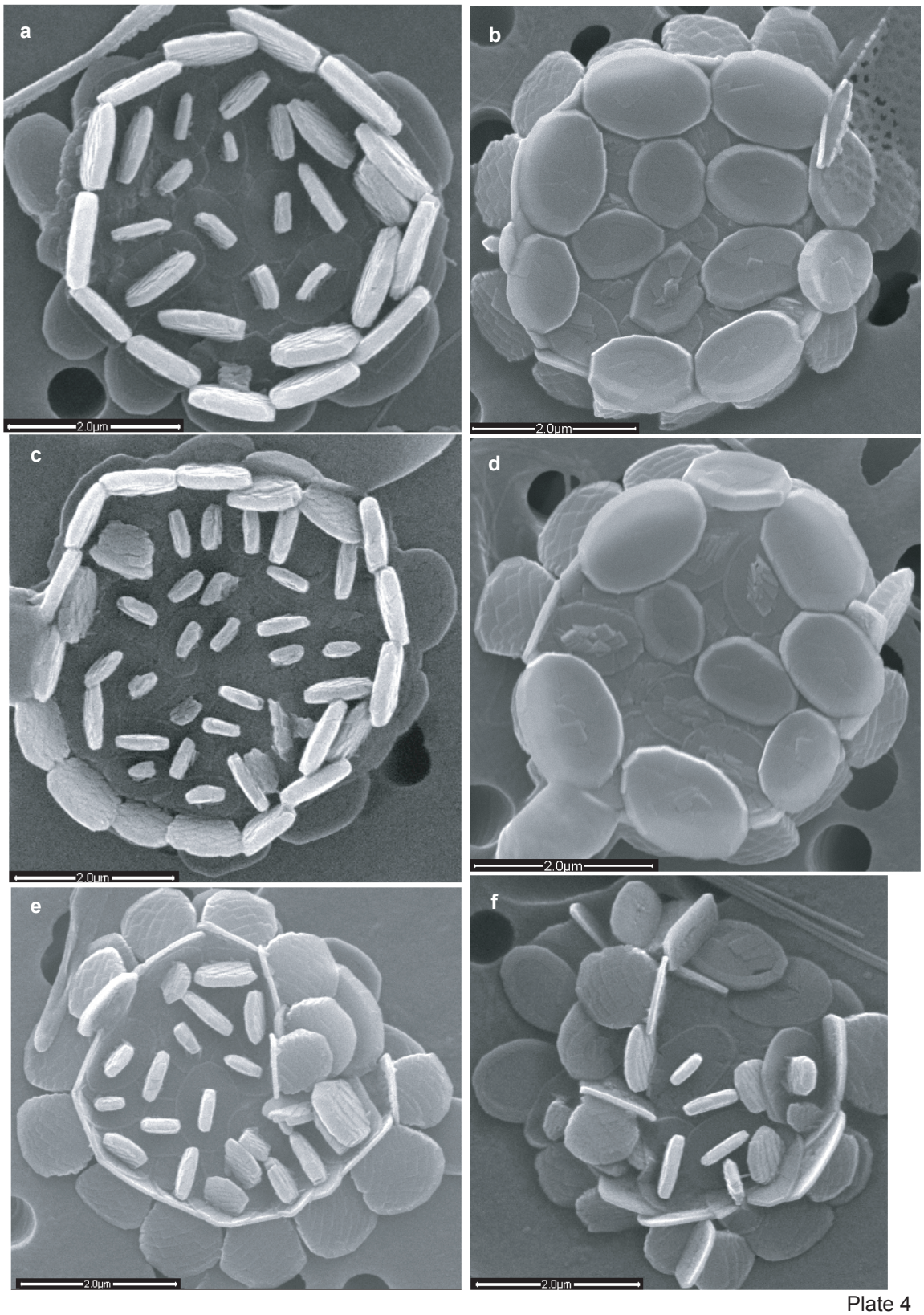

Plate 4

Solisphaera blagnacensis coccospheres

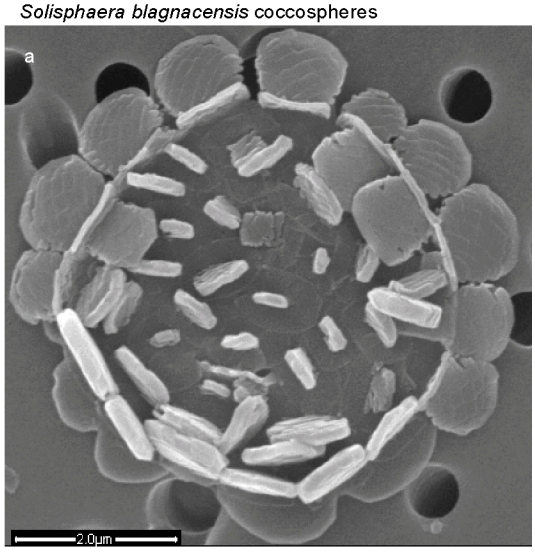

Solisphaera emidasia coccospheres

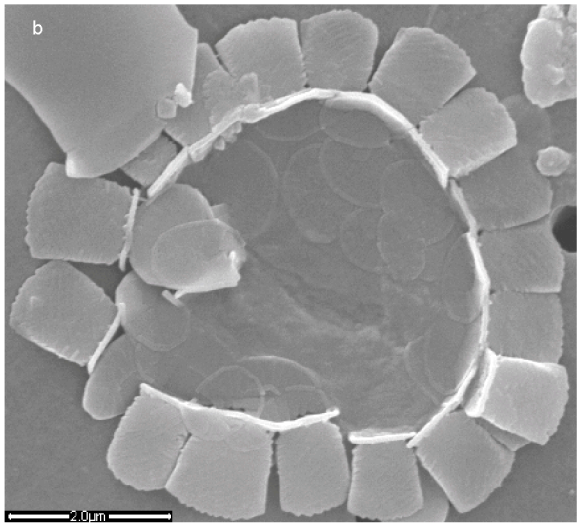

Florisphaera profunda coccospheres

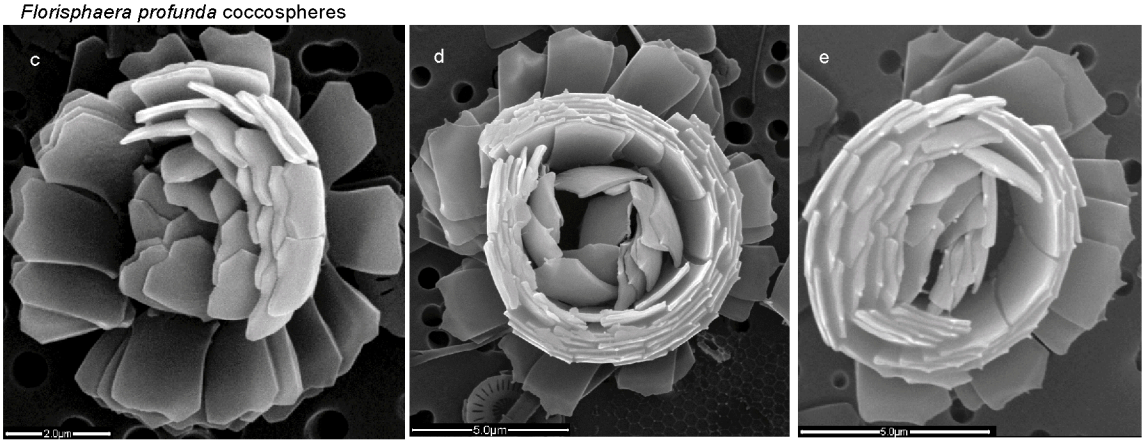

Plate 5

Chapter 3

Intraspecific variability in the deep photic zone coccolithophorids of the Indian Ocean

Abstract

This sample, taken at 120 m depth in the southern Indian Ocean, provides a rich assemblage of deep photic zone coccolithophore taxa, preserved predominantly as whole coccospheres. Most notable in this sample is the uniformity in intraspecific variability of coccoliths and coccospheres in the deep photic zone. I also note that the coccospheres of the deeper dwelling genera are often asymmetric and slightly elongate, comprised of imbricated coccoliths. The widespread homogeneity in morphology noted of the deeper dwelling genera in the southern Indian Ocean may indicate convergent adaptation to the low light, high nutrient conditions within the stable deep photic zone environment.

1- Introduction

The species distribution among coccolithophores generally follows latitude, with diversity decreasing with increasing latitude. Distribution also broadly depends on depth in temperate and tropical regions where the deeper part (~150-200 m) of the photic zone is inhabited by a characteristic community of cocolithophores that includes *Florisphaera profunda, Gladiolithus flabellatus, Oolithotus antillarum, Algirosphaera robusta* (Okada and Honjo 1973), plus the newly described *Solisphaera* spp. (Aubry and Kahn 2006; Bollmann et al. 2006) and *Navilithus altivelum* (Young and Andruleit 2006). This deep photic zone (hereon referred to as the DPZ) community inhabits the water mass below the thermocline and the deep chlorophyll maximum, at which depth (80-120 m) the amount

of solar radiation available for photosynthesis is 1% that at the sea surface (Venrick 1973). As noted by Takahashi and Okada (2000), the characteristic DPZ community (comprised of the abovementioned species typically found together in the DPZ) is not strictly restricted to the physico-chemically defined DPZ. The sample described here, recovered at 120 m water depth, is dominated by *F. profunda*, and secondarily dominated by the abovementioned DPZ community. Because they live in a light depleted environment, the DPZ dwelling coccolithophorids may have a distinct life strategy relative to size of the cell and size and structure of the coccosphere. Qualitative and quantitative analyses of morphological variation herein are used to discuss variability and coccosphere and coccolith function. I propose, in concert with Aubry (personal communication), that the DPZ is a morphologically convergent community that has evolved adaptive structural features in parallel.

I have documented elsewhere the intraspecific variability among selected species of the upper photic zone, using two exceptionally rich plankton samples recovered during the 2003 HV Melville Cruise in the southern Indian Ocean (Kahn and Aubry 2006; Ch. 1 of this dissertation). Here, I document the intraspecific variability among the species of the 4 major genera (excluding *Oolithotus* due to its rarity in the sample) of the deep-water communities. Sample VANC10MV07D provides a rich community of deep-water taxa, preserved predominantly as whole coccospheres. The large number of coccospheres of these species in the sample allows us to complement previous studies (e.g., Okada and Honjo 1973) in further analysis of the DPZ community.

Site VANC10MV07 is influenced by the Agulhas Current and the South Equatorial Current, transporting water from the mid-Indian Ocean towards the southern Atlantic Ocean (Wyrtkie 1973).

2- Methods

2.1- Sampling

I analyzed a single sample recovered at a depth of 120 m on the eastern side (33°17.91' S, 45° 21.72' E) of the Indian Ocean during the HV Melville Hydroacoustic and Biological Sampling Cruise (Fig. 1). Sample VANC10MV07D was taken on May 3, 2003 (between 16:49 and 17:45 h). Seawater temperature and salinity at the sample location (120 m) were 18^{o}C, and 35.67‰, respectively; in contrast to that close to the sea surface (6 m), 21^{o}C and 35.73‰, respectively. Five liters of seawater were vacuum filtered onto a polycarbonate (Osmonics) filter 47 mm in diameter with a 0.8 µm pore size. The filter was made available to us by Colomban de Vargas (Institute of Marine and Coastal Science at Rutgers University).

2.2- S.E.M Preparation

To avoid sampling bias the polycarbonate filter half was cut into 2 x 4 mm^2 subsections from the center to the edge of the filter sample on opposite ends of the filter. The sub-samples were mounted onto separate stubs and sputter coated with gold and palladium at the Electron Imaging Facility, Division of Life Sciences at Rutgers, the State University of NJ and further analyzed with a FEI Quanta 400 E.S.E.M. in the Geology Department at Bucknell University. The scanning of the entire triangular sub-samples was conducted

at a magnification of 2000x. Each coccosphere was carefully examined using magnifications up to 120,000x. All (670) coccospheres encountered were photographed for subsequent measurements.

2.3- Quantitative Analysis

Measurements were conducted on the S.E.M. photographs using Image J graphics measuring program. For explanation of the measured dimensions refer to Figure 2 and the Terminology section below. The measurements discussed here exclusively concern coccoliths occurring in situ on coccospheres.

3- Terminology

I discuss here intraspecific variations in 3 species and 6 variants of *Florisphaera* (Okada and Honjo 1973), 2 species of *Gladiolithus* (Jordan and Chamberlain 1993), 1 species of *Algirosphaera* (Schlauder 1945), and 5 species of *Solisphaera* (Aubry and Kahn 2006; Bollmann et al. 2006). Although these show commonality in coccosphere morphology, they differ in the morphology and structure of their coccoliths. Coccospheres and coccoliths of the abovementioned genera are illustrated in Figure 2.

Species in *Gladiolithus* secrete 2 kinds of coccoliths (Hagino and Okada 1998; Young et al. 1997; Jordan and Chamberlain 1993; Young 1992). The proximal slightly convex side of the coccosphere is covered by elliptical to rounded planoliths (general term for polygonal coccoliths) termed lepidoliths due to their rounded outline. Striate (*G. striatus*) or smooth (*G. flabellatus*), lepidoliths are composed of two elements with a suture across

the center. Tubular coccoliths cover the slightly convex distal side of the coccosphere, and are composed of 6 vertical elements, which together form a hollow tube.

Algirosphaera species secrete characteristic rhabdoliths (Aubry 1999; Kleijne 1992); the terminology that applies to their rhabdoliths is the same as for rhabdoliths described in Kahn and Aubry (2006). The innermost cycle (of 3) consists of lamellar elements developing into a globular-structured protrusion. The thin often broken distal end of the stem reveals the thick inner sides typical of a labiatiform stem (Aubry 1999).

The term nannolith has been used to describe the plates of species such as *Florisphaera profunda*, without the typical structural features of coccoliths. These forms are not formally classified as haptophytes, although their nannoliths may merely be unfamiliar or adapted coccoliths (Bown and Young 1998). I accept *Florisphaera* as a haptophyte, due to its calcite plates, which strongly resemble those of recognized coccoliths (such as *Gladiolithus striatus* and *G. flabellatus*), pending genetic testing, and therefore do not use the term nannolith. Instead the single crystals of polygonally-shaped calcite (see explanation in Quinn et al. 2005) that species in the genus *Florisphaera* secrete are termed polygolith. I use the terms anterior and posterior to refer to the wider and narrower ends of the polygolith, respectively, as discussed in Quinn et al. (2005).

The hemispheric coccospheres of each species within the genus *Solisphaera* consist of 3 types of cedrilith. I refer to the convex cedriliths on the antidomal side of the coccospheres of both *S. turbinella* and *S. galbula* as tumular due to the mound-shape into which the polygonal elements rise (Aubry and Kahn 2006; Ch. 2 of this dissertation). The concave discoidal cedriliths of *S. turbinella*, *S. blagnacensis*, *S. emidasia*, and *S. helianthiformis* are termed cupuliform due to their depressed central area. The cedriliths

observed only on coccospheres of *S. galbula* are termed gibbous due to their long narrow protrusion. I refer to the scaley, slightly convex cedriliths on the antidomal side of the coccospheres of *S. blagnacensis*, *S. emidasia*, and *S. helianthiformis* as scutate. The domal-side cedriliths are referred to as sacculiform (*S. turbinella* and *S. galbula*), peltiform (*S. blagnacensis*, *S. emidasia*), or petaliform (*S. helianthiformis*) cedriliths due to their cylindrical swollen or flattened protrusion, respectively.

4- Current Taxonomic Framework

Descriptions are paraphrased from the authors of the genera/species, unless otherwise referenced.

Family Rhabdosphaeraceae Haeckel 1894

Genus *Algirosphaera* Schlauder 1945 emend. Norris 1984

Dimorphic rhabdoliths on monothecate rhabdosphere. Rhabdoliths consist of 3 distinct cycles: 1. narrow outer rim, 2. inner cycle of spaced radial rectangular elements 3. inner cycle rising into labiatiform protrusion. Currently a single species is assigned to the genus although 6 taxa have been distinguished (Aubry 1999).

Algirosphaera robusta (Lohmann 1902) Norris 1984

The central area of the body rhabdoliths protrudes into a labiatiform distal shape that is hollow in the center and is composed of radial polygonal elements. That of the 3-4 circum-flagellar rhabdoliths protrudes higher than that of the body coccoliths into a flattened concavo-convex shape. The circum-flagellar rhabdoliths are centrally located

on one side of the rhabdosphere, forming an opening to the spherical to sub-spherical rhabdosphere.

Family *incertae sedis*

Genus *Gladiolithus* Jordan and Chamberlain 1993

Dimorphic coccoliths form widely cylindrical coccospheres, concave on the proximal side, convex on the distal side. Coccoliths are termed lepidoliths, flat elliptical to rounded rectangular plates overlapping to form the base of coccosphere, and 3-dimensional hollow tubular coccoliths composed of 6 vertical elements (Cros and Fortuño 2000). The 2 proximal peripheral elements have peg-like structures at their bases. The two species are currently differentiated based on the presence (*G. striatus*) or absence (*G. flabellatus*) of striations on the both tubular coccoliths and lepidoliths. In addition, *G. striatus* lepidoliths are dimorphic.

Gladiolithus flabellatus (Halldal and Markali 1955) Jordan and Chamberlain 1993

Lepidoliths are elliptical planoliths joined along a transverse suture. The spine-like tubular coccoliths can be featureless, or have small spines rising at irregular intervals from distal side of the coccolith along the sutures between the vertical elements. The top of the tube terminates in a crown shape formed by the 6 vertical elements.

Gladiolithus striatus Hagino and Okada 1998

Two types of striated lepidoliths cover the base of the coccosphere; elliptical planoliths with a suture perpendicular to the long axis separating them into 2 equal elements, and

rectangular planoliths with slightly rounded edges and a suture at a 45º angle to the long or short axis. Striations are perpendicular to the short axis. Lepidoliths are slightly curved, and overlap each other, increasing in number towards the center of the base of the coccosphere. Tubular coccoliths have striations parallel to the short axis, terminating in a straight line close to the top of the tube. The top of the tube has no striations, and terminates in a three-pronged crown-like shape.

Genus *Florisphaera* Okada and Honjo 1973

The genus name *Florisphaera* designates monomorphic coccospheres in the shape of a multi-petalled flower, consisting of polygonal plates (polygoliths) arranged by concentric, imbricated rows into a tightly layered rosette. One to two peg-like structures are seen on the posterior end of most plates presumably to secure the plates together. Three varieties are distinguished in the single species *Florisphaera profunda* Okada and Honjo 1973. *Florisphaera profunda* var. *profunda* (Okada and McIntyre 1977; Okada and Honjo 1973) is characterized by polygonal polygoliths terminating in an offset triangular peak. By contrast, *Florisphaera profunda* var. *elongata* (Okada and McIntyre 1977; Okada and Honjo, 1973) has polygoliths that are more elongate but also rise into an offset peak. *F. profunda* var. *rhinocera* possesses a distinct spine projecting from the dextral corner of the anterior end of the polygolith (Quinn et al. 2005). Several more morphotypes are proposed here, based on polygolith morphology.

Family Solisphaeraceae (*incertae sedis* aff. Rhabdosphaeraceae Bollmann, Cortés, Kleijne, Østergaard and Young 2006) Aubry and Kahn 2006

Genus *Solisphaera* (Bollmann, Cortés, Kleijne, Østergaard and Young 2006) emend. Kahn and Aubry in Aubry and Kahn 2006

Solisphaera turbinella Kahn and Aubry in Aubry and Kahn 2006

Solisphaera galbula Kahn and Aubry in Aubry and Kahn 2006

Solisphaera blagnacensis (Bollmann 2006) emend. Kahn and Aubry in Aubry and Kahn 2006

For complete descriptions of the genus *Solisphaera* and the species *S. turbinella, S. galbula,* and *S. blagnacensis* please refer to Chapter 2 of this dissertation.

5- Distribution and abundance of the DPZ community

Florisphaera profunda variants (42.3%) and *Solisphaera* species (8%) dominate the coccolithophore community recovered from Sample VANC10MV07D. *Solisphaera* is a newly identified DPZ dwelling genus, various morphotypes of which have been found in the southern Indian Ocean (this study), North Atlantic, equatorial Pacific, and Gulf of Mexico (Bollmann et al. 2006), and the Northwestern Mediterranean Sea (Cros and Fortuño 2002; labeled as Coccosphere sp.1, but subsequently classified within the *Solisphaera* genus (Aubry and Kahn 2006).

Less abundant are coccospheres of *Emiliania huxleyi* (4.7%), *Algirosphaera robusta* (4.0%), *Gladiolithus flabellatus* (1.9%) and *G. striatus* (0.9%). *Gephyrocapsa* spp. (1.9%), *Umbilicosphaera anulus* (1.9%), *Turrilithus latericidoides* (1.3%), and *Ophiaster*

formosus (0.9%) are also found in this sample, but in lesser numbers. Although *E. huxleyi* is found relatively frequently in this sample, and at varying depths at other sites, it is not discussed here because it is not classified as a DPZ species, but instead as highly cosmopolitan (Okada and Honjo 1973).

6- Quantitative analysis of DPZ genera

6.1- *Florisphaera profunda*

A total of 177 intact coccospheres were observed and photographed. Of those, 169 were complete, intact coccospheres and thus appropriate for measurement. These can be grouped according to distinctive features of the anterior end of their polygoliths, which differ by asymmetry and/or concavity/convexity of the triangular terminations and the intensity of serration. Based on these variations and sometimes the imbrication of the polygoliths on the coccosphere, the coccospheres of *F. profunda* were amenable to separation into 6 morphotypes, plus the 3 accepted species (Plates 1-3, Table 1).

6.1.1- *F. profunda* var. *elongata* (Plate 1, figs. a and b)

The polygoliths of *F. profunda* var. *elongata* were described by Okada and Honjo (1973) as polygonal plates more elongate than *F. profunda* var. *profunda*. The smooth plates terminate in an asymmetrical wide triangle and are identically shaped throughout the coccosphere. I estimated an average of 158 polygoliths per coccosphere, with a minimum of 92 and a maximum of 224 (Table 2). The length of the polygoliths varied between 1.9 µm and 4.1µm, averaging 2.3 µm (Fig. 5a). The width of the polygoliths varied between 1.0 µm and 2.5 µm, with an average of 1.4 µm (Fig. 5a). The maximum

width and length were recorded from polygoliths on the same coccosphere, which was itself significantly larger than any other observed coccosphere of *F. profunda* var. *elongata* in our sample (Table 3). The difference in widths of the polygoliths on a single coccosphere was approximately 0.5 µm, with the diffference in length on the order of 0.2 µm. The standard deviation in polygolith length and width per coccosphere ranged from 0.04-0.5 µm and 0.1-0.17 µm, respectively (Figs. 4a and 5a). With one exception, the width of the polygoliths of *F. profunda* var. *elongata* did not vary significantly between coccospheres (see above explanation).

6.1.2- *F. profunda* var. *profunda* (Plate 1, fig. c and d)

The polygoliths of *F. profunda* var. *profunda* are less elongate than those of *F. profunda* var. *elongata* (Okada and Honjo 1973), and their anterior end is concave, forming a V of variable sharpness. On the adjacent sides of the V, the anterior end either rises into a peak, or remains flat. I estimated an average of 151 polygoliths per coccosphere (Table 2). The average width, 1.5 µm, of the polygoliths was among the shorter of the morphotypes described here, with a relatively small size range compared to the other morphotypes (minimum=1.0 µm, maximum=2.0 µm) (Table 3). The length of the polygoliths averaged 2.0 µm, ranging from 1.5-2.3 µm. Variation was seen both on measurements of polygoliths on a single coccosphere, and among those on different coccospheres, with standard deviation on length and width of the polygoliths on each coccosphere ranging from 0.04-0.2 µm and 0.1-0.2 µm, respectively (Figs. 4b and 5b).

6.1.3- *F. profunda* var. *rhinoceri* (Plate 3, fig. e)

As described by Quinn et al. (2005), the polygoliths of *F. profunda* var. *rhinoceri* are polygonal plates with distinct spines projecting from the dextral corner of their anterior ends. I found 1 individual of this species in our sample. The polygoliths of this form were exceptionally wide (Table 3), averaging 2.4 µm, with little variation (minimum=2.2 µm; maximum=2.6 µm). Because of the position of the coccosphere on the filter (Plate 1, fig. c), measurement of the length of the polygoliths was not permitted. I estimated the number of polygoliths on a single coccosphere to be 135 (Table 2).

6.1.4- *F. profunda* var. *C* (Plate 1, figs. d and e)

This variety is characterized by tightly packed coccospheres with only slightly curved polygoliths. The polygoliths have a relatively flat and slightly serrated anterior end, without the typical triangular termination described in polygoliths of *F. profunda* var. *profunda* (Quinn et al. 2005; Okada and Honjo 1973). Most polygoliths were relatively similar in length and width. The average length of the polygoliths was 1.9 µm, among the shorter of the *Florisphaera* morphotypes (maximum=2.3 µm, minimum=1.4 µm), with a range in standard deviation per coccosphere of 0.005-0.3 µm (Fig. 4c). The average width of the polygoliths was 1.5 µm, ranging to a maximum of 2.6 µm and a minimum of 0.9 µm, with a range in standard deviation per coccosphere of 0.05-0.4 µm (Fig. 5c). The average number of estimated polygoliths was 145 (Table 2).

6.1.5- *F. profunda* var. *D* (Plate 2, figs. a and b)

The polygoliths of this variety are characterized by their asymmetry and serrations at both their anterior and posterior ends. The smaller polygoliths generally are more

irregularly shaped than the larger more polygonal ones. The polygoliths ranged in length on a single coccosphere by 1.5 µm (Fig. 4d). The length and width of the polygoliths of *F. profunda* var. *D* were the shortest of all morphotypes measured here, the width averaged 1.4 µm (range of 0.9-2.4 µm) and the length averaged 1.7 µm (range of 0.7-2.6 µm). Both on single coccospheres and between them, the length was variable (standard deviation per coccosphere: 0.008-0.5 µm), whereas the width, though variable, was more consistent with a standard deviation ranging from 0.06-0.2 µm (Fig. 4d and 5d). The coccospheres consisted of an average of 160 asymmetrical polygoliths.

6.1.6- *F. profunda* var. *E* (Plate 2, figs. c and d)

The average-sized polygoliths of this variety (relative to all *F. profunda* species and morphotypes) have distinctive tabs at the posterior ends and terminate in an off-centered V on the anterior ends. The distal end of the polygoliths is thus divided asymmetrically. The shorter side of the anterior end rises into a triangular point, while the longer side remains flat or slightly convex. The average number of polygoliths per coccosphere was calculated as 162 (Table 2). These polygoliths were not as long relative to their width as some morphotypes of *F. profunda*, with an average length of 2.1 µm (minimum=1.3 µm; maximum=2.6 µm), and width of 1.5 µm (minimum=1.0 µm; maximum=2.5 µm) (Figs. 4e and 5e). The standard deviation in length and width per coccosphere ranged from 0.02-0.3 µm and 0.07-0.2 µm, respectively (Figs. 4e and 5e).

6.1.7- *F. profunda* var. *F* (Plate 2, figs. e and f)

The polygoliths of this variety are similar to those of *F. profunda* var. *elongata*, terminating in an asymmetrical triangle. Unlike the smooth polygoliths of *elongata*, however, those of *F. profunda* var. *F* are serrate. The average number of polygoliths per coccosphere was 145 (Table 2). The average length of the polygoliths was 2.2 µm, with a maximum length of 4.2 µm and minimum of 1.4 µm, and range in standard deviation of 0.05-0.6 µm (Fig. 4f). The average width of these long polygoliths was among the least of the *F. profunda* morphotypes, 1.5 µm (maximum= 2.8 µm; minimum= 1.1 µm), with a range in standard deviation per coccosphere of 0.05-0.4 µm (Fig. 5f).

6.1.8- *F. profunda* var. *G* (Plate 3, figs. a and b)

Similar to those of *F. profunda* var. *E*, the polygoliths of *F. profunda* var. *G* rise into off-center triangular peaks. The longer side of the anterior end of the polygoliths is concave, with varying deepness, and the triangle terminates in a narrow sharp spine, similar, but shorter, to that of *F. profunda* var. *rhinoceri*. I estimated an average of 141 polygoliths per coccosphere (Table 2). The average length of polygoliths was the 2nd largest of all the morphotypes measured here, and the average width was the greatest (Table 3). These relatively large polygoliths averaged 2.6 µm in length, with a minimum of 2.0 µm and a maximum of 3.2 µm (Table 3). The average width of the polygoliths was 2.2 µm, ranging from a minimum of 1.2 µm and a maximum of 2.6 µm (Table 3). I observed variation among the length of polygoliths betIen coccospheres but generally little on a single coccosphere; standard deviation per coccosphere ranged from 0.02-0.3 µm (Fig. 4g). By contrast, I saw variation in polygoliths width on single coccospheres, but less so among different coccospheres (this is of course partially due to the greater

variety on single coccospheres); standard deviation per coccosphere ranges from 0.06-0.3 µm (Fig. 5g).

6.1.9- *F. profunda* var. *H* (Plate 3, fig. c and d)

The polygoliths of this variety are characterized by featureless polygonal plates that are smooth and flat to rounded on the anterior end. The length averaged 2.3 µm, with a considerable range from 1.7 µm to 3.1 µm and a standard deviation per coccosphere of 0.2 µm (Fig. 4h). The width also varied significantly, from 1.0 µm to 3.2 µm, and averaged 1.7 µm, with a range in standard deviation per coccosphere of 0.7-0.3 µm (Fig. 5h). There were relatively fewer of these large polygoliths per coccosphere, with an average of 92 (Table 2).

6.2- *Gladiolithus flabellatus* (Plate 4, figs. d and f)

6.2.1- Coccosphere and coccoliths

A total of 12 coccospheres were observed, 11 of which were collapsed, and 1 of which was intact (Table 4). Of those 11 collapsed, 3 were considered complete. The length of the tubular coccolith averaged 6.9 µm, with a wide range from 4.4-11.1 µm and standard deviation per coccosphere of 0.1-0.5 µm (Fig. 6a). The average width of the top and base of the tubular coccolith was 1.9 µm and 1.3 µm, respectively, both with standard deviations per coccosphere of 0.06-0.2 µm (Fig. 6b and c). The width of the top had a smaller range (1.1-2.8 µm) than that of the base (0.9-1.7 µm). The average length of the elliptical lepidoliths was 1.7 µm (ranging 1.5-2.2 µm), with standard deviation per

coccosphere of 0.1 µm (Fig. 6d). The width of the lepidoliths averaged 1.2 µm (ranging 1.0-1.5 µm) and standard deviation per coccospher eof 0.1 µm (Fig. 6e).

6.3- *Gladiolithus striatus* (Plate 4, figs. a-c and e)

6.3.1- Coccosphere and coccoliths

A total of 5 coccospheres were observed; 3 intact and 2 collapsed but considered complete (Table 4). The length of the tubular coccolith ranged from 4.0-5.1 µm, with an average of 4.6 µm; standard deviation per coccosphere of 0.2 µm (Fig. 6a). The width of the 3 elements at the top of the tubular coccolith averaged 1.6 µm (range=1.3-2.0 µm), with a standard deviation per coccosphere of 0.05-0.2 µm (Fig. 6b). At the base the width averaged and ranges slightly less; 1.1 µm, 0.9-1.2 µm, respectively, with a range in standard deviation per coccosphere of 0.5-0.8 µm (Fig. 6c). The lepidoliths were elliptical to rounded rectangular, with an average length of 1.8 µm, and average width of 1.3 µm (Fig. 6d and e). The standard deviation per coccosphere in lepidolith length and width was 0.1 µm and 0.1 µm, respectively (Fig. 6d and e).

6.4- *Algirosphaera robusta* (Plate 5)

6.4.1- Rhabdosphere

A total of 19 rhabdospheres were observed in this sample, 11 of which were intact, 5 collapsed, and 3 malformed. The long diameter of the rhabdosphere averaged 11.8 µm, the short, 10.8 µm (Table 4). One pole of the rhabdosphere has a flagellar opening surrounded by 3-4 flattened circum-flagellar rhabdoliths (Plate 5, fig. d), which rise above the body rhabdoliths. Considering the asymmetry of the rhabdosphere, it was

difficult to estimate the total number of rhabdoliths per rhabdosphere; nonetheless, assuming sphericity, I calculated that the number of rhabdoliths ranged from 45-116, malformed individuals with generally fewer rhabdoliths per rhabdosphere than normal individuals (45 and 62) (Table 4).

6.4.2- Rhabdoliths

Algirosphaera robusta coccospheres are dimorphic, consisting predominantly of body rhabdoliths, and 3-4 circum-flagellar rhabdoliths. The body rhabdoliths are composed of 3 cycles, the central cycle rising into a labiatiform protrusion. This protrusion obscures the base of the rhabdoliths and the inner rhabdosphere from view (Plate 5, figs. a-c). The labiatiform protrusion was often slightly broken at the distal end, so that the inner structure of the protrusion was visible (Plate 5, fig. f). The average length of the distal end of the protrusion was 2.5 µm, with a range of 1.6 µm to 3.7 µm (Fig. 7a), and standard deviation of 0.5 µm (Table 4). The average width of the distal end of the protrusion was 1.1 µm, ranging from 0.9 µm to 1.6 µm (Fig. 7b), with standard deviation of 0.2 µm (Table 4). The base of the body rhabdoliths, visible only when the rhabdosphere was broken, averaged 2.2 µm and 1.6 µm in length and width, respectively (Fig. 7c and d). The height of the labiatiform protrusion ranged from 1.4 µm to 3.0 µm, with an average of 2.1 µm (Fig. 7e), and standard deviation of 0.3 µm (Table 4).

6.5- *Solisphaera turbinella* (Plate 4, fig. g)

Trimorphic coccospheres with cupuliform cedriliths on the antidomal side of the coccosphere, sacculiform cedriliths on the domal side, and tumular cedriliths positioned equatorially.

6.5.1- Coccosphere

The coccosphere is minuscule, averaging 4.5 µm in diameter, but ranges considerably from 3.1-5.3 µm (Table 5). The average number of sacculiform cedriliths is 50, ranging from 34-70 cedriliths per coccosphere (Table 5). That of the tumular and cupuliform discoidal cedriliths are 25 and 17, respectively, ranging less than the sacculiform cedriliths, from 20-30 and 13-21 tumular and cupuliform cedriliths, respectively (Table 5). Depending on the orientation of the coccosphere, only particular types of cedriliths are visible.

6.5.2- Cedriliths

The long axis of tumular cedriliths averages 1.1 µm, ranging from 0.9-1.2 µm, with a standard deviation per coccosphere of 0.01-0.2 µm (Fig. 8a). The short axis of tumular cedriliths averages 0.8 µm (minimum=0.7 µm, maximum=0.9 µm), with a standard deviation of 0.03-0.05 µm (Fig. 8b). The long axis of cupuliform cedriliths averages 1.0 µm, slightly less than the long axis of the tumular cedriliths, with a large range from 0.7-1.2 µm and standard deviation of 0.05-0.2 µm (Fig. 8c). Their short axis averages 0.8 µm, ranging slightly less than the long axis, from 0.6-0.9 µm, with a standard deviation of 0.008-0.08 µm (Fig. 8d). The base of the sacculiform cedriliths is more circular than that of the tumular or cupuliform cedriliths (Fig. 8e, f, g), averaging in

length and width, 0.77 µm and 0.75 µm, respectively (Fig. 8g). The range between the length and the width, however, varies in numeric value and amplitude: 0.1-1.0 µm, 0.7-0.8 µm, respectively. The height of the sacculiform protrusion is smaller than that of *S. galbula*, averaging 0.5 µm, with a greater range of 0.2-0.7 µm and standard deviation of 0.1 µm (Table 5). The height of the spine exuding from the distal end of the sacculiform protrusion averages 0.1 µm, with a relatively large range of 0.05-0.2 µm (Fig. 8h), and an average standard deviation of 0.03 µm (Table 5).

6.6- *Solisphaera galbula* (Plate 4, fig. h)

Trimorphic coccospheres with gibbous cedriliths on the antidomal side of the coccosphere, tumular cedriliths positioned equatorially, and sacculiform cedriliths on the domal side.

6.6.1- Coccosphere

A total of 14 coccospheres of varying orientation were found on the filter. The average diameter of the coccosphere is 5.0 µm, ranging from 4.2 µm to 5.9 µm (Fig. 9a). The average number of sacculiform cedriliths per coccosphere is 51 (similar to *S. turbinella*), and the average number of the tumular and gibbous cedriliths is 29 and 33, respectively per coccosphere (note the contrast with those values for *S. turbinella*) (Table 5).

6.6.2- Cedriliths

The diameter of the long axis of the tumular cedrilith averages 1.1 µm, with a range from 0.8-1.3 µm and standard deviation per coccosphere of 0.02-0.1 µm (Fig. 9b). The short axis of the tumular cedrilith averages 0.6 µm, with a range from 0.5 to 0.7 µm (Fig. 9c). The gibbous cedriliths are more variable in size and less elliptical than those of the tumular cedriliths. The average diameter of the long axis of the base is 1.0 µm, with a standard deviation per coccosphere of 0.04-0.1 µm (Fig. 9d), the short axis, 0.6 µm, with a standard deviation of 0.03 µm (Fig. 9e). The range of the long and short axes is, respectively, 0.6-1.2 µm, and 0.5-1.1 µm (Fig. 9d, e). The base of the cylindrical sacculiform protrusion is circular, its long axis averaging 0.7 (minimum=0.6 µm, maximum=0.9 µm) (Fig. 9f); its width also averages 0.7µm (minimum=0.68 µm, maximum=0.73 µm) (Table 5). The height of the protrusion averages 0.6 µm, with a small range from 0.5-0.7 µm (Fig. 9g). The top of the sacculiform protrusion averages 0.8 µm (long axis) and 0.2 µm (short axis) (Table 5).

6.7- *Solisphaera blagnacensis* (Plate 4, fig. i)

Trimorphic coccospheres with scutate cedriliths on the antidomal side of the coccosphere, cupuliform cedriliths positioned equatorially, and peltiform cedriliths on the domal side.

6.7.1- Coccosphere

I found 14 coccospheres of this species. The average diameter of the coccosphere is very small, 4.8 µm, but ranges considerably from 4.1 µm to 6.2 µm (Table 5). The

average number of peltiform cedriliths is 41 per coccosphere (Table 5). On the apical side of the coccosphere, the average number of cupuliform cedriliths is 13 per coccosphere, and the average number of scutate cedriliths is 11 (Table 5), but because they are overlapping and many are underneath the cupuliform cedriliths I may have missed some.

6.7.2- Cedriliths

The diameter of the base of the peltiform cedriliths averages 1.0 µm in length (standard devation per coccosphere= 0.01-0.2) (Fig. 10a), 0.7 µm in width. The height of the peltiform protrusion averages 0.8 µm, ranging from 0.6-1.0 µm, with a standard deviation per coccosphere of 0.05-0.2 µm (Fig. 10b). The top of the peltiform protrusions average 1.0 µm and 0.2 µm in length and width, respectively (Fig. 10c). On the planar side of the coccosphere, the long and short axes of the cupuliform cedriliths average 1.3 µm (standard deviation= 0.2 µm) and 1.0 µm (standard devation= 0.1 µm), respectively, fitting into 2 size groups (Fig. 10d). The scutate cedriliths could not be measured due to their position underneath the cupuliform cedriliths.

7- Discussion

7.1- Morphotypic variation in *Florisphaera profunda*

Florisphaera profunda is a ubiquitous DPZ dweller, identified off the coast of Japan (Okada 1973), in the Red Sea (Okada and Honjo 1975), the Mediterranean Sea (Thomson et al., 2004; Cros and Fortuño 2002), the equatorial (Molfino and McIntyre 1990) and northern (Okada and Honjo 1973) Atlantic Ocean, the western (Okada 1983; Okada and

Honjo 1975), equatorial (Hagino et al. 2000; Molfino and McIntyre 1990; Okada and Honjo 1973), and northern (Reid 1980) Pacific Ocean, the northern (Andruleit et al. 2005; Okada and Matsuoka 1996), and southern (this study) Indian Ocean.

Recent morphological analysis of *F. profunda* indicates that it should be split into 3 morphospecies (Quinn et al. 2005). Here I have found broad variation in polygolith shape, indicating further splitting of the species. Variation in polygolith (instead of coccosphere) shape distinguishes the morphotypes as shown in this study and in recent work. Minor size variation (Tables 2, 3) in both polygoliths and coccospheres (less so) emphasizes the differentiation in shape. All forms were found at the same location and their collective presence indicates that the variation in their morphologies may not be functional. It may also indicate that the salinity and/or temperature and/or nutrient conditions at 120 m depth at Site VANC10MV07D were ideal for the *Florisphaera* genus, which therefore flourished in many forms. The homogeneity in *overall* morphology (e.g., size *and* shape) of the coccospheres - the dominant rectangular shape of the elements, and the imbrication of those component elements - indicates that the coccosphere of *F. profunda* may be an adaptation to stable, low light, high nutrient DPZ conditions that is shared across DPZ dwelling genera.

F. profunda var. *C* (Plate 1, figs. d and e) and *F. profunda* var. *D* (Plate 2, figs. a and b) may be along a continuum of similarity, because at first glance their contrast may not appear obvious and they differ only slightly in size (Tables 2, 3). However, *F. profunda* var. *D* is irregular on both anterior and posterior ends of the polygolith, with deep serrations misshaping the typical polygon, described by Okada and Honjo (1975) as possibly malformed. Polygoliths of *F. profunda* var. *C* only have serrations on the

overall flat-shaped anterior end so that the polygoliths maintain a polygonal shape. The fundamental difference is extremity and location of serrations on individual polygoliths, both characteristics contrasting notably between the morphotypes.

F. profunda var. *G* (Plate 3, figs. a and b) is among the largest of the *F. profunda* morphotypes in both coccosphere and polygoliths, whereas *F. profunda* var. *elongata* and *F. profunda* var. *F* consist of among the smaller polygoliths, although their coccospheres measure approximately average that of all the morphotypes. Polygoliths of *F. profunda* var. *elongata, F. profunda* var. *F,* and *F. profunda* var. *G*, are all elongate polygons as first described by Okada and Honjo (1973), varying in shape of the anterior end of the polygonal element. *F. profunda* var. *elongata* raises into a slightly offset triangular peak (Plate 1, figs. a and b). The perimeter of this peak, as well as of the entire element, is smooth. By contrast, in *F. profunda* var. *F*, the perimeter of the same offset peak is serrated (Plate 2, figs. e and f). That peak is further modified in *F. profunda* var. *G*, in which the moderately serrate to smooth peak rises into a narrow spine (Plate 3, figs. a and b). One side of the anterior end sometimes rises into a blunt protrusion slightly above the top of the polygolith, but below the level of the spine.

F. profunda var. *E* and *F. profunda* var. *profunda* both are composed of below average-sized polygoliths which form above average-sized coccospheres (Tables 2 and 3). Although they contrast little in size, the shape of the anterior ends of their polygoliths is very different. Polygoliths of *F. profunda* var. *E* have a flat anterior end that rises abruptly into a small triangle on one side (Plate 2, figs. c and d). By contrast, the polygoliths of *F. profunda* var. *profunda* indent into a shallow V located usually at the center of the anterior end (Plate 1, figs. c and d).

F. profunda var. *H* has very smooth polygoliths with rounded to slightly rounded anterior ends (Plate 3, figs. c and d). The polygoliths are short but often very wide relative to their length, as well as to the widths of the polygoliths of other variants. These are the most featureless of the polygoliths, very different from other *F. profunda* morphotypes.

7.2- Intra- and interspecific variation in *Gladiolithus flabellatus* and *Gladiolithus striatus*

Gladiolithus flabellatus is found in the DPZ in the northern (Reid 1980) and western central equatorial (Hagino et al. 2000) Pacific Ocean, the northern Atlantic Ocean (Okada and Honjo 1973; Halldal and Markali 1955), and the northern (Okada and Matsuoka 1996) and southern (this study) Indian Ocean. Much scarcer, *G. striatus* is found in the DPZ of the Pacific Ocean (Hagino et al. 2000; Hagino and Okada 1998) and the southern Indian Ocean (this study).

Although their coccospheres are structured virtually identically, several variations in their coccolith morphologies confirm the strong differentiation between *G. flabellatus* and *G. striatus* (Hagino and Okada 1998). Here I will discuss both features of the coccoliths and the overall structure of the coccosphere.

7.2.1- Coccosphere

The coccospheres of both *G. flabellatus* and *G. striatus* are structured asymmetrically as short cylinder, flat at the base, and spiked at the top due to the 3-pronged structure of its tubular coccoliths (Fig. 3). The base is covered by elliptical or rounded rectangular lepidoliths, which form a thin layer around the outside of the cylinder, thickening as more lepidoliths are layered towards the middle of the base (Plate 4, fig. b). This thickening

towards the middle reduces the potential concavity of the coccosphere base, flattening out the overall basal structure.

The tubular coccoliths appear thickest at their base, thinning towards the middle of the coccolith, and then thickening slightly to make a hollow tube at the top (Plate 4, figs. e and f). The described structure plus a minimal to moderate curvature of the coccolith contributes to the packing of the coccosphere. The coccoliths fit together with the concave side proximal to the convex side of the one in front. This creates a small opening in the middle of the coccosphere above the area of the thickest layer of lepidoliths, where the cell presumably can fit (Lohmann 1902).

Due to its asymmetry, counting the exact number of coccoliths per coccosphere is difficult. To estimate I counted the number of tubular coccoliths in a row and then counted the number of rows. I will assume here that those for which I could not count the rows contained 7 rows of tubular coccoliths. Some coccospheres were wholly visible (both collapsed and intact) so that I could count the total number of tubular coccoliths. I counted the number of visible lepidoliths, assuming that overlap notwithstanding, all of the lepidoliths would be at least partially visible. The 5 collapsed but whole coccospheres of *G. striatus* consisted of 58-91 tubular coccoliths and 34-36 lepidoliths, and the 3 of *G. flabellatus* consisted of 57-98 tubular coccoliths, and 74 lepidoliths (Table 4).

A single intact measurable coccosphere of each *G. flabellatus* and *G. striatus* (2 more intact coccospheres also found, but measurements were not taken due to the orientation of the coccospheres) yielded coccosphere measurements as follows: diameter of base, 7.9

and 8.3 µm, respectively; diameter of top, 10.7 and 12.6 µm, respectively; height, 5.062 and 4.5 µm, respectively.

7.2.2- Coccoliths

Interestingly, certain coccolith features are smaller in *G. flabellatus*, and some smaller in *G. striatus*. Also, as to be expected, the intra- and interspecific size range varies between feature and species. Tubular coccoliths of *G. striatus* contrast relatively little in length intraspecifically (1 µm), whereas those of *G. flabellatus* contrast significantly (6.7 µm) (Fig. 6a). The shorter tubular coccoliths contrast little in size intra- and interspecifically between *G. flabellatus* and *G. striatus* (Fig. 6a). However, interspecific variation among the tubular coccoliths is greater in the longer coccoliths. The width of the proximal side of the tubular coccoliths of *G. striatus* is generally less than that of *G. flabellatus* (compare average widths: 1.1 µm, 1.3 µm, respectively) (Fig. 6b). The range in width of the proximal side of the tubular coccoliths is also less among *G. striatus* individuals (0.3 µm) than among *G. flabellatus* individuals (0.8 µm) (Table 4). The distal side of the tubular coccoliths of *G. striatus* are narrower (0.3 µm difference in average width) and vary less intraspecifically than *G. flabellatus* (contrast range of 0.7 to 1.7 µm, respectively) (Fig. 6c). There is little interspecific variation in the lengths of lepidoliths with the average of *G. striatus* only 0.1 µm greater than that of *G. flabellatus* (Fig. 6d). Intraspecific variation in the length of the lepidolith is minimal too, 0.4 and 0.7 µm, respectively. The average width of lepidoliths of *G. striatus* is slightly greater (0.1 µm) than that of *G. flabellatus*, with little interspecific variation (Fig. 6e). The above

measurements are comparable to those of Hagino and Okada (1998) (Table 4), with minor variation in range.

7.3- Morphology of *Algirosphaera robusta* coccospheres

Algirosphaera robusta is found in the Mediterranean Sea (Cros and Fortuño 2002), the Red Sea (McIntyre 1969), Pacific and North Atlantic Ocean basins (Okada and McIntyre 1977), and the northern (Okada and Matsuoka 1996) and southern (this study) Indian Ocean. Generally assumed to be a spherical species, observation here and in culture (Probert, pers. comm. 2006) indicates that the tightly packed *A. robusta* rhabdospheres in fact range in structure from spherical to hemispheric. Previously used to classify junior synonyms of *A. robusta*, these variations in coccosphere sphericity are not currently considered significant enough for species designation (Young et al. 2003; Kleijne 1992). The rhabdospheres and constituent rhabdoliths found in this sample vary by similar magnitude to the coccospheres and polygoliths of *F. profunda* variants, and far less than those of *Gladiolithus* species. The rhabdospheres vary by ~3-4x the long axis of their diameter. They are notably larger (138%-150%) than those of Kleijne (1992), which were collected at 0-5 m water depth. Measurements of the rhabdoliths are similar to those of Kleijne (1992), though those from our samples generally range slightly larger (Table 4). I cannot make global generalizations from this comparison because of the sample size. Further quantification is necessary.

Though designated as a DPZ dweller, *A. robusta* is also found in surface waters (Triantaphyllou pers. comm. 2006; Kleijne 1992) and the unique features of its rhabdospheres are not consistently comparable with those of the other DPZ coccospheres.

The structure may reflect adaptation to such water column cosmopolitanism, but further research of such depth-ranging species is needed for clarification.

7.4- Interspecific variability in the genus *Solisphaera*

The average diameter of the coccospheres of *S. turbinella, S. galbula,* and *S. blagnacensis* fall along a continuum of (as measured from collapsed coccospheres) from smallest (*S. turbinella*) to largest (*S. galbula*) but overlap in size range (Fig. 11a; Table 5). Interestingly, though the average diameter of the coccospheres of *S. blagnacensis* falls in the middle of the 3 species (though the maximum diameter I measured was greater than the maximum diameter of the coccospheres of either *S. turbinella* and *S. galbula*) the number of peltiform cedriliths on the domal side is significantly less (~50%) than the number of sacculiform cedriliths on those of *S. turbinella* and *S. galbula* (Table 5). The sacculiform cedriliths of *S. turbinella* and *S. galbula* are far more densely packed on the domal side. The diameter of the coccosphere is ~10% smaller in *S. turbinella* than *S. galbula* (Fig. 11a), although the average number of sacculiform cedriliths is approximately the same (Table 5). The planar side of the coccosphere of *S. turbinella* has fewer discoidal cedriliths (68%) than *S. galbula* (they are slightly larger and cover a smaller coccosphere).

Solisphaera turbinella has wider range in height of the protrusion of the sacculiform cedrilith, but *S. galbula* is 0.1 µm larger in average height (Fig. 11b). The bases of the peltiform cedriliths of *S. blagnacensis* are larger and more elliptical than those sacculiform cedriliths of *S. turbinella* and *S. galbula* (Table 5).

Solisphaera turbinella has generally smaller cupuliform discoidal cedriliths, but I do observe overlap between the ranges of the 2 species (Fig. 11c). Interestingly, the average diameter of the long axis is the same, but the average diameter of the short axis in *S. turbinella* is 0.2 µm larger than that of *S. galbula* (this is not necessarily illustrated in the Fig. 11 compilations, which show only those cedriliths with measurements of both long and short axes). The tumular discoidal cedriliths are generally larger in *S. turbinella* than *S. galbula*. Although the short axis of *S. turbinella* averages 0.2 µm larger than *S. galbula*, the average diameters of the long axes are the same (Fig. 11d). I also observe 2 size groupings in the cupuliform discoidal cedriliths of *S. blagnacensis*, the larger of which is much larger than the equivalent cupuliform discoidal cedriliths of *S. turbinella*. The smaller grouping, however, overlaps the sizes observed in *S. turbinella* (Fig. 11e).

7.5- Summary of DPZ intraspecific variability

The species within the genera *Florisphaera, Gladiolithus*, *Solisphaera*, and *Algirosphaera* occupy a fairly limited generic niche in the DPZ. As shown above, I have quantified low magnitude intra- and interspecific variability in both coccospheres and coccoliths of those species in the DPZ of the southern Indian Ocean; this is in significant contrast to the high intraspecific variability analyzed in the SPZ within the family Rhabdosphaeraceae (Kahn and Aubry 2006).

7.5- Structure and Morphology of DPZ coccospheres

DPZ coccolithophorids occupy a contrasting ecological niche from SPZ species (Okada and Honjo 1973). Particular coccosphere shapes are almost omnipresent in the DPZ. In the SPZ, I observe a wide variety of coccosphere shapes, including, but not limited to, those coccospheres I analyzed in the DPZ. The strong variability in size as well as shape of the coccospheres and coccoliths in the SPZ indicates that no particular morphology defines that zone. By contrast, due to their lack of overall morphological variability (as demonstrated here), and relatively unique coccolith and coccosphere structure, the DPZ dwelling species appear to have adapted a common morphology to the low light, high nutrient conditions of 100-200 m water depth near the thermo/nutricline. I discuss this further below and in section 7.6.

Although some species can live in both the SPZ and the DPZ (e.g., *Gephyrocapsa* spp., *E. huxleyi*), the globally dominant species in the DPZ are well characterized: *F. profunda, G. flabellatus, O. antillarum,* and *A. robusta* (Okada and Honjo 1973). I also add *S. turbinella, S. galbula*, and *S. blagnacensis* (Aubry and Kahn 2006; Bollmann et al. 2006) and *Navilithus altivelum* (Young and Andruleit 2006). Because they live in a relatively eutrophic environment compared to the SPZ dwellers, the deeper dwelling coccolithophorids may differ in life strategy. Although classified as a DPZ species, *A. robusta* is also found throughout the photic zone and its structure does not consistently fit into the DPZ morphology I describe here.

This study is in agreement with Aubry (2007) in that among the features that distinguish the SPZ from the DPZ dwelling heterococcolithophorids are size of the cell, structure, shape and size of the coccosphere, and number and position of the coccoliths. The

coccospheres of the deep-living genera display 2 especially notable morphostructures most common to the DPZ: 1. imbricated and elongate, 2. hemispheric. The coccoliths of *F. profunda* and *O. antillarum* are imbricated, forming slightly elongate coccospheres from the progressive layers (Fig. 3a, b). The imbrication requires that all the coccoliths are oriented in the same direction at slightly varying angles towards the flagellar opening. Coccospheres of *Solisphaera* spp., *G. flabellatus, G. striatus,* and sometimes, *A. robusta,* are hemispheric, with a defined base and convex/domed top (Fig. 3c, d). These asymmetrical coccospheres are characterized by differently structured coccoliths on the planar vs. convex/domal side. Those convex/domal side coccoliths are comprised of a base with a protrusion (labiatiform, sacculiform, tubular, or peltiform). They are oriented so that they rise outwards from the coccosphere. The planar side coccoliths (lepidoliths or discoidal cedriliths) overlap to form a flat slightly convex base (Pl. 4b). Though the structure of *A. robusta* is sometimes hemispheric, it is not comprised of different rhabdoliths on opposing sides of the coccosphere. The asymmetry of the otherwise morphologically homogeneous rhabdosphere is caused by its flagellar opening, which is surrounded by 3-4 flattened elongate rhabdoliths. These circumflagellar rhabdoliths are differentiated from the surrounding labiatiform rhabdoliths by their increased height, and 2-dimensionality. The hemispheric rhabdosphere is differentiated only by its overall shape, not by its constituent rhabdoliths.

Whether elongate cylinders or hemispheric, the DPZ coccospheres are generally asymmetrical with obviously differentiated poles (though distinguishing apical from antapical pole, and alignment of the coccosphere relative to the air-sea interface can be difficult). *Oolithotus antillarum* is one minor exception, as its coccosphere can be more

spherical and symmetrical than the other deep photic forms; yet, the coccosphere is generally slightly elliptical, and always floriform, imbricated, and opens at one pole (features common in the DPZ dwellers). *Gladiolithus*, *Solisphaera*, and to a lesser degree, *Florisphaera*, all have one pole (apical) with mono-directional coccoliths parallel to the short axis of the coccosphere (Pl. 4a-b; Pl. 1-2d, e, f). The coccoliths on the other pole (antapical) or domal side are mono-directional and oriented perpendicular to the short axis (Pl. 4a, c-d, e-g; Pl. 3b, e).

The DPZ coccolithophorids appear to have larger calcite volumes relative to the size of their cells than their counterparts in the SPZ. The coccospheres, particularly those of *F. profunda*, *G. flabellatus*, and *G. striatus*, are tightly packed, held together presumably by the 2 peg-like structures at the proximal (posterior) base of each of their vertically-oriented coccoliths. These peg-like structures are not seen in other species (shallow or deep), and appear to be a unique adaptation for the structure these genera exhibit; indeed, they appear to facilitate the imbricated structure of the coccosphere. Additionally, the relatively 1-dimensional structure of their coccoliths (contrast to placoliths, with their 2 layered shields) and concave shape permits a considerable number of coccoliths to fit multiple layers within a small volume. The asymmetrical coccospheres have relatively little space for their cells due to this packing structure.

The actual location of the cell within the coccosphere is unknown, but Lohmann (1902) proposes that in *Gladiolithus sensu* lato it sits in the center of the lepidolith-covered anti-domal side, surrounded by the slightly curved tubular coccoliths. Similarly, the coccosphere of *Florisphaera sensu lato* appears to hold the cell at its domal side, with significantly fewer polygoliths overlapping, in contrast with the antidomal side, with

similarly multiple layers of polygoliths as the tubular coccoliths of *Gladiolithus* coccosphere. However, on the coccospheres of *Florisphaera*, the polygoliths imbricate and rotate outwards from the base, forming a thickening cone; whereas, the entire coccosphere of *Gladiolithus* bends, creating a comparable shape, without spiraling imbricated tubular coccoliths.

The coccospheres of some SPZ species have similar characteristics to those of the DPZ, as Aubry (in press) proposes, indicating that several morphostructural groups exist to categorize genera of both the extant and extinct coccospheres and coccoliths, spanning across depth "boundaries" (i.e., genera with (un)limited depth ranges overlap groups). *Alisphaera gaudii* Kleijne et al. 2002, *A. pinnigera* Kleijne et al. 2002, *A. unicornis* Okada and McIntyre 1977, *Helicosphaera wallischi* (Lohmann 1902) Okada and McIntyre 1977, *H. carteri* (Wallich 1877) Kamptner 1954, *H. hyalina* Gaarder 1970 are all SPZ coccolithophorids with imbricated coccoliths, and often a cylindrical coccosphere structure. The above species of *Helicosphaera* are composed of fewer larger coccoliths than those above of *Alisphaera*, which are comprised of smaller, more abundant coccoliths. The imbrication of numerous small coccoliths is strikingly similar to that of the DPZ coccospheres; however, the SPZ coccospheres are large, and range from slightly elliptical to spherical, unlike the small, floriform and asymmetrical coccospheres of the DPZ. In addition, the DPZ species (namely, *Florisphaera*, *Solisphaera*, *Gladiolithus*) are imbricated and thickly layered or strongly asymmetrical (Fig. 3), so that a small space is left for the cell, unlike the larger single-layered SPZ coccospheres. The coccospheres of *O. antillarum*, similar to the SPZ imbricating coccospheres, are comprised of a single layer of imbricating coccoliths (Fig. 3); however, the coccoliths are relatively large

compared to the coccosphere, sometimes measuring almost 1/3 the height of the coccosphere.

It is likely that the relative instability in the SPZ that creates different types of habitats also forces variation in coccosphere morphology. In contrast, the DPZ, with low light and high nutrient concentrations, is considerably more stable an environment, unaffected by the air-sea interface, such that they only require efficient light harvesting for photosynthesis, or perhaps nutrient harvesting for possible heterotrophy. As such, the similarity of some SPZ coccospheres to those in the DPZ is not surprising, as variable turbidity, wind/wave conditions, temperature, nutrient conditions, etc., will force SPZ coccospheres to be adaptable to a modifiable SPZ, or specifically thrive in particular SPZ conditions (that can sometimes be similar to those in the DPZ).

7.6- Adaptive functionality of coccoliths

It is unknown whether DPZ dwellers are exclusively photosynthetic or in fact heterotrophic (Brand 1994). Although it is tempting to hypothesize that these genera would be unable to exclusively photosynthesize in conditions of such reduced sunlight, their size and shape in fact indicate that they are well suited for autotrophy. Coccolithophore cells contain 2-4 lens shaped chloroplasts, overlapping or layering underneath the cell walls (Kirk 1994). The shape of an elongate cell (in contrast to that of a spherical one) reduces the amount of chloroplast layering so that the chloroplasts are all closer to the cell wall and more efficient at light collection (Kirk 1994).

The elongate (or floriform) structure observed in some DPZ coccospheres (Fig. 3) improves cellular light absorption (Kirk 1994; Young 1994), plus a smaller cell has a

larger surface area to volume ratio, again optimizing light absorption (Finkel 2001; Peters 1983). The reduced cell size, in combination with the particular elongation of the DPZ coccospheres thus clearly indicates a selection towards efficient light collection, possibly so that these species can remain exclusively photosynthetic. Additionally, at depth the coccolithophores have a competitive advantage for nutrients over light, so that the nutrients necessary for efficient photosynthesis are not limiting.

It has been shown that light and nutrient competitive ability are found in inverse concentrations in the water column (Klausmeier and Litchman 2001). In the ocean I also see inverse vertical concentrations of light and nutrients within the photic zone so the SPZ coccolithophores must in general (exceptions including turbidity) be more effective nutrient competitors, whereas, DPZ coccolithophores must be more effective light competitors.

8- Conclusions

Although the extant coccolithophores are relatively uniform in size compared to those found in the fossil record (Aubry 2007), the comparison in intraspecific variability between the SPZ and DPZ remains quantifiable and of importance in interpreting possible convergence through time. I also propose that the lack of size variability can be extrapolated to the fossil record in reconstructing the paleodepth habitats of particular coccolithophore species. The unusual morphologies observed in the DPZ, seen less commonly in shallower communities, seem to indicate morphological adaptation to the DPZ ecological niche. Those coccospheres with comparable morphologies in the SPZ may be responding to forcing mechanisms similar to those in the DPZ. I also suggest that

species with wider depth ranges, such as *A. robusta*, but who inhabit the DPZ, may differ in morphological utility than those that live exclusively in the DPZ.

I measured several dimensions of each type of coccolith for each species analyzed here. I found that certain measurements were more useful than others and summarize here:

1- *Florisphaera profunda*

Length and width dimensions are crucial in analyzing variability in *F. profunda* due to 1. relative ease of accessibility to take measurements, 2. comparability with other geometrically-shaped polygoliths, 3. inter- and intra-generic comparability. It is considerably easier to measure the width of the polygoliths because of the imbricated nature of the coccosphere, such that the overlapping polygoliths block view of their full lengths. *Florisphaera profunda* has unusually low variability both on any given coccosphere, within a particular species, and among multiple morphotypes (i.e., generically).

2- *Gladiolithus flabellatus and G. striatus*

The coccospheres of *G. flabellatus and G. striatus* are strongly asymmetrical. Measurements of width and height of the coccosphere differentiate the height of the tubular coccoliths and the total width of all overlapping lepidoliths. Determining the important measurements on these coccoliths depends on the aim of the study (more so than the other species discussed here). To determine intraspecific variability, the most useful measurements are the length and width of the lepioliths, the length of the tubular coccoliths, and the width of the top of the coccoliths. I do not include the width of the

base of the coccolith here due to the greater difficulty in measurement, but more importantly, due to the similarity in relative variability with the width of the top of the tubular coccoliths. For analyses of relative dimensions on and structure of the coccosphere, the width of the base of the tubular coccolith should be taken.

3- *Algirosphaera robusta*

The dimensions of the coccosphere of *A. robusta* must be carefully analyzed due the variable asymmetry of the coccosphere, ranging from elliptical to round more so than the other coccospheres in the DPZ. It also has slightly higher standard deviation in most dimensions than the other DPZ genera. *Algirosphaera robusta* has been found ranging in depth from the SPZ to DPZ, which perhaps explains its greater variability. Further analysis of depth-ranging species may elucidate how to morphologically differentiate them from the depth-specific species. Dimensions of the coccoliths on coccospheres of *A. robusta* are difficult to measure, unless the coccosphere has collapsed, due to the large size of the labiatiform protrusion preventing observation of the entire coccolith base. As such, the measurements easiest to make, and thus more statistically accurate (greater number of measurements), are the length and width of the top of the labiatiform protrusion of the body rhabdoliths. The height of the labiatiform protrusion is also useful, and comparable to that of the protrusions of coccoliths of other species.

4- *Solisphaera turbinella, S. galbula, S. blagnacensis*

The coccospheres of the genus *Solisphaera* are similar to those of the genus *Gladiolithus*, in the differentiation in type of coccolith on domal versus anti-domal side. Unlike the

coccospheres of *Gladiolithus*; however, which are comprised of 2 types of coccoliths (tubular coccoliths and lepidoliths), those of *Solisphaera* are comprised of 3 different types of coccoliths. Measurements of the sacculiform/peltiform coccoliths (cedriliths) are comparable to other coccoliths with protrusions, such as the rhabdoliths of *A. robusta*. Despite the unique morphology of the particular cedriliths (cupuliform, tumular, gibbous), their elliptical shape makes their measureable dimensions easily comparable to other elliptical coccoliths. The scutate cedriliths are endothecal and not fully visible; as such they are not measured. The relevant measurements of cedriliths are the diameters of their long and short axes, and the height of the sacculiform/peltiform protrusions. Both long and short axes should be measured, due to some variability in standard deviation between the 2 dimensions.

Acknowledgements

This study would not have been possible without the enthusiastic support and technical expertise of Dr. Christopher Daniel who has given us access to the S.E.M. in the Department of Geology at Bucknell University. I am most grateful to him. I thank Colomban de Vargas for sharing with us the filter from the HV Melville Hydroacoustic and Biological Sampling Cruise. I also thank Zoe Finkel for discussion of the manuscript. This study was partially funded by the John Mason Clark 1877 Fellowship in Paleontology and Geology from Amherst College (AK).

References

AUBRY, M.-P., 1992. Late Paleogene calcareous nannoplankton evolution: a tale of climate deterioration. In: Prothero, D., Berggren, W.A., Eds., *The Eocene-Oligocene Climatic and Biotic Changes*, Princeton, Princeton University Press: 272-309.

AUBRY, M.-P., 1999. *Handbook of Cenozoic Calcareous Nannoplankton, Book 5: Heliolithae (Zygoliths and Rhabdoliths)*. New York, Micropaleontology Press: 1-368.

AUBRY, M.-P., 2007. A Major Mid-Pliocene Calcareous Nannoplankton Turnover: Change in Life Strategy in the Photic Zone. In: Monechi, S., Rampino, M., Coccioni, R., Eds., *Mass Extinctions and Other Large Ecosystem Perturbations: Causes and Consequences*, Geological Society of America, Special Paper 424: 25-51.

AUBRY, M.-P., Kahn , A., 2006. Coccolithophores from the deep photic zone of the Indian Ocean: A case for morphological convergence as a forcing mechanism in the evolution of the calcareous nannoplankton, Micropaleontology.

ANDRULEIT, H., Rogalla, U., Stäger, S., 2005. Living coccolithophores recorded during the onset of upwelling conditions in Oman in the western Arabian Sea. Journal of Nannoplankton Research, 27(1): 1-14.

BALCH, W.M., Holligan, P.M., Kilpatrick, K.A., 1992. Calcification, photosynthesis and growth of the bloom-forming coccolithophore, *Emiliania huxleyi*. Continental Shelf Research, 12:1353-1374.

BERNARD, F., 1939. Coccolithophorides nouveaux ou peu connu observés á Monaco en 1938. Arch. Zool. Exp. et gén., notes et revue, 81: 33-44.

BOLLMANN, J., Cortés, M.Y., Kleijne, A., Østergaard, J., Young, J., 2006. *Solisphaera* gen. nov. (Prymnesiophyceae), a new coccolithophore genus from the lower photic zone. Phycologia, 45(4): 465-477.

CROS, L., Fortuño, J., 2002. Atlas of northwestern Mediterranean coccolithophores. Scientia Marina, 66(1): 7-182.

FINKEL, Z.V., 2001. Light absorption and size scaling of light-limited metabolism inmarine diatoms. Limnology and Oceanography, 46(1): 86-94.

GAARDER, K.R., 1970. Three new taxa of Coccolithineae. Nytt Magasin for Botanikk, 17(2): 113-126.

GIRAUDAU, J. and Pujos, A., 1990. Fonction de transfert basée sur les nannofossiles calcaires du Pleistocéne des Caraïbes. Oceanologica Acta, 13: 453-469.

HAGINO, K., Okada, H., Matsuoka, H., 2000. Spatial dynamics of coccolithophore assemblage in the equatorial western-central Pacific Ocean. Marine Micropaleontology, 39: 53-57.

HAGINO, K., Okada, H., 1998. *Gladiolithus striatus* sp. nov. (Prymnesiophyceae), a living coccolithophore from the lower photic zone of the Pacific Ocean. Phycologia, 37:246-250.

HALLDAL, P., Markali, J., 1955. Electron Microscope studies on coccolithophorids from the Norwegian Sea, the Gulf Stream and the Mediterranean. Norske Videnske. - Akad. Oslo, Avh., Mat.-Nat., Kl., 1: 1-30.

JORDAN, R.W., Chamberlain, A.H.L., 1993. *Vexillarius cancellifer* gen. sp. nov., and its possible affinities with other living coccolithophorids. In: Hamrsmíd, B. and Young, J.R., Eds., Nannoplankton Research Vol. 2. Tertiary biostratigraphy and paleoecology; Quaternary coccoliths. Knihovnicka zemniho plynu a nafty, 14b: 305-325.

KAHN, A., Aubry, M.-P., 2006. Intraspecific morphotypic variability in the Family Rhabdosphaeraceae. Micropaleontology, 52(4): 317-342.
KAMPTNER, E., 1954. Untersuchungen über den feinbau der coccolithen. Anzeiger. Österreichische Akademie der Wissenschaften. Mathematische-Naturwissenschaftliche Klasse. Wien, 87: 152-158.
KIRK, J.T.O, 1994. Light and photosynthesis in aquatic ecosystems, 2nd edition. Cambridge University Press, Great Britain.
KLAUSMEIER, C.A., Litchman, E., 2001. Algal games: the vertical distribution of phytoplankton in poorly mixed water columns. Limnology and Oceanography, 46(8): 1998-2007.
KLEIJNE, A., 1992. Extant Rhabdosphaeraceae (cocolithophorids, class Prymnesiophyceae) from the Indian Ocean, Red Sea, Mediterranean Sea and North Atlantic Ocean. Scripta Geologica, 100: 1-63.
KLEIJNE, A., Jordan, R.W., Heimdal, B.R., Samtleben, C., Chamberlain, A.H.L., and Cros, L. 2002. Five new species of the coccolithophorid genus *Alisphaera* (Haptophyta) with notes on their distribution, coccolith structure and taxonomy. Phycologia, 40(6): 583-601.
KNAPPERTSBUSCH, M., 1993. Geographic distribution of living and Holocene coccolithophorids in the Mediterranean Sea. Marine Micropaleontology, 21: 219-247.
LOHMANN, H., 1902. Die coccolithophoridae, eine monographie der coccolithen bildenden flagellaten, zugleich ein Beeitrag zur Kenntnis des Mittelmeerauftriebs. Arch Protistenkd, 1: 89-165.
MOLFINO, B., McIntyre, A., 1990. Precessional forcing of nutricline dynamics in the equatorial Atlantic. Science, 249(4970): 766-769.
MCINTYRE, A., 1969. The Coccolithophorida in Red Sea sediments. In: Degens, E.T. and Ross, D.A., Eds., *Hot Brines and recent heavy metal deposits in the Red Sea; a geochemical and geophysical account*. New York, Springer-Verlag: 299-305.
OKADA, H., 1983. Modern nannofossil assemblages in sediments of coastal and marginal seas along the western Pacific Ocean. Utrecht Micropaleontological Bulletin, 30: 171-187.
OKADA, H., Honjo, S., 1975. Distribution of coccolithophores in marginal seas along the western Pacific Ocean and in the Red Sea. Marine Biology, 31: 271-285.
OKADA, H., Honjo, S., 1973. The distribution of oceanic coccolithophorids in the Pacific. Deep Sea Research, 20: 355-374.
OKADA, H., Matsuoka, M., 1996. Lower-photic nannoflora as an indicator of the late Quaternary monsoonal palaeo-record in the tropical Indian Ocean. In: Moguilevsky, A., Whatley, R., Eds., *Proceedings of the ODP and the marine biosphere international conference*, Aberystwyth, 231-245.
OKADA, H., McIntyre, A., 1977. Modern coccolithophores of the Pacific and North Atlantic Oceans, Micropaleontology, 23(1):1-55.
PETERS, R.H., 1983. The ecological implications of body size. Cambridge University Press.
PROBERT, I., Fresnel, J., Billard, C., Geisen, M., Young, J.R., in preparation. Light and electron microscope observations of *Algirosphaera robusta* (Haptophyceae).

QUINN, P.S., Cortés, M.Y., Bollmann, J., 2005. Morphological variation in the deep dwelling coccolithophore *Florisphaera profunda* (Haptophyta). European Journal of Phycology, 40(1): 123-133.
REID, F., 1980. Coccolithophorids of the North Pacific Central Gyre with notes on their vertical and seasonal distribution. Micropaleontology, 26: 151-176.
SAMTLEBEN, C. and Schröder, A., 1992. Living coccolithophore communities in the Norwegian-Greenland Sea and their record in sediments. Marine Micropaleontology, 19: 333-354.
SCHLAUDER, J.,1945. Recherches sur les flagellés calcaires de la Baie d'Alger. University d'Alger, Dipl. Fac. Sci., pp. 1-51, pls. 1-9.
TAKAHASHI, K., Okada, H., 2000. Environmental control on the biogeography of modern coccolithophores in the southeastern Indian Ocean offshore of Western Australia. Marine Micropaleontology, 39(1): 73-86.
THOMSON, J., Crudeli, D., de Lange, G.J., Slomp, C.P., Erba, E., Corselli, C., 2004. *Florisphaera profunda* and the origin and diagenesis of carbonate phases in eastern Mediterranean sapropel units. Paleoceanography, 19: 1-19.
VENRICK, E.L., 1973. Deep maxima of photosynthetic chlorophyll in the Pacific Ocean. *Fishery Bulletin*, 71: 41-52.
WALLICH, G.C., 1877. Observations on the coccosphere. Annals and Magazine of Natural History, 19: 342-350.
WINTER, A. and Seisser, W.G., 1994. Atlas of Living Coccolithophores. In: Winter, A. and Seisser, W.G., Eds., *Coccolithophores*. Cambridge, Cambridge University Press: 107-159.
WYRTKIE, K., 1973. Physical oceanography of the Indian Ocean. In: Zeitzschel, B., Ed., *The Biology of the Indian Ocean*. Berlin, Springer-Verlag: 18-36.
YANG, T.-N. and Wei, K.-Y., 2003. How many coccoliths are there in a coccosphere of the extant coccolithophorids? A compilation. Journal of Nannoplankton Research, 25(1): 7-15.
YOUNG, J.R., Andruleit, H., 2006. *Navilithus altivelum*: a remarkable new genus and species of deep photic coccolithophores. Journal of Micropalaeontology, 25(2): 141-152.
YOUNG, J.R., Geisen, M., Cros, L., Kleijne, A., Sprengel, C., Probert, I., Østergaard, J., 2003. A guide to extant coccolithophore taxonomy. Journal of Nannoplankton Research, Special Issue 1, 1-125pp.
YOUNG, J.R., Bown, P.R., 1997. Cenozoic calcareous nannoplankton classification. Journal of Nannoplankton Research, 19: 36-47.
YOUNG, J.R., 1994. Neogene. In: Bown, P.R., Ed., *Calcareous nannofossil biostratigraphy*. London, Kluwer Academic Publishers: 225-265.

Chapter 3

Table captions

Table 1: Number of coccospheres of *Florisphaera profunda* counted and number of those measured in sample VANC10MV07D.

Table 2: Measurements of coccospheres of *F. profunda* compared with published measurements.

Table 3: Measurements of width and length of polygoliths of *F. profunda* compared with published measurements.

Table 4: Measurements of coccospheres and coccoliths of *G. striatus, G. flabellatus, A. robusta* and comparison with published data.

Table 5: Measurements of coccospheres and cedriliths of *S. turbinella, S. galbula*, and *S. blagnacensis* compared with published measurements. Adapted for Table 1 in Aubry and Kahn 2006. Measurements from published manuscripts are: *S. galbula* (Cros and Fortuño 2002); *S. blagnacensis* (Bollmann et al. 2006).

Table 6: Comparison between published measurements of numbers of coccoliths per coccosphere in *F. profunda, A. robusta, G. flabellatus* and *striatus, S. blagnacensis* and our data (also including measurements of *S. turbinella* and *S. galbula*). Values from several different sources: a) Okada and Honjo 1973, b) Giraudau and Pujos 1990, c) Knappertsbusch 1993, d) Yang and Wei 2003, e) Kleijne 1992, f) Samtleben and Schröder 1992 and Knappertsbusch 1993, g) Winter and Seisser 1994, h) Bernard 1939, i) Hagino and Okada 1998.

Chapter 3
Tables

Florisphaera profunda variant	Number of coccospheres present	Number of coccospheres measured
F. profunda var. *elongata*	18	18
F. profunda var. *profunda*	2	2
F. profunda var. *rhinoceri*	1	1
F. profunda var. *A*	48	45
F. profunda var. *B*	32	24
F. profunda var. *C*	26	23
F. profunda var. *D*	21	20
F. profunda var. *E*	20	15
F. profunda var. *F*	8	8
F. profunda var. *G*	6	6

Table 1.

			Long diameter of coccosphere			**Short diameter of coccosphere**		
***F. profunda* variant**	# counted coccoliths	# calculated coccoliths	min	max	average	min	max	average
var. *elongata*	82	158	4.7	10.5	8.3			
Okada & Honjo 1973			8.3	13.2	10.8			
var. *profunda*	46	138			5.1			5.0
Okada & Honjo 1973		30-100	3.7	8.5	6.3			
var. *rhinoceri*	45	135			9.1			9.3
Quinn et al. 2006		30-100	7.1	12	9.1			
var. *A*	75	145	5.8	10.3	8.0	5.4	9.6	7.7
var. *C*	66	162	6.8	9.6	8.1	6.6	9.6	8.2
var. *B*	80	160	7.4	10.2	8.5	7.1	9.5	8.4
var. *D*	75	145	6.6	9.2	7.6			
var. *E*	69	141	7.6	12.4	9.5	8.3	12.0	9.9
var. *F*	79	151			9.6			
var. *G*	46	92			6.1			
average of average					8.0			8.1
min of average					5.1			5.0
max of average					9.6			9.9

Table 2.

	Width of polygolith				**Length of polygolith**			
F. profunda variant	min	max	avg	std dev	min	max	avg	std dev
var. *elongata*	1.0	2.5	1.4	0.2	1.9	4.1	2.3	0.4
Okada & Honjo 1973	1.3	5.0			1.7	7.8	4.3	
var. *profunda*	1.3	1.6	1.4	0.1	1.6	1.7	1.7	0.1
Okada & Honjo 1973	0.7	2.5	1.5		0.8	3.1	2.0	
var. *rhinoceri*					2.2	2.6	2.4	0.1
Quinn et al. 2006	0.9	3.8	1.9	0.2	1	3.8	2.7	0.2
A	0.9	2.6	1.5	0.2	1.4	2.3	2.0	0.2
C	1.0	2.5	1.5	0.2	1.3	2.6	2.1	0.2
B	0.9	2.4	1.4	0.2	0.7	2.6	1.7	0.4
D	1.1	2.8	1.5	0.3	1.4	4.2	2.2	0.6
E	1.2	2.6	2.2	0.3	2.0	3.2	2.6	0.4
F	1.0	2.0	1.5	0.2	1.5	2.3	2.0	0.3
G	1.1	3.2	1.7	0.6	1.7	3.1	2.3	0.5
average of average			1.7				2.1	
min of average			1.4				1.7	
max of average			2.4				2.7	
max of average			2.4				2.7	

Table 3.

	min	max	avg	std dev	min	max	average
G. striatus					Hagino & Okada 1998		
total coccospheres	5						
intact	3						
tubular coccolith L	4.0	5.1	4.6	0.2	3.8	4.3	
tubular coccolith top W	1.3	2.0	1.6	0.1	1.1	1.5	
tubular coccolith base W	0.9	1.2	1.1	0.1			
lepidolith L	1.6	2.0	1.8	0.1	1.5	1.9	
lepidolith W	1.1	1.4	1.3	0.2	1.1	1.4	
G. flabellatus					Jordan & Chamberlain 1993		
total coccospheres	12						
intact	1						
tubular coccolith L	4.4	11.1	6.9	2.1	6.5	12	
tubular coccolith top W	1.1	2.8	1.9	0.4			2.0
tubular coccolith base W	0.9	1.7	1.3	0.2			1.6
lepidolith L	1.5	2.2	1.7	0.2			2.0
lepidolith W	1.0	1.5	1.2	0.1			1.4
A. robusta					Kleijne 1992		
total coccospheres	19						
intact	11						
malformed	3						
Long axis of coccosphere	9.9	13.2	11.8	1.2	6.5	9.6	
Short axis of coccosphere	7.3	12.5	10.8	1.9			
Length top of body rhabdoliths	1.6	3.7	2.5	0.5	1.1	3.6	
Width top of body rhabdoliths	0.9	1.6	1.1	0.2	0.3	1.1	
Long axis of base of body rhabdoliths	1.4	3.3	2.2	0.5	1.6	2.6	
Short axis of base of body rhabdoliths	0.8	2.5	1.6	0.6	1.1	1.8	
Height of protrusion of body rhabdoliths	1.4	3.0	2.1	0.3	0.8	1.8	

Table 4.

		this paper				Cros & Fortuño 2002 and Bollmann et al. 2006		
		avg	**min**	**max**	**std dev**	avg	min	max
S. turbinella								
total # of individuals		**21**						
# with all cedriliths visible		**7**						
coccosphere	diameter	**4.5**	**3.1**	**5.3**	**0.8**			
# with domal side visible		**9**						
sacculiform cedriliths	#	**50**	**34**	**70**				
sacculiform cedriliths base	long axis	**0.8**	**0.1**	**1.0**	**0.2**			
sacculiform cedriliths base	short axis	**0.8**	**0.7**	**0.8**	**0.1**			
sacculiform cedriliths	height to papilla	**0.5**	**0.2**	**0.7**	**0.1**			
sacculiform cedriliths	height of papilla	**0.1**	**0.1**	**0.2**	**0.03**			
# with antidomal side visible		**5**						
tumular cedriliths	#	**25**	**20**	**30**				
tumular cedriliths	long axis	**1.1**	**0.9**	**1.2**	**0.1**			
tumular cedriliths	short axis	**0.8**	**0.7**	**0.9**	**0.1**			
cupuliform cedriliths	#	**17**	**13**	**21**				
cupuliform cedriliths	long axis	**1.0**	**0.7**	**1.2**	**0.1**			
cupuliform cedriliths	short axis	**0.8**	**0.6**	**0.9**	**0.1**			
S. galbulus								
total # of individuals		**14**				*Not given*		
# with all cedriliths visible		**2**						
coccosphere	diameter	**5.0**	**4.2**	**5.9**	**0.5**		*4.5*	*6.5*
# with domal side visible		**6**						
sacculiform cedriliths	#	**51**	**32**	**63**				
sacculiform cedrilith base	long axis	**0.7**	**0.6**	**0.9**	**0.1**		*0.9*	*1.5*
sacculiform cedrilith base	short axis	**0.7**	**0.7**	**0.7**	**0.02**			
sacculiform cedrilith	height	**0.6**	**0.5**	**0.7**	**0.1**			
sacculiform cedrilith distal end	long axis	**0.8**	**0.6**	**0.9**	**0.1**			
sacculiform cedrilith distal end	short axis	**0.3**	**0.2**	**0.3**	**0.04**			
# with antidomal side visible		**5**						
tumular cedriliths	long axis	**1.1**	**0.8**	**1.3**	**0.1**			
tumular cedriliths	short axis	**0.6**	**0.5**	**0.7**	**0.04**			
gibbous cedriliths	#	**33**	**27**	**41**				
gibbous cedriliths	long axis	**1.0**	**0.6**	**1.2**	**0.1**			
gibbous cedriliths	short axis	**0.6**	**0.5**	**1.1**	**0.1**			
S. blagnacensis								
total # indiv		**14**				Not given		
coccosphere	diameter	**4.8**	**4.1**	**6.2**	**0.7**	7.5		
# with domal side visible		**11**						
peltiform cedriliths	#	**41**	**32**	**51**			51	68
peltiform cedrilith proximal side	long axis	**1.0**	**0.7**	**1.3**	**0.1**		0.9	1.4
peltiform cedrilith proximal side	short axis	**0.7**	**0.6**	**0.8**	**0.1**		0.6	0.9
peltiform cedrilith	height	**0.8**	**0.6**	**1.0**	**0.1**			
peltiform cedrilith distal side	long axis	**1.0**	**0.6**	**1.2**	**0.2**			
peltiform cedrilith distal side	short axis	**0.2**	**0.1**	**0.3**	**0.1**			
# with antidomal side visible		**4**						
cupuliform cedriliths	#	**13**	**11**	**14**			10	14
cupuliform cedrilith	long axis	**1.3**	**0.9**	**1.6**	**0.2**	1.4		
cupuliform cedrilith	short axis	**0.9**	**0.7**	**1.1**	**0.1**	1.0		
scutate cedriliths	#	**11**	**9**	**13**				

Table 5.

		(Yang and Wei 2003)		Our data	
		Number of coccoliths per coccosphere			
Species	Type of Coccolith	Average	Range	Average	Range
F. profunda	polygoliths	a) 200 b) 76 c) ~120	d) 30->100	143	92-162
A. robusta	sacculiform circum-flagellar	e) 92 e) 3	f) 60-80	76 3	49-116
G. flabellatus	tubular lepidoliths	c) 18 g) 120 h) 56 c) 86 g) ~40			57-98
G. striatus	tubular lepidoliths		i) 100-140 i) 60-80		58-91 34-35
		Bollmann et al. 2006		Our data	
S. turbinella	sacculiform discoidal type a discoidal type b			50 25 17	34-70 20-30 13-21
S. galbulus	sacculiform discoidal type a discoidal type c			51 29 33	32-63 21-36 27-41
S. blagnacensis	sacculiform discoidal type b discoidal type d		51-68 10-14	41 13 11	32-51 11-14 9-13

Table 6.

Chapter 3

Figure captions

Figure 1: Map of southern Indian Ocean transect of the HV Melville Hydroacoustic and Biological Sampling Cruise. Infilled circles= sample sites, with site VANC10MV07 labelled.

Figure 2: Illustration of dimensions measured.

a: *A. robusta* rhabdosphere and rhabdoliths.

b: *F. profunda* coccospheres with antapical and lateral views; measurements of polygolith shown on coccosphere.

c: *G. striatus* coccosphere and tubular coccoliths; measurements of lepidoliths shown on coccosphere.

d: *S. blagnacensis* coccosphere to illustrate measurements of coccospheres within the genus *Solisphaera*; cedriliths listed below:

S. turbinella: 1a) sacculiform cedrilith; 1b) tumular cedrilith; 1c) cupuliform cedrilith.

S. galbula: 2a) sacculiform cedrilith; 1b) tumular cedrilith; 2b) gibbous cedrilith.

S. blagnacensis: 3a) peltiform cedrilith; 1c) cupuliform cedrilith.

Figure 3: Illustrations of DPZ coccospheres showing the triangular asymmetry in shape.

a: *O. antillarum*

b: *F. profunda*

c: *G. flabellatus*

Figure 4: Lengths of polygoliths of morphotypes of *F. profunda*.

Range- diamond= average length on each coccosphere; bars= minimum and maximum on each coccosphere.

Standard deviation- diamond= average length on each coccosphere; bars= standard deviation of lengths of polygoliths per coccosphere.

a: *Florisphaera profunda* var. *elongata*

b: *Florisphaera profunda* var. *profunda*

c: *Florisphaera profunda* var. *C*

d: *Florisphaera profunda* var. *D*

e: *Florisphaera profunda* var. *E*

f: *Florisphaera profunda* var. *F*

g: *Florisphaera profunda* var. *G*

h: *Florisphaera profunda* var. *H*

Figure 5: Widths of polygoliths of morphotypes of *F. profunda*.

Range- diamond= average width on each coccosphere; bars= minimum and maximum on each coccosphere.

Standard deviation- diamond= average width on each coccosphere; bars= standard deviation of widths of polygoliths per coccosphere.

a: *Florisphaera profunda* var. *elongata*

b: *Florisphaera profunda* var. *profunda*

c: *Florisphaera profunda* var. *C*

d: *Florisphaera profunda* var. *D*

e: *Florisphaera profunda* var. *E*

f: *Florisphaera profunda* var. *F*

g: *Florisphaera profunda* var. *G*

h: *Florisphaera profunda* var. *H*

Figure 6: Comparative measurements of *G. flabellatus* and *G. striatus*.

Range- diamond= all measurements of coccoliths of *G. flabellatus*; square= all measurements of coccoliths of *G. striatus*.

Standard deviation- diamond= average measurement of coccoliths per coccosphere of *G. flabellatus*; square= average measurement of coccoliths per coccosphere of *G. striatus*; bar= standard deviation.

All measurements in order of increasing value.

a: Length of tubular coccolith.

b: Width of proximal side of tubular coccolith.

c: Width of distal side of tubular coccolith.

d: Length of short axis of lepidolith.

e: Length of long axis of lepidolith.

Figure 7: Measurements of *A. robusta*.

Diamond= individual rhabdolith dimension.

a: Length of the long axis of the distal end of all labiatiform protrusions measured.

b: Length of the short axis of the distal end of all labiatiform protrusions measured.

c: Length of the long axis of the proximal end of all labiatiform protrusions measured.

d: Length of the short axis of the proximal end of all labiatiform protrusions measured.

e: Height of all labiatiform protrusions measured.

Figure 8: Intraspecific variability in *S. turbinella*.

a: Range- measurements of long axes of tumular cedriliths on each coccosphere.

Standard deviation- diamond: average of long axes of tumular cedriliths on each

coccosphere; bars: standard deviation of long axes of tumular cedriliths on each coccosphere.

b: Range- measurements of short axes of tumular cedriliths on each coccosphere. Standard deviation- diamond: average of short axes of tumular cedriliths on each coccosphere; bars: standard deviation of short axes of tumular cedriliths on each coccosphere.

c: Range- measurements of long axes of cupuliform cedriliths on each coccosphere. Standard deviation- diamond: average of long axes of cupuliform cedriliths on each coccosphere; bars: standard deviation of long axes of cupuliform cedriliths on each coccosphere.

d: Range- measurements of short axes of cupuliform cedriliths on each coccosphere. Standard deviation- diamond: average of short axes of cupuliform cedriliths on each coccosphere; bars: standard deviation of short axes of cupuliform cedriliths on each coccosphere.

e: Plot of long to short axes of tumular cedriliths.

f: Plot of long to short axes of cupuliform cedriliths.

g: Plot of long to short axes of bases of sacculiform cedriliths.

h: Plot of length of spine of sacculiform cedrilith to height of sacculiform cedrilith.

Figure 9: Intraspecific variability in *S. galbula*.

a: Diameter of coccospheres in ascending order.

b: Mean diameter of short axes of tumular cedriliths per coccosphere in ascending order.

c: Range- diamond: mean long axis of tumular cedriliths on each coccosphere, bars: minimum to maximum measurements of long axes. Standard deviation – diamond: mean

long axis of tumular cedriliths on each coccosphere, bars: standard deviation of long axis per coccosphere.

d: Range- diameters of long axis of gibbous cedriliths on each coccosphere. Standard deviation- diamond: mean long axis of gibbous cedriliths on each coccosphere, bars: standard deviation of long axis per coccosphere.

e: Range- diameter of short axis of gibbous cedriliths on each coccosphere. Standard deviation- diamond: mean short axis of gibbous cedriliths on each coccosphere, bars: standard deviation of short axes per coccosphere.

f: Range of diameters of long axis of tumular cedriliths on each coccosphere

g: Range of height of sacculiform protrusions on each coccosphere.

Figure 10: Intraspecific variability in *S. blagnacensis*.

a: Range- plot of short to long axes of base of all measured peltiform cedriliths. Standard deviation- diamond: average diameter of long axis of base of peltiform cedriliths on each coccosphere; bars: standard deviation of diameter of long axes per coccosphere.

b: Range- heights of all peltiform cedriliths measured on each coccosphere. Standard deviation- diamond: average height of peltiform cedriliths on each coccosphere; bars: standard deviation of height per coccosphere.

c: Range- plot of long to short axes of cupuliform cedriliths. Standard deviation- diamond: average diameter of cupuliform cedriliths on each coccosphere; bars: standard deviation of diameter per coccosphere.

Figure 11: Interspecific variability in the genus *Solisphaera*.

Infilled diamond= *S. galbula*. Infilled triangle= *S. blagnacensis*. Open square= *S. turbinella*.

a; Comparison of coccosphere diameters of *S. galbula*, *S. blagnacensis*, *S. turbinella*; each in order of increasing size.

b: Comparison of heights of sacculiform cedriliths of *S. galbula* and *S. turbinella*; cedriliths in order of increasing size.

c: Diameters of short axis of cupuliform cedriliths (*S. turbinella*) and gibbous cedriliths (*S. galbula*) plotted against the diameters of their long axis.

d: Diameters of short axis of tumular cedriliths (*S. turbinella* and *S. galbula*) plotted against the diameters of their long axis.

e: Diameters of short axis of cupuliform cedriliths (*S. turbinella* and *S. blagnacensis*) plotted against the diameters of their long axis.

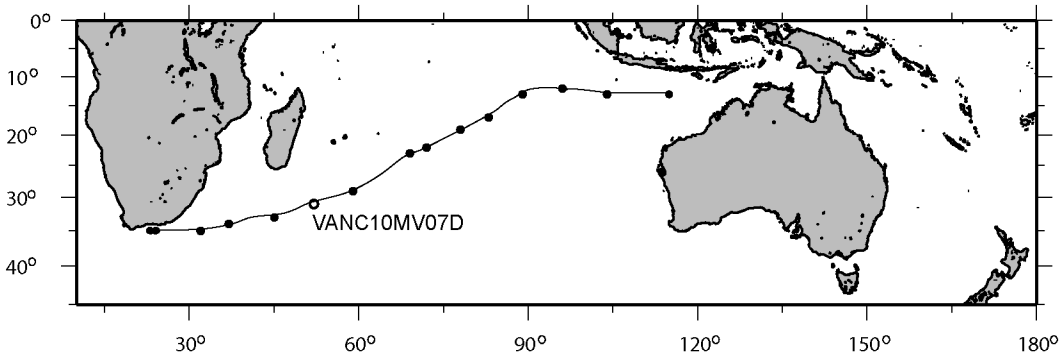

GMT 2006 Apr 27 16:59:44 R.Earley 2006

Figure 1

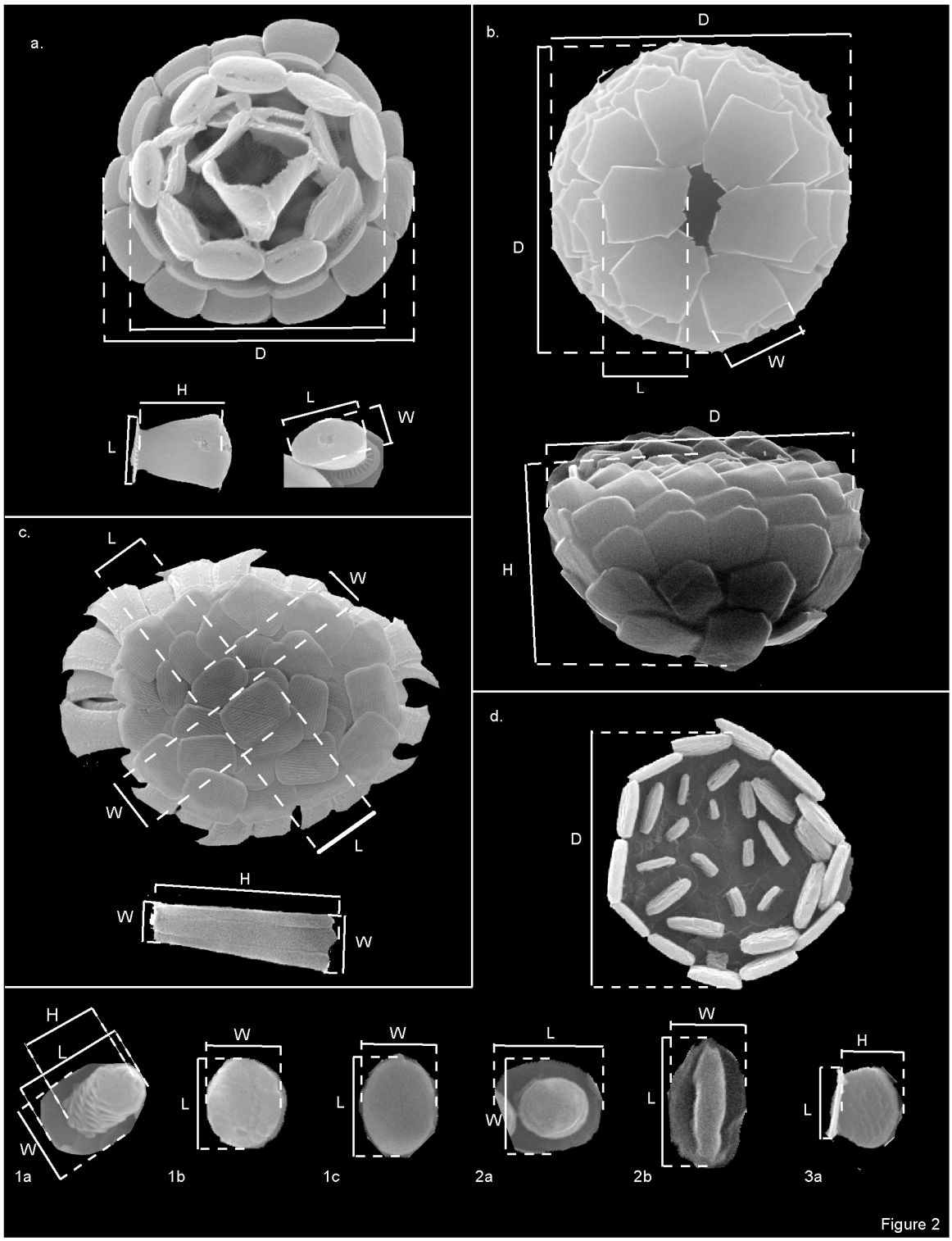

Figure 2

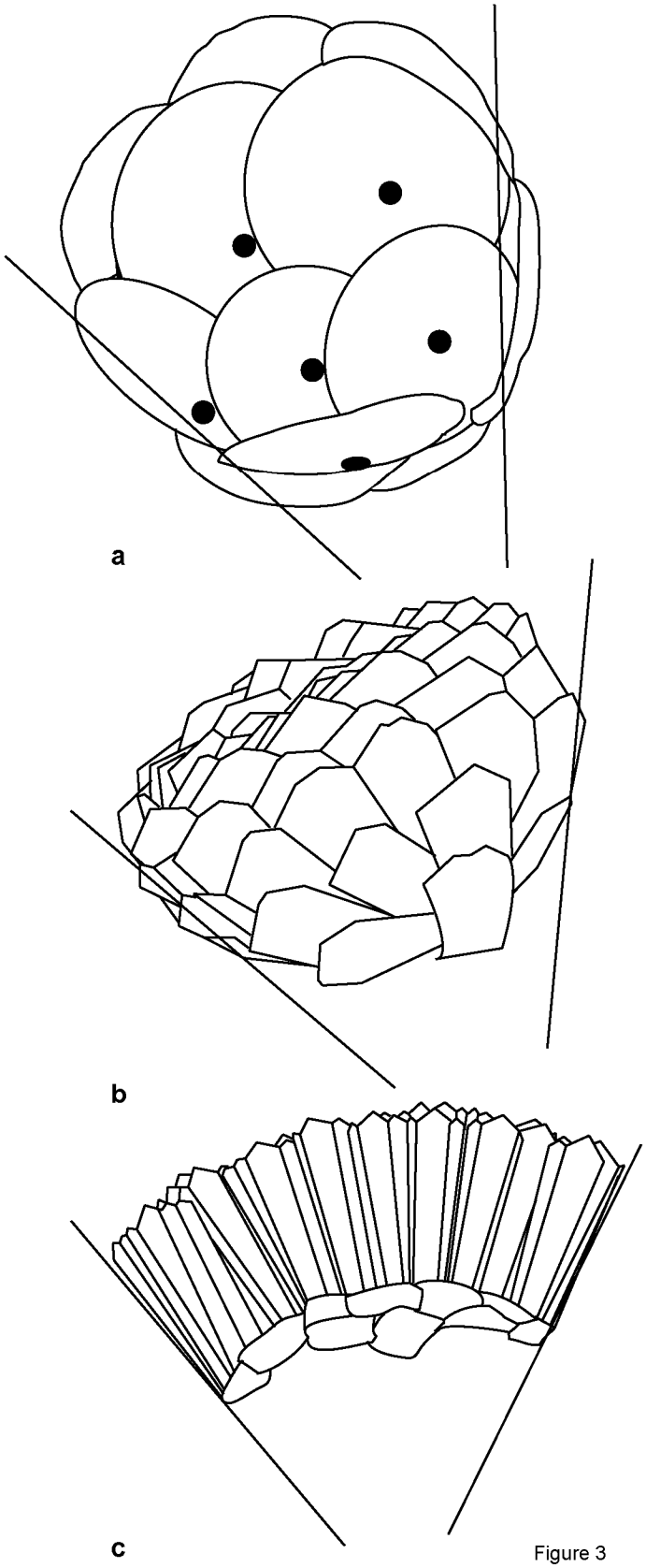

Figure 3

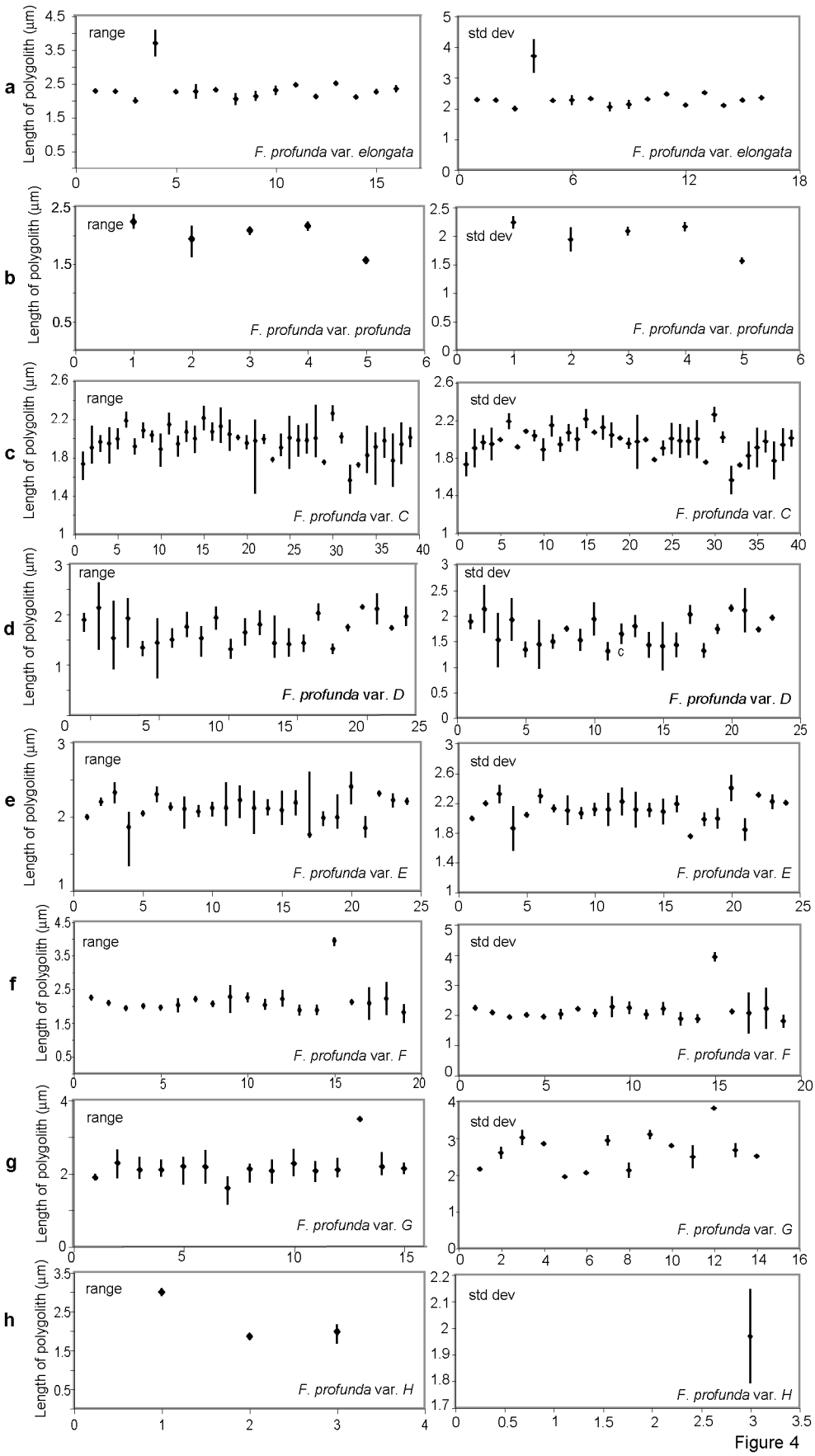
a
b
c
d
e
f
g
h
Length of polygolith (µm)
range
std dev
F. profunda var. elongata
F. profunda var. profunda
F. profunda var. C
F. profunda var. D
F. profunda var. E
F. profunda var. F
F. profunda var. G
F. profunda var. H

Figure 4

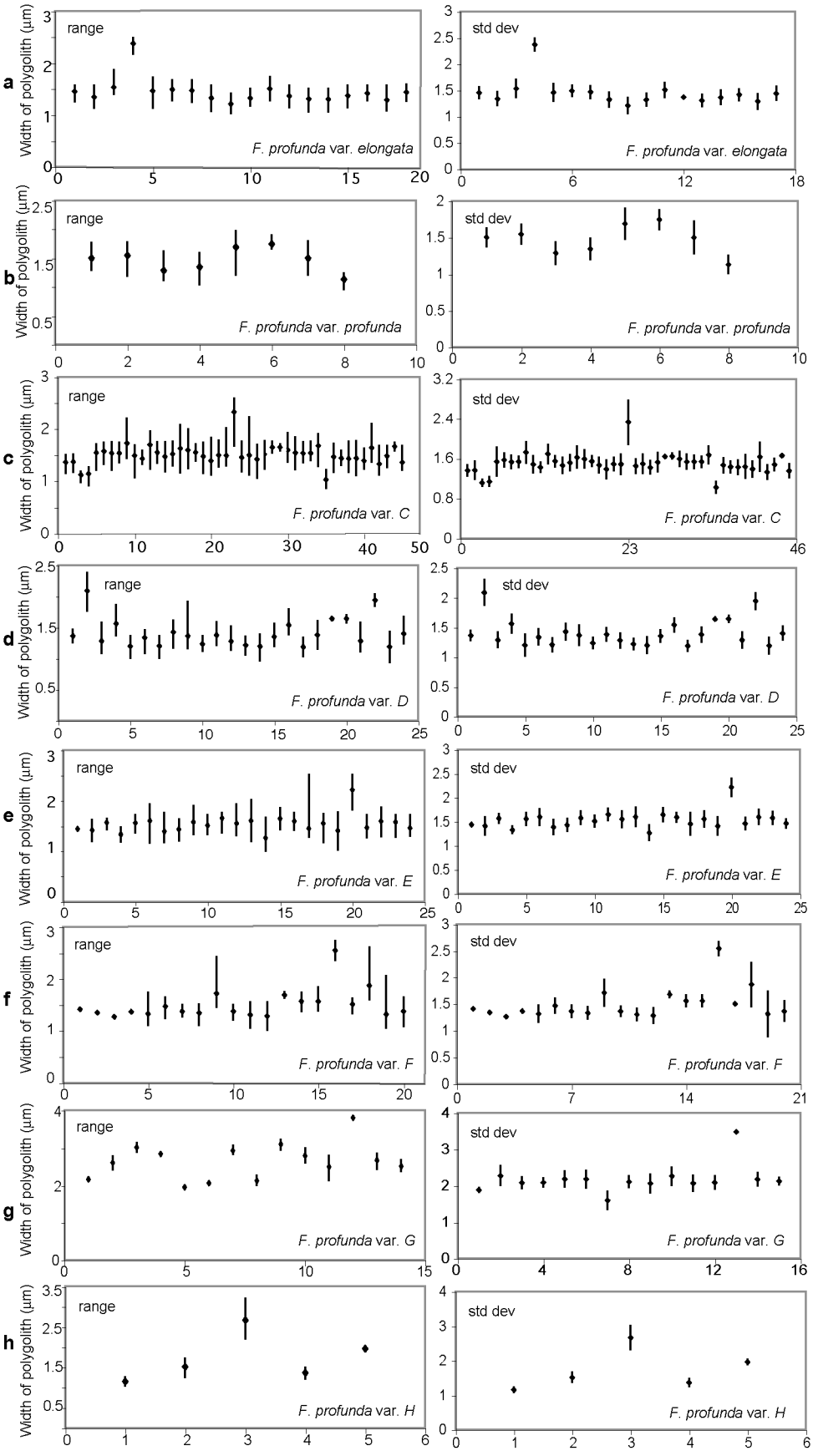
a
b
c
d
e
f
g
h
Width of polygolith (µm)
range
std dev
F. profunda var. elongata
F. profunda var. profunda
F. profunda var. C
F. profunda var. D
F. profunda var. E
F. profunda var. F
F. profunda var. G
F. profunda var. H

Figure 5

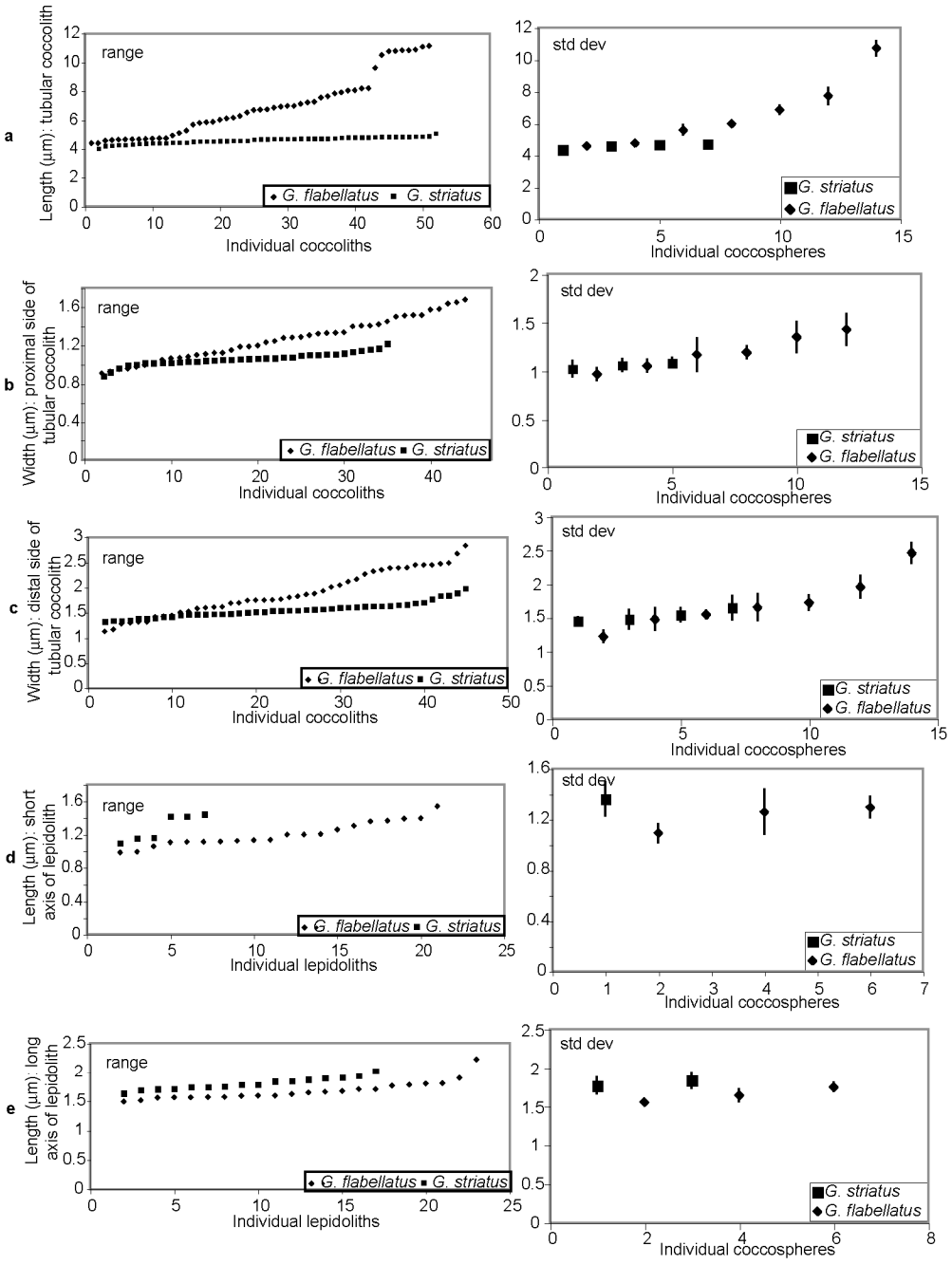
a
Length (µm): tubular coccolith
range
G. flabellatus
G. striatus
Individual coccoliths
std dev
G. striatus
G. flabellatus
Individual coccospheres
b
Width (µm): proximal side of tubular coccolith
range
G. flabellatus
G. striatus
Individual coccoliths
std dev
G. striatus
G. flabellatus
Individual coccospheres
c
Width (µm): distal side of tubular coccolith
range
G. flabellatus
G. striatus
Individual coccoliths
std dev
G. striatus
G. flabellatus
Individual coccospheres
d
Length (µm): short axis of lepidolith
range
G. flabellatus
G. striatus
Individual lepidoliths
std dev
G. striatus
G. flabellatus
Individual coccospheres
e
Length (µm): long axis of lepidolith
range
G. flabellatus
G. striatus
Individual lepidoliths
std dev
G. striatus
G. flabellatus
Individual coccospheres

Figure 6

a

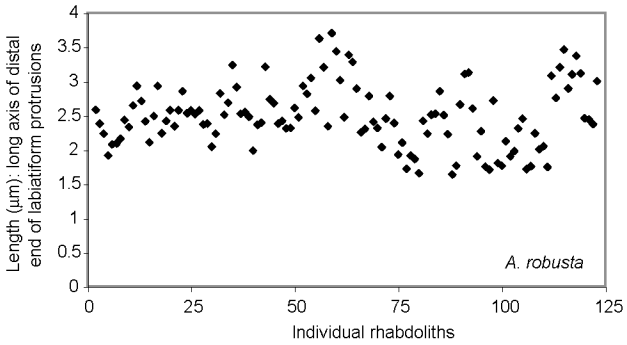

b

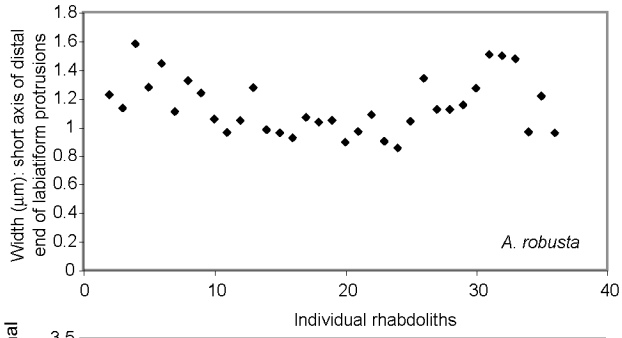

c

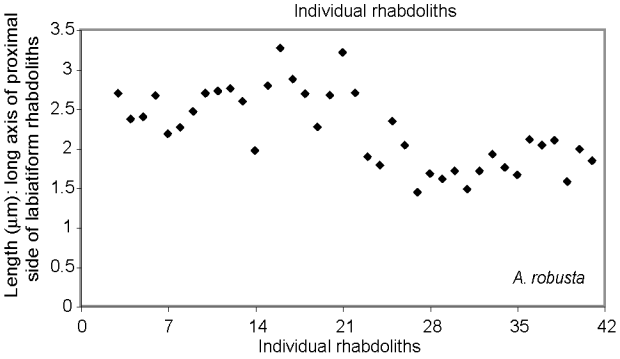

d

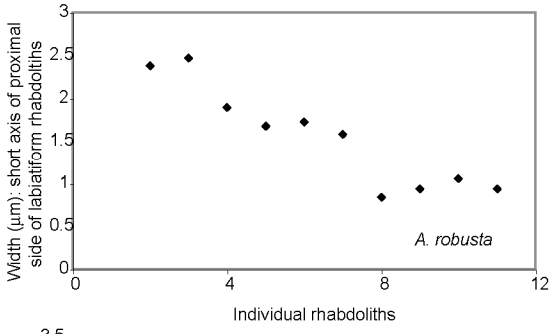

e

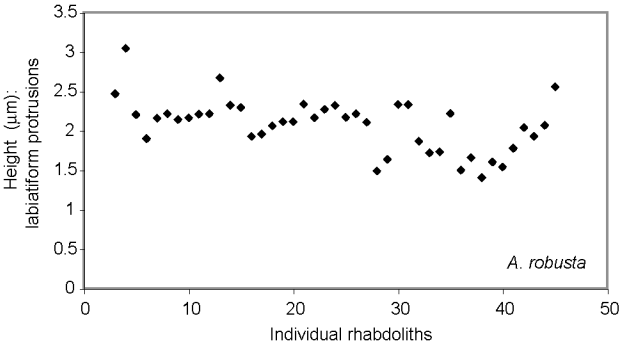

Figure 7

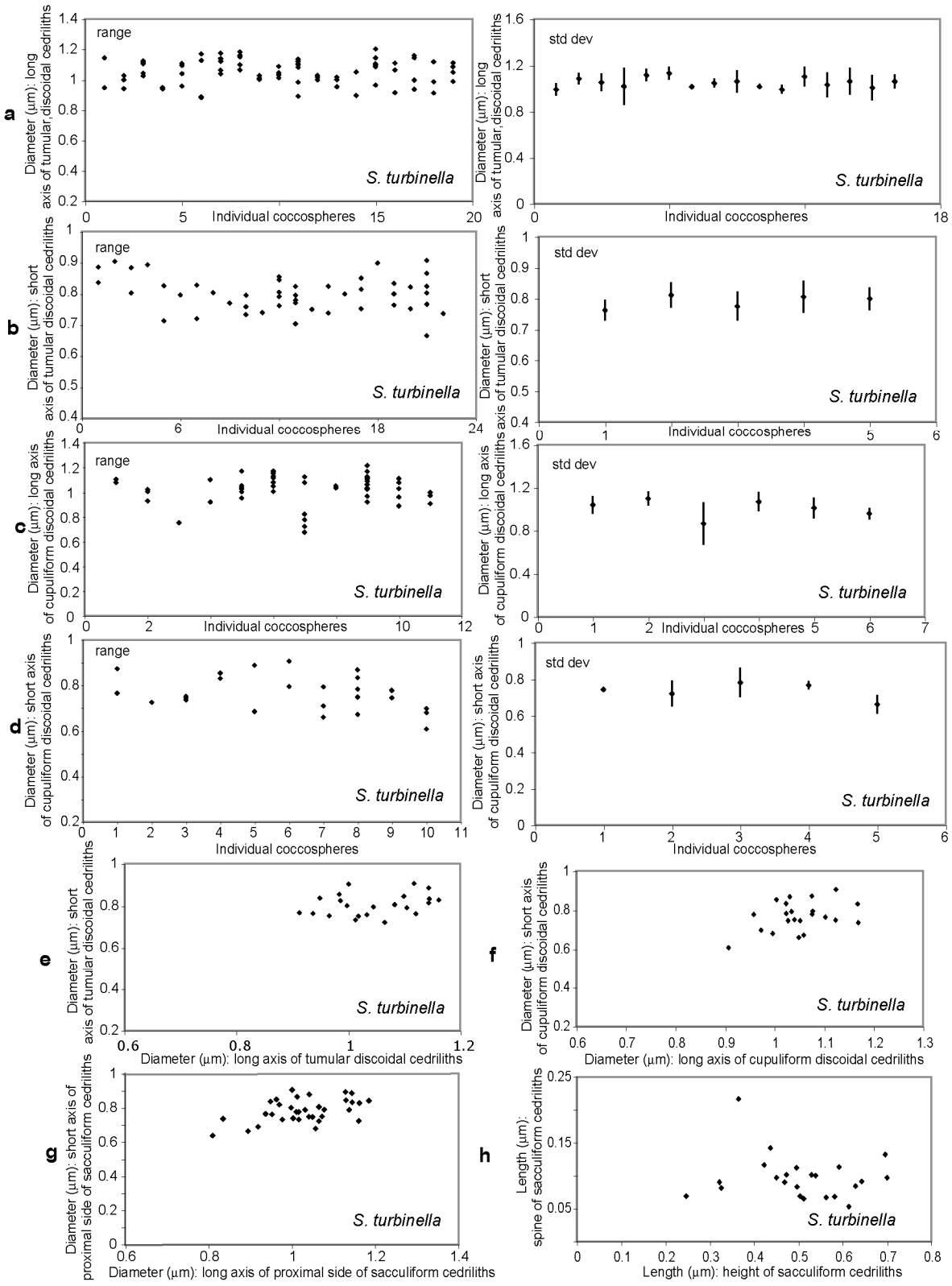
a
range
Diameter (µm): long axis of tumular discoidal cedriliths
Individual coccospheres
S. turbinella
std dev
b
range
Diameter (µm): short axis of tumular discoidal cedriliths
std dev
c
range
Diameter (µm): long axis of cupuliform discoidal cedriliths
std dev
d
range
Diameter (µm): short axis of cupuliform discoidal cedriliths
std dev
e
Diameter (µm): short axis of tumular discoidal cedriliths
Diameter (µm): long axis of tumular discoidal cedriliths
f
Diameter (µm): short axis of cupuliform discoidal cedriliths
Diameter (µm): long axis of cupuliform discoidal cedriliths
g
Diameter (µm): short axis of proximal side of sacculiform cedriliths
Diameter (µm): long axis of proximal side of sacculiform cedriliths
h
Length (µm): spine of sacculiform cedriliths
Length (µm): height of sacculiform cedriliths

Figure 8

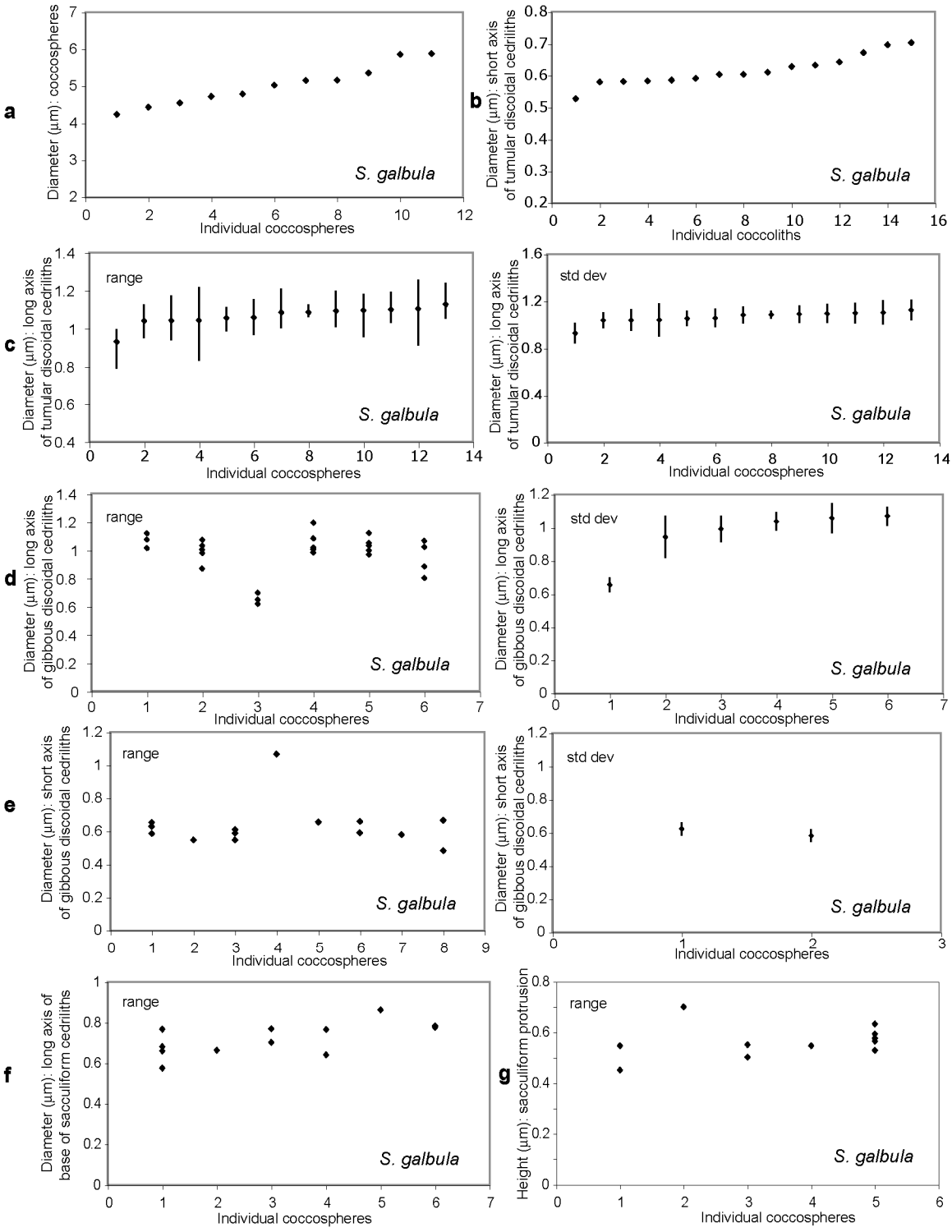
a
Diameter (µm): coccospheres
Individual coccospheres
S. galbula
b
Diameter (µm): short axis of tumular discoidal cedriliths
Individual coccoliths
S. galbula
c
Diameter (µm): long axis of tumular discoidal cedriliths
range
Individual coccospheres
S. galbula
std dev
Individual coccospheres
S. galbula
d
Diameter (µm): long axis of gibbous discoidal cedriliths
range
Individual coccospheres
S. galbula
std dev
Individual coccospheres
S. galbula
e
Diameter (µm): short axis of gibbous discoidal cedriliths
range
Individual coccospheres
S. galbula
std dev
Individual coccospheres
S. galbula
f
Diameter (µm): long axis of base of sacculiform cedriliths
range
Individual coccospheres
S. galbula
g
Height (µm): sacculiform protrusion
range
Individual coccospheres
S. galbula

Figure 9

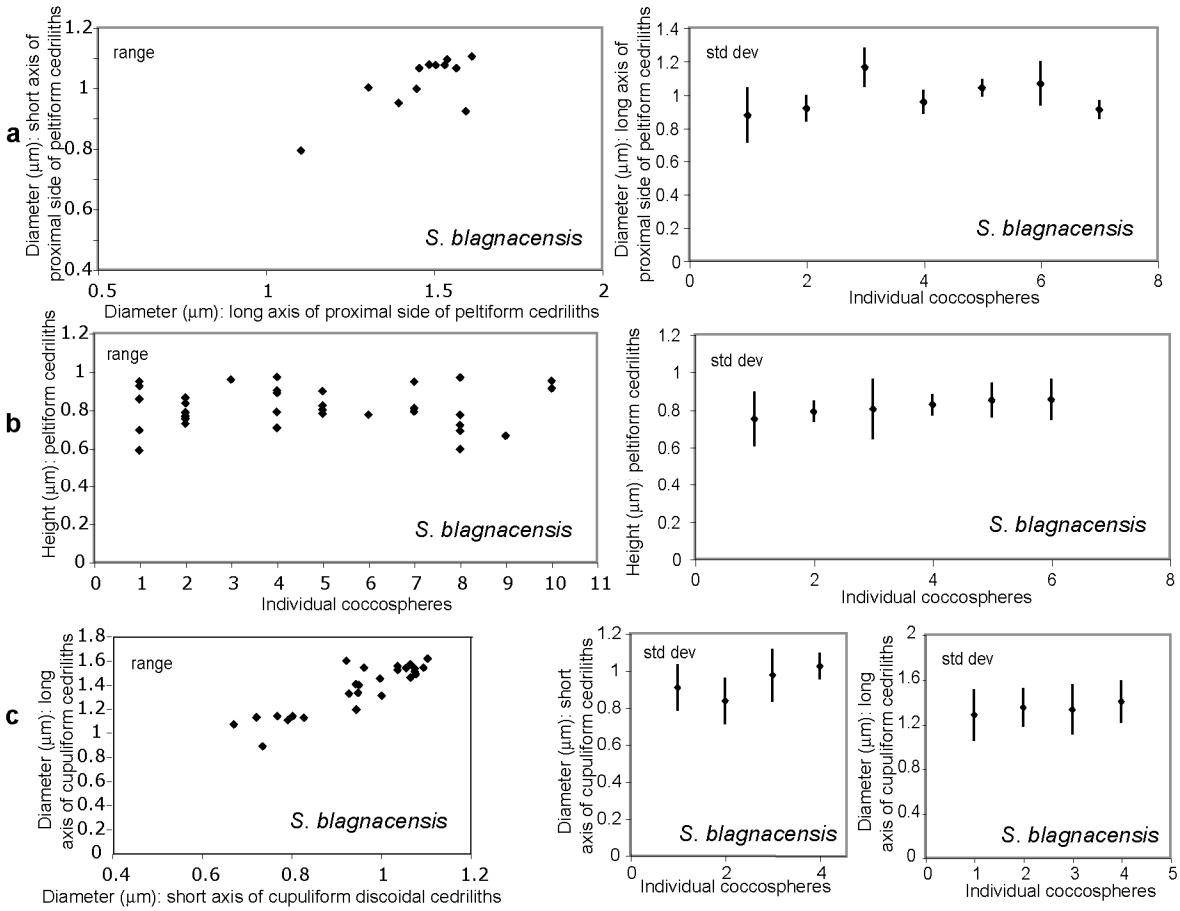
a
range
Diameter (µm): short axis of proximal side of peltiform cedriliths
Diameter (µm): long axis of proximal side of peltiform cedriliths
S. blagnacensis
std dev
Diameter (µm): long axis of proximal side of peltiform cedriliths
Individual coccospheres
S. blagnacensis
b
range
Height (µm): peltiform cedriliths
Individual coccospheres
S. blagnacensis
std dev
Height (µm) peltiform cedriliths
Individual coccospheres
S. blagnacensis
c
range
Diameter (µm): long axis of cupuliform cedriliths
Diameter (µm): short axis of cupuliform discoidal cedriliths
S. blagnacensis
std dev
Diameter (µm): short axis of cupuliform cedriliths
Individual coccospheres
S. blagnacensis
std dev
Diameter (µm): long axis of cupuliform cedriliths
Individual coccospheres
S. blagnacensis

Figure 10

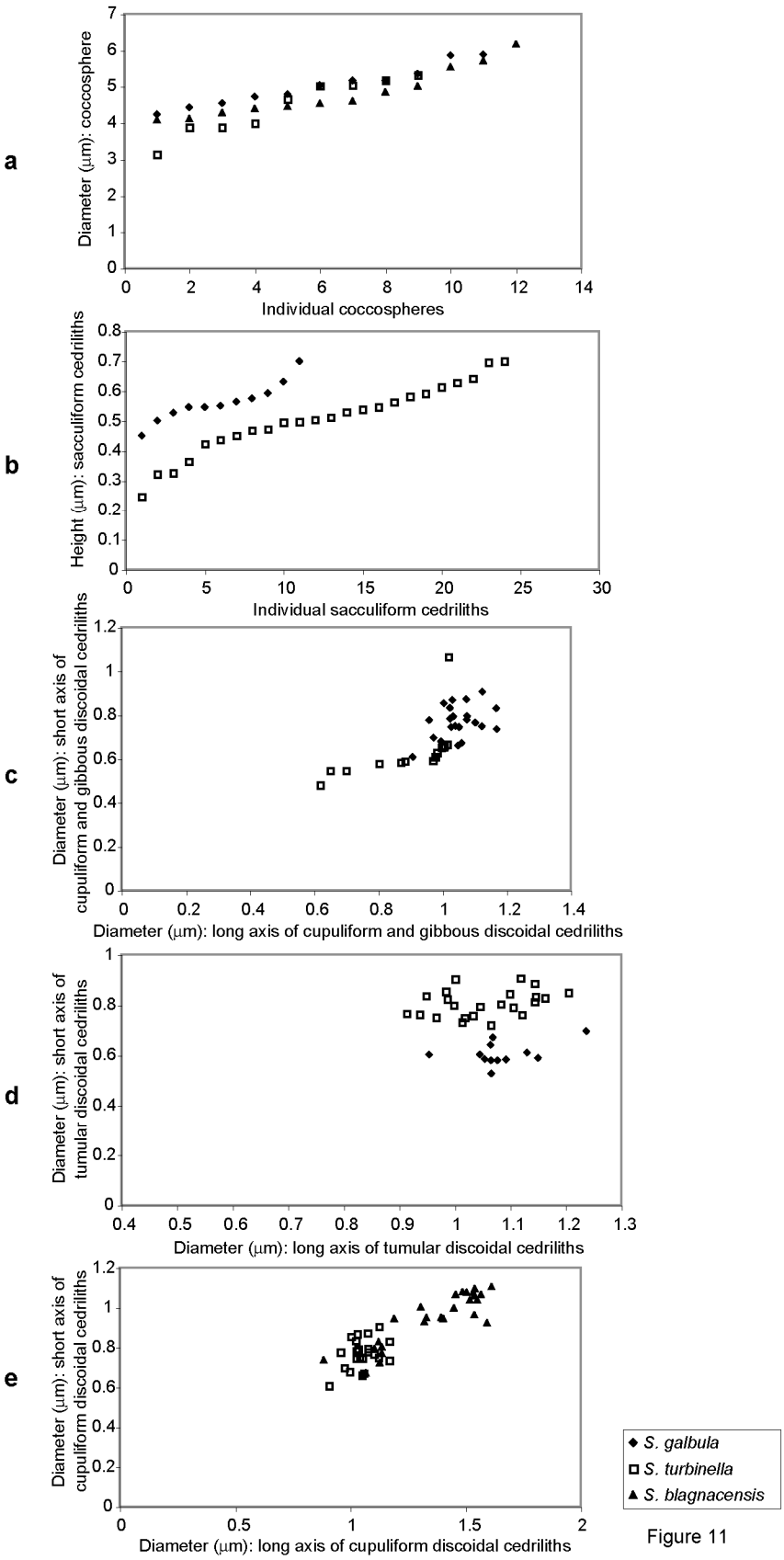
a
Diameter (μm): coccosphere
Individual coccospheres
b
Height (μm): sacculiform cedriliths
Individual sacculiform cedriliths
c
Diameter (μm): short axis of cupuliform and gibbous discoidal cedriliths
Diameter (μm): long axis of cupuliform and gibbous discoidal cedriliths
d
Diameter (μm): short axis of tumular discoidal cedriliths
Diameter (μm): long axis of tumular discoidal cedriliths
e
Diameter (μm): short axis of cupuliform discoidal cedriliths
Diameter (μm): long axis of cupuliform discoidal cedriliths
S. galbula
S. turbinella
S. blagnacensis

Figure 11

Chapter 3

Plate captions

Plate 1: *Florisphaera profunda* coccospheres. Figs. a, c, e; bar= 2 µm. Figs. b, d, f; bar= 5 µm. a-b. *Florisphaera profunda* var. *elongata*. c-d. *Florisphaera profunda* var. *profunda*. e-f. *Florisphaera profunda* var. *C.*

Note anterior end of polygolith on each coccosphere.

a: Lateral view with antapical polygoliths sliding off coccosphere, revealing the arrangement of the polygoliths.

b: Antapical view of coccosphere, Note asymmetrical termination of smooth polygolith.

c: Apical view of coccosphere collapsing both inwards and outwards to form a corona of collapsed polygoliths.

d: Antapical view of coccosphere with polygoliths sliding off to reveal anterior ends of packed polygoliths. Note also the broad V-shape of the posterior end of the polygoliths.

e: Apical view of coccosphere. Note serration of anterior end of polygoliths.

f: Antapical view of coccosphere with polygoliths collapsing inward.

Plate 2: *Florisphaera profunda* coccospheres. Figs. a; bar= 5 µm. Figs. b-f ; bar= 2 µm. a-b. *Florisphaera profunda* var. *D*. c-d. *Florisphaera profunda* var. *E*. e-f. *Florisphaera profunda* var. *F*.

a: Lateral view of collapsed coccosphere. Note extreme serration and varimorphism of polygoliths.

b: Antapical view of slightly collapsed coccosphere.

c: Lateral view of coccosphere.

d: Antapical view of coccosphere. Note dextral side of posterior end of polygolith which rises into a broad triangular point.

e: Lateral view of coccosphere. Note slight serration along and asymmetrical triangular termination of posterior end of polygoliths.

f: Antapical view of coccosphere.

Plate 3: *Florisphaera profunda* coccospheres. Figs. a, b, e; bar= 5 µm. Figs. c, d; bar= 2 µm. a-b. *Florisphaera profunda* var. *G*. c-d. *Florisphaera profunda* var. *H*. e. *Florisphaera profunda* var. *rhinoceri*.

a: Apical view of coccosphere with artifical corona of collapsed polygoliths.

b: Lateral view of coccosphere. Note sharp triangular termination of the polygoliths and concavity of sinistral side of their posterior ends.

c: Lateral view of coccosphere. Note smooth, flat to slightly convex posterior end of polygoliths.

d: Antapical view of coccosphere.

e: Antapical view of coccosphere. Note width of polygoliths, and the spines on the dextral corners of their anterior ends.

Plate 4: Figs. a-f; bar= 5 µm. Figs. g-i; bar= 2 µm. a-c, e. *Gladiolithus striatus*. d, f. *Gladiolithus flabellatus*. g. *Solisphaera turbinella*. h. *Solisphaera galbula*. i. *Solisphaera blagnacensis*.

a: Lateral view of coccosphere. Note concave antapical side and convex apical side.

b: Apical view of coccosphere. Note range of elliptical to rectangular lepidoliths, which increase in number and overlap towards the center of the apical side.

c: Lateral view of slightly collapsed coccosphere.

d: Lateral view of coccosphere without lepidoliths.

e: Apical view of collapsed coccosphere. Note thickness and concavo-convexity of tubular coccoliths.

f: Collapsed coccosphere. Note spines along tubular coccoliths.

g: Domal side of collapsed coccosphere. Note partially visible girdle of tumular cedriliths proximal to sacculiform cedriliths, and several cupuliform cedriliths.

h: Collapsed coccosphere with tumular, gibbous, and sacculiform cedriliths in a random arrangement.

i: Domal side of collapsed coccosphere with some peltiform cedriliths collapsed outwards into a partial corona. Note other peltiform cedriliths that have remained upright or collapsed inwards. Antidomal cupuliform and scutate cedriliths are not visible here.

Plate 5: Figs. a-d; bar= 5 µm. Figs. e-f; bar= 2 µm. a-f. *Algirosphaera robusta*.

a-c: Antapical view of intact rhabdospheres.

d: Apical side of rhabdosphere with 4 circum-flagellar rhabdoliths surrounding the flagellar opening.

e: Detailed view of proximal side of rhabdoliths, plus several rhabdoliths in lateral and distal view.

f: Distal view of rhabdoliths showing detail of inner sides of the labiatiforrm stem.

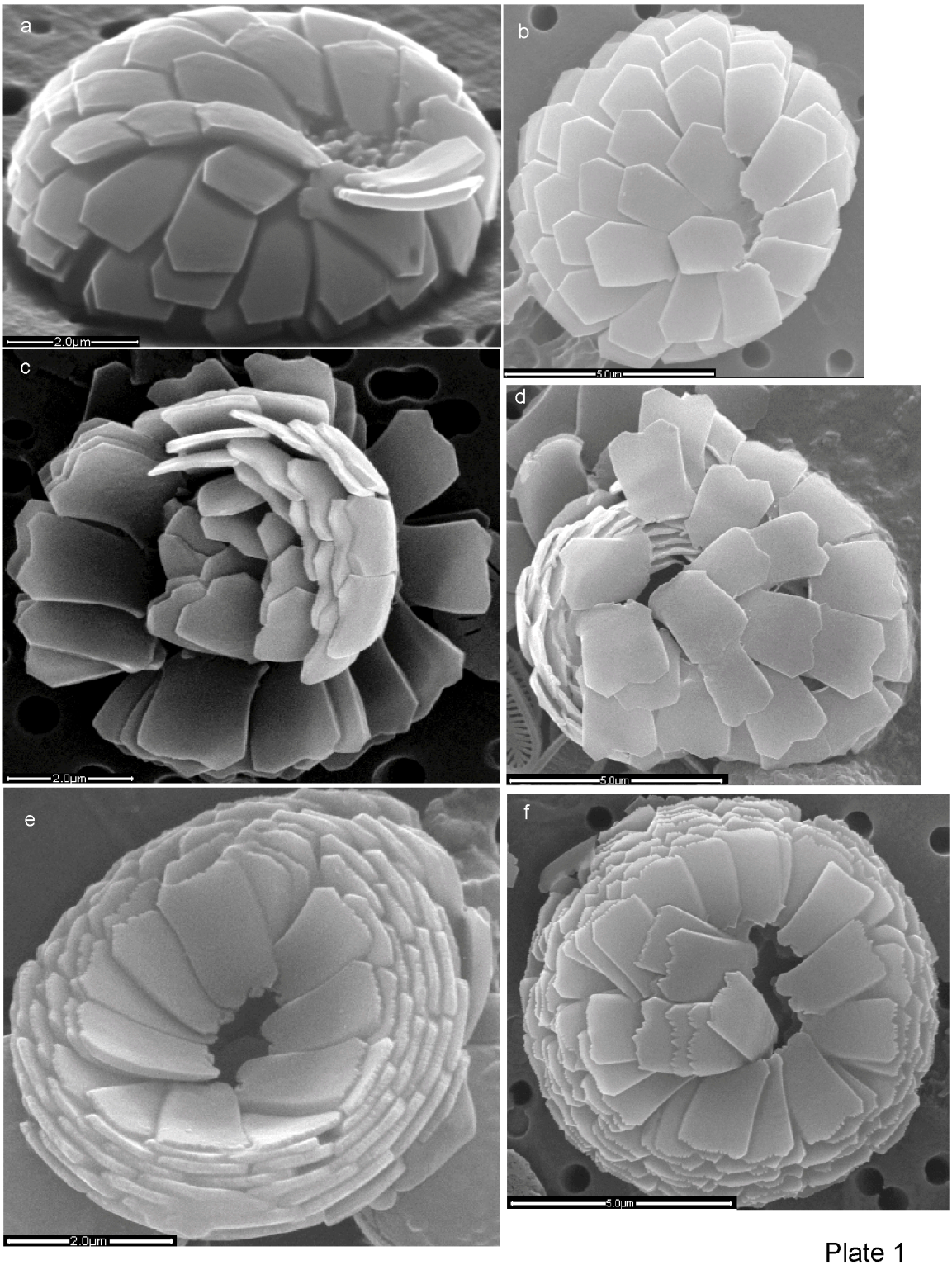

Plate 1

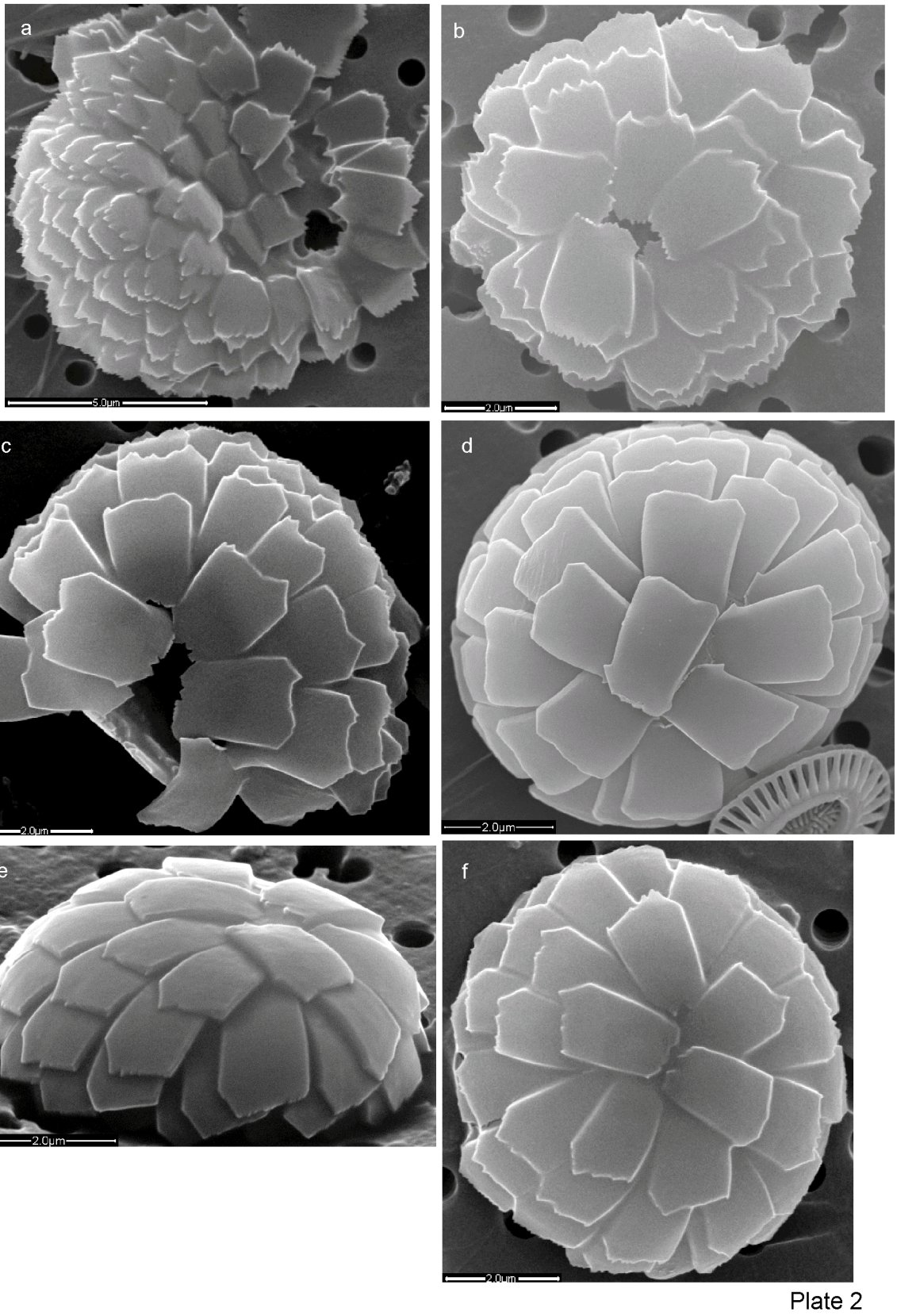

Plate 2

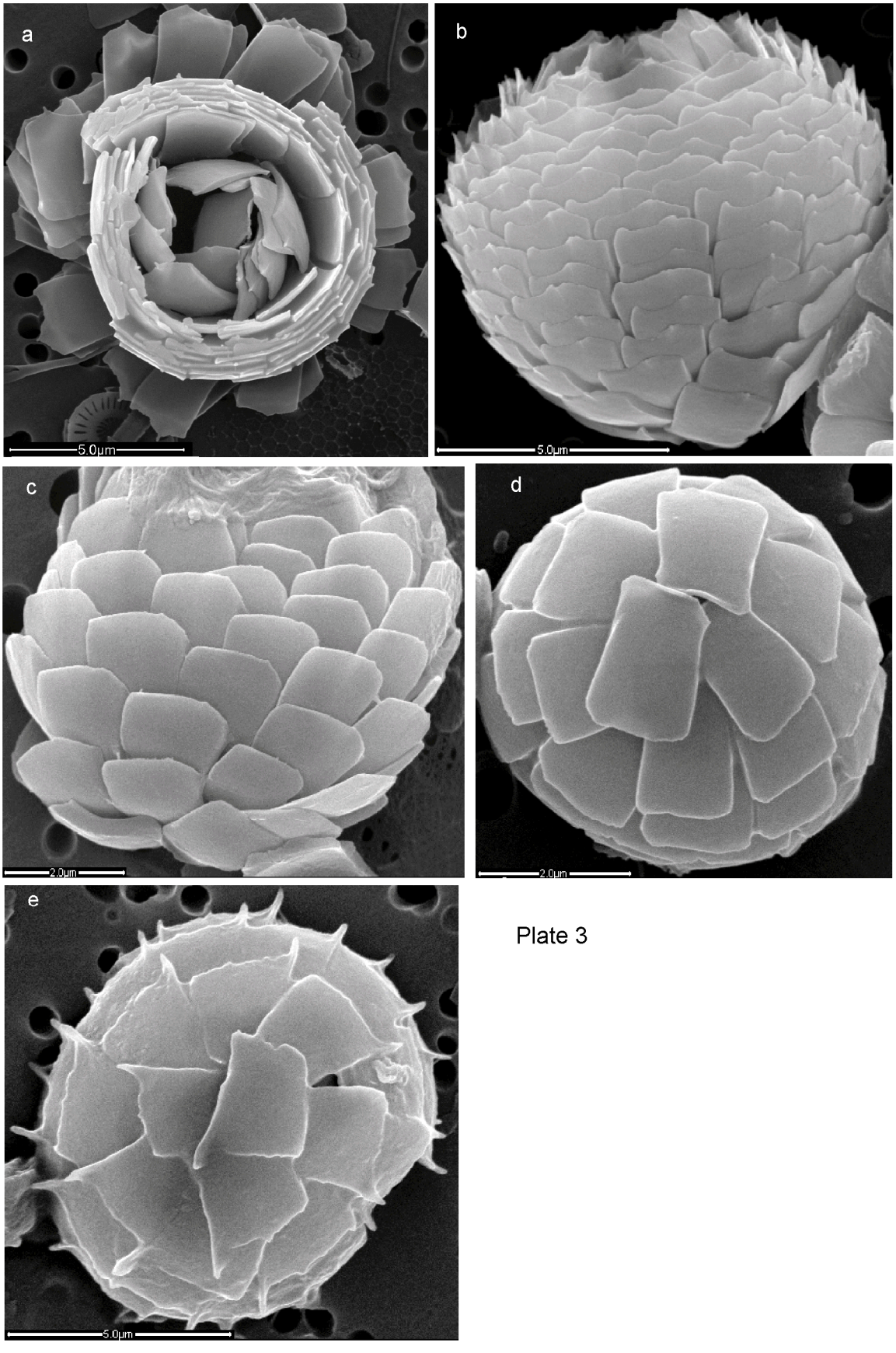

Plate 3

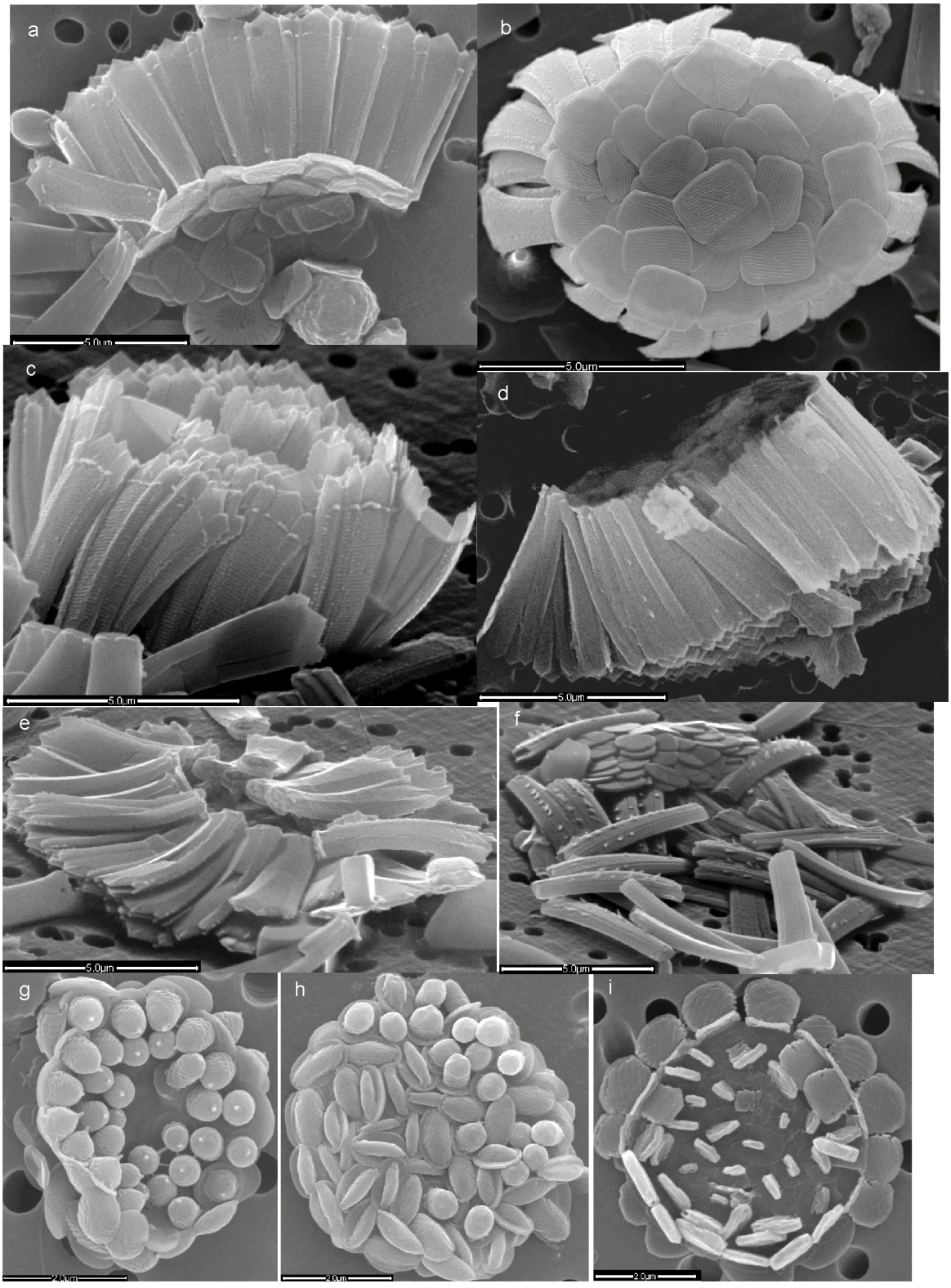

Plate 4

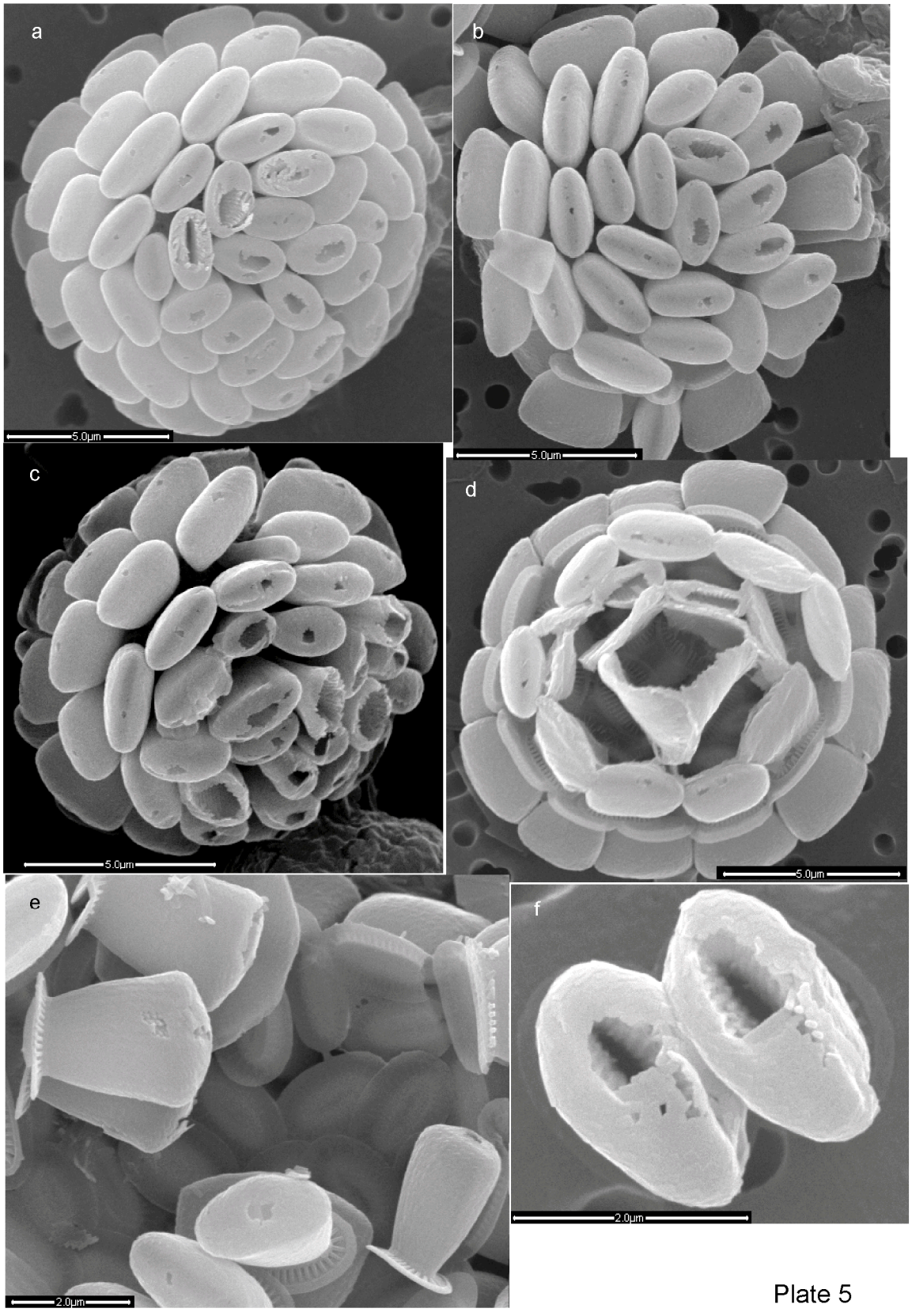

Plate 5

Chapter 4

Size variability in *Minylitha convallis* (Bukry 1973) emend. Theodoris 1984: implications for paleodepth reconstruction

Abstract

Intraspecific variability in the extant coccolithophores contrasts markedly between the shallow and the deep photic zone. Considerable intra- and interspecific variability in coccolith and coccosphere size characterizes the shallow photic zone, whereas low intraspecific size variability distinguishes coccospheres and coccoliths of the deep photic zone. It is this contrast in size variability that one can use in examining the fossil record (Aubry 2007). To estimate the depth at which Late Miocene species *Minylitha convallis* may have lived, I have quantified its size variability and compared it with that in extant deep photic zone taxa, *Florisphaera profunda sensu lato*, plus *Solisphaera* spp., and *Gladiolithus* spp. The size of the nannoliths of *M. convallis* remained constant through time, with overall low variability in all samples, indicating that it likely lived in the deep photic zone in a stratified water column.

1- Introduction

Ocean depth preferences of the modern coccolithophores may be applicable to the fossil record, assuming that size variability can imply habitat (see Ch. 3 of this dissertation). The underlying assumption of this pilot study is that intraspecific variability in coccolith size can be used in paleo-reconstruction of water column stratification; I do not discuss variability in cocco*sphere* size because coccospheres of *M. convallis* have not yet been

found. I therefore make a quantitative comparison of the size variability of the coccoliths of the modern deep photic zone coccolithophore species and those of the Late Miocene *M. convallis*. I particularly focus on *F. profunda sensu lato* due to the similarity in shape of its polygoliths with the nannoliths of *M. convallis*.

Coccospheres of *M. convallis* have never been found, and although inorganic origins are mostly ruled out due to its restricted stratigraphic range (Gartner 1992), its plates are classified as nannoliths. The Late Miocene nannoliths are found from nannofossil zones CN8 through CN9a (NN10 to top NN11a) (Young 1998; Gartner 1992), ranging in age from 9.43 to 7.2 Ma (Berggren et al. 1995; Aubry 1993a, b). Gartner (1992) has identified *M. convallis* as an analog to the Late Miocene through Holocene taxon, *F. profunda*. Gartner (1992) therefore hypothesized that *M. convallis*, like *F. profunda*, thrived in the nutrient-abundant lower photic zone in a well-stratified water column and is an indicator of high productivity.*Minylitha convallis* has been found in Antarctic margin Upper Miocene sediments, indicating possible warming of the southern polar areas during the late Miocene or a tolerance for cooler temperatures (Pospichal 2002).

Florisphaera profunda is a monospecific genus with numerous varieties (Ch. 3 this dissertation; Kahn and Aubry in preparation; Quinn et al. 2005; Okada and McIntyre 1977; Okada and Honjo 1973) comprised of polygonal plates termed polygoliths (Quinn et al. 2005). It ranges from the Late Miocene (7 Ma) (Okada 1983) to today. *Florisphaera profunda* is found predominantly in the deep photic zone in the Atlantic and Pacific tropical to transitional watermasses (Okada & McIntyre, 1977), presumably adapted to the low light and high nutrient conditions (Cortés et al. 2001; Brand 1994;

Jordan et al. 1994). Its relative abundance to other species is used to estimate paleo-stratification of the water column, shallowing or deepening of the thermo/nutricline (Kinkel et al. 2000; Henriksson 2000; McIntyre and Molfino 1996; Molfino and McIntyre 1990), turbidity in the upper photic zone (Ahagon et al 1993), and upwelling and primary productivity (Andruleit et al. 2005; Beaufort et al. 2001).

The genus *Gladiolithus* includes *G. flabellatus* (Halldal and Markali 1955) Jordan and Chamberlain 1993 and *G. striatus* Hagino and Okada 1998; that of *Solisphaera* includes 5 species, *S. blagnacensis* (Bollmann 2006) Aubry and Kahn 2006, *S. helianthiformis* Bollmann 2006, *S. emidasia* Bollmann 2006, *S. turbinella* Kahn and Aubry (in Aubry and Kahn 2006), and *S. galbulus* Kahn and Aubry (in Aubry and Kahn 2006). These genera have been studied in less detail with regard to paleo/ecology than *F. profunda* but because they are classified as DPZ genera (Aubry and Kahn 2006; Bollmann et al. 2006; Okada and Honjo 1973) I use them here along with *F. profunda* as indicators of deep thermo/nutricline and a stratified water column.

2- Methods

Samples for *M. convallis* are from ODP Leg 138, Site 846, hole B, cores 29 (sections 1 to 7) and 30 (sections 1 to 4) in the Eastern Equatorial Pacific, (3°5.70 N, 90°49.08 W) (Fig. 1a). Two cc sediment samples were taken at approximately 40 cm intervals from 264 mbsf to 280 mbsf (sample 846-29-1, 0 cm, to 846-30-4, 130 cm). Smear slides were prepared on the cover slip using Ayac. Microscope work was conducted using a Zeiss Axiovision optical microscope at 100x magnification. Photographs and subsequent measurement of the coccoliths were taken using the Axio Vision measuring program

calibrated to the microscope. Fifty nannoliths of *M. convallis* per slide were photographed and their length and width measured; 100 nannoliths were originally measured per slide, but the average and range of measurements were the same as for 50 nannoliths (Table 1). The nannolith is shaped like a diamond, so that the length was measured across the obtuse angles, and the width was measured across the acute angles (Plate 1a). No coccospheres of this species were found.

Coccoliths on coccospheres of *F. profunda sensu lato*, *Solisphaera*, and *Gladiolithus* were analyzed from a filter taken during the HV Melville Hydroacoustic and Biological Sampling Cruise. Sample VANC10MV07D was taken at 120 m depth on the eastern side of the southern Indian Ocean (33°17.91'S, 45° 21.72'E) (Fig. 1b). An 8 mm^2 piece of filter was mounted on a stub and sputter coated with gold and palladium in the Electron Imaging Facility, Division of Life Sciences at Rutgers, the State University of NJ. All 181 coccospheres of *F. profunda sensu lato* were photographed on a FEI Quanta 400 E.S.E.M. at Bucknell University and the length and width of constituent coccoliths measured using the Image J measuring program. Morphological variants of *F. profunda* were combined for the purposes of this study to quantify overall size variation within both genera. I combined all measured species within each of the genera *Solisphaera* and *Gladiolithus* for comparative consistency with those of *M. convallis* and *F. profunda sensu lato*. The coccoliths of 49 coccospheres of the genus *Solisphaera*, and 17 coccospheres of the genus *Gladiolithus*, were measured to show size variation Measurements of individual species are shown in Figs. 6, 8 to 11 of Chapter 3 of the dissertation.

3- Stratigraphy of Leg 138, Site 846, hole B

Cores from Ocean Drilling Project Leg 138 were drilled from sites in the eastern equatorial Pacific. Samples were taken from hole B of Site 846, located ~300 km south of the Galapagos Islands on the southern limb of the Carnegie Ridge (Hey 1977) where the Southern Equatorial Current and the Peru Current converge (Mayer et al. 1992). The core was selected from hole B of Site 846 due to the availability of published astrochonology and stable isotope stratigraphy (Shackleton et al. 1991a; Shackleton et al. 1991b) that provided age constraint for our samples.

The sediments in the core are divided into 2 lithologic units of dominantly biogenic silica and calcium carbonate with low clay input. These units are comprised of common to abundant radiolarians and diatoms. Calcareous nannofossils are abundant and moderately to well preserved throughout, except for the lowermost upper Miocene, where they are rare and poorly preserved. Planktonic foraminifera are rare and poorly preserved in the Miocene and generally through the core (Mayer et al. 1992).

Unit 1, which is a continuous sedimentary sequence with a high sedimentation rate of ~40 m/my (Mayer et al. 1992), is characterized by alternating carbonate and siliceous oozes with calcium carbonate concentration ranging from 0 to 90%. It is further subdivided into Subunits 1A (0 to 262.7 mbsf) and 1B (262.7 to 317.0 mbsf). Subunit 1B (~10.6 to 7.0 Ma (Mayer et al. 1992)) is highly siliceous, comprised dominantly of diatom and radiolarian oozes with minor interbedded nannofossil oozes (Mayer et al. 1992). Calcareous nannofossil assemblages of Subunit 1B are characterized by slightly dissolved placoliths (*Reticulofenestra* spp. and *Coccolithus* spp. in particular), discoasters

with some overgrowth, helicoliths, sphenoliths, and ceratoliths (Raffi and Florés 1995; Mayer et al. 1992).

Our samples (264 to 280 mbsf) are within Subunit 1B, ranging from CN8 to CN9a in the Late Miocene (~8.8 to 6.4 Ma). Samples were taken through both carbonate and siliceous oozes throughout the range of *M. convallis* within this core.

4- Results

4.1- *Minylitha convallis* (Pl. 1)

I prepared 35 samples for measurements. Twenty-four samples had abundant nannoliths of *M. convallis*. Eleven samples had very rare nannoliths of *M. convallis*, so that I found fewer than 50 nannoliths to measure (ranging from 0 to 13 nannoliths). Of those 11 samples, I encountered 4 that were barren of *M. convallis* but generally abundant in discoasters, diatoms, and silicoflagellates. Nannoliths of *M. convallis* are highly resistant to dissolution, as are discoasters and sphenoliths, so that their concurrence with those genera and siliceous fossils (diatoms and silicoflagellates) implies poor preservation that has resulted in almost monospecific assemblages.

Although the average length (7.5 µm) of all specimens measured is greater than the average width (7.1 µm), many specimens are wider than long (Fig. 2a). The average lengths and widths per sample are 5.8 to 8.6 µm and 6.4 to 7.8 µm, respectively (Fig. 2b to c). The highest frequencies in average length per sample range between 7.2 and 7.4 µm, whereas the most common average widths per sample are 7.1 to 7.2 µm and 7.4 to 7.5 µm (Fig. 2b to c). The standard deviation of the lengths and widths of all nannoliths

measured in all 35 samples is 1.2 µm and 1.0 µm, respectively. The average standard deviation for each sample is 1.1µm (length) and 1.0 µm (width).

The total range in length is 4.4 to 11.5 µm, in contrast to a slightly larger range in width, from 4.3 to 11.7 µm (Fig. 2d to e). The dominant length of all nannoliths measured is 6.2 µm (Fig. 2d), but I see no corresponding peak in width measurements (Fig. 2e). Samples with small ranges in width correspond to small ranges in length (Fig. 2f). Similarly, large ranges in width generally correspond to large ranges in length (Fig. 2f).

Interestingly, although I see change in average length and width of the nannoliths between samples, the overall change through time is minimal. I see virtual unimodality in the range of width through time and within samples (Figs. 2e, g). In contrast, the range in length is more variable both from sample to sample, and within samples (Figs. 2d, h). The ratio of average length to width is constant from sample to sample (Fig. 2a), but I see a small range in the minimum and maximum lengths and widths (Figs. 3a to b). Variation in length and width of nannoliths in all samples ranges from 2.3 µm to 6.3 µm and 2.4 µm to 6.8 µm, respectively (Table 2).

4.2- *Florisphaera profunda sensu lato* (Pl. 1i, j)

A total of 2158 width measurements were taken from the polygoliths of 161 coccospheres, and 593 length measurements from those of 146 coccospheres. The length was more difficult to measure due to the imbrication of the polygoliths. Nannoliths of *F. profunda sensu lato* show unimodal distribution across morphotypes in both length and width (Figs. 4a to b). The correlation between average length and width of all measured polygoliths per coccosphere shows that most measurements cluster from approximately

1.6 to 2.4 µm (length) and 1.3 to 1.7 µm (width) (Fig. 4c). The average length and width of the polygoliths is 2.1 µm and 1.5 µm, respectively, with a spread of all polygoliths from 0.7 to 4.2 µm (length) and 0.9 to 3.5 µm (width) and standard deviation of 0.4 µm and 0.3 µm (Table 3), respectively. The average length and width of polygoliths on each individual coccosphere ranges from 1.3 µm to 3.9 µm (Fig. 4d, Table 3) and 1.0 µm to 3.5 µm (Fig. 4e, Table 3), respectively, with an average standard deviation of 0.2 and 0.2 (Fig. 4f to g), respectively. The total variation in length of polygoliths per coccosphere ranges from 0.01µm to 1.3 µm. Total variation in width of polygoliths is slightly less than that of the variation in length, ranging from 0.1 µm to 1.1 µm per coccosphere.

4.3- *Gladiolithus* spp.

A total of 17 coccospheres were found and their constituent coccoliths measured (Table 4). The average length of the 102 tubular coccoliths measured 5.8 µm (ranging from 4.0 to 11.1 µm), with a standard deviation of 1.9 µm (Table 4). The average length of tubular coccoliths on each coccosphere ranges from 4.4 to 7.7 µm (Fig. 5a), with a range in standard deviation per coccosphere from 0.1 to 0.5 µm (Fig. 5a). The widths of the distal and proximal side of the tubular coccoliths average 1.7 µm and 1.2 µm, respectively (Table 4). The proximal width ranges less from 0.9 to 1.7 µm, with a lower standard deviation of 0.2 µm (Table 4). The average proximal width of tubular coccoliths on each coccosphere ranges from 1.0 to 1.4 µm (Fig. 5b), with a range in standard deviation per coccosphere from 0.05 to 0.2 µm (Fig. 5b). The distal width ranges from 1.1 to 2.8 µm, with a standard deviation of 0.4 µm (Table 4). The average distal width of the tubular coccoliths on each coccosphere ranges from 1.2 to 2.0 µm (Fig. 5c), with a

range in standard deviation per coccosphere from 0.05 to 0.2 µm (Fig. 5c). The standard deviation of the length of the short axis of the lepidoliths is 0.2 µm, with an average width of 1.2 µm (range= 1.0 to 1.5 µm) (Table 4). The average length of the short axis of lepidoliths on each coccosphere ranges from 1.1 to 1.4 µm (Fig. 5d), with a range in standard deviation per coccosphere from 0.1 to 0.2 µm (Fig. 5d). Similarly, the length of the long axis of the lepidoliths averages 1.7 µm, with a range of 1.5 to 2.2 µm and standard deviation of 0.2 µm (Table 4). The average length of the long axis of the lepidoliths on each coccosphere ranges from 1.6 to 1.8 µm (Fig. 5e), with a range in standard deviation per coccosphere from 0.04 to 0.1 µm (Fig. 5e).

4.4- *Solisphaera* spp.

The dimensions of the cedriliths of 49 coccospheres of the genus *Solisphaera* were measured (Table 5). I combined the measurements of the sacculiform and peltiform cedriliths. Although the two types of cedriliths are from different species, they are equivalent in position on the coccosphere, and similar in shape (see discussion in Ch. 2 of this dissertation; Aubry and Kahn 2006). The diameter of the long axis of the cupuliform cedriliths averaged 1.1 µm, with a standard deviation of 0.1 µm (Table 5). The range in average diameter of the long axis on each coccosphere was 0.9 to 1.4 µm (Fig. 6a), with a range in standard deviation from 0.05 to 0.2 µm (Fig. 6a). The diameter of the short axis of the cupuliform cedriliths averaged 0.8 µm, with a standard deviation of 0.1 µm (Table 5). The range in average diameter of the short axis on each coccosphere was 0.7 to 1.0 µm (Fig. 6b), with a range in standard deviation from 0.01 to 0.1 µm (Fig. 6b). The diameter of the long axis of the tumular cedriliths averaged 1.1 µm, with a standard

deviation of 0.1 µm (Table 5). The range in average diameter of the long axis on each coccosphere was 0.9 to 1.1 µm (Fig. 6c), with a range in standard deviation from 0.01 to 0.2 µm (Fig. 6c). The diameter of the short axis of the tumular cedriliths averaged 0.7 µm (Table 5), with a standard deviation of 0.03 µm (Table 5). The diameter per coccosphere ranges from 0.6 to 0.8 µm (Fig. 6d), with a range in standard deviation of 0.006 to 0.05 µm (Fig. 6d). The average measurement of the long axis of the base of the sacculi/peltiform cedriliths was 0.9 µm with a standard deviation of 0.1 µm (Table 5). The average measurement of the base of the sacculi/peltiform cedriliths per coccosphere ranges from 0.8 to 1.2 µm (Fig. 6e), with a range of standard deviation from 0.02 to 0.16 µm (Fig. 6e). The average height of the sacculi/peltiform cedriliths was 0.7 µm, with a standard deviation of 0.1 µm (Table 5). Per coccosphere, the average height ranged from 0.5 to 0.9 µm (Fig. 6f), with the standard deviation ranging from 0.05 to 0.16 µm (Fig. 6f).

5- Discussion

I discuss here the quantitative measurements of the nannoliths, with attention to their application to coccosphere shape and paleo-ecological reconstruction.

5.1- Quantitative analysis

I see no pattern in size variability between *M. convallis* samples through time; average length and width varies from sample to sample, but with no overall trend (Fig. 2a). Due to the lack of trend in size change through time, I did not sample at higher resolution.

Coccoliths from deep photic zone coccospheres in the modern Indian Ocean similarly show low intraspecific variability.

Each sample from which I measured nannoliths of *M. convallis* (across a ~3 million year range) represents ~250 to 500 years of sedimentation, whereas the age of the sample from which I measured the coccoliths of *F. profunda sensu lato, Gladiolithus sensu lato,* and *Solisphaera sensu lato* is known precisely, to the particular time of day of the sampling (May 3, 2003 between 16:49 and 17:45 h). Nannoliths of *M. convallis* are on average 375% and 440% larger (length and width) than the polygoliths of *F. profunda sensu lato*. The average length of *M. convallis* is 7.5 µm versus 2.0 µm of *F. profunda sensu lato*. The average width is 7.1 µm in *M. convallis*, versus 1.5 µm in *F. profunda sensu lato*. This is expected, as modern coccospheres and coccoliths are generally smaller than most of those in the fossil record, as discussed in Aubry in press.

Variability among the nannoliths in each sample and polygoliths/tubular coccoliths/lepidoliths/cedriliths of individual coccospheres differs in relative scale. I directly compare length and width of the nannoliths of *M. convallis* and polygoliths of *F. profunda sensu lato*, due to parallels in coccolith outline, and compare overall range with coccoliths of *Gladiolithus sensu lato* and *Solisphaera sensu lato*. The size variability in nannoliths of *M. convallis* is minimal, comparable to that of *F. profunda sensu lato* and the other above-listed DPZ species, and unlike that of shallow photic zone species, which are far more variable in size (Kahn and Aubry 2006). Polygoliths on individual coccospheres of *F. profunda sensu lato* have remarkably low variability, even when compared with other DPZ species, which typically exhibit low intraspecific variability in size (Ch. 3 this dissertation). Polygoliths on single coccospheres of *F. profunda sensu*

lato vary in length and width by an average of 17% and 30%, respectively. In contrast, a comparison of all polygoliths measured in sample VANC10MV07D demonstrates far greater variability, the average range being 167% and 173% of the average length and width, respectively. Nannoliths of *M. convallis* range by approximately 63% of their average length, and 58% of their average width (Fig. 2). The size range of the most frequently occurring lengths and widths of the nannoliths of *M. convallis* is minimal, approximately 3% of the average. The less frequently occurring measurements may be representative of different morphotypes of *M. convallis* that should be separated at the species level.

Although the size range appears to be low, the standard deviation of the most frequently occurring measurements of the nannoliths of *M. convallis* (height: 6.0 to 8.8 µm; width: 6.0 to 8.5 µm) is 0.75 µm (height) and 0.68 µm (width), which is higher than that of most of the dimensions of the DPZ coccoliths (Tables 2 to 4). *Solisphaera sensu lato* and *Gladiolithus sensu lato* show very low variability, with standard deviation averaging ~0.2 µm for most coccolith dimensions (Tables 3 to 4). The average standard deviation per coccosphere of the length and width of all the measured polygoliths of *Florisphaera profunda sensu lato* is also 0.2 µm. Comparing the standard deviation of the coccoliths among the above modern deep photic zone genera to that of all measured nannoliths of *M. convallis*, shows a marked contrast, with the standard deviation of the length and width of the nannoliths of *M. convallis* averaging 1.1 µm and 1.0 µm, respectively, per sample. Although the standard deviation of *M. convallis* is generally higher than that of the extant species of the DPZ, it is lower than that calculated for many of the coccoliths within the shallow photic zone (Kahn and Aubry 2006).

Although the standard deviation shows a greater spread in the measurements of nannoliths of *M. convallis* than the coccoliths of *Solisphaera sensu lato, Gladiolithus sensu lato,* and *F. profunda sensu lato,* it is still considerably less than that of the shallow photic zone species (please see Kahn and Aubry 2006 or Ch. 1 of this dissertation for further explanation of and data on SPZ size variability). The low variability I observe among the nannoliths of *M. convallis* indicates that the Miocene form may have inhabited the deep photic zone. As such, greater relative abundance of *M. convallis*, like that of *F. profunda*, should indicate a highly stratified paleo-ocean, deep nutricline, and warmer climate, whereas reduced abundance relative to other coccolithophore species should indicate a cooler climate and shallow nutricline.

5.2- Paleoecological reconstruction

I observe that in the southern Indian Ocean, shallow photic zone coccospheres have high intraspecific variability relative to those in the deep photic zone (Kahn and Aubry 2006; Kahn and Aubry in prep.; Chs. 1 and 3 this dissertation). The possibility that one can distinguish intraspecific size variability between the upper and lower photic zone extends from our (Kahn and Aubry) working hypothesis that shallow and deep photic zone dwellers may have adapted specialized coccospheres to inhabit particular depth niches, and occur in varying concentrations depending on stratification of the photic zone and depth of the thermo/nutricline due to seasonal surface water mixing.

The geometric outline and simple morphology of the nannoliths of *M. convallis* is similar to that of the coccoliths on many of the extant deep photic zone coccospheres (*Florisphaera* polygoliths, *Gladiolithus* lepidoliths). In addition, low intraspecific

variability in size characterizes the nannoliths within any given sample and through time. These morphological parallels indicate that *M. convallis* inhabited the deep photic zone.

5.3- Coccosphere reconstruction

Because coccospheres of *M. convallis* have never been observed and I see parallels in nannolith morphology with *F. profunda sensu lato*, I briefly consider the structure of the coccospheres and polygoliths of *F. profunda sensu lato* as a hypothetical coccosphere configuration. The nannoliths are flat, thick, raised-rimmed polygons with a central depression (Bukry 1973), comprised of 2 curved calcite elements (Theodoris 1984), similar namely in geometric outline to those of the flat, slightly concave polygoliths of *F. profunda sensu lato*. The polygoliths are rectangular and massive, whereas the nannoliths are composed of 2 polygonal elements (visible from the side), which form a trapezoidal outline, and with a distinct raised rim (Theodoris 1984). Large numbers (>100) of multi-layered polygoliths imbricate to form the floriform coccospheres of *F. profunda sensu lato*. The polygoliths fit tightly, probably attached by small tabs on the proximal side of their posterior ends. I do not observe similar tabs on the nannoliths of *M. convallis*; however, their central depressions may serve as dents in which the next layer of nannoliths can sit. Consideration of the strong 3-dimensionality of the rims of the nannoliths; however, may invalidate this theory. An alternative could be constructed with adjacent nannoliths forming a cylindrical coccosphere. Morphostructural analysis is necessary for further extrapolation.

Should I assume a certain parallel in shape between the coccospheres of *F. profunda sensu lato* and *M. convallis*, then I also assume that they would consist of similar

numbers of coccoliths. I can therefore calculate the total number of coccospheres of *M. convallis* from the number of nannoliths I counted per sample (as compiled in Yang and Wei (2003) and Chapter 3 of this dissertation) (Table 6). I measured 50 nannoliths of *M. convallis* in each sample; therefore, the estimated number of coccospheres analyzed (again, note the assumptions outlined above) ranges from 1/3 of a coccosphere to 1 coccosphere.

6- Conclusions

The coccoliths of *M. convallis, F. profunda sensu lato, Gladiolithus sensu lato, Solisphaera sensu lato* show significant lack of overall size variability. This, plus minimal intraspecific variability in size through time and in the dominant lengths and widths within samples, indicates that the distinctly-shaped *M. convallis* could have been a deep photic zone dweller. Quantification of polygoliths of *F. profunda* in the fossil record may further clarify these two genera due to more comparable preservation conditions, and experimental technique. Additionally, measuring the polygoliths and nannoliths during their coexistence should elucidate paleoecological parallels. I propose that coccolith and coccosphere morphologies of depth-specific coccolithophore species may be increasingly useful in paleoceanographic interpretation as we increase the database of dimensions of coccoliths globally. The conclusions can be corroborated by isotopic analysis of coccoliths of the deep and shallow photic zone species with comparison to the tests of depth-stratified planktonic foraminifera.

Acknowledgements

I greatly appreciate the support of Dr. Christopher Daniel for his technical expertise and the use of his S.E.M. at the Geology Department at Bucknell University. Our sincere thanks to Dr. Connie Sancetta for her Latin translations. I thank Ryan Earley for help drafting the maps and David Bord for data entry.

References

AHAGON, N., Tanaka, Y., Ujiie, H., 1993. *Florisphaera profunda*, a possible nannoplankton indicator of late Quaternary changes in sea-water turbidity at the northwestern margin of the Pacific. Marine Micropaleontology, 22:255-273.

ANDRULEIT, H., Rogalla, Stäger, S., 2005. Living coccolithophores recorded during the onset of upwelling conditions off Oman in the western Arabian Sea. Journal of Nannoplankton Research, 27(1): 1-14.

AUBRY, M.-P., 2007. A Major Mid-Pliocene Calcareous Nannoplankton Turnover: Change in Life Strategy in the Photic Zone. In: Monechi, S., Rampino, M., Coccioni, R., Eds., *Mass Extinctions and Other Large Ecosystem Perturbations: Causes and Consequences*, Geological Society of America, Special Paper 424: 25-51.

AUBRY, M.-P., 1993a. Calcareous nannofossil stratigraphy of the Neogene formations of eastern Jamaica. In: Wright, R.M., and Robinson, E., Eds., *Biostratigraphy of Jamaica.* Memoirs of the Geologic Society of America, 182: 131-178.

AUBRY, M.-P., 1993b. Neogene Allostratigraphy and Depositional History of the De Soto Canyon Area, Northern Gulf of Mexico. Micropaleontology, 39(4): 327-366.

AUBRY, M.-P., 1992. Late Paleogene calcareous nannoplankton evolution: a tale of climatic deterioration. In: Prothero, D.R., & Berggren, W.A., Eds., *Eocene-Oligocene Climatic and Biotic Evolution*. Princeton University Press, Princeton, 272-309.

AUBRY, M.-P., Kahn, A., 2006. Coccolithophores from the deep photic zone of the Indian Ocean: a case for morphological convergence as a forcing mechanism in the evolution of the calcareous nannoplankton. Micropaleontology, 52(5): 27-47.

BEAUFORT, L., de Garidel Thoron , T., Mix, A.C., Pisias, N.G., 2001. ENSO-like forcing on Oceanic Primary Production during the late Pleistocene. Science, 293(5539): 2440-2444.

BERGGREN, W.A, Kent, D.V., Swisher, C.C., III, Aubry, M.-P., 1995. A revised Cenozoic geochronology and chronostratigraphy. In: Berggren, W.A. Kent, D.V., Aubry, M.-P., Hardenbol, J., Eds., *Geochronology, Time Scales and Global Stratigraphic Correlation*. SEPM Special Publication, Society of Sedimentary Geologists, 54: 129-212.

BOLLMANN, J., Cortés, M.Y., Kleijne, A., Østergaard, J., Young, J., 2006. *Solisphaera* gen. nov. (Prymnesiophyceae), a new coccolithophore genus from the lower photic zone. *Phycologia*, 45(4): 465-477.

BRAND, L.E., 1994. Physiological ecology of marine coccolithophores. In: Winter, A., Seisser, W.G., Eds., *Coccolithophores*, Cambridge University Press, Cambridge, 39-50.
BUKRY, D., 1973. Coccolith stratigraphy, Eastern Equatorial Pacific, Leg 16 Deep Sea Drilling Project. Proceedings of the Deep Sea Drilling Project, 653- 711.
CORTÉS, M., Bollmann, J., Thierstein, H.R., 2001. Coccolithophore ecology at the HOT stations ALOHA, Hawaii.
GARTNER, S., 1992. Miocene nannofossil chronology in the North Atlantic, DSDP Site 608. Marine Micropaleontology, 18: 307-331.
HEY, R., 1977. Tectonic evolution of the Cocos-Nazca spreading center. Geological Society of America Bulletin, 88: 1404-1420.
JORDAN, R., Kleijne, A., 1994. A classification system for living coccolithophores. In: Winter, A., Seisser, W.G., Eds., *Coccolithophores*, Cambridge University Press, Cambridge, 83-105.
KAHN, A., Aubry, M.-P., 2006. Intraspecific morphotypic variability in the Family Rhabdosphaeraceae. Micropaleontology, 52(4): 317-342.
KAHN, A., Aubry, M.-P., in preparation. Intraspecific variability in the deep photic zone coccolithophorids of the Indian Ocean.
MAYER, L.A., Psias, N.G., Janecek, T.R., and Shipboard Scientific Party, 1992. Site 846. Proceedings of the Ocean Drilling Program, Initial Reports, 138: 265-333.
OKADA, H., 1983. Modern nannofossil assemblages in sediments of coastal and marginal seas along the western Pacific Ocean. Utrecht Micropaleontological Bulletin, 30: 171-187.
OKADA, H., Honjo, S., 1973. The distribution of oceanic coccolithophorids in the Pacific. *Deep Sea Research*, 20: 355-374.
OKADA, H., McIntyre, A., 1977. Modern coccolithophores of the Pacific and North Atlantic Oceans, Micropaleontology, 23(1):1-55.
POSPICHAL, J.J., 2002. Speculations on the occurrence of the Late Miocene species, *Minylitha convallis* in Antarctic margin sediments. Journal of Nannoplankton Research, 24:195-197.
QUINN, P.S., Cortés, M.Y., Bollmann, J., 2005. Morphological variation in the deep-dwelling coccolithophore *Florisphaera profunda* (Haptophyta). European Journal of Phycology, 40(1): 123-133.
RAFFI, I., Florés, J.-A., 1995. Pleistocene through Miocene calcareous nannofossils from eastern equatorial Pacific Ocean (Leg 138). In: Psias, N.G., Mayer, L.A., Janecek, T.R., Palmer-Jutson, A., van Andel, T.H., Eds., Proceedings of the Ocean Drilling Program, Scientific Results, 138: 233-286.
SHACKLETON, N.J., Crowhurst, S., Hagelberg, T., Pisias, N.G., Schneider, D.A., 1991a. A new late Neogene time scale: application to Leg 138 sites. Proceedings of the Ocean Drilling Program, Scientific Results, 138:73-104.
SHACKLETON, N.J., Hall, M.A., Pate, D., 1991b. Pliocene stable isotope stratigraphy of Site 846. Proceedings of the Ocean Drilling Program, Scientific Results, 138: 337-356.
THEODORIS, S., 1984. Calcareous nannofossil biozonation of the Miocene and revision of the helicoliths and discoasters. Utrecht Micropaleontological Bulletin, 32.
YANG, T.-N., and Wei, K.-Y., 2003. How many coccoliths are there in a coccosphere of the extant coccolithophorids? A compilation, Journal of Nannoplankton Research, v. 25, p. 7-15.

YOUNG, J.R., Geisen, M., Cros, L., Kleijne, A., Sprengel, C., Probert, I., Østergaard, J., 2003. A guide to extant coccolithophore taxonomy. *Journal of Nannoplankton Research Special Issue* 1: 1-125.
YOUNG, J.R., 1998. Neogene. In: Bown, P.R., Ed., *Calcareous Nannofossil Biostratigraphy*. British Micropaleontological Society Publication Series. Chapman & Hall/Kluwer Academic, London: 225-265.

Chapter 4

Table captions

Table 1: Comparison of measurements of 50 versus 100 nannoliths of *M. convallis* showing the similarity in average , range, and standard deviation.

Table 2: Measurements of dimensions of nannoliths of *M. convallis*. Each sample is shown with ODP sample information and corresponding depth (mbsf) and average, minimum and maximum measurements of all measured nannoliths per sample. Fifty nannoliths were measured in most samples (those represented by fewer than 50 nannoliths due to sparse or barren nannoliths are blank in the table).

Table 3: Average, minimum, and maximum length and widths of all *F. profunda sensu lato* polygoliths measured in HV Melville sample HV10MV07D.

Table 4: Average and average standard deviation of all the length and widths of all coccoliths of *Gladiolithus* spp. measured from HV Melville sample HV10MV07D.

Table 5: Average and average standard deviation of all the length and widths of all coccoliths of *Solisphaera* spp. measured from HV Melville sample HV10MV07D.

Table 6: Comparison of total number of polygoliths per coccosphere of *F. profunda* from our data and from Yang and Wei (2003).

Chapter 4
Tables

	846_30_4_130	
	Height	**Width**
50 nannoliths		
average	7.3	6.8
min	5.7	5.1
max	9.4	8.9
std devia	1.0	0.9
average	7.2	6.7
min	5.1	5.0
max	9.8	8.9
std devia	1.1	0.9
100 nannoliths		
average	7.3	6.7
min	5.1	5.0
max	9.8	8.9
std devia	1.0	0.9

Table 1.

Hole	Core	Section	cm	Depth (mbsf)	Avg L (µm)	Min L (µm)	Max L (µm)	Std Dev	Avg W	Min W (µm)	Max W (µm)	Std Dev
846	29	1	0	264.2	8.6	4.8	11.1	2.6	7.8	5.9	10.2	1.7
846			40	264.6								
846			80	265								
846		2	0	265.7	7.7	5.7	10.6	1.2	7.5	5.3	9.6	1.0
846			40	266.1	7.9	6.5	10.1	0.9	7.4	6.0	9.5	0.8
846			100	266.7								
846		3	0	267.2	7.2	5.6	8.7	0.8	7.2	5.1	8.3	0.8
846			60	267.8	7.0	6.0	8.8	1.0	6.7	5.5	8.4	0.8
846			100	268.2	7.4	5.4	10.4	1.2	7.1	5.0	9.2	1.0
846			140	268.6	7.4	5.5	9.6	1.0	7.1	4.9	9.1	0.8
846		4	0	268.7	7.4	5.7	9.2	0.8	7.4	6.0	9.6	0.8
846			40	269.1	5.8				6.6			
846			80	269.5								
846			120	269.9	7.5	5.9	10.1	1.2	7.4	5.5	9.5	1.2
846		5	0	270.2	7.1	4.9	10.2	1.0	7.2	5.2	10.0	1.0
846			40	270.6	8.5				7.4			
846			60	270.8	7.2	5.2	9.4	1.0	7.1	4.9	8.9	0.9
846			140	271.6	7.4	5.2	10.4	1.0	7.1	4.6	9.8	1.0
846		6	40	272.1	7.4	5.5	10.9	1.0	7.3	5.4	9.6	1.0
846			80	272.5	7.5	5.9	9.5	0.8	7.5	6.1	9.2	0.8
846			120	272.9	8.0	5.3	10.5	1.3	7.6	6.0	9.3	1.0
846		7	0	273.2	7.9	6.2	10.5	1.1	7.7	5.6	10.8	1.1
846			40	273.6	7.1	5.5	10.7	1.0	6.8	4.9	11.7	1.1
846	30	1	40	274.3	6.3	4.4	9.0	1.0	6.4	4.3	8.0	0.8
846			100	274.9	7.6	5.2	11.5	1.3	7.0	4.8	9.4	1.0
846			140	275.3	6.7	5.8	8.1	0.7	6.6	5.5	7.9	0.7
846		2	40	275.8	8.3	5.6	10.9	1.2	7.3	5.3	9.5	0.9
846			80	276.2	8.0	5.6	10.6	1.3	7.2	4.7	9.9	1.1
846			120	276.6	8.4	5.8	11.9	1.4	7.5	5.4	10.1	1.1
846		3	40	277.3	6.8	4.7	10.5	1.2	6.6	4.8	8.8	1.0
846			80	277.7	7.2	4.9	11.0	1.3	6.7	4.6	9.0	1.0
846			100	277.9	7.5	5.2	10.1	1.2	7.0	4.8	9.7	1.0
846		4	10	278.5	8.5	6.1	11.5	1.5	7.5	5.3	10.3	1.2
846			90	279.3	7.8	5.3	9.5	1.1	7.2	5.7	9.0	0.8
846			130	279.7	7.2	5.1	9.8	1.1	6.7	5.0	8.9	0.9
Avg total					7.9				7.4			
Min total					4.4				4.3			
Max total					11.9				11.7			
Std dev total					2.1				1.9			
Avg std dev					1.1				1.0			

Table 2.

Florisphaera profunda sensu lato	Polygolith length (µm)	Polygolith width (µm)
total # of polygoliths measured	593	2158
Average of all polygoliths	2.1	1.5
Minimum of all polygoliths	0.7	0.9
Maximum of all polygoliths	4.2	3.5
Standard deviation of all polygoliths	0.4	0.3
Avg of average per coccosphere	2.1	1.6
Avg of minimum per coccosphere	1.3	1.0
Avg of maximum per coccosphere	3.9	3.5
Avg standard deviation per coccosphere	0.2	0.2

Table 3.

Gladiolithus sensu lato		min	max	avg	std dev
total coccospheres	17				
total # tubular coccoliths L measured	102				
tubular coccolith L (µm)		4.0	11.1	5.8	1.9
total # tubular coccoliths top W measured	88				
tubular coccolith top W (µm)		1.1	2.8	1.7	0.4
total # tubular coccoliths base W measured	77				
tubular coccolith base W (µm)		0.9	1.7	1.2	0.2
total # lepidoliths L measured	38				
lepidolith L (µm)		1.5	2.2	1.7	0.2
total # lepidoliths W measured	26				
lepidolith W (µm)		1.0	1.5	1.2	0.2

Table 4.

Solisphaera sensu lato		average	std dev
total # of coccospheres	49		
sacculi/peltiform cedriliths base	long axis	0.9	0.1
sacculiform cedriliths	height	0.7	0.1
tumular cedriliths	long axis	1.1	0.1
tumular cedriliths	short axis	0.7	0.03
cupuliform cedriliths	long axis	1.1	0.1
cupuliform cedriliths	short axis	0.8	0.1

Table 5.

		(Yang and Wei 2003)		Our data
		Number of coccoliths per coccosphere		
Species	Type of coccolith	Mean	Range	Mean
F. profunda	Polygoliths	a) 200 b) 76 c) ~120	d) 30->100	143

Table 6.

Chapter 4

Figure captions

Fig.1: Location maps

a: HV Melville transect and location of Site VANC10MV07.

b: Location of ODP Leg 138, Site 846, with time scale and $\partial^{18}O$ data from Shackleton et al. 1991a, and Shackleton et al. 1991b.

Fig. 2: Quantitative measurements of nannoliths of *Minylitha convallis*.

a: X-axis: samples from left to right from 264 mbsf to 280 mbsf.

Y-axis: diamond=average length divided by average width in each sample.

b: Distribution of average widths of all samples.

c: Distribution of average lengths of all samples.

d: Distribution of all length measurements in all samples.

e: Distribution of all width measurements in all samples.

f: Range in average length per sample plotted against range in average width per sample in each sample.

g: Range- X-axis: each sample from left to right from 264 mbsf to 280 mbsf

Y-axis: diamond=average width of all nannoliths per sample, bar=range from minimum to maximum width in each sample.

Standard deviation: X-axis: samples from left to right from 264 mbsf to 280 mbsf

Y-axis: diamond=average width of all nannoliths per sample, bar= standard deviation per sample.

h: Range- X-axis: samples from left to right from 264 mbsf to 280 mbsf

Y-axis: diamond=average length of all nannoliths per sample, bar=range from minimum to maximum length in each sample.

Standard deviation: X-axis: samples from left to right from 264 mbsf to 280 mbsf

Y-axis: diamond=average length of all nannoliths per sample, bar= standard deviation per sample.

Fig. 3: Quantitative measurements of nannoliths of *Minylitha convallis*.

a: X-axis: samples from left to right from 264 mbsf to 280 mbsf

Y-axis: diamond=minimum length divided by minimum width in each sample.

b: X- axis: samples from left to right from 264 mbsf to 280 mbsf

Y-axis: diamond=maximum length divided by maximum width in each sample.

Fig. 4: Quantitative measurements of polygoliths of *Florisphaera profunda*.

a: Distribution of length of all polygoliths measured.

b: Distribution of width of all polygoliths measured.

c: Length plotted against width of all polygoliths.

d: Range- X-axis: all polygoliths measured per each coccosphere.

Y-axis: diamond= average length, bar= range from minimum to maximum length on each coccosphere.

Standard deviation- X-axis: all polygoliths measured per each coccosphere.

Y-axis: diamond= average length, bar= standard deviation per coccosphere

e: Range- X-axis: all polygoliths measured per each coccosphere.

Y-axis: diamond= average width, bar= range from minimum to maximum width on each coccosphere.

Standard deviation- X-axis: all polygoliths measured per each coccosphere.

Y-axis: diamond= average width, bar= standard deviation per coccosphere.

Fig. 5: Quantitative measurements of tubular coccoliths and lepidoliths of *Gladiolithus* spp..

a: Length of tubular coccolith.

Range- diamond= average length per *Gladiolithus* spp. coccosphere; bar= range from minimum to maximum length on each coccosphere.

Standard deviation- diamond= average length per *Gladiolithus* spp. coccosphere; bar= standard deviation per coccosphere.

b: Width of proximal side of tubular coccolith.

Range- diamond= average width per *Gladiolithus* spp. coccosphere; bar= range from minimum to maximum width on each coccosphere.

Standard deviation- diamond= average width per *Gladiolithus* spp. coccosphere; bar= standard deviation per coccosphere.

c: Width of distal side of tubular coccolith.

Range- diamond= average width per *Gladiolithus* spp. coccosphere; bar= range from minimum to maximum width on each coccosphere.

Standard deviation- diamond= average width per *Gladiolithus* spp. coccosphere; bar= standard deviation per coccosphere.

d: Length of short axis of lepidolith.

Range- diamond= average length per *Gladiolithus* spp. coccosphere; bar= range from minimum to maximum length on each coccosphere.

Standard deviation- diamond= average length per *Gladiolithus* spp. coccosphere; bar= standard deviation per coccosphere.

e: Length of long axis of lepidolith.

Range- diamond= average length per *Gladiolithus* spp. coccosphere; bar= range from minimum to maximum length on each coccosphere.

Standard deviation- diamond= average length per *Gladiolithus* spp. coccosphere; bar= standard deviation per coccosphere.

Fig. 6: Quantitative measurements of the cedriliths of *Solisphaera spp.*.

a: Diameter of long axis of cupuliform cedrilith.

Square= average diameter per coccosphere; bar= standard deviation per coccosphere.

b: Diameter of short axis of cupuliform cedrilith.

Square= average diameter per coccosphere; bar= standard deviation per coccosphere.

c: Diameter of long axis of tumular cedrilith.

Square= average diameter per coccosphere; bar= standard deviation per coccosphere.

d: Diameter of short axis of tumular cedrilith.

Square= average diameter per coccosphere; bar= standard deviation per coccosphere.

e: Diameter of long axis of base of sacculiform/peltiform cedrilith.

Square= average diameter per coccosphere; bar= standard deviation per coccosphere.

f: Height of sacculiform/peltiform cedrilith.

Square= average height per coccosphere; bar= standard deviation per coccosphere.

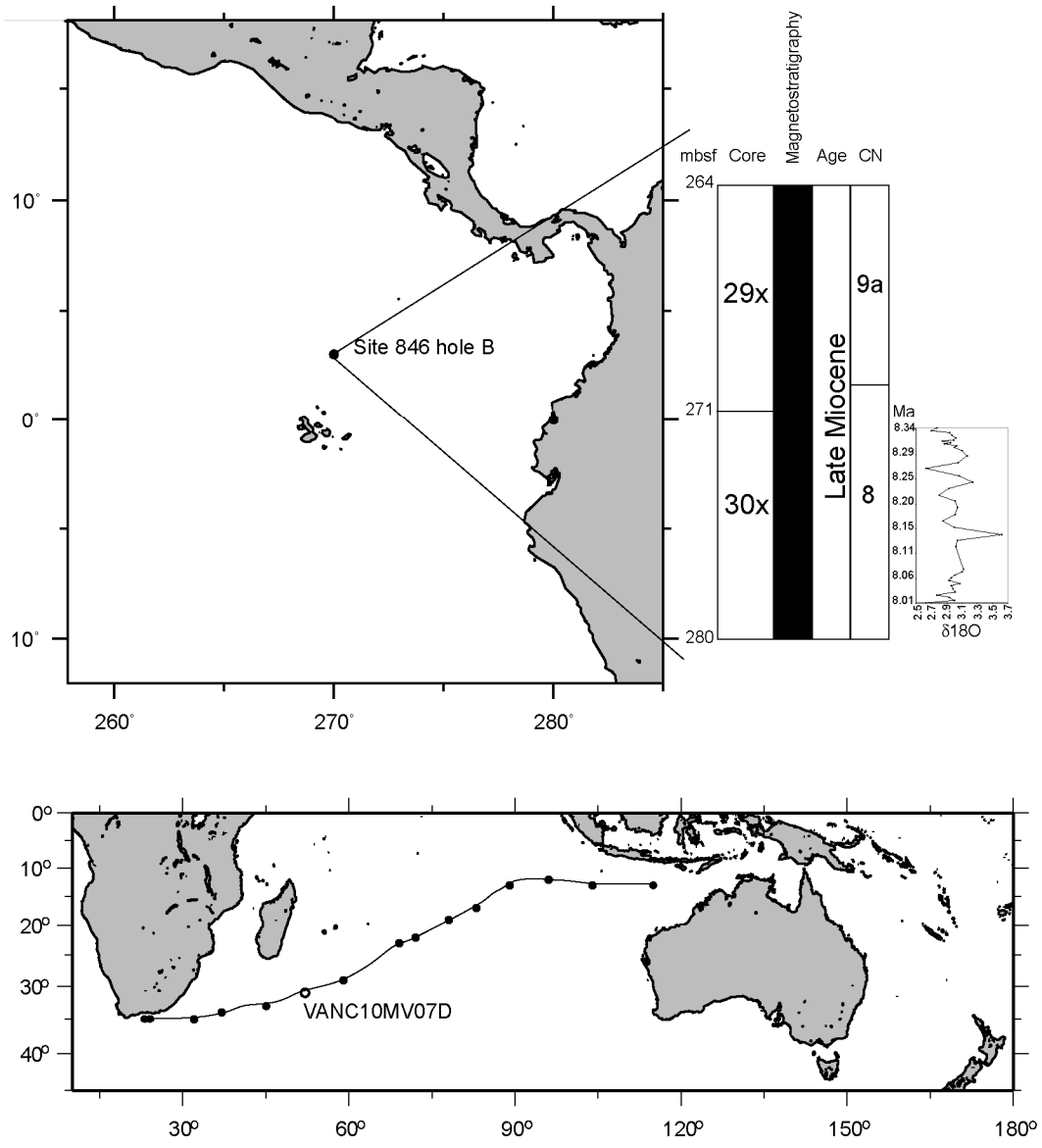

GMT 2006 Apr 27 16:59:44 R.Earley 2006

Figure 1

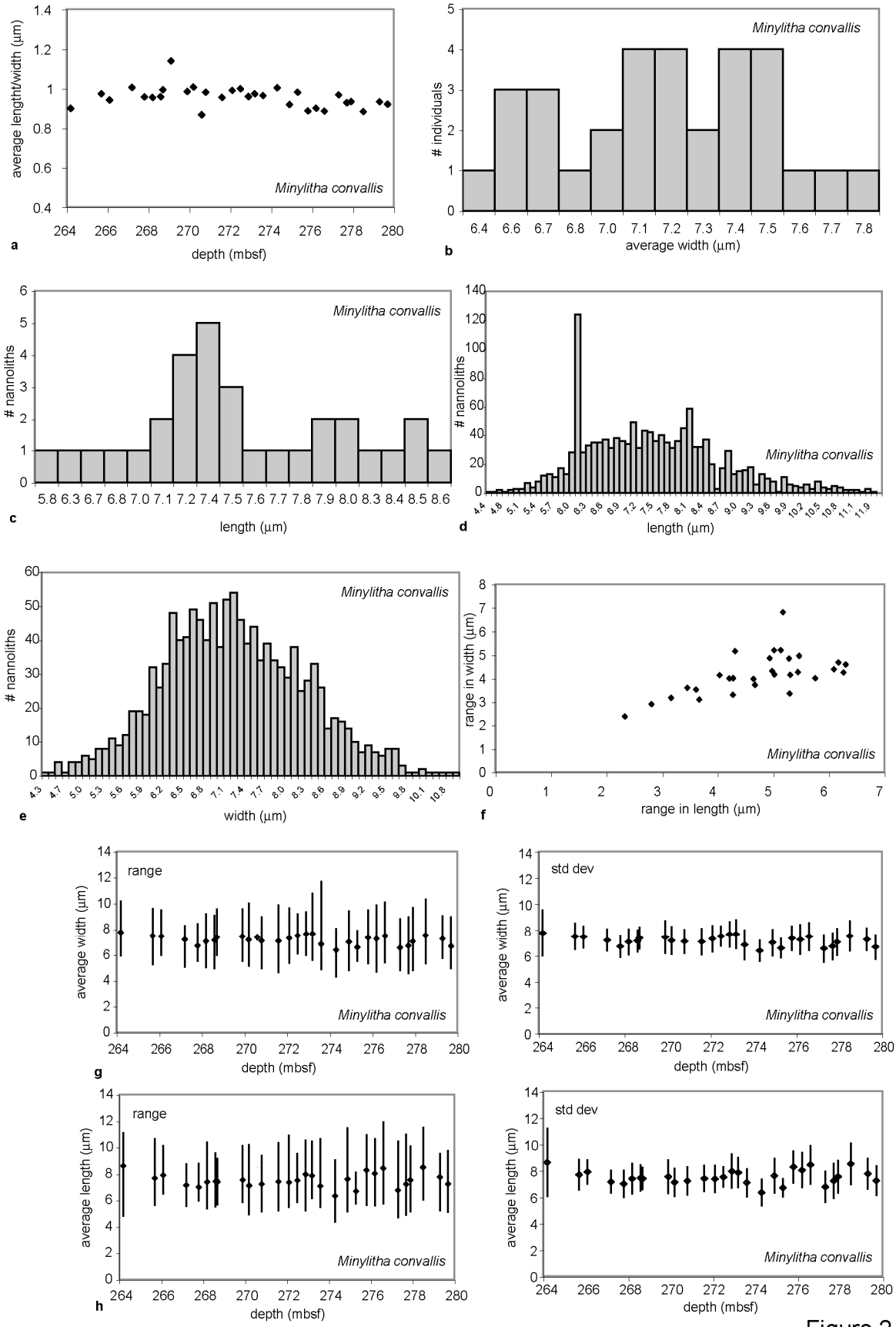
a
average lengtht/width (µm)
depth (mbsf)
Minylitha convallis
b
individuals
average width (µm)
Minylitha convallis
c
nannoliths
length (µm)
Minylitha convallis
d
nannoliths
length (µm)
Minylitha convallis
e
nannoliths
width (µm)
Minylitha convallis
f
range in width (µm)
range in length (µm)
Minylitha convallis
g
range
average width (µm)
depth (mbsf)
Minylitha convallis
std dev
average width (µm)
depth (mbsf)
Minylitha convallis
h
range
average length (µm)
depth (mbsf)
Minylitha convallis
std dev
average length (µm)
depth (mbsf)
Minylitha convallis

Figure 2

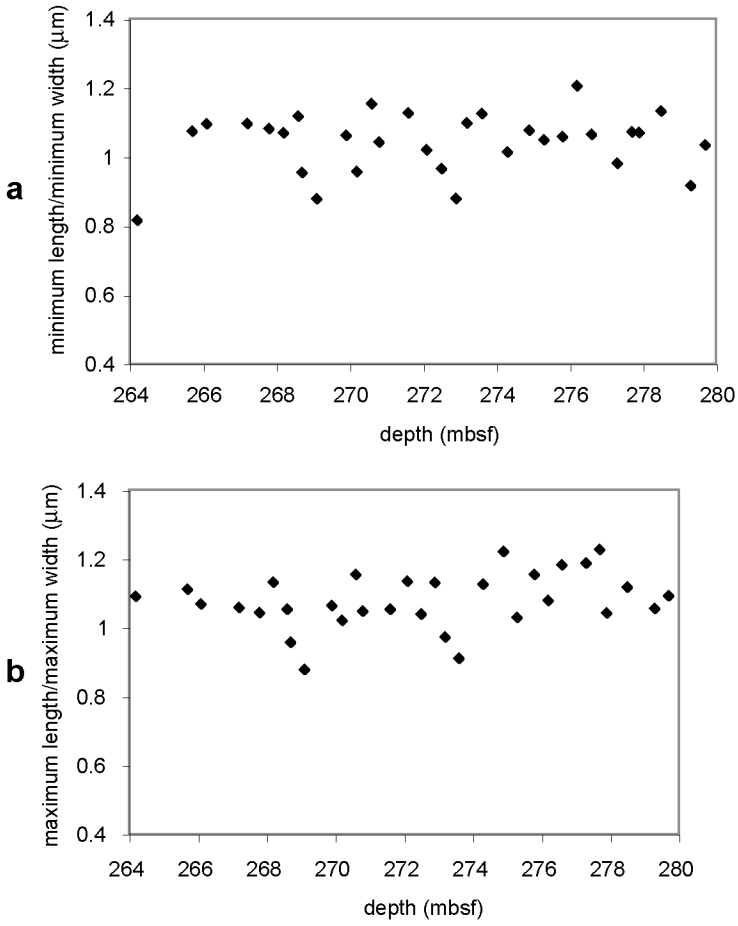
a
minimum length/minimum width (µm)
1.4
1.2
1
0.8
0.6
0.4
264
266
268
270
272
274
276
278
280
depth (mbsf)
b
maximum length/maximum width (µm)
1.4
1.2
1
0.8
0.6
0.4
264
266
268
270
272
274
276
278
280
depth (mbsf)

Figure 3

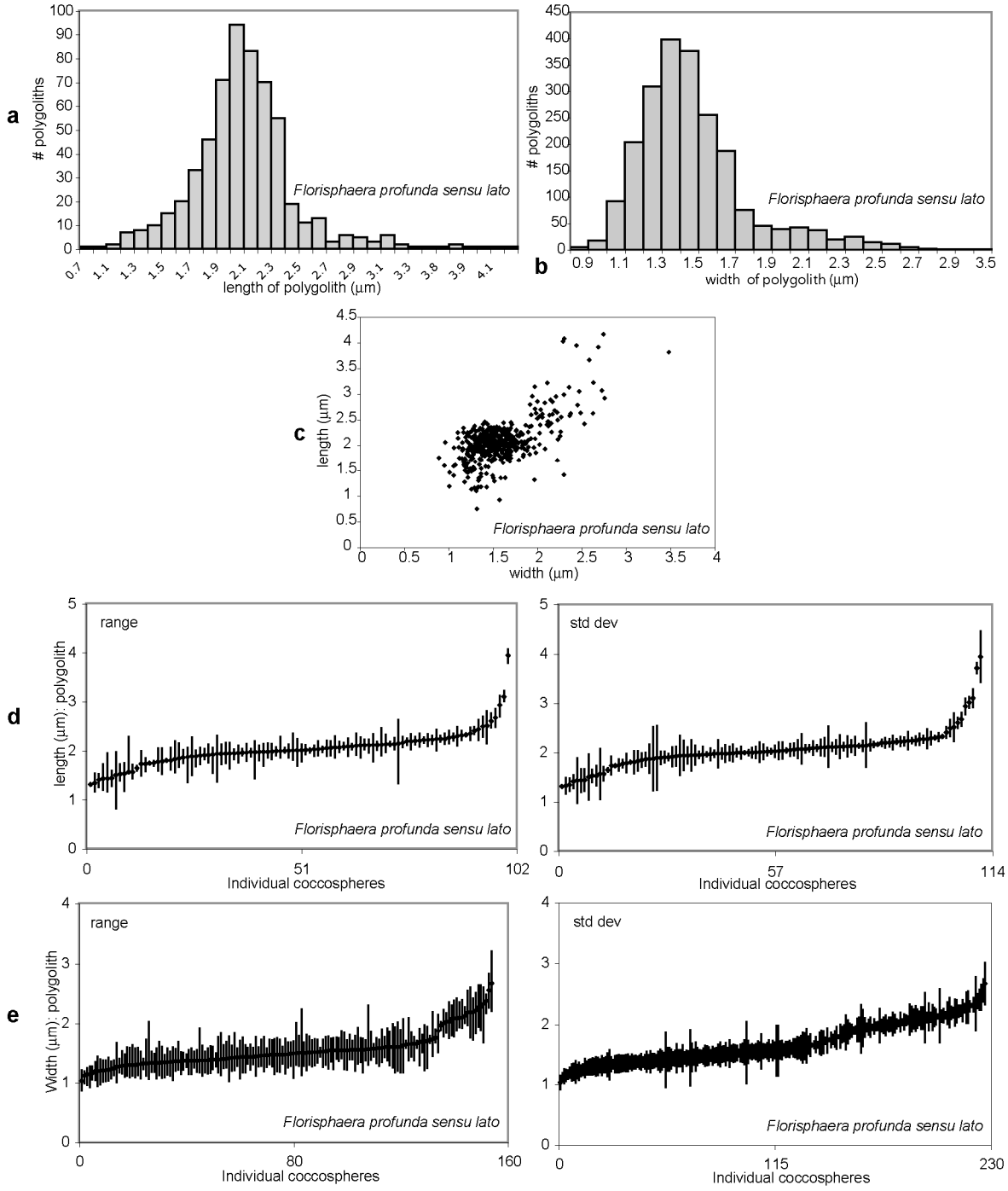
a
polygoliths
length of polygolith (µm)
Florisphaera profunda sensu lato
b
polygoliths
width of polygolith (µm)
Florisphaera profunda sensu lato
c
length (µm)
width (µm)
Florisphaera profunda sensu lato
d
range
std dev
length (µm): polygolith
Individual coccospheres
Florisphaera profunda sensu lato
e
range
std dev
Width (µm): polygolith
Individual coccospheres
Florisphaera profunda sensu lato

Figure 4

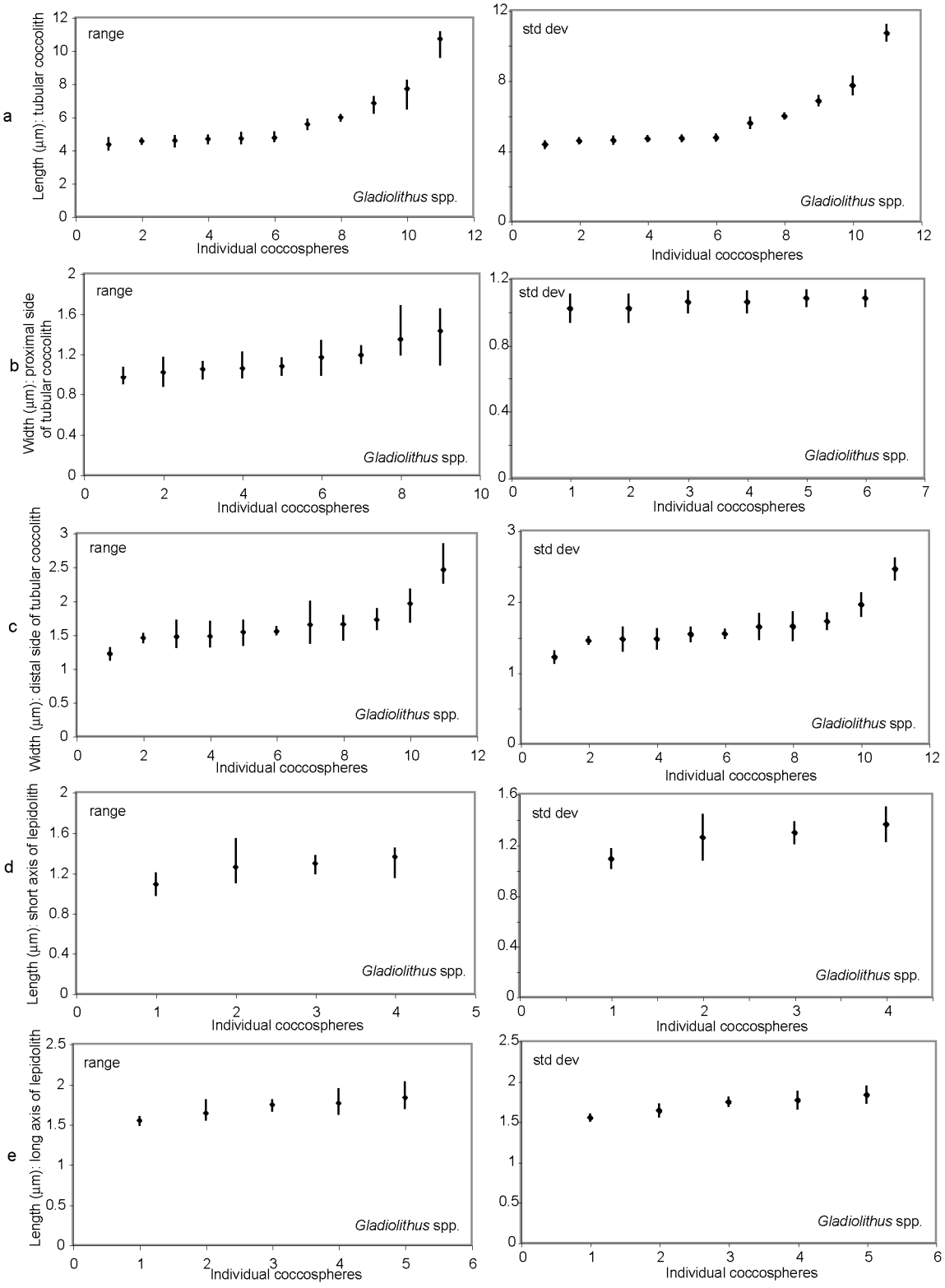
a
Length (µm): tubular coccolith
range
std dev
Gladiolithus spp.
Individual coccospheres
b
Width (µm): proximal side of tubular coccolith
c
Width (µm): distal side of tubular coccolith
d
Length (µm): short axis of lepidolith
e
Length (µm): long axis of lepidolith

Figure 5

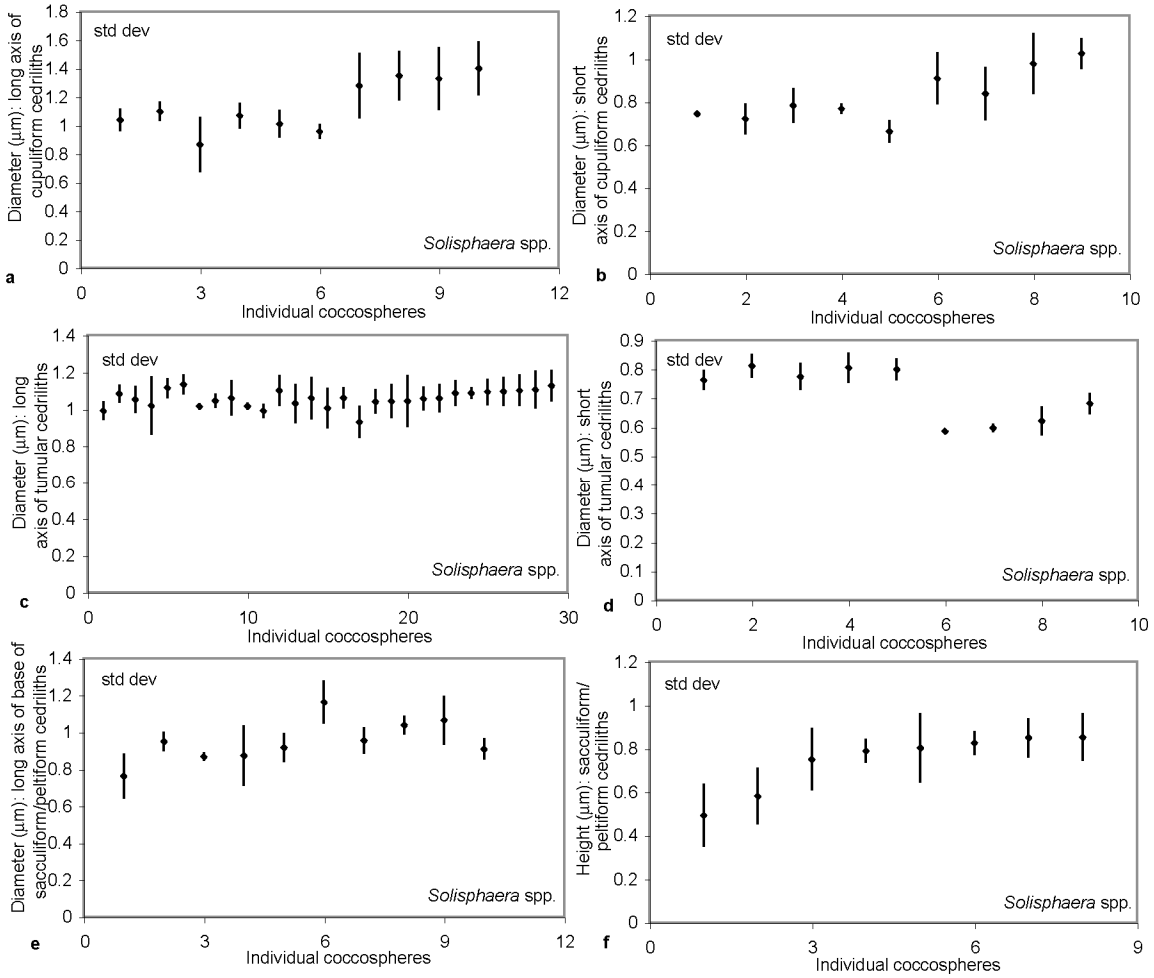
a
Diameter (µm): long axis of cupuliform cedriliths
std dev
Solisphaera spp.
Individual coccospheres
b
Diameter (µm): short axis of cupuliform cedriliths
std dev
Solisphaera spp.
Individual coccospheres
c
Diameter (µm): long axis of tumular cedriliths
std dev
Solisphaera spp.
Individual coccospheres
d
Diameter (µm): short axis of tumular cedriliths
std dev
Solisphaera spp.
Individual coccospheres
e
Diameter (µm): long axis of base of sacculiform/peltiform cedriliths
std dev
Solisphaera spp.
Individual coccospheres
f
Height (µm): sacculiform/ peltiform cedriliths
std dev
Solisphaera spp.
Individual coccospheres

Figure 6

Chapter 4

Plate captions

Plate 1: Figs. a-h; bar= 2 µm. *Minylitha convallis*. ODP Leg 138, Site 846, hole B. Photographs in stratigraphic order from 268.2-279.7 mbsf. Photographs taken from a Zeiss Axiom Light Microscope at 8000x magnification.

Fig. i; bar= 2 µm. Fig. j: scale bar= 5 µm. *Florisphaera profunda*. Filter-sample VANC10MV07D. Photographs taken from FEI Quanta 400 E.S.E.M.

a: Core 29, section 3, 100 cm; 268.2 mbsf.

b: Core 29, section 5, 0 cm; 270.2 mbsf.

c: Core 29, section 6, 80 cm; 272.5 mbsf.

d: Core 30, section 1, 100 cm; 274.9 mbsf.

e: Core 30, section 4, 90 cm; 279.3 mbsf.

f: Core 30, section 4, 90 cm; 279.3 mbsf.

g: Core 30, section 4, 130 cm; 279.7 mbsf.

h: Core 30, section 4, 130 cm; 279.7 mbsf.

i: *Florisphaera profunda* var. *F*

j: *Florisphaera profunda* var. *C*

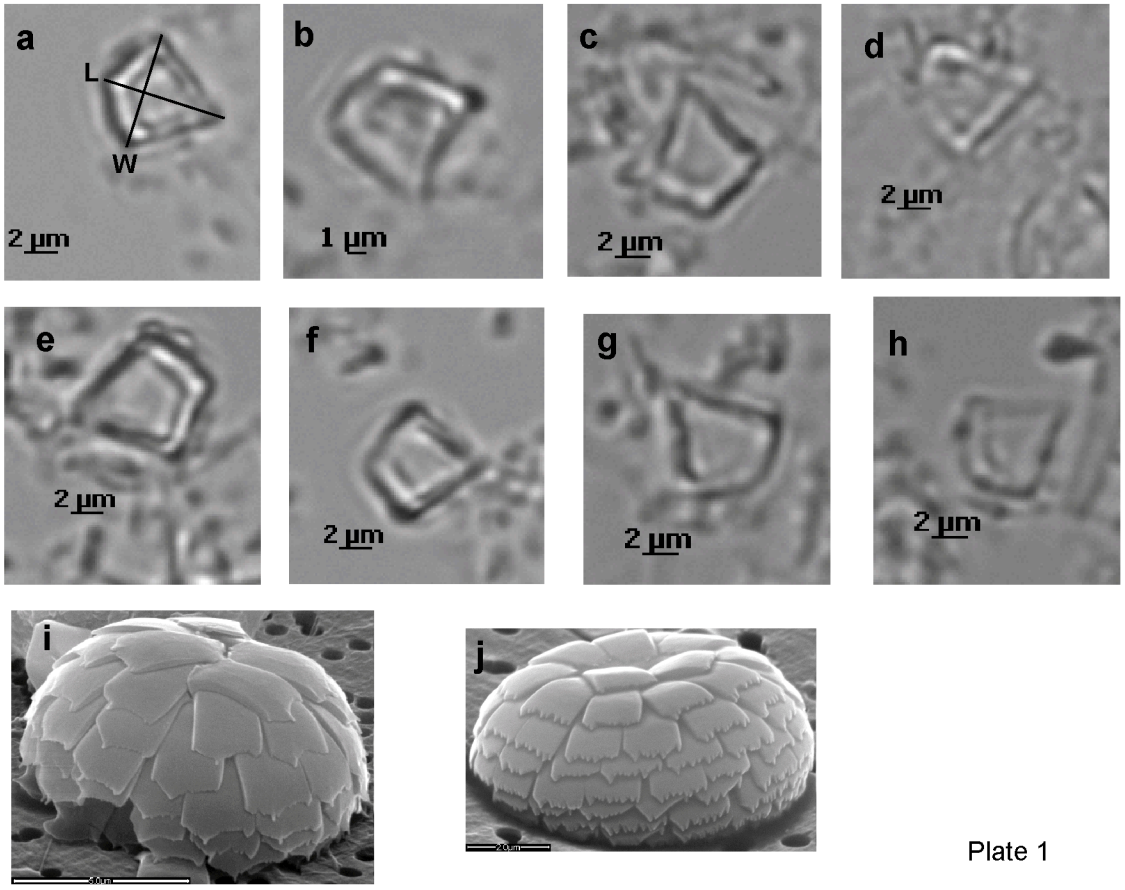

Plate 1

Synthesis of the Dissertation

Recent publications quantifying morphology of the modern coccolithophores focus on particular ocean basins and broadly describe certain families or collections (not necessarily communities) of species/genera. Here I have quantified a shallow water family and the deep-water community in the Indian Ocean basin to clarify that differentiation that exists between (and perhaps defines) depth-stratified species. Many of the species measured in this dissertation are the single formally described species in their genus (i.e., *Discosphaera, Palusphaera vandelli, Florisphaera profounda, Algirosphaera robusta*), and all are defined to a precise depth in the upper water column or photic zone (as partitioned by the depth of the thermo/nutricline.

Modern coccolithophore communities are depth stratified. Deep photic zone (DPZ) coccolithophorids occupy a contrasting ecological niche from the shallow water species. Although some species can live in both the shallow and the DPZ (*Gephyrocapsa* spp., *E. huxleyi*), the globally dominant species in the DPZ are well-defined; *F. profunda, G. flabellatus, O. antillarum, A. robusta* (Okada & Honjo, 1973). I demonstrate the unique morphological features and intraspecific variability of coccoliths and coccospheres, which differentiate communities at 2 different depths within the photic zone. Although conclusions for the shallow photic zone (SPZ) have limited application due to the narrow scope of the study, those of the DPZ coccolithophores are more broadly applicable due to the lower species diversity and therefore larger relative number of analyzed species. Subsequent extrapolation into the fossil record permits interpretation of stratification in the paleo-ocean.

Within the SPZ family Rhabdosphaeraceae I observe two monospecific genera, *Discosphaera* and *Palusphaera*. I propose that despite significant morphological variation, the species designations are appropriate. Rhabdospheres of these genera are comprised of varimorphic rhabdoliths, whose varimorphism is a defining characteristic. I emphasize that high intraspecific variability characterizes these SPZ species. Further quantification of these SPZ species and those of different families and in different ocean basins will increase the database for the SPZ. With such a database, as started here with the family Rhabdosphaeraceae, patterns should emerge that may corroborate my conclusions of low intraspecific variability defining the SPZ. Measurements of the length of coccolith protrusions, and the long and short axes of (sub-) elliptical coccoliths appear to be the easiest to make and the most comparable (and thus useful).

Unique morphologies link coccospheres of various genera in the DPZ. Low intraspecific variability, as well as particular coccosphere shape, differentiates these genera from SPZ dwelling coccolithophore genera. The less variable DPZ forms a stable, low light, high nutrient, lower temperature habitat with highly decreased wave energy as compared to the highly changeable SPZ. As such, the DPZ coccolithophores should be more similar across the globe than the SPZ coccolithophores. Although I cannot make ubiquitous conclusions from this preliminary work in the SPZ and more extensive work in the DPZ (which also needs to be further quantified), I have compared my data with that from published measurements which indicate that the data herein is comparable to that in the literature. Even so, such large databases as compiled here must be done for the other ocean basins. As with the SPZ coccolithophores, those measurements that are most

important are the length of protrusions, length and width of geometrically-shaped coccoliths, and diameter of the long and short axes of elliptical coccoliths.

The nannoliths of the Late Miocene *M. convallis* are similar in shape to polygoliths of *F. profunda sensu lato*. As such, and due to overlapping stratigraphic ranges, Gardner (1992) proposed that *M. convallis* is ancestral to *F. profunda*. Should the two species be related it should follow that *M. convallis* was deep photic dweller in the Miocene, similar to *F. profunda* from the late Miocene to today. This correlation is highly relevant for application to paleoceanography. *Florisphaera profunda* is used to extrapolate paleoceanographic conditions and climate cyclity back to its first occurrence at ~7 Ma. If the tie between *M. convallis* and *F. profunda* can be more tightly constrained, such paleoceanographic extrapolations can be applied to the first occurrence of *M. convallis* ~11 Ma. Additionally, should morphologies indicate depth habitat of the calcareous nannoplankton/fossils and as such paleo-ocean dynamics, I have established another tool for constraint of stratification of the paleo-ocean and associated paleo-ocean and paleo-climate conditions.

The variability in *M. convallis* is more similar to the deeper photic zone coccolithophores that to that of the SPZ coccolithophores. Similarity in low intraspecific variability and coccolith morphology with *F. profunda sensu lato* and other DPZ genera indicates that *M. convallis* may have been a DPZ dweller and that peaks in its abundance during the Miocene imply a stratified upper ocean and deep nutricline.

References

GARTNER, S., 1992. Miocene nannofossil chronology in the North Atlantic, DSDP Site 608. Marine Micropaleontology, 18: 307-331.

OKADA, H., Honjo, S., 1973. The distribution of oceanic coccolithophorids in the Pacific. *Deep Sea Research*, 20: 355-374.

Future Outlook from the dissertation

1- Morphological analysis:

To confirm the magnitude of intraspecific morphological variation among depth-stratified coccolithospheres, further quantification of their morphological homo- and heterogeneity is necessary. Particularly relevant are the morphologies of coccoliths and coccospheres of those genera that inhabit a range of depths (0-200 m), e.g.; *Oolithotus* and *Algirosphaera.*

In collaboration with Dr. M. Triantaphyllou of the University of Athens I have measured the diameter of rhabdospheres of *A. robusta* from the Aegean Sea (0 m), southern Indian Ocean (120 m), and from published photographs (0-160 m). I observe from preliminary data that size may be correlatable with depth (Tables 1a-d), however, a greater number of coccospheres need to be measured.

I have also measured coccospheres of the DPZ dwelling, *O. antillarum*, and the shallower, *O. fragilis*, from Indian Ocean sample VANC10MV03B (Table 2) at 35 m depth. Both species are found in this SPZ sample likely due to its proximity to the Agulhas Current and resultant increased mixing. Coccospheres of the genus *Oolithotus* are comprised of imbricated coccoliths, making measurement of constituent coccoliths difficult. As such, I have measured only completely visible coccoliths, approximately 3-4 per coccosphere. Measurements of both species plotted together show bimodality in coccolith diameter, but high variability in coccosphere diameter. Due to the low number of coccoliths that can be measured per coccosphere, collection of more coccospheres is

necessary; I measured 44 coccospheres with 43 measurements of the diameter of the long axis of the coccoliths, and 108 measurements of the short axis.

Finally, quantification of length and width of fossil polygoliths of *F. profunda* for comparison with those measurements from *M. convallis* in Chapter 4 of this dissertation would provide a better comparative framework for contrasting the 2 species. Both currently monospecific, these taxa may both require that their genera be split into multiple species based on intraspecific variability in both structure and size.

2- Phylogenetic analysis:

Molecular biology has revealed that calcareous nannoplankton speciation is much greater than morphological analysis might indicate (Sáez et al. 2003) such that small morphologic differences may characterize different species rather than reflect intraspecific variability. Genetic sequencing has been used to refine morphological taxonomy of foraminifera and more recently, coccolithophores (de Vargas 2004). Construction of primers for unknown genetic sequences is most effective with monospecific communities.

In the process of designating field samples appropriate for molecular analysis, I found 3 samples along the Indian Ocean transect which have single species dominating their coccolithophore communities: VANC10MV05B – *D. tubifera*, VANC10MV07D – *F. profunda sensu lato*, VANC10MV26A – *P. vandelii*. Total DNA can be extracted from these samples so that various couples of primers targeting different taxonomic ranges within the coccolithophores can be used to PCR amplify the LSU rDNA of chosen morphospecies, genus, or even families. Once interpreted (with morphological data), the

molecular phylogenies of the sequenced genes may be used to inter-calibrate genetic and morphological variations at the species level. The use of combined morphogenetic datasets will be a necessary condition to accurately define which characters of the coccoliths or coccospheres are relevant to biological species recognition. More specific to this study, we will be able to genetically confirm the monospecificity in *D. tubifera* and *P. vandelii*, the validity of the 2 species *Rhabosphaera clavigera* and *R. stylifera*, and the splitting of the morphotypes of *F. profunda*.

References

DE VARGAS, C., Sáez, A.G., Medlin, L.K., Thierstein, H.R., 2004. Super-species in the calcareous plankton. In: Thierstein, H.R., Young, J.R., Eds., *Coccolithophores: from molecular processes to global impact*. Berlin, Springer-Verlag: 271-298.

SÁEZ, A.G., Probert, I., Geisen, M., Quinn, P., Young, J.R., Medlin, L.K., 2003. Pseudo-cryptic speciation in coccolithophores. *Proceedings of the National Academy of Sciences*, 100(12): 7163-7168.

3- Isotopic analysis:

Isotopic comparison between DPZ and SPZ species should corroborate the morphological differentiation described in this dissertation. Fossil polygoliths of *F. profunda* have been isolated using a density settling technique and then analyzed isotopically (Stoll and Ziveri 2002). Although Stoll and Ziveri (2002) did not analyze bulk samples, the isotopic values between *F. profunda* and other species differ by ~1 to 2‰ for $\delta^{13}C$, and ~0.2 to 3.0‰ for $\delta^{18}O$.

The isotopes clearly indicate vital effect, but its full magnitude is as yet unclear. Replication of the data and testing of controls should indicate the effectiveness of the separation technique for isotopic analysis. Analyses should be compared to values from depth-specific planktonic foraminifera and bulk sediment for all samples as controls, to

note the vital effect of the separated assemblage, and to compare the isotopic difference in foraminifera at varying depths. The mass spectrometer standard should be treated with the same density settling method as the coccoliths to identify any sources of contamination. This is a time consuming and complex technique (see Appendix II Methods), but one that may substantiate hypotheses of depth stratification of fossil coccolithophores. Based on previous work on isotopic differentiation in depth-stratified foraminifera, I anticipate that the SPZ versus DPZ coccospheres will have lighter : heavier isotopic values, respectively.

Future outlook

Table captions

Table 1: *Algirosphaera robusta*.

Comparison of measurements taken from published photographs from samples in the Pacific, Atlantic, and Indian Oceans, and unpublished S.E.M. photographs taken from samples in the Mediterranean Sea and Indian Ocean.

a: 0-5 m water depth

b: 60 m water depth

c: 90 m water depth

d: 120-160 m water depth

Table 2: *Oolithotus antillarum, O. fragilis*.

Average, minimum, and maximum measurements from coccospheres found on filter-sample VANC10MV03B.

Future outlook
Tables

0-5 meters			
Sample	Diameter 1	Diameter 2	No. of rhabdoliths
Western Arabian (Kleijne 1992)	9.6		43
N. Atlantic (Kleijne 1992)	8.7	7.9	39
Western Arabian (Kleijne 1992)	7.8		39
Western Arabian (Kleijne 1992)	8.3		45
Medit 5m (Cros & Fortuño 2002)	7.9		38
Pacific 0-5m (Nishida 1979)	8.9	8.3	43
Pacific 0-5m (Nishida 1979)	10.6	10.0	26
Medit T1-2-0March (Kahn unpub. data)	10.5		52
Medit 1T1-2-0March (Kahn unpub. data)	10.4		52
Kleijne 1992 compilation			60-80
Kleijne 1992 max	6.5		
Kleijne 1992 min	9.6		
Average	**9.0**	**8.8**	**41.9**
Minimum	**6.5**	**7.9**	**26**
Maximum	**10.6**	**10.0**	**52**

Table 1a.

60 meters			
Sample	Diameter 1	Diameter 2	No. of rhabdoliths
Medit 60m (Cros & Fortuño 2002)	11.3	10.9	45
Medit 60m (Cros & Fortuño 2002)	10.1	9.4	28
Medit T3-1-45Au01 (Kahn unpub. data)	9.3		31
Average	**10.2**	**10.1**	**34.7**
Minimum	**9.3**	**9.4**	**28**
Maximum	**11.3**	**10.9**	**45**

Table 1b.

90 meters	Mediterranean Sea (Kahn unpub. data)		
Sample	Diameter 1	Diameter 2	No. of rhabdoliths
T3-1-90Au02	9.9	8.7	35
3T3-1-90Au01	8.8		42
1T3-1-90Au02	9.5	9.0	49
2T3-1-90Au01	10.2		43
T3-1-90Au01	8.5		42
Alg890	8.3	8.2	53
Alg1690	8.1		46
Alg1590	8.1	6.5	37
Alg1490	6.9	5.9	37
Alg1390	7.7		34
Al1190	8.6	8.0	49
Alg1090	8.3	8.1	34
Alg990	8.5	8.0	40
Alg590	8.0		27
Alg490	8.0		29
Alg390	10.7		60
Alg290	8.9		53
Alg190	8.7		36
Al1090Au	8.8		41
Al1190Au	9.4	7.6	57
Al1290Au	8.9		41
Al1390Au	10.1	8.7	43
Al1490Au	9.7	9.4	46
Al1590Au	11.9	11.0	60
Al1690Au	10.0	9.9	49
Al1790Au	8.1		39
Al1890Au	7.7		37
Al1990Au	9.8	9.0	48
Al2090Au	8.1	7.9	44
Alg190Au	8.8	7.9	45
Alg290Au	8.6	8.9	49
Alg390Au	7.6		44
Alg490Au	10.2	9.9	42
Alg590Au	8.5	7.4	33
Alg690Au	11.1		78
Alg790Au	10.7	10.2	48
Alg890Au	9.3		38
Alg990Au	7.9		36
Algrobusta3_T3190Au01	7.5		37
Algrobusta2_T3190Au01	8.3	8.2	39
Average	**8.9**	**8.5**	**43.5**
Minimum	**6.9**	**5.9**	**27**
Maximum	**11.9**	**11.0**	**78**

Table 1c.

120-160 meters			
Sample	Diameter 1	Diameter 2	No. of rhabdoliths
Pacific 140-160m (Reid 1980)	13.0		51
S.China Sea 150m (Yang)	8.1	7.2	43
Kahn 07D 120m (Kahn, Chapter 3)			
Kahn, Chapter 3 avg	11.8	10.8	
Kahn, Chapter 3 min	9.9	7.3	
Kahn, Chapter 3 max	13.2	12.5	
Kahn 24D 121m (Kahn unpub. data)	11.0	10.3	45
Average	**11.2**	**9.6**	**46.3**
Minimum	**8.1**	**7.2**	**43**
Maximum	**13.2**	**12.5**	**51**

Table 1d.

O. antillarum			**Avg**	**Min**	**Max**	**Std Dev**
coccosphere	#	23				
	height		7.9	6.6	9.8	1.0
	width		7.4	5.6	10.0	1.1
coccolith	long axis		3.8	3.2	4.4	0.3
	short axis		3.4	2.6	4.3	0.4
O. fragilis	#	14				
coccosphere	width		7.8	6.9	8.4	0.8
	long axis		3.5	3.1	4.1	0.3
coccolith	short axis		3.4	2.7	4.3	0.3

Table 2.

Appendix I
Quantitative Data

All quantitative data from dissertation in excel format and photographs in PDF format.
Hard copy users please see attached cd.

Appendix II
Methods

Methodology for coccolith separation in sediment samples

(approx. 3-day procedure, plus another 4 days under the hood to evaporate ammonia from vials for mass spectrometer analysis)
Modified from Stoll and Ziveri, 2002 (modifications from references noted below)

All procedures to be performed in a hood with appropriate safety equipment. Keep NH_4OH separate from NaClO and H_2O_2.

Carbonate-saturated 2% ammonia solution with density of 0.90 (Andruleit, H., pers. comm., Feb. 2004; Stoll, H., pers. comm., Feb. 2004; Bollmann et al., 2002; Andruleit et al., 2000)
950 mL deionized water
50 mL 20% NH_4OH
0.980 g $CaCO_3$ (technical carbonate – chemically precipitated and therefore relatively free of ions)
Vacuum filter
0.8-0.45 micron polycarbonate or nitrocellulose mixed ester filter

Mix together in a hood, shake, and leave for at least 24 hours. Vacuum filter with to remove excess carbonate. Store solution in hood.

Metal clean
Leach overnight in 1N HCl all plastics to be used (polypropylene centrifuge tubes, squirt bottle, polypropylene bottle, etc.) Wash thoroughly in deionized water.

Isolate 20 micron fraction of sample
~1/8 cc sediment
saturated NH_4OH
20 micron sieve
"jam jar" (polypropylene jar with 3 inch diameter, same as sieve diameter)

Wet sieve sediment with ammonium solution over "jam jar", and then pour fraction that went through the sieve into clean 50 mL centrifuge tube.
Wash sieve thoroughly with DI.

Disaggregate organic matter
Shaker table
50 mL centrifuge tubes with sample in ammonium solution
Centrifuge
Deionized water
Gently shake ~24 hours.

To clean ammonia from sediments centrifuge at 2500 rpm for 45 minutes (be sure no sediment remains in supernatant). Decant ammonium solution without removing any sediment. Fill tubes with DI and use disposable pipette to pull sediment from bottom into solution. Repeat centrifuge and decanting, refill with with DI and repeat once more.

Oxidation of organic matter (Bairbakhish et al.,1999; Bollmann, J., pers. comm., Feb. 2004; Stoll, H., pers. comm., Feb. 2004)
1000 µm deionized H_2O
1000 µm 2-3% NaClO
1000 µm 35% H_2O_2
Ultrasonicator
13 mL test tubes (borosilicate glass) – for carbon and oxygen isotopes (plastic for metals)
100-1000 µL adjustable micropipetter with tips
Vacuum filter
0.8 micron polycarbonate or nitrocellulose mixed ester filter
Clean 50 mL polypropylene centrifuge tubes
Carbonate-saturated NH_4OH

Pipette sample and DI into test tube. Pipette, in the following order, NaClO, and H_2O_2, into test tube. Place test tube in rack in ultrasonicator and sonicate 5 seconds. Every 10 minutes for 50 minutes ultrasonicate for 5 seconds and add one drop of NaClO (add the NaClO to keep the pH constant).
Vacuum filter mixture in test tube, adding DI to wash sample (~200 mL). Under a hood, place filter in centrifuge tube and squirt with carbonate-saturated NH_4OH to remove sediment into tube.
Note: For *F. profunda* only fill the tube up to 4 cm (~20 mL).

Settling
50 mL centrifuge tubes with 4 cm high sample plus carbonate-saturated NH_4OH
100-1000 µL adjustable micropipetter with tips
glass vials for mass spectrometer analysis
0.8 micron polycarbonate or nitrocellulose mixed ester filter
glass cover slip

Allow tubes to settle for 3 hours (for *F. profunda*). Pipette 150-200 µL from settling column within top ½ of supernatant into glass vials, cover with kimwipe and allow to evaporate in hood. Pipette small amount of supernatant onto cover slip or nitrocellulose mixed ester filter (light microscope analysis) or onto polycarbonate filter (scanning electron microscope analysis).
When solution has evaporated from vial, it is ready for analysis in mass spectrometer for carbon and oxygen isotopes.

References
ANDRULEIT, H., Köthe, A., Stäger, S., Bruns, A., 2000. Some comments concerning sample processing and dissolution. Journal of Nannoplankton Research, 22, 3, 201.

ANDRULEIT, H., 1996. A filtration technique for quantitative studies of coccoliths. Micropaleontology, 42, 2, 403-406.
BAIRBAKHISH, A.N., Bollmann, J., Sprengel, C., Thierstein, H.R., 1999. Disintegration of aggregates and coccospheres in sediment trap samples. Marine Micropaleontology, 37, 219-223.
BOLLMAN, J., Cortés, M.Y., Haidar, A.T., Brabec, B., Close, A., Hofmann, Palma, S., Tupas, L., Thierstein, H.R., 2002. Techniques for quantitative analyses of calcareous marine phytoplankton. Marine Micropaleontology, 44, 163-185.
STOLL, H., Ziveri, P., 2002. Separation of monospecific and restricted coccolith assemblages from sediments using differential settling velocity. Marine Micropaleontology, 46, 209-221.

Personal Communication
Andruleit, Harald, Feb. 2004.
Bollmann, Jörg, Feb. 2004.
Stoll, Heather, Feb. 2004.

Curriculum Vita
Alicia Catherine Muzika Kahn

Education

October 2007: Ph.D., Rutgers University Geological Sciences, N.J.
Morphometric variability in the extant coccolithophores: implications for the fossil record

May 2003: M.Sc., Rutgers University Geological Sciences, N.J.
Protist Provincialism during the Paleocene/Eocene Thermal Maximum: Temporal Constraint of the *Rhomboaster* spp. – *Discoaster araneus* Association

May 1998: B.A., Amherst College Geology, M.A.
Honors thesis (Sedimentology) with distinction
Newly Evaluated Paleosols and Gaps in the Basal Conemaugh Record, Upper Potomac Coal Fields, Western Maryland

Teaching Positions

September 2005-May 2006: Professor for Introduction to Physical Geology, Rutgers University

September 2004-May 2005: Head Teaching Assistant for Introduction to Geology laboratory, Rutgers University

September-December 2004: Tutor for Introduction to Geology, Rutgers University

September-December 2004: Tutor for Global Environments, Rutgers University

May-June 2004: Adjunct Professor for Introduction to Oceanography, Rider University

September-December 2003: Tutor for Introductory Oceanography, Rutgers University

April 2001: Tutor for Introduction to Geology, Rutgers University

January-May 2001: Tutor for online Introduction to Geology course

September 2000 – May 2005: Teaching Assistant, Rutgers University
- September-May 2000-2001, 2003-2005: Introduction to Geology Laboratory
- September-December 2001: Sedimentology Laboratory
- January-May 2000-2001: Stratigraphy Laboratory

Professional Positions

September 2006-present: Biostratigrapher in the Shallow Water Stratigraphy Team in the Energy Technology Company within Chevron Corporation

June-August 2005: Internship in the Biostratigraphy and Geostatistics Team at ChevronTexaco Corporation

July, October, December 2001, September 2003, October 2004: Field geologist (stratigraphy), New Jersey drilling projects

May-September 2000: Geochemistry/Micropaleontology Laboratory technician, Institute of Marine and Coastal Science, Rutgers University

August-December 1999: Curatorial intern, Rancho Santa Ana Botanic Garden herbarium, C.A.

June-August 1999: Forestry Technician, U.S. Forest Service, Big Bear, C.A.

June-December 1998: Carbonate Soils Technician, USFS, Big Bear, C.A.

Publications

Peer-reviewed Papers

Aubry, M.-P. and Kahn, A., 2006. Coccolithophores from the deep photic zone of the Indian Ocean: a case for morphological convergence as a forcing mechanism in the evolution of the calcareous nannoplankton. Micropaleontology, 52(5): 411-431.

Kahn, A., Aubry, M.-P., 2006. Intraspecific morphotypic variability in the Family Rhabdosphaeraceae. Micropaleontology, 52(4): 317-342.

Aubry, M.-P., Bord, D., Beaufort, L., Kahn, A., Boyd, S., 2005. Trends in Size Changes in the Calcareous Nannoplankton during the Mesozoic: A Pilot Study. Micropaleontology, 51(4): 309-318.

Kahn, A., Aubry, M.-P., 2004. Provincialism associated with the Paleocene/Eocene Thermal Maximum: Temporal constraint. Marine Micropaleontology, 52:117-131.